

Thèse

Présentée à

L'Université de Lille – Faculté Science et Technologies

Par

Despoina Andriotou

En vue d'obtenir le grade de

Docteur de l'Université de Lille

Filière : Molécules et Matière Condensée

Discipline : Chimie des matériaux



Synthèse de complexes et de polymères de coordination avec des cations de métaux de haute valence (Nb) ou d'actinides (Th, U)

Rapporteur	M. Thomas Devic	Directeur de recherche CNRS – Institut Des Matériaux de Nantes Jean Rouxel
Rapporteur	M. Nicolas Clavier	Directeur de recherche CNRS – ICSM Marcoule
Examineur	M. Guillaume Rogez	Directeur de recherche CNRS – Université de Strasbourg
Examineur et président du jury	M. Sébastien Royer	Professeur des universités – Université de Lille
Directeur de thèse	M. Thierry Loiseau	Directeur de recherche CNRS – Université de Lille
Co-directeur de thèse	M. Christophe Volkringer	Professeur des universités – Centrale Lille

Thèse soutenue publiquement le 13/01/2023

Thèse réalisée à l'Unité de Catalyse et Chimie du Solide UMR CNRS 8181

Thesis

Presented at

University of Lille – Faculty of Science and Technology

By

Despoina Andriotou

For obtaining the title of

Doctor of philosophy of University of Lille

Sector: Molecules and Condensed Matter

Discipline: Material Chemistry



Synthesis of complexes and coordination polymers with high valence transition metals (Nb) or actinide cations (Th,U)

Rapporteur	M. Thomas Devic	Research director CNRS – Institute of Materials Jean Rouxel, University of Nantes
Rapporteur	M. Nicolas Clavier	Research director CNRS – ICSM Marcoule
Examiner	M. Guillaume Rogez	Research director CNRS – University of Strasbourg
Examiner and president of the jury	M. Sébastien Royer	Professor – University of Lille
Thesis director	M. Thierry Loiseau	Research director CNRS – University of Lille
Thesis co-director	M. Christophe Volkringer	Professor – Centrale Lille

Thesis defended in public the 13/01/2023

Thesis executed in the Unit of Catalysis and Solid-State Chemistry (UCCS) UMR CNRS 8181

Table of content

Acknowledgements.....	7
General Introduction.....	9
Chapter I – State of the art.....	13
I. 1 General characteristics of niobium.....	14
I. 2 The world of niobium carboxylates.....	15
I. 2.1 Introduction.....	15
I. 2.2 Nb ^{III} carboxylate complexes.....	16
I. 2.3 Nb ^{IV} carboxylate complexes.....	19
I. 2.4 Nb ^V carboxylate complexes.....	24
I. 2.5 Niobium carboxylate complexes containing heteroatoms.....	33
I. 3 Towards niobium-containing multi-dimensional networks.....	36
I. 4 From actinide(IV) clusters to multidimensional networks using carboxylic acids as complexing linkers.....	42
I. 4.1 Mixed Th-U based carboxylates.....	48
I. 5 Summary.....	51
I. 6 Purpose of the thesis.....	52
I. 7 References.....	55
Chapter II – Niobium(IV) pyridine-carboxylate complexes.....	63
II. 1 Synthesis of molecular mononuclear Nb(IV) carboxylate complexes.....	65
II. 1.1 Synthesis of [Nb(Hqui) ₄ ·0.8(CH ₃ CN)] (Nb(IV)-1).....	66
II. 1.2 Synthesis of [Nb(Hqui) ₄ ·0.7CH ₃ CN·2pyr] (Nb(IV)-2).....	66
II. 1.3 Synthesis of [Nb(qui)(Hqui) ₃ ·Cl·Hpyr·HTEA·1.5H ₂ O] (Nb(IV)-3).....	67
II. 1.4 Synthesis of [Nb(Hicc) ₄ ·6DMF] (Nb(IV)-4).....	67
II. 1.5 Synthesis route discussion.....	68
II. 2 Structural description.....	69
II. 2.1 Complex 1 [Nb(Hqui) ₄ ·0.8(CH ₃ CN)].....	70
II. 2.2 Complex 2 [Nb(Hqui) ₄ ·0.7CH ₃ CN·2pyr].....	72
II. 2.3 Complex 3 [Nb(qui)(Hqui) ₃ ·Cl·Hpyr·HTEA·1.5H ₂ O].....	74
II. 1.4 Synthesis of [Nb(Hicc) ₄ ·6DMF].....	77

II. 3 Infrared spectroscopy in Nb(IV) carboxylate complexes.....	78
II. 4 Magnetism in Nb(IV) carboxylate complexes.....	79
II. 5 Electron Paramagnetic Resonance in Nb(IV) carboxylate complexes.....	83
II. 6 X-Ray Photoelectron Spectrometry in Nb(IV) carboxylate complexes.....	85
II. 7 Conclusions.....	86
II. 8 References.....	89
Chapter III – Pentavalent niobium carboxylate poly-oxo clusters.....	91
III. 1 Nb(V) monocarboxylate poly-oxo clusters.....	94
III. 1.1 Synthesis of Nb(V) monocarboxylate poly-oxo clusters.....	94
III. 1.1.2 Synthesis route discussion.....	98
III. 1.2 Structural description.....	99
III. 1.3 Infrared study in Nb(V) monocarboxylate complexes.....	113
III. 1.4 Nuclear Magnetic Resonance study (liquid state)	116
III. 1.5 Discussion.....	125
III. 2 Nb(V) polycarboxylate poly-oxo clusters.....	131
III. 2.1 Synthesis of Nb(V) polycarboxylate poly-oxo clusters.....	131
III. 2.2 Structural description.....	133
III. 2.2.1 Structural discussion.....	138
III. 2.3 Infrared study in Nb(V) polycarboxylate complexes.....	139
III. 2.4 Nuclear Magnetic Resonance study (liquid state)	142
III. 3 ⁹³ Nb solid state NMR of the coordination niobium(V) complexes.....	143
III. 4 Conclusions.....	147
III. 5 References.....	150
Chapter IV – Coordination polymers of thorium(IV) with azobenzene-polycarboxylate ligands.....	153
IV. 1 Thorium(IV) coordination polymers with 4,4'-azobenzenedicarboxylic acid.....	155
IV. 1.1 Synthesis of precursors.....	155
IV. 1.2 Composition diagram of the system ThCl ₄ /H ₂ abdc/modulator/DMF/H ₂ O.....	156
IV. 1.3 The thorium azobenzenedicarboxylate (Th-abdc-1) phase.....	158
IV. 1.3.1 Synthesis of Th-abdc-1.....	158
IV. 1.3.2 Structural description of Th-abdc-1.....	162

IV. 1.3.3	Characterization of Th-abdc-1 by infrared and thermogravimetric analysis.....	167
IV. 1.3.4	Modulator content (formic acid)	169
IV. 1.3.5	Gas sorption experiments and enthalpies of adsorption of the Th-abdc-1.....	173
IV. 1.4	The thorium azobenzenedicarboxylate (Th-abdc-2) phase.....	178
IV. 1.4.1	Synthesis of Th-abdc-2.....	178
IV. 1.4.2	Structural description of Th-abdc-2.....	180
IV. 1.4.3	Characterization of Th-abdc-2 by infrared and thermogravimetric analysis.....	184
IV. 1.4.4	Gas sorption experiments in Th-abdc-2.....	186
IV. 2	Thorium(IV) coordination polymers with 3,3',5,5'-azobenzenetetracarboxylic acid.....	187
IV. 2.1	Composition diagram of the system $\text{ThCl}_4/\text{H}_4\text{abtc}/\text{modulator}/\text{DMF}/\text{H}_2\text{O}$	187
IV. 2.2	The thorium azobenzenetetracarboxylate (Th-abtc-1) phase.....	189
IV. 2.2.1	Synthesis of Th-abtc-1 phase.....	189
IV. 2.2.2	Structural description of Th-abtc-1.....	190
IV. 2.2.3	Characterization of Th-abtc-1 by infrared and thermogravimetric analysis.....	194
IV. 2.3	The thorium azobenzenetetracarboxylate (Th-abtc-2) phase.....	196
IV. 2.3.1	Synthesis of Th-abtc-2 phase.....	196
IV. 2.3.2	Structural description of Th-abtc-2.....	197
IV. 2.3.3	Characterization of Th-abtc-2 by infrared and thermogravimetric analysis.....	200
IV. 2.3.4	Gas sorption experiments and enthalpies of adsorption for Th-abtc-2.....	202
IV. 3	Conclusions.....	203
IV. 4	References.....	205
Chapter V – Elaboration of mixed thorium(IV)/uranium(IV) carboxylate compounds.....		207
V. 1	Th(IV)/U(IV) hexameric cluster stabilized by anthracene-9-carboxylic acid.....	209
V. 1.1	Synthesis of actinide(IV) chloride precursors.....	209
V. 1.2	Synthesis of the actinide(IV) anthracene-9-carboxylate: $\text{Th}_{6-x}\text{U}_x\text{-anth}$	210
V. 1.3	Structural description of $\text{Th}_6\text{-anth}$	211
V. 1.4	Characterization of the $\text{Th}_{6-x}\text{U}_x\text{-anth}$ compounds.....	213
V. 2	Study of the (Th,U) composition in the $\text{Th}_{6-x}\text{U}_x\text{-UiO-67-NH}_2$ series.....	219
V. 2.1	Synthesis of $\text{Th}_{6-x}\text{U}_x\text{-UiO-67-NH}_2$	219

V. 2.2 Structural description of Th _{6-x} U _x -UiO-67-NH ₂	220
V. 2.3 Characterization of Th _{6-x} U _x -UiO-67-NH ₂	222
V. 3 Study of the Th/U-fumarate series.....	226
V. 3.1 Synthesis of Th _{1-x} U _x -fum.....	226
V. 3.2 Structural description of Th _{1-x} U _x -fum.....	228
V. 3.3 Characterization of Th _{1-x} U _x -fum.....	230
V. 3.4 CO ₂ sorption and enthalpies of adsorption for Th _{1-x} U _x -fum.....	235
V. 4 Conclusions.....	239
V. 5 References.....	241
General conclusion and perspectives.....	243
Abstract/Resumé.....	250

Acknowledgements

At first, I would like to thank and express my gratitude to my two directors: my thesis supervisor Thierry Loiseau, research director in CNRS and head of the team “**MAT**ériaux **HYB**rides” and my co-supervisor Christophe Volkringer, professor in Central Lille.

I am extremely grateful to be guided and supported by Thierry. Someone whose advices and guidance throughout the three years of this thesis, made me evolve as a scientist and for that I would be always in his favor.

I would also like to extend my deepest gratitude to Christophe Volkringer. His help was precious as he never runs out of ideas and he provided me with encouragement and patience throughout the duration of this project.

I would like to thank Ecole Doctorale (SMRE) in the University of Lille for funding my thesis.

I would like to address my sincere thanks to all the members of the jury. First the rapporteurs Nicolas Clavier, Directeur de recherche CNRS in the ICSM Marcoule and Thomas Devic, Directeur de recherche CNRS in the Institut des Matériaux de Nantes Jean Rouxel that have accepted to read carefully this manuscript, enrich this work and for the fruitful discussion during my thesis defense. I would like to equally thank the examiners Guillaume Rogez, Research director CNRS in the University of Strasbourg and Sebastien Royer Professor in University of Lille and president of the jury for attending my defense and upgrade the scientific discussion.

Special thanks should go to Sylvain Duval (MATHYB, UCCS), who played a decisive role in this work. His practical suggestions, relentless support and his optimism always gave me a boost to continue.

I also had great pleasure of collaborating with many researchers in Lille and not only: Xavier Trivelli (UGSF, Univ. Lille) for the liquid NMR experiments, Till Bousquet (CASECO/UCCS) for the advice on organic chemistry, Frederique Pourpoint (RM2i/UCCS) for the solid-state NMR experiments, Pardis Simon (UCCS) for the XPS analysis, Angel Arevalo-Lopez (MISSP/UCCS) for magnetism measurements, Hérve Vezin (LASIRE, Lille) for EPR experiments, Caroline Mellot-Draznieks (Collège de France) and Adel Mesbah (IRCELYON) for the structural calculations and refinement.

I would like to recognize the assistance of many people of the UCCS lab, especially the Solid-State department: Philippe Devaux who can fix everything, Frédéric Capet for always being there during single-crystal X-ray diffraction, Natacha Henry for all the help in indexing and structural solving problems, Laurence Burylo and Pascal Roussel for the DRX, Nora Djelal for the TGA, Céline Delabre for elementary analyses, Alexander Fadel (UMET) for SEM training and support, Edouard Capoen and Maxence Vandewalle for the technical support, Geoffrey Bassez, David Porier, Sandrine Berton and Barbara Declerck-Boulanger for the administration part. Thanks to all the staff of UCCS for these amazing three years.

I gratefully acknowledge the assistance of the interns I supervised: Moumin Atteyeh Djimaleh and Gabrielle Rudeau, thanks for your work.

I also had a great pleasure to meet and interact with numerous PhD students and post-docs and at this part I would like to thank them for all the wonderful moments these last three years.

Maëva (come and get your love..!), Nelly (bike trip partner), Orfeas (the aesthetics director), Iro (for always being there), Amandine (radioactive partner), Pauline (my office view), Julie (breakthrough!), Mohammed (photo-truc, monsieur solution pour tout!), Pedro (Brazilian or Greek bbq?), Soukaina (la stagiaire), Atulya, Jean-Baptiste, the “downstairs” guys: Nico (eau de mort), Teddy, Bertha, the “next door” guys: Catharina (stay strong girl!), Mickaël (master of argon), Xavier (love your T-shirts), Nathan, and also Ibrahim, Victor, and Eleonora.

I cannot leave UCCS without mentioning Julien Dupont, my boyfriend who I met and loved in this lab. You were always there when I needed you the most and you filled these three years with the most wonderful and unforgettable memories.

Last, but not least, I would like to thank my family. My grandparents, my parents Nikos and Antonia and my sister Konstantina for their profound belief in my abilities and their unconditional love and support.

General introduction

Once Maria Skłodowska-Curie said: *“Nothing in life is to be feared, it is only to be understood. Now is the time to understand more, so that we may fear less.”* Research in natural sciences is all about understanding the world we are living in and set the bases for future innovations. Fundamental research in domains like coordination chemistry can set these bases and leads to the generation of new materials with new properties and future prospects.

In 1995, Omar Yaghi introduced a new class of porous materials, named Metal-Organic Frameworks (MOFs). These hybrid crystalline compounds consisted of the association of inorganic and organic building units, that self-assemble towards open frameworks. The resulting porosity can vary depending on the length of the organic chain and belongs to the micropore up to mesopore scale, with applications in gas capture, storage and separation, sensing, drug delivery, etc. Another important aspect, is the plethora of new structural topologies that can be found, since the combinations of the inorganic with the organic SBUs seem limitless. Since then, more than 90,000 MOF-like structures have been synthesized and identified.^[1] This great dynamic shows already the potential of this class of porous hybrid materials.

Whereas many of the different metals in the periodic table have been exploited to generate a large number of MOF structures, there are some, like niobium, that so far, is rarely investigated. Niobium is a metal with different oxidation states (+2, +3, +4, +5) that can be interesting in catalytical processes (for example N₂ reduction reaction (NRR) to produce ammonia). Thus, exploring the reactivity around niobium in order to isolate the first niobium-based porous framework poses a real challenge.

On the same time, MOFs bearing heaviest elements such as actinides starts to become a sub-class of this porous family, especially those represented by the parent analogy of the well-known UiO-n archetypes with the tetravalent actinides (Th, U, Np, Pu). In a sense, the latter exhibits also a way to “capture” these actinides into inorganic building bricks upon specific mild conditions in the presence of carboxylic acids, which plays the role of connecting ligands. Particularly, the interest in uranium comes from its use as combustible in nuclear power plants for the generation of electricity. The hexavalent and most stable oxidation state

of uranium has been extensively studied compared to the tetravalent one. However, the oxide used as combustible in nuclear reactors is the UO_2 , where uranium is in the tetravalent state. Thus, the behavior of tetravalent uranium in the environment needs to be thoroughly studied, as it can be stabilized by complexing agents present in nature (carboxylates, phosphates, etc) and precipitate.

The research work of the team “**MAT**eriaux **HYB**rides” (MATHYB) of the Unit of Catalysis and Solid-state Chemistry (UCCS) in University of Lille is focused in the generation of new hybrid materials like coordination polymers (CPs), metal-organic frameworks (MOFs) and polyoxometalates (POMs). These compounds are then used in catalytical applications, in gas sorption and depollution. In October 2019, my supervisors Thierry LOISEAU and Christophe VOLKRINGER, entrusted me a thesis work around the exploration of new type of crystalline materials, a project that had two distinct approaches. The first one was to study the chemistry around niobium carboxylates, since its reactivity has little yet been investigated. The second one is to extend the work of actinide-based MOFs for which the MATHYB team has now acquired a long experience. This particular work deals with structures made with long home-made organic ligands and investigates the possibility to produce mixed actinide (Th,U) compounds.

Therefore, this manuscript is separated in five chapters:

In the first chapter, the state of the art for the two main subjects is introduced. The first one is dedicated to the reported examples of trivalent, tetravalent and pentavalent niobium carboxylate complexes, as well as the first attempts to incorporate niobium cations in multidimensional systems. The second one is related to the isolation of clusters and coordination polymers with tetravalent actinides (uranium and thorium). Uranium is used in nuclear power plants and their reactivity (like hydrolysis, reduction, oxidation, complexation, adsorption, agglomeration) is important to be studied. The short reviews open the way for the possible formation of three-dimensional hybrid networks containing high valence elements and poses the hypothesis of using less studied elements such as niobium (IV or V) in this strategy, as well as the further use of actinides (IV) with non-conventional organic ligands or involved in mixed metallic systems (typically Th, U).

In the second chapter of this thesis, the reactivity of tetravalent niobium with carboxylates will be thoroughly studied as mimicking the chemical behavior of other transition metals such as Ti(IV) or Zr(IV), for which numerous MOF-like compounds have been isolated with the most promising porosity properties. In our investigations, four new coordination complexes were isolated by using derivatives of pyridine-based dicarboxylic acids, and shows only the assembly of discrete 0D molecular systems, which exhibits different topologies due to the variety of hydrogen bond networks with encapsulated organic solvent molecules (acetonitrile, pyridine, triethylamine, etc...). These compounds will be deeply characterized by X-ray diffraction (single crystal and powder), infrared spectroscopy, magnetism, electron paramagnetic resonance and X-ray photoelectron spectroscopy, in order to confirm the oxidation degree and the coordination sphere around Nb⁴⁺.

Due to some issues of tetravalent niobium stability found in some coordination complexes, we focused our effort to the reactivity of pentavalent niobium towards mono- and polycarboxylates in the third chapter. By controlling the hydrolysis process, in a way that will be discussed in details, numerous molecular poly-oxo-niobates were isolated with nuclearities varying from {Nb₂} up to {Nb₁₂}. These entities were also deeply characterized, by infrared and liquid nuclear magnetic resonance spectroscopies and attempts of characterization by solid-state nuclear magnetic resonance of ⁹³Nb are presented.

The fourth chapter presents new multidimensional frameworks with tetravalent thorium and the use of azobenzene poly-carboxylate ligands. Different synthetical conditions as well as the nature and the quantity of monocarboxylic acid as modulator were tested for their influence on the crystal growth. These systems were characterized with single crystal X-ray diffraction (single-crystal and powder), infrared spectroscopy, thermogravimetric analysis and gas sorption experiments.

The fifth chapter contains an initiative towards the exploration of mixed U/Th compounds. From clusters to coordination polymers, a protocol to isolate mixed U/Th compounds around the desired percentage was developed. These systems were characterized by single-crystal X-ray diffraction for the determination of the crystal structure and by powder X-ray diffraction for the comparison between the mixed systems. Thermogravimetric analysis proved also to be a primary helpful tool in order to compare their thermostability and SEM-

EDX and cartography studies to evaluate the homogeneity and determine the accuracy of the doping.

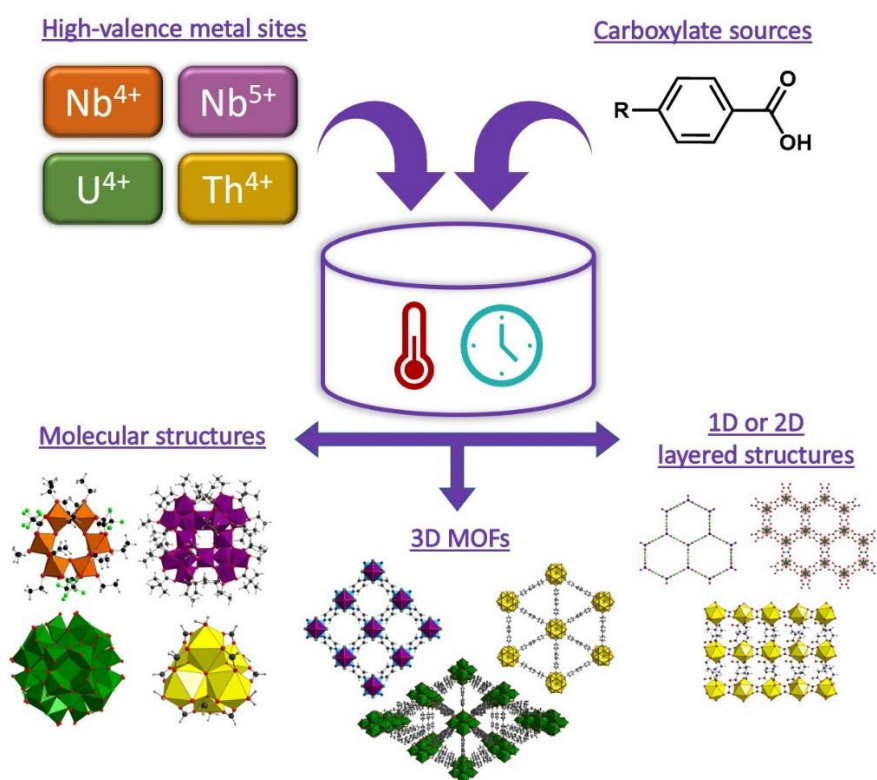
This manuscript finishes with conclusions and the perspectives on the thesis subject.

References

- [1] S. M. Moosavi, A. Nandy, K. M. Jablonka, D. Ongari, J. P. Janet, P. G. Boyd, Y. Lee, B. Smit, H. J. Kulik, *Nat. Commun.* 2020 111 **2020**, 11, 1–10.

Chapter I

State of the art



The bibliographic chapter is focused on two distinct families related to the metal carboxylate crystal chemistry. At first, an up to date review describes niobium carboxylate compounds from molecular level to their incorporation into multidimensional networks. A second part reports well-known and studied tetravalent uranium and thorium polyoxo/hydroxo clusters involved in coordination polymers.

CHAPTER I – State of the art

The synthesis of hybrid inorganic-organic materials is a continuous tendency in the field of materials chemistry, with a very large number of such mixed compounds described in literature.^[1] Hybrid materials are attracting the interest of researchers as they exploit the advantages of both the inorganic and the organic parts. A well-studied category of these materials is the Metal-Organic Frameworks (MOFs) that are a class of porous hybrid coordination polymers. These crystalline solids are built up from a self-assembly of different types of metal-centered Secondary Building Units (SBUs) associated with polytopic organic linkers, giving rise to multidimensional frameworks.^[2] According to the size of these ligands and the type of the inorganic SBU, a broad variety of different topologies can be generated and lead to different pores sizes.^[3] MOFs are considered to be microporous (< 2 nm) and sometimes mesoporous (2-50 nm) materials.^[4] By taking a look on the periodic table, many metals of different groups have already been already introduced as an inorganic SBU (mononuclear cation or polynuclear cluster) incorporated in MOF structures.^[5] However, in Group V (V, Nb, Ta), only vanadium has been really involved in MOF structures^[6], as for example MIL-47^[7], MIL-68^[8] and MIL-71.^[9] There is also only one example of a Ta-MOF reported in 2017^[10], although no detail about the crystal structure was described. But there is still no report of single metal Nb-MOF, except a series of oxyfluorinated niobium compounds obtained by using pillaring pyridine-derived ligands for the production of small-pore network systems.^[11] Thus, this observation incited us to explore the chemistry around niobium and its reactivity with the aim to exploit this metal that, so far, it is not widely studied and fill in a missing piece in the participation of Group V elements (specifically niobium) in MOF structures.

I.1 General characteristics of niobium

Niobium is a d-block transition element with atomic number 41, atomic relative mass of 92,90638 and is located in the 5th group and 5th period of the periodic table. It exists in nature as one only stable isotope, ⁹³Nb, usually in the form of the minerals of pyrochlore-type ((Na,Ca)₂Nb₂O₆(OH,F)) or columbite ((Fe, Mn)Nb₂O₆). The electronic distribution of niobium is [Kr] 4d⁴ 5s¹ and can be found in the oxidation states of 2+ (NbO)^[12,13], 3+ (Nb₂O₃), 4+ (NbO₂) and 5+ (Nb₂O₅) from which only 5+ is considered stable, where +4 and +3 states commonly

exist as halides^[14]. By looking deeper in the ionic radii of niobium at its common oxidation states, which depends on the coordination environment (Table I-1)^[15], we observe that these values are situated between the first and third rows of the transition metals in the periodic table. It is noticeable to consider the close ionic radii of tetravalent metals in eight-fold coordination for Zr⁴⁺ (0.98 Å) or Hf⁴⁺ (0.97 Å), compared to that of Nb⁴⁺ (0.93 Å), since the Zr and Hf-based carboxylate compounds give rise to the generation of the famous UiO-n like MOF.^[16] Related to the six-fold coordination, the ionic radius of Nb⁵⁺ (0.78 Å) is slightly higher than that found for Ti⁴⁺ (0.745 Å), for which well-known MIL-125 MOF^[17] compound has been described. These considerations would open the way for the elaboration of MOF-like materials containing niobium elements.

Table I-1. Ionic radii of niobium and some common M⁴⁺ (M= Ti, Zr and Hf) ions.^[15]

Ion	Coordination	Ionic radius (Å)
Nb³⁺	VI	0.86
Nb⁴⁺	VI	0.82
Nb⁴⁺	VIII	0.93
Nb⁵⁺	VI	0.78
Nb⁵⁺	VII	0.83
Nb⁵⁺	VIII	0.88
Ti⁴⁺	VI	0.745
Ti⁴⁺	VIII	0.88
Zr⁴⁺	VI	0.86
Zr⁴⁺	VII	0.92
Zr⁴⁺	VIII	0.98
Zr⁴⁺	IX	0.103
Hf⁴⁺	VI	0.85
Hf⁴⁺	VII	0.90
Hf⁴⁺	VIII	0.97

I.2 The world of niobium carboxylates

I.2.1 Introduction

There is still a growing interest about niobium compounds, especially niobium oxides and its catalytical applications.^[14,18,19] Even if they are incorporated in a system of mixed oxides associating other metals (like Si and Al), it was proven that niobium could enhance the activity, the selectivity and the long-term stability of the materials it is doped in.^[19–23] More specifically, when niobium oxides are combined with other oxides (Nb₂O₅–SiO₂, Nb₂O₅–Al₂O₃) known for their catalytical properties, they present acidity, redox properties and

photosensitivity.^[21,24] The hydrated form of niobium pentoxide can be used in acid-catalyzed reactions by exchanging water molecules.^[21] Photochromism properties have been evidenced in niobium oxalates like (bpyH₂)(bpyH)[NbO(C₂O₄)₃] \cdot 2H₂O as photoactive compounds. As proposed mechanism, the nitrogen-based counter cation absorbs the daylight irradiation. The energy is transferred to the oxalato-niobate and then back to the base with an electron transfer (mechanism proposed based on Density Functional Theory calculations).^[25] The literature of Nb^V is much more explored than the one of Nb^{IV} and Nb^{III}, for which it is less documented. Due to their unstable oxidation state, laboratories working with the lower oxidation states of niobium need to be specifically equipped (e.g. glove box) in order to handle them. Most of Nb^{IV} and Nb^{III} precursors are halides, stabilized molecules as tetrahydrofuran (THF), tetrahydrothiophene (THT) or 1,2-dimethoxyethane (DME).^[26,27]

Continuous efforts have been made to develop coordination or organometallic complexes with possible multiple metal-oxo bonded moieties of Nb, especially in the low oxidation states of 3+ and 4+. In this manner, resulting niobium cluster compounds were reported and further studied since 1912^[28–32], with most common coordination numbers to vary from six to eight. Our bibliographic survey will now focus on the family of compounds bearing the niobium element associated with carboxylic acids, and then its occurrence in MOF-like materials. The classification of niobium carboxylates will first follow the different oxidation states of niobium from 3+ to 5+.

1.2.2 Nb^{III} carboxylate complexes

In order to generate niobium complexes, coordination with carboxylate functions were investigated. A few Nb^{III} carboxylate complexes have been reported so far and are related to the use of common monocarboxylic acids. They are summarized in Table I-2.

Table I-2. Summary of Nb^{III} carboxylate complexes

Chemical formula	Nb(III) nuclearity	Ligand	Ref
(NMe ₄)[Nb ₂ Cl ₂ (THT)(acetate) ₅]CH ₂ Cl ₂	dimer	Acetic acid	[33]
[Nb ₃ (μ -O) ₂ (O ₂ CC ₆ H ₅) ₆ (THF) ₃][NbOCl ₄ (THF)] \cdot n(THF)	trimer	Benzoic acid	[34]
[Nb ₃ (μ -O) ₂ (O ₂ CC(CH ₃) ₃) ₆ (THF) ₃][B(C ₆ H ₅) ₄]	trimer	Pivalic acid	[34]
[Nb ₃ O ₂ (O ₂ CMe) ₆ (THF) ₃][NbOCl ₄ (THF)]	trimer	Acetic acid	[35]

The main investigations have been performed by the group of F. Albert Cotton. Two distinct nuclearities have been identified, as either dimeric or trimeric niobium-centered entities. There is only one dimer, which exhibits an acetate-bridged complex of Nb^{III} (Figure I-1), for the compound (NMe₄)[Nb₂Cl₂(THT)(acetate)₅]CH₂Cl₂, (THT= tetrahydrothiophene), in which the two niobium atoms create a Nb-Nb bond with a length of 2,764 Å.^[33] Starting by the precursor Nb₂Cl₆(THT)₃ mixed with CH₃CO₂NMe₄ (tetramethylammonium acetate) in dichloromethane, the group of F. A. Cotton achieved to replace most of the chloride molecules with acetate that derive from the partial degradation of CH₃CO₂NMe₄. Each niobium atom is 7-coordinate with a coordination sphere consisting of five carboxyl oxygens, two of them coming from one chelating acetate ligand, two others from two bidentate acetate ligands with two neighbored niobium centers, and the fifth one coming from monodentate acetate ligand. The rest of the coordination sphere consists of one terminal chloride and one bridging sulfur coming from the THT molecule. The dinuclear entity is viewed as two niobium sites with an edge-sharing-polyhedral geometry. The resulting anionic [Nb₂Cl₂(THT)(acetate)₅]⁻ species is compensated by the positive charge of tetramethylammonium.

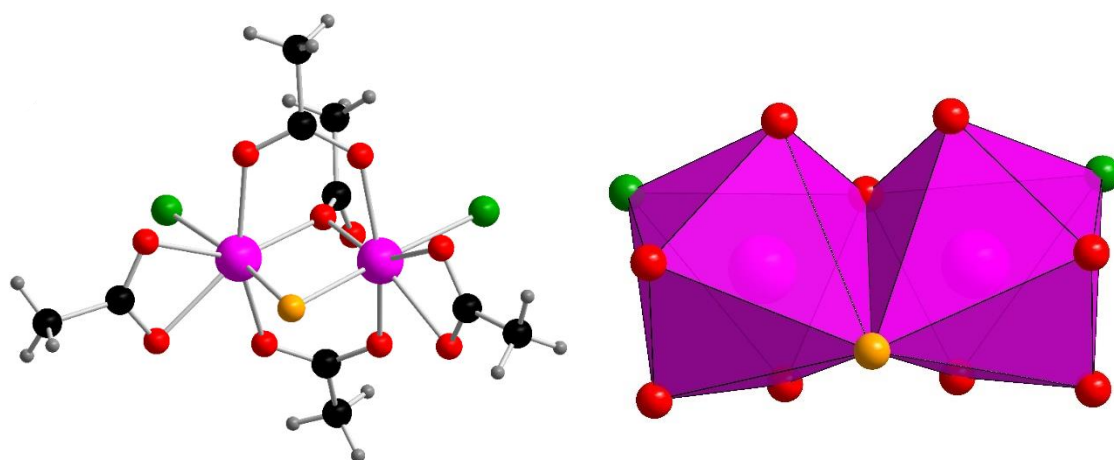


Figure I-1. Crystal structure of the anionic complex [Nb₂Cl₂(THT)(acetate)₅]⁻ (left), dimer niobium-centered cluster with the polyhedral representation (right). (color code: niobium, pink; oxygen, red; chlorine, green; carbon, black; hydrogen, grey)

In order to isolate a higher nuclearity cluster, a different synthetical procedure was adopted and a trimer of Nb^{III} was stabilized by different monocarboxylate functions. At first, the synthesis of [Nb₃(μ₃-O)₂(O₂CC₆H₅)₆(THF)₃][NbOCl₄(THF)]·n(THF) and [Nb₃(μ₃-O)₂(O₂CC(CH₃)₃)₆(THF)₃][B(C₆H₅)₄] were introduced (Figure I-2), where niobium atoms create a trinuclear oxo-cluster with two bridging μ₃-oxygens and carboxyl oxygens deriving from benzoic and pivalic acids accordingly. As for the synthetical procedure, Nb₂Cl₆(SMe₂)₃ was the

starting precursor which was dissolved in a mixture of benzene-THF and into which afterwards the sodium benzoate and sodium pivalate was added. The organic monocarboxylate precursors are already deprotonated and that may be the key to the successful isolation after layering with hexane at RT for $[\text{Nb}_3(\mu_3\text{-O})_2(\text{O}_2\text{CC}_6\text{H}_5)_6(\text{THF})_3][\text{NbOCl}_4(\text{THF})]\cdot n(\text{THF})$ and at low temperature (-4°C) for $[\text{Nb}_3(\mu_3\text{-O})_2(\text{O}_2\text{CC}(\text{CH}_3)_3)_6(\text{THF})_3][\text{B}(\text{C}_6\text{H}_5)_4]$.^[34] The averaged oxidation degree of niobium in this case was found to be +3.66 as all niobium atoms are considered to be equal. The trinuclear niobium cation is formed by two bridging μ_3 -oxygens creating $\text{Nb}_3\text{O}_2^{7+}$ units, in which the niobium atoms have a monocapped trigonal-bipyramidal geometry. Each niobium site is 7-coordinate with oxygens from which two of them derived from condensation between niobium sites, four are coming from bidentate carboxyl oxygens that bridge the niobium trinuclear unit and one oxygen from a terminal THF molecule (Figure I-2). The $[\text{Nb}_3(\mu_3\text{-O})_2(\text{O}_2\text{CC}_6\text{H}_5)_6(\text{THF})_3]^+$ entities are positively charged and are compensated by $[\text{NbOCl}_4(\text{THF})]^-$ in case of benzoate ligand and $[\text{B}(\text{C}_6\text{H}_5)_4]^-$ (tetraphenylborate) in case of pivalate ligand.

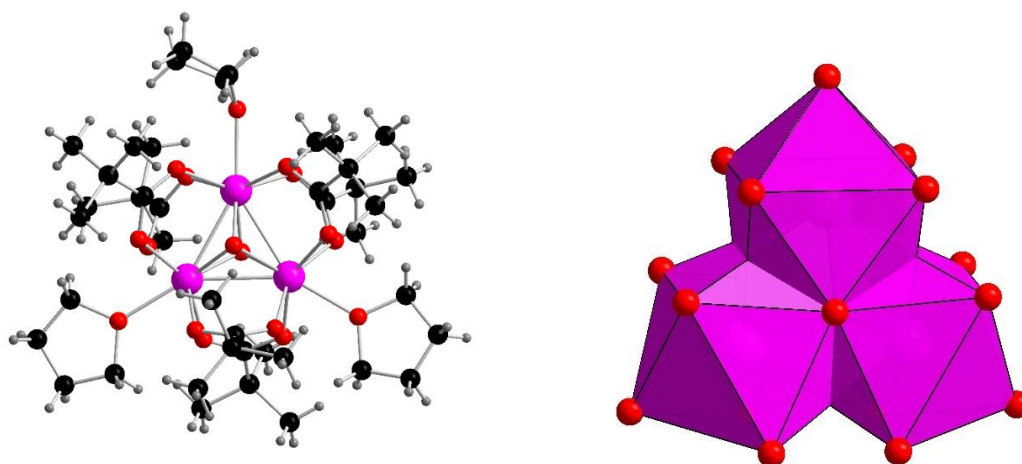


Figure I-2. Crystal structure of $[\text{Nb}_3(\mu_3\text{-O})_2(\text{O}_2\text{CC}(\text{CH}_3)_3)_6(\text{THF})_3]^+$ (left) and its polyhedral representation (right). (color code: niobium, pink; oxygen, red; carbon, black; hydrogen, grey)

Following this work, couple of years after, another trinuclear niobium(III)-carboxylate complex was isolated ($[\text{Nb}_3\text{O}_2(\text{O}_2\text{CMe})_6(\text{THF})_3][\text{NbOCl}_4(\text{THF})]$). The geometry of the trimeric niobium cluster remains the same, but this time the monocarboxylate source was the acetate.^[35] It was reported that the synthetical protocol of the previous trinuclear complex using sodium benzoate and sodium pivalate has been tested as well, but unsuccessfully. Thus, another precursor was used ($\text{Nb}_2\text{Cl}_3(\text{THT})$), it was dissolved in THF and by adding a 1:1 mixture

of deoxygenated acetic acid/acetic anhydrite, crystals of $[\text{Nb}_3\text{O}_2(\text{O}_2\text{CMe})_6(\text{THF})_3][\text{NbOCl}_4(\text{THF})]$ were observed.

Finally, it is of high importance to notice that all procedures in the reported publications were performed under Schlenk lines under inert atmosphere, in order to prevent the oxidation of niobium(III). The resulting dimeric or trimeric Nb(III)-complexes are found to be unstable in air, due to a probable loss of solvent, together with oxidation of the niobium centers.

1.2.3 Nb^{IV} carboxylate complexes

The field of Nb^{IV} carboxylates complexes is also poorly explored and we may notice six carboxylate compounds involved in molecular assemblies of mononuclear or hexanuclear moieties (Table I-3).

Table I-3. Summary of Nb^{IV} carboxylate complexes.

Chemical formula	Nb(IV) nuclearity	Ligand	Ref
$\text{K}_4\text{Nb}(\text{C}_2\text{O}_4)_4 \cdot 4\text{H}_2\text{O}$	monomer	Oxalic acid	[36]
$\text{Nb}(\text{O}_2\text{CNR}_2)_4$	monomer	$\text{CO}_2 + \text{HNR}_2$ (R=Et, Pr ⁱ)	[37]
$[\text{Nb}(\text{edta})(\text{H}_2\text{O}) \cdot 2\text{H}_2\text{O}]$	monomer	Ethylenediaminetetraacetic acid	[38]
$[\text{Nb}(\text{pyc})_4] \cdot 2\text{C}_2\text{H}_5\text{OH}$	monomer	2-pyridinecarboxylic acid	[39]
$[(\text{Cp}'_2\text{Nb})_2(1,4-(\kappa^2\text{-O},\text{O}'\text{-OOC})_2(\text{C}_6\text{H}_4))]$	monomer	Terephthalic acid	[40]
$\text{Nb}_6(\mu_2\text{-O})_3(\mu^2\text{-O}_2\text{CCF}_3)_6(\mu^2\text{-OC}_2\text{H}_5)_6(\text{OC}_2\text{H}_5)_6$	hexamer	Trichloroacetic acid	[41]

The first report of a monomeric niobium(IV)-carboxylate was made in 1987, when the group of F.A. Cotton described an eight-coordinate tetrakis(oxalato)niobium(IV) complex.^[36] $\text{Nb}_2\text{Cl}_6(\text{THT})_3$ was used as a starting material, dissolved in THF at 0°C with the addition of a concentrated solution of hydrochloric acid. After evaporation, the dried green residue was re-dissolved into water where $\text{K}_2\text{C}_2\text{O}_4 \cdot \text{H}_2\text{O}$ was added in a metal to ligand ratio 1:5. According to the ratio of the crystal structure (Table I-3) which is 1:4 (niobium to oxalate), a slight excess of the organic ligand is required in order to obtain the anionic complex $[\text{Nb}(\text{C}_2\text{O}_4)_4]^{4-}$. After the addition of oxalate, a dark red residue was formed, which was removed by filtration and the remaining red solution was layered with mixture of water:ethanol to obtain crystals of $[\text{Nb}(\text{C}_2\text{O}_4)_4]^{4-}$. Each niobium atom is eight-coordinate and the coordination sphere around it consists of four oxalate ligands surrounded by their carboxylic groups and resulting in a

dodecahedral geometry. The negative charge of the Nb-oxalate unit is compensated by potassium cations deriving from $K_2C_2O_4 \cdot H_2O$ precursor.

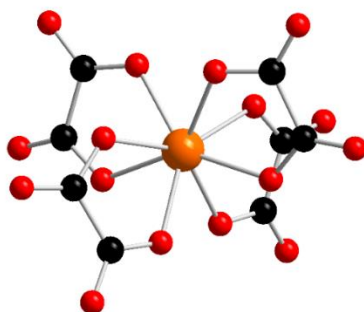
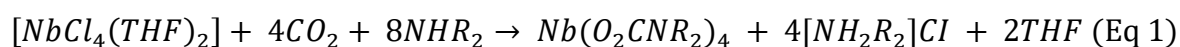


Figure I-3. Crystal structure of the anionic complex $[Nb(C_2O_4)_4]^{4-}$. (color code: niobium, orange; oxygen, red; carbon, black; hydrogen, grey)

Among the efforts to isolate oxalato-niobium(IV) monomeric complexes, it is important to remark another study, in which the authors achieved to isolate the same eight-coordinate oxalato-niobium(IV) anion through a different synthetic route, via the reduction of $NbCl_5$ using Zn metal in a concentrated HCl-ethanol solution.^[42] The result was a brown intermediate that was followed by a complexation with oxalate and led to $[Nb(C_2O_4)_4]^{4-}$ species, with the same counter-cation ($K_4[Nb(C_2O_4)_4]$).

About a decade later, mononuclear complexes of tetrakis(diisopropylcarbamato)- and tetrakis(diethylcarbamato)-niobium(IV) were reported, with the type $Nb(O_2CNR_2)_4$, where R = Et or Pr.^[37] According to the synthetic protocol, $[NbCl_4(THF)_2]$ was used as the metal precursor, which was mixed with a solution of a secondary amine (HNR_2) in toluene that was treated with CO_2 in order to generate the carboxylate functions.^[37] All procedures were performed under argon atmosphere in Schlenk line tubes to avoid oxidation of Nb^{IV} . The reaction can be resumed in equation 1 and after single-crystal X-ray diffraction experiment on crystals of $Nb(O_2CNEt_2)_4$, the crystal structure of the eight-coordinate niobium(IV) complex was revealed and is shown in Figure I-4. The niobium atom is coordinated by eight carboxyl oxygens, which derive from four diethylcarbamato groups, and result in a dodecahedral symmetry.



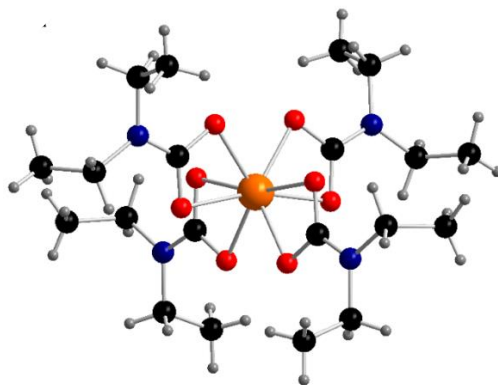


Figure I-4. Crystal structure of $\text{Nb}(\text{O}_2\text{CNEt}_2)_4$. (color code: niobium, orange; oxygen, red; nitrogen, blue; carbon, black; hydrogen, grey)

So far, all of the mononuclear Nb(IV) carboxylate complexes with an eight-fold coordination adopt a dodecahedral geometry for the niobium(IV) center. The first example of an eight-coordinate Nb(IV) carboxylate complex with square antiprismatic geometry was reported at 1998 by Ooi et al. [38] NbCl_5 was reduced into Nb(IV) in an HCl-ethanol (1:6) solution with the addition of zinc powder. Once the reduction is done and the color changes to black-green, the solution is filtered to remove the zinc and ethylenediaminetetraacetic acid (edta) is added. The reaction mixture is left at 4°C for several weeks and after this period, dark-brown crystals were obtained. The Nb(IV) center is eight-coordinate with four carboxyl oxygen atoms, two oxygen atoms coming from coordinated water molecules and two ethylenediamine nitrogen atoms to complete the coordination sphere. This arrangement gives to a distorted square-antiprismatic symmetry. The .cif file of the crystal structure did not surprisingly contain any coordinates data, so a representation of the molecular structure as shown in the publication can be found in Table I-5.

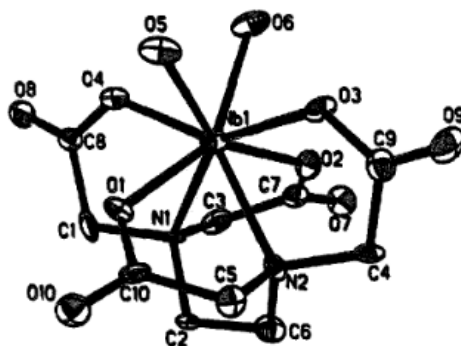


Figure I-5. Representation of the crystal structure of $[\text{Nb}(\text{edta})(\text{H}_2\text{O})_2] \cdot 2\text{H}_2\text{O}$.

Another type of coordination around Nb(IV) species has been reported with the use of 2-pyridinecarboxylic acid as it introduced a coordination with carboxyl oxygens and pyridyl nitrogens.^[39] Niobium(V) pentachloride was reduced in an ethanolic solution with zinc powder by stirring during 3 hours. After reducing Nb(V) to Nb(IV), 2-pyridinecarboxylic acid is added, the reaction mixture was stirred for 30 min and then left to crystallization at 4 °C. Some deep-red crystals were obtained overnight and after performing single-crystal X-ray diffraction analysis, an eight-coordinate Nb(IV) carboxylate complex was revealed (Table I-6). The geometry around the niobium(IV) atoms defines a dodecahedral environment (D_{2d} symmetry) as expected for eight-fold coordination system of $\{MA_4B_4\}$ unit for d^1 transition cations. The structure includes two ethanol molecules (solvent) linked with hydrogen atoms (1.7883(16) and 1.7379(16) Å) by the non-bonded carboxyl oxygens.

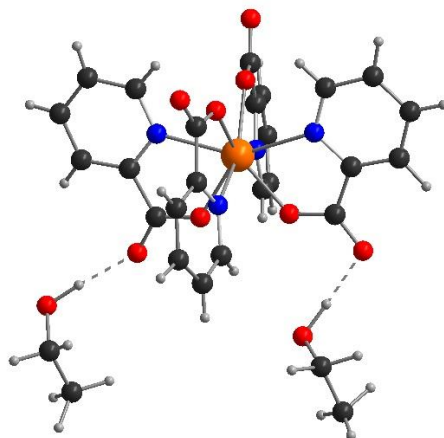


Figure I-6. Crystal structure of $[Nb(pyc)_4] \cdot 2C_2H_5OH$. (dashed line, hydrogen bond. color code: niobium, orange; oxygen, red; nitrogen, blue; carbon, black; hydrogen, grey)

The fifth mononuclear Nb^{IV}-carboxylate complex was reported upon studying the reactivity of complexes Cp'_2NbH_3 (where $Cp' = \eta^5-C_5H_4SiMe_3$) with different carboxylic acids as ligands, like benzoic acid $C_6H_5(COOH)$, terephthalic acid $(1,4-COOH)_2(C_6H_4)$, isophthalic acid $(1,3-COOH)_2(C_6H_4)$ and trimesic acid $(1,3,5-COOH)_3(C_6H_3)$, under stirring in mild thermal conditions (50 °C) in dry THF.^[40] After evaporation and washing steps, a dark green solid was isolated, which corresponds to $[(Cp'_2Nb)_2(1,4-(\kappa^2-O,O'-OOC)_2(C_6-H_4))]$ (Table I-7). Same complexes have been identified with the monocarboxylic acid (benzoic acid), but also some di- and tri-carboxylic acid ligands mentioned above (terephthalic, isophthalic and trimesic acid). The final structure consists of two niobium atoms (when a dicarboxylic acid is used) that

each of them is coordinated to a cyclopentadienyl rings in a η^5 -mode and two carboxyl oxygens from a chelating dicarboxylate ligand, that has a planar arrangement to niobium sites. When the tricarboxylic acid is used (here trimesic acid), each carboxylate arm is coordinated with one $\text{Cp}'_2\text{Nb}$, resulting in a three niobium-centers entity.

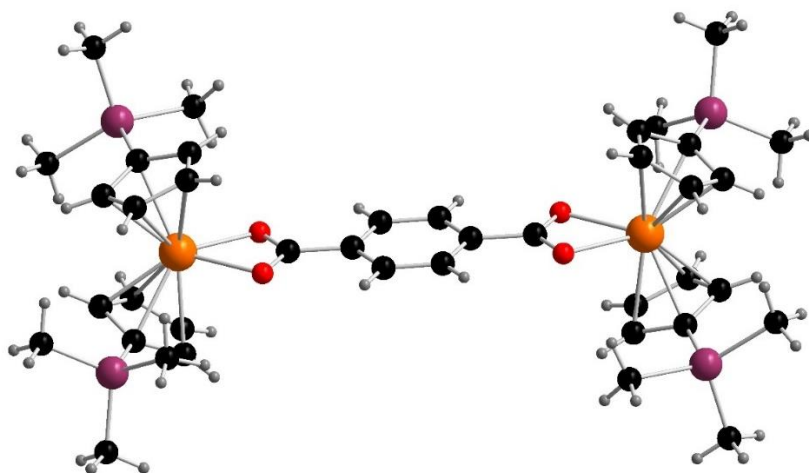


Figure I-7. Crystal structure of $[(\text{Cp}'_2\text{Nb})_2(1,4-(\kappa^2\text{-O,O'-OOC})_2(\text{C}_6\text{H}_4))]$. (color code: niobium, orange; silicon, purple; oxygen, red; carbon, black; hydrogen, grey)

The Nb^{IV} -carboxylate complex with the highest nuclearity so far contains an hexanuclear core.^[41] Starting from NbCl_5 and adding powdered zinc in absolute ethanol, the color of the solution turned from yellow to brown, corresponding to the reduction of Nb^{V} to Nb^{IV} . After 2 days the solution was filtered and re-dissolved in ethanol where trifluoroacetic acid was also added with a 4 times molar excess. Finally, plate-like brown reddish crystals of $\text{Nb}_6(\mu_2\text{-O})_3(\mu_2\text{-O}_2\text{CCF}_3)_6(\mu_2\text{-OC}_2\text{H}_5)_6(\text{OC}_2\text{H}_5)_6$ were isolated (Table I-8). A similar crystal structure was also isolated in the same work with trichloroacetic acid. Basically, we can observe a combination of two identical and equivalent trimers, creating the hexanuclear ring-like structure, in which each niobium is 6-fold coordinated with an octahedral geometry of six oxygens coming from two bridging carboxyl oxygens, two bridging ethoxo groups, one bridging oxo group and one terminal ethoxo group.

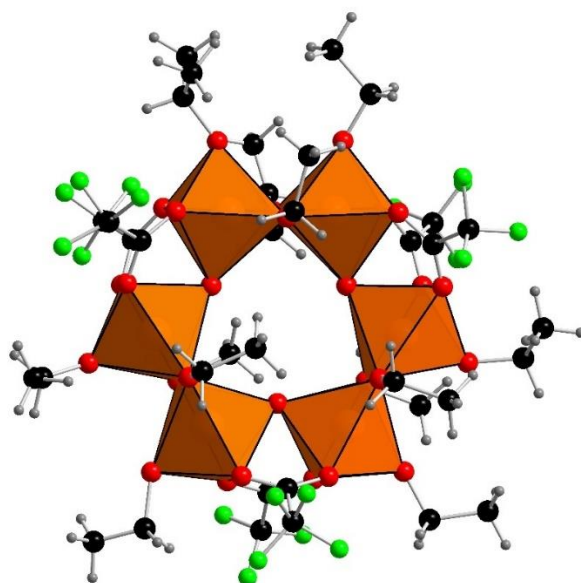


Figure I-8. Crystal structure of $Nb_6(\mu^2-O)_3(\mu^2-O_2CCF_3)_6(\mu^2-OC_2H_5)_6(OC_2H_5)_6$. (color code: niobium, orange; oxygen, red; fluorine, green; carbon, black; hydrogen, grey)

Since this is the only reported example of an hexanuclear structure, it confirms that the condensation of niobium(IV) is challenging. Most of the reported Nb^{IV} alkoxo complexes started from the precursor niobium(V) pentachloride, which is then reduced by using zinc powder dissolved into an alcoholic solution.^[43–46]

I.2.4 Nb^V carboxylate complexes

As it is reported from literature, Nb^V can be found in the vast majority of Nb-carboxylate complexes, as summarized in Table I-4. These coordination complexes show nuclearities that vary from monomers to tetramers and up to a recent report of a hexadecamer.

Table I-4. Summary of Nb^V carboxylate complexes

Chemical formula	Nb(V) nuclearity	Ligand	Ref
$(NH_4)_3NbO(C_2O_4)_3 \cdot H_2O$	Monomer	Oxalic acid	[47]
$(NH_4)_3Nb(O_2)_2(C_2O_4)_2 \cdot H_2O$	Monomer	Oxalic acid	[48]
$KNb(O_2)_3(C_{12}H_8N_2) \cdot 3H_2O$	Monomer	Phenanthroline	[49]
$KNb(O_2)_3(C_{12}H_8N_2) \cdot 3H_2O \cdot H_2O_2$	Monomer	Phenanthroline	[49]
$A_3[Nb(O_2)_2(edta)] \cdot xH_2O \cdot yH_2O_2$ (A= NH_4^+ $CN_3H_6^+$)	Monomer	Ethylenediaminetetraacetic acid	[50]
$A_3[Nb(O_2)_2(pdta)] \cdot xH_2O \cdot yH_2O_2$ (A= NH_4^+ $CN_3H_6^+$)	Monomer	propylenediaminetetraacetic acid	[50]
$(gu)_5[Nb_2(O_2)_4(tart)(Htart)] \cdot 4H_2O$	Dimer	Tartaric acid	[51]
$(gu)_5[Nb_2(O_2)_4(tart)(Htart)] \cdot 6H_2O \cdot H_2O_2$	Dimer	Tartaric acid	[51]
$[Nb_2O_2(OH)(C_4H_3O_5)_2] \cdot 4H_2O$	Dimer	Malic acid	[52]

$[(\text{NbCl}_3(\text{O}_2\text{CPh}))_2\text{O}]$	Dimer	Benzoic acid	[53]
$[\text{NbCl}_4(\text{O}_2\text{CC}_6\text{F}_5)_2]$	Dimer	Pentafluorobenzoic acid	[54]
$[\text{Nb}_2\text{Cl}_4(\text{OEt})_4(\text{O}_2\text{CPh})_2]$	Dimer	Benzoic acid	[55]
$[\text{Nb}(\mu\text{-O}_2\text{CCMe}_3)(\text{OCH}_2\text{CMe}_3)_3]_2(\mu\text{-O})$	Dimer	Methacrylic acid	[56]
$[\text{Nb}_2(\mu\text{-O})_2(\mu\text{-O}_2\text{CCH}_2\text{CMe}_3)_2(\text{OCH}_2\text{CMe}_3)_4]_2$	Tetramer	Methacrylic acid	[56]
$[\text{Nb}^{\text{V}}_4(\mu\text{-O})_4(\mu,\eta^2\text{-Me})_4(\text{OPr}')_8]$	Tetramer	Methacrylic acid	[56]
$[\text{Nb}_4(\mu\text{-O})_4(\text{OAc})_4(\text{OPr}')_8]$	Tetramer	Acetic acid	[57]
$[\text{Nb}_4(\mu\text{-O})_4(\mu,\eta^2\text{-O}_2\text{CCMeCH}_2)_4(\text{OPr}')_8]$	Tetramer	Trimethylacetic acid	[58]
$\text{Nb}_{16}(\text{O})_{28}(\text{OEt})_{12}(\text{piv})_{12}$	Hexadecamer	Pivalic acid	[59]

Two of the reported monomers were stabilized by oxalates. The first one reported is an oxotrioxalate-niobium(V) complex $(\text{NH}_4)_3\text{NbO}(\text{C}_2\text{O}_4)_3 \cdot \text{H}_2\text{O}$ (Table I-9, middle) that was synthesized by mixing oxalic acid and ammonium oxalate with the Nb precursor according to the method of F. Russ in 1902.^[47,60] These authors started by digesting columbite, making a hydrated niobic acid ($\text{Nb}_2\text{O}_5 \cdot n\text{H}_2\text{O}$). This solid was mixed in water with potassium dioxalate to give crystals of the niobium oxalate complex $\text{Nb}_2\text{O}_5 \cdot 5\text{K}_2\text{O}_{10}\text{C}_2\text{O}_3 \cdot 8\text{H}_2\text{O}$. The niobium site is seven-coordinate with a pentagonal bipyramidal arrangement of seven oxygens, six of them coming from the oxalates, in which the carboxylate groups are semi-bidentate, and one terminal hydroxo oxygen. These anionic niobium oxalates precipitate as salts with the following chemical formula $[\text{A}][\text{NbO}(\text{C}_2\text{O}_4)_2(\text{H}_2\text{O})_2] \cdot x\text{H}_2\text{O}$ ($\text{A} = \text{NH}_4^{+ [61],[62]}$ or $\text{Cs}^{+ [63]}$) (Table I-9, left) or $[\text{A}]_3[\text{NbO}(\text{C}_2\text{O}_4)_3] \cdot x\text{H}_2\text{O}$ ($\text{A} = \text{NH}_4^{+ [60]}$ or $\text{Rb}^{+ [64]}$). These can be further associated with various pyridine-based molecules (phenanthroline, bipyridine, etc...)^[25] or divalent transition metals complexes with $[\text{Zn}(\text{bpy})]^{2+ [65]}$, $[\text{Co}(\text{terpy})]^{2+ [66]}$, including a series of $[(\text{Fe-Zn})(\text{bpy})]^{2+ [67]}$ ($\text{bpy} = 2,2'$ -bipyridine, $\text{terpy} = 2,2':6',2''$ -terpyridine), or with rare-earth cations^[68]. Other niobium oxalates have been identified in the presence of barium in $[\text{Ba}_2(\text{H}_2\text{O})_5][\text{NbO}(\text{C}_2\text{O}_4)_3][\text{HC}_2\text{O}_4] \cdot \text{H}_2\text{O}$ ^[69].

A very similar to the later niobioxalate^[60] is also the anion $[\text{Nb}(\text{O}_2)_2(\text{C}_2\text{O}_4)_2]^{3-}$ that was also synthesized in 2003.^[70] This type of oxalates has been introduced by the isolation of the diperoxodioxalate-niobium(V) complex $(\text{NH}_4)_3\text{Nb}(\text{O}_2)_2(\text{C}_2\text{O}_4)_2 \cdot \text{H}_2\text{O}$ (Table I-9, right) by inserting hydrogen peroxide as a solvent.^[48] The niobium center is eight-coordinate with a dodecahedral geometry of eight oxygen atoms deriving from two oxalate groups, that coordinate with the same way as in the previous structure ($[\text{NH}_4^+]_3[\text{NbO}(\text{C}_2\text{O}_4)_3] \cdot x\text{H}_2\text{O}$, Table I-9, middle) and two terminal peroxy groups.

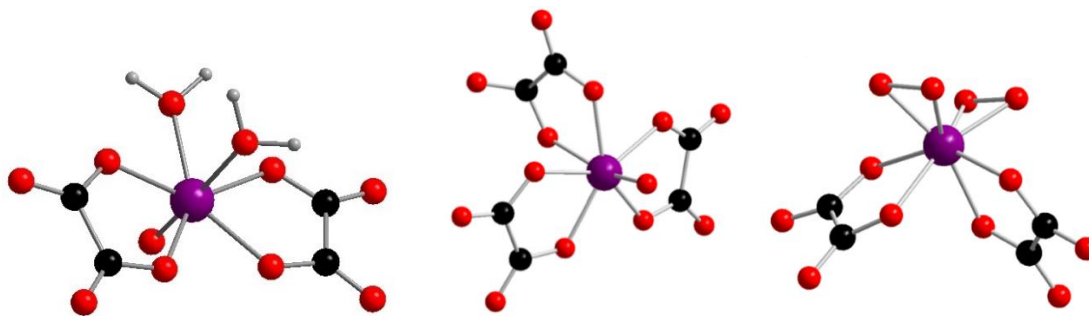


Figure I-9. Crystal structure of the anionic complexes $[\text{NbO}(\text{C}_2\text{O}_4)_2(\text{H}_2\text{O})_2]^-$ (left), $[\text{NbO}(\text{C}_2\text{O}_4)_3]^{3-}$ (middle) and $[\text{Nb}(\text{O}_2)_2(\text{C}_2\text{O}_4)_2]^{3-}$ (right) (color code: niobium, purple; oxygen, red; carbon, black)

Another study reported an eight-coordinate peroxy[polyaminocarboxylato bis(N-oxido)]niobate(V) complex (Figure I-10) by starting from niobic acid ($\text{Nb}_2\text{O}_5 \cdot n\text{H}_2\text{O}$) as metal precursor and using H_4edta (ethylenediaminetetraacetic acid) or H_4pdt (propylenediaminetetraacetic acid) as a carboxylic linker in a solution of H_2O_2 and ammonia.^[50] The hydrogen peroxide was chosen for oxidizing the nitrogen sites (N-oxide derivative ligands).

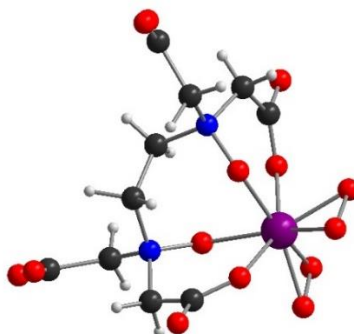


Figure I-10. Crystal structure of the $[\text{Nb}(\text{O}_2)_2(\text{edta})]^{3-}$ anion. (color code: niobium, purple; oxygen, red; nitrogen, blue; carbon, black; hydrogen, grey)

The last monomer, was reported in a study, in which the authors synthesized a Nb(V) peroxy-tartrate complex, by using tartaric acid ($\text{HO}_2\text{CC}_2\text{H}_2\text{CO}_2\text{H}$) instead of oxalic acid.^[51] The structure reveals, as expected, an eight-fold coordination for the Nb(V) center (Figure I-11), where two ligands are bridging two niobium sites and the coordination is completed by two peroxy groups per niobium site.

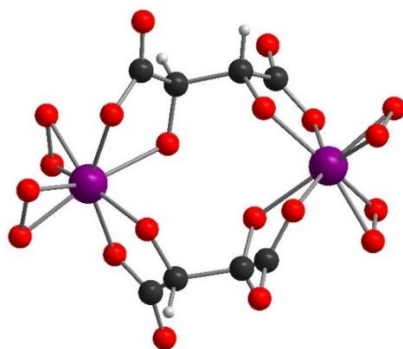


Figure I-11. Crystal structure of $[\text{Nb}_2(\text{O}_2)_4(\text{tart})(\text{Htart})]^{5-}$. (color code: niobium, purple; oxygen, red; carbon, black; hydrogen, grey)

So far, the coordination around niobium(V) consisted only with oxygen atoms. Another study showed that it is possible to incorporate in the coordination sphere both a N-donor ligand and a carboxylate O-donor, by synthesizing the triperoxo-(o-phenanthroline)niobate(V).^[49] In a solution of hydrogen peroxide at 0 °C, phenanthroline and potassium niobate was mixed. After the addition of the right amount of alcohol just to make the solution saturated and by letting the solution rest at room temperature, crystals of $\text{KNb}(\text{O}_2)_3(\text{C}_{12}\text{H}_8\text{N}_2) \cdot 3\text{H}_2\text{O} \cdot \text{H}_2\text{O}_2$ can be obtained (Figure I-12). The niobium site of the structure is eight-coordinate with a trigonal bipyramidal arrangement of six oxygens and two phenanthroline nitrogens.

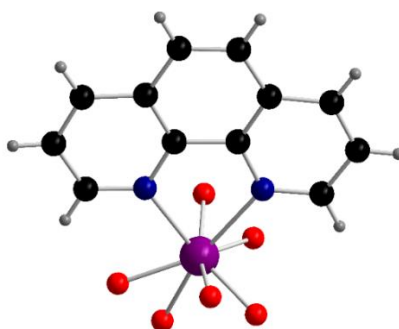


Figure I-12. Coordination sphere of $\text{KNb}(\text{O}_2)_3(\text{C}_{12}\text{H}_8\text{N}_2) \cdot 3\text{H}_2\text{O} \cdot \text{H}_2\text{O}_2$. (color code: niobium, purple; oxygen, red; nitrogen, blue; carbon, black; hydrogen, grey)

There are also some studies related to synthesized dimeric cores of Nb^{V} . N. Brnicevic et al. reported dinuclear malato complexes of Nb^{V} by dissolving hydrated niobium pentoxide into a 5 % aqueous solution (pH = 2.6) of a racemic malic acid, giving the precipitate $(\text{A})[\text{Nb}_2\text{O}_2(\text{OH})(\text{C}_4\text{H}_3\text{O}_5)_2] \cdot 4\text{H}_2\text{O}$ (A=Na, K, $(\text{C}_6\text{H}_5)_4\text{P}$, $(\text{C}_6\text{H}_5)_4\text{As}$) (Figure I-13) after 1 week of refrigeration.^[52] The authors proposed a structure model based on infrared spectroscopy and

a previously reported analogous Mo(VI) complex^[71]. The hypothetical structure contains a niobium dimer which is stabilized by two malate molecules. Each niobium is 6-fold coordinated, with two oxygen atoms that come from carboxylate functions (malic acid), two terminal oxygen atoms and two μ_3 -O.

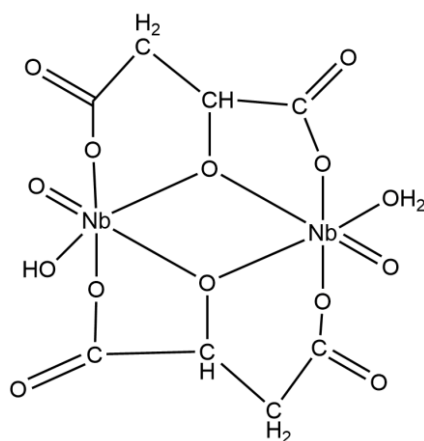


Figure I-13. Suggested crystal structure of $[\text{Nb}_2\text{O}_2(\text{OH})(\text{C}_4\text{H}_3\text{O}_5)_2] \cdot 4\text{H}_2\text{O}$.

Another study aiming on the synthesis of oxoniobium carboxylates, made by the group of D. A. Brown, resulted in the binuclear species $[\{\text{NbCl}_3(\text{O}_2\text{CPh})\}_2\text{O}]$.^[53] This complex was synthesized by mixing NbCl_5 with benzoic acid in a slight excess of the ligand (1:1.5), dissolved and refluxed in chloroform. A brown-orange solution was cooled and dried under vacuum, resulting to a yellow powder of $[\{\text{NbCl}_3(\text{O}_2\text{CPh})\}_2\text{O}]$ (Figure I-14, top). Each niobium atom is six-coordinate with an octahedral arrangement of three terminal chlorides and three oxygen atoms. One single oxygen is bridging the two niobium sites and two oxygens are coming from two bidentate benzoate molecules.

One year after, in 1994, the same group synthesized a dinuclear niobium chlorocarboxylate, starting again from NbCl_5 , but using pentafluorobenzoic acid, instead of benzoic acid. By keeping the same synthetic protocol, they isolated $[\text{NbCl}_4(\text{O}_2\text{CC}_6\text{F}_5)]_2$ (Figure I-14, middle), that does not exhibit an oxo bridge as in the above complex^[54]. A same structure has been also isolated by using TaCl_5 as a metal precursor and *p*-chlorobenzoic acid.

A series of dinuclear niobium chloro alkoxy carboxylates of the type $[\text{Nb}_2\text{Cl}_4(\text{OEt})_4(\text{O}_2\text{CR})_2]$ ($\text{R}=\text{Ph}$, *p*- FC_6H_4 , *p*- ClC_6H_4 , *p*- IC_6H_4 , *p*- MeC_6H_4) were synthesized by using as precursors NbCl_5 and carboxylic acids in EtOH (Figure I-14, bottom).^[55] The hexacoordinated

niobium sites are stabilized by two bridging bidentate carboxylate functions and connected by two terminal ethoxy ligands and two chloride anions.

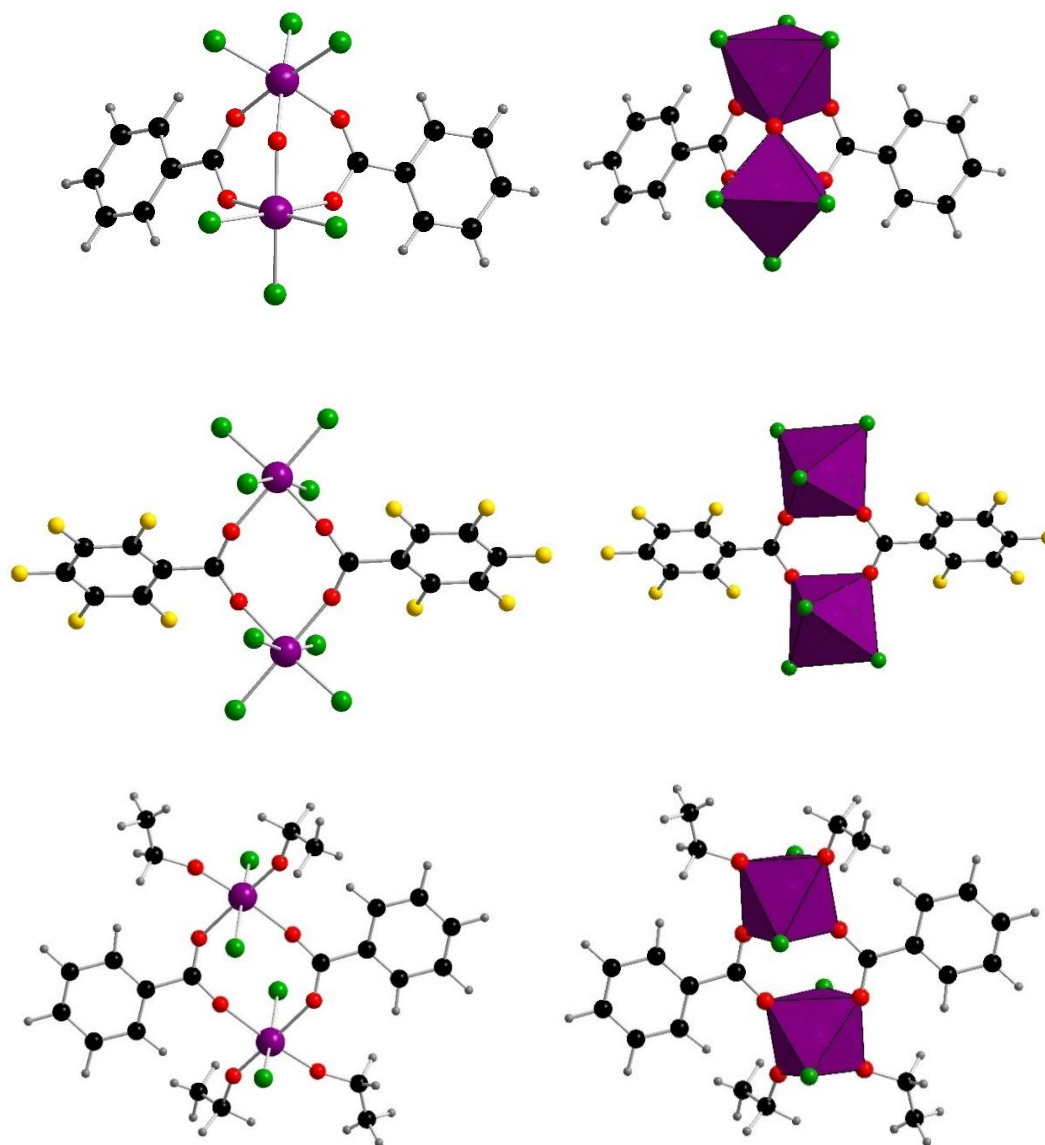


Figure I-14. Crystal structure of $[(\text{NbCl}_3(\text{O}_2\text{CPh}))_2\text{O}]$ (top), $[\text{NbCl}_4(\text{O}_2\text{CC}_6\text{F}_5)]_2$ (middle) and $[\text{Nb}_2\text{Cl}_4(\text{OEt})_4(\text{O}_2\text{CPh})_2]$ (bottom).
(color code: niobium, purple; oxygen, red; chlorine, green; carbon, black; hydrogen, grey)

Whereas monomers and dimers are generally synthesized from niobium halides, niobium alkoxides seem to be more adapted to synthesize higher nuclearity clusters. Alkoxides are materials of the type $\text{M}(\text{OR})_n\text{-xG}$, where OR and G are two different types of ligands, with $\text{R} = -\text{CH}_3$, $-\text{CH}_2\text{CH}_3$, or $-\text{CH}(\text{CH}_3)_2$, and G is a monocarboxylic acid. These ligands (G) can bridge other metallic cations and give an extended network, as previously reported by few examples^[58,72–74]. These precursors have already a starting condensed form of niobium since

there is an equilibrium between $\text{Nb}(\text{OEt})_5$ and $\text{Nb}_2(\text{OEt})_{10}$ (with alkoxo bridging groups) as proved for $\text{Nb}_2(\text{OMe})_{10}$ structural model.^[75]

The esterification process (Equation 2) can also result to hydrolysis and niobium condensation. There is a bright example in 2002 from T. J. Boyle, who used as a metal precursor the ethoxides of Nb^{V} and Ta^{V} .^[76] First, $[\text{Nb}(\mu\text{-OCH}_2\text{CH}_3)(\text{OCH}_2\text{CMe}_3)_4]_2$ was synthesized by adding $\text{HOCH}_2\text{CMe}_3$ (pivalic acid) to a stirring solution of $\text{Nb}(\text{OEt})_5$ in toluene followed by heating at $60\text{ }^\circ\text{C}$ for 12h.^[56] The solvent was removed under vacuum giving an off-white precipitate. Point to be made is that X-ray quality crystals were obtained when slow cooling a hot toluene solution. Then, HO_2CCMe_3 was dissolved in toluene, added to the previously synthesized $[\text{Nb}(\mu\text{-OCH}_2\text{CH}_3)(\text{OCH}_2\text{CMe}_3)_4]_2$ and the mixture was left for slow evaporation in a glove box for 12 hours to give $[\text{Nb}(\mu\text{-O}_2\text{CCMe}_3)(\text{OCH}_2\text{CMe}_3)_3]_2(\mu\text{-O})$ (Figure I-15). Each niobium site in the dimer adopts an octahedral fashion. The number of oxo ligands (one μ_2 -oxo group in this case) formed from the esterification pathway in equation 2 is believed to be dependent by the temperature of the reaction mixture, as well as the steric bulk (three methyl group) of the carboxylate ligand.^[76]

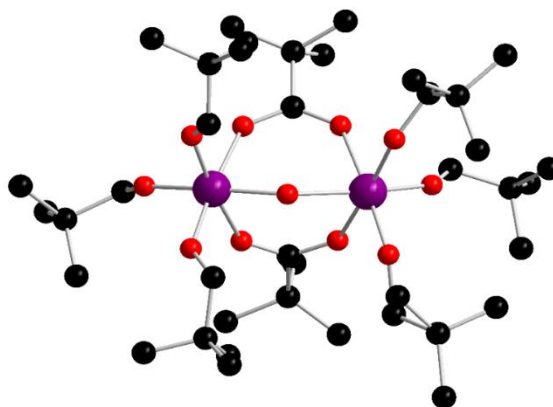
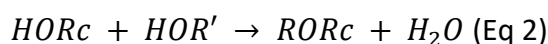
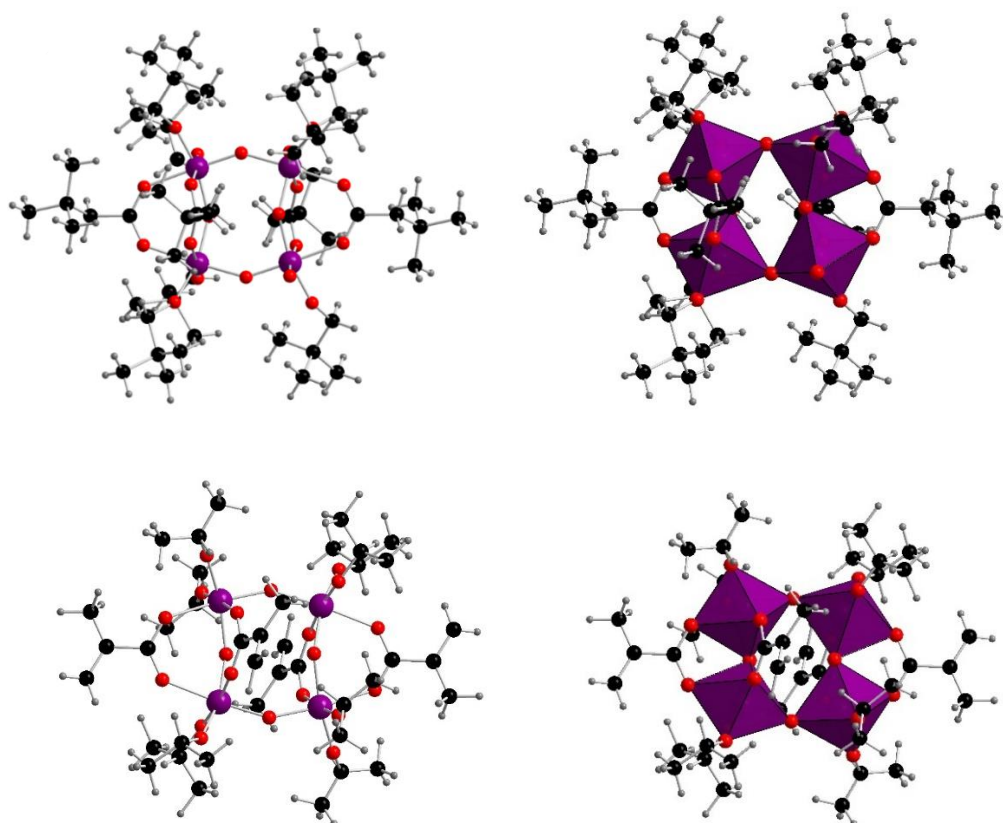


Figure I-15. Crystal structure of $[\text{Nb}(\mu\text{-O}_2\text{CCMe}_3)(\text{OCH}_2\text{CMe}_3)_3]_2(\mu\text{-O})$. Hydrogen atoms were removed for clarity. (color code: niobium, purple; oxygen, red; carbon, black)

The same procedure was used to synthesize tetrameric niobium units that can be better described as two identical dimers, where each niobium site is six-coordinate and has a strongly distorted octahedral geometry (in L.G.Hubert-Pfalzgraf's article, it is mentioned a trigonal prismatic environment). The coordination sphere is consisted of six oxygen atoms, from which

two oxo bridging oxygens and four oxygen atoms deriving from the carboxylate functions. The different ligands are *tert*-butylacetic acid ($\text{HO}_2\text{CCH}_2\text{CMe}_3$), methacrylic acid ($\text{HO}_2\text{CCH}_2\text{CH}_3$) and acetic acid (HO_2CCH_3) that give rise to the structures $\text{Nb}_2(\mu\text{-O})_2(\mu\text{-O}_2\text{CCH}_2\text{CMe}_3)_2(\text{OCH}_2\text{CMe}_3)_4$,^[76] $[\text{Nb}^{\text{V}}_4(\mu\text{-O})_4(\mu,\eta^2\text{-Me})_4(\text{OPr}')_8]$,^[58] and $\text{Nb}_4\text{O}_4(\text{OAc})_4(\text{OPr}')_8$,^[57] respectively (Figure I-16). Their reaction pathway is similar. $[\text{Nb}(\text{OPr}')_5]_2$ and the monocarboxylic acid (1:2 ratio) were dissolved in toluene or isopropanol at room temperature, which after stirring gives an oily clear solution. Subsequent controlled hydrolysis in $\text{Pr}'\text{OH}$ at room temperature allowed the precipitation of a white crystalline material. For this series, starting with niobium alkoxides play a key-role in the synthesis of niobium(V) carboxylate coordination complexes as the esterification process that is induced by the alkoxy groups (leaving as alcohol) and the carboxylic acid groups results in the production of water molecules and the creation of μ_2 -oxo-bridges between niobium(V) atoms.



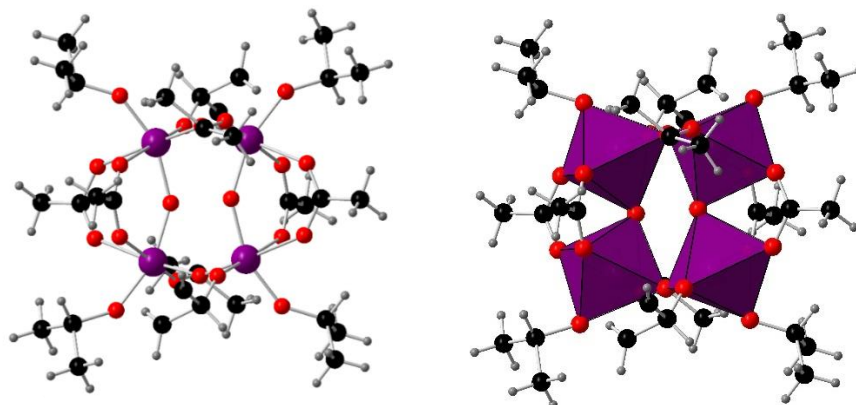


Figure I-16. Crystal structure of the tetrameric cluster presented in polyhedral (top left) and of $[\text{Nb}_2(\mu\text{-O})_2(\mu\text{-O}_2\text{CCH}_2\text{CMe}_3)_2(\text{OCH}_2\text{CMe}_3)_4]_2$ (top right). Crystal structure of $[\text{Nb}_4(\mu\text{-O})_4(\mu,\eta^2\text{-Me})_4(\text{OPr}')_8]$ (down left) and $\text{Nb}_4\text{O}_4(\text{OAc})_4(\text{OPri})_8$ (down right) (color code: niobium, purple; oxygen, red; carbon, black; hydrogen, grey)

Except of dinuclear and tetranuclear niobium complexes, the octanuclear $\text{Nb}_8\text{O}_{10}(\text{OEt})_{20}$ was also reported, but in absence of any carboxylate bridges.^[77] Each Nb(V) is six-fold coordinated with six oxygen atoms, forming NbO_6 units that adopt an octahedral arrangement (Figure I-17).

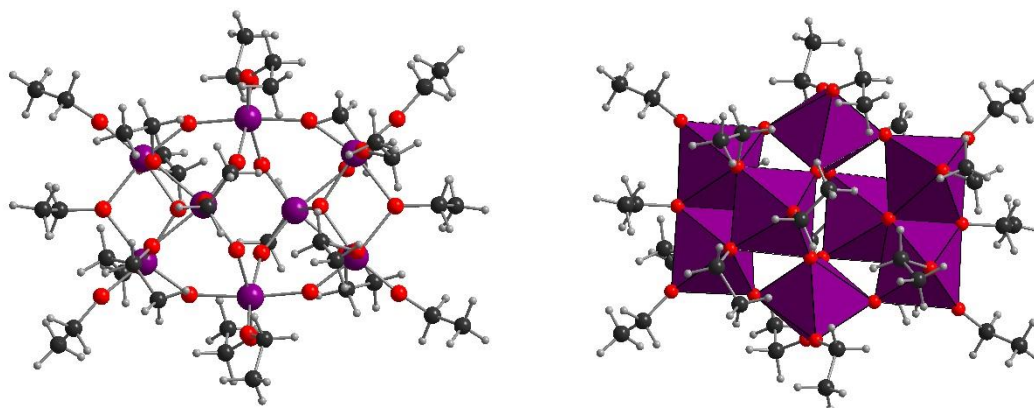


Figure I-17. Crystal structure of the octanuclear cluster $\text{Nb}_8\text{O}_{10}(\text{OEt})_{20}$ (left) and presented in polyhedral (right)

Lately, in 2020, Dinca *et al.* reported a high nuclearity Nb_{16} cluster (Figure I-18) by reacting $\text{Nb}(\text{OEt})_5$ with trimethylacetic acid (pivalic acid) in acetonitrile under reflux at 100 °C for 4 days.^[59] In this case, despite the anhydrous conditions, the oxo groups come from the esterification process that generates ethyltrimethylacetate and water. The structure consists of sixteen niobium(V) centers, 6-fold octahedrally coordinated and connected with oxo groups. As depicted in Figure I-18 (along *c* and *a* axis), we observe that four of them form a central 4-ring crown (blue octahedra) and each pair of these is connected with a peripheral trimer (purple octahedra). Pivalate and ethoxy groups stabilize this core, that represents one

of the latest steps in the generation of high nuclearity niobium clusters, stabilized by carboxylate species.

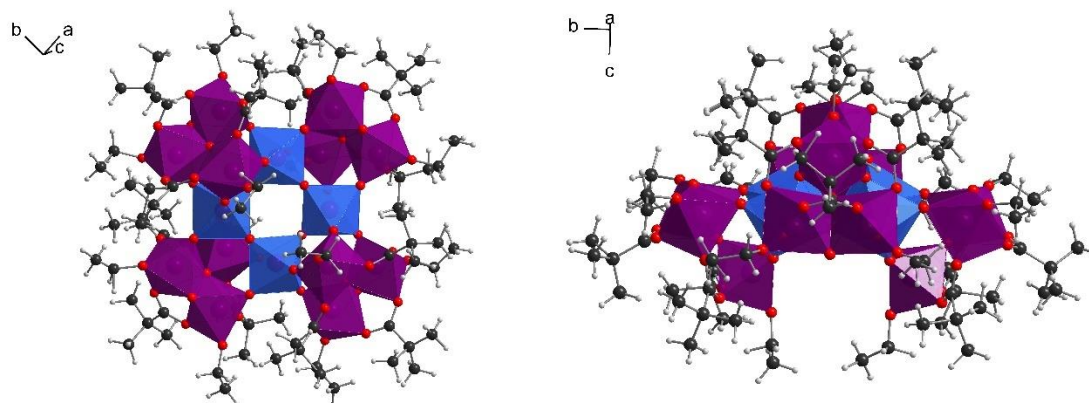


Figure I-18. Cluster of $Nb_{16}O_{28}$ along the c (left) and a axis (right). (color code: niobium, purple; oxygen, red)

I.2.5 Niobium carboxylate complexes containing heteroatoms

Niobium carboxylates have been also found in structural arrangement involving heterometallic centers.

Supramolecular structures based on the use of oxalate linker of the type $[M(\text{bpy})_3]_2[\text{NbO}(\text{C}_2\text{O}_4)_3]\text{Cl}\cdot n\text{H}_2\text{O}$ ($M=\text{Fe}^{2+}$, Co^{2+} , Ni^{2+} , Cu^{2+} and Zn^{2+} ; $n=11$, 12 ; bpy = 2,2'-bipyridine) (Figure I-19, left) and $[\{\text{Zn}(\text{bpy})_2\}_2(\mu\text{-C}_2\text{O}_4)][\text{Zn}(\text{bpy})_2(\mu\text{-C}_2\text{O}_4)\text{NbO}(\text{C}_2\text{O}_4)_2]\cdot 0,5\text{bpy}\cdot 7\text{H}_2\text{O}$ (Figure I-16, right) have been lately reported by M. Juric *et al.*^[78,79] In the first case, an aqueous solution of $\text{Na}_3[\text{NbO}(\text{C}_2\text{O}_4)_3]\cdot 4\text{H}_2\text{O}$ was combined with $[\text{M}(\text{bpy})_3]\text{Cl}_2\cdot 6\text{H}_2\text{O}$ and after a period between three days and two weeks, crystals were formed. Single crystal X-ray diffraction analysis revealed two independent $[\text{M}(\text{bpy})_3]^{2+}$ cations and one $[\text{NbO}(\text{C}_2\text{O}_4)_3]^{3-}$ anion. The charge is compensated with a Cl^- anion. The niobium oxalate anionic arrangement is identical to those crystallizing with alkali cations that were previously reported and described above.^[60,64]

A specific case occurs for the dimetallic Zn-Nb complex (Figure I-19, right), in which the Zn site is six-coordinate with an octahedral arrangement of four bipyridine nitrogen atoms and two oxalate oxygens chelating with the seven-coordinate niobium site (pentagonal bipyramid).

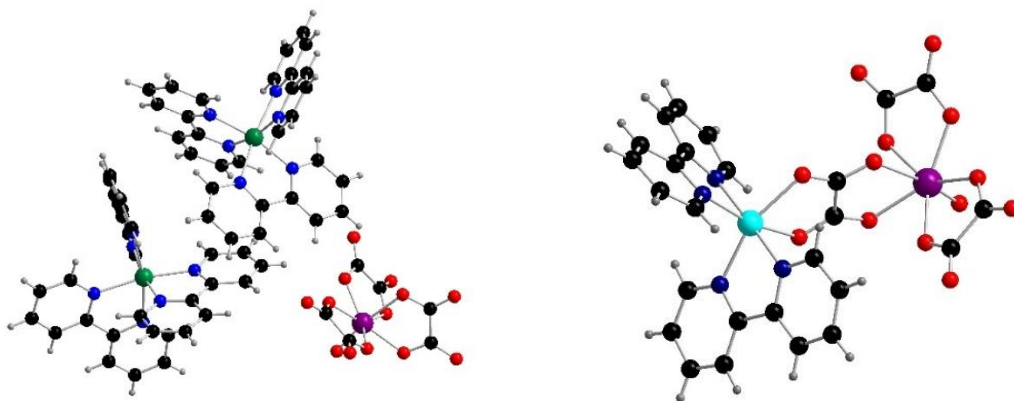


Figure I-19. Crystal structure of $[\text{Cu}(\text{bpy})_3]_2[\text{NbO}(\text{C}_2\text{O}_4)_3]\text{Cl}\cdot 7\text{H}_2\text{O}$ (top) and $[\{\text{Zn}(\text{bpy})_2\}_2(\mu\text{-C}_2\text{O}_4)][\text{Zn}(\text{bpy})_2(\mu\text{-C}_2\text{O}_4)\text{NbO}(\text{C}_2\text{O}_4)_2]\cdot 0,5\text{bpy}\cdot 7\text{H}_2\text{O}$ (bottom). (color code: niobium, purple; cooper, light blue; copper, green; oxygen, red; nitrogen, blue; carbon, black; hydrogen,

A study with lanthanides has been reported too. In 2018, C. N. Muniz et al. described a series of rare earth niobate oxalate coordination complexes with the type $((\text{CH}_3)_2\text{SO})_3(\text{RE})\text{NbO}(\text{C}_2\text{O}_4)_3$ (RE=La, Ce, Pr, Nd, Sm, Eu, Gd, Tb) (Figure I-20).^[68] The niobium site remains like the previous case of Zn^{II} , whereas in this case the Ln^{III} site is nine-coordinate, with a tricapped trigonal prismatic geometry. The two metal centers are connected with an oxalate group and the coordination of lanthanides is completed with three terminal DMSO (dimethylsulfoxide) molecules.

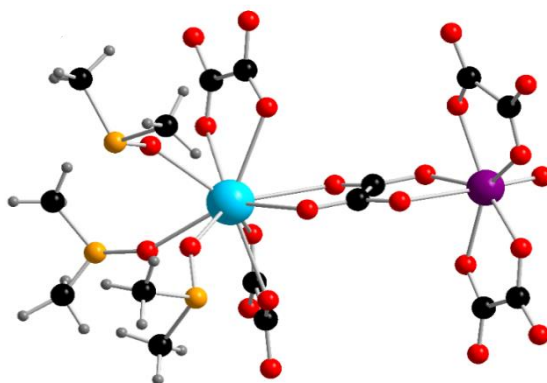


Figure I-20. Crystal structure of $((\text{CH}_3)_2\text{SO})_3(\text{La})\text{NbO}(\text{C}_2\text{O}_4)_3$. (color code: niobium, purple; lanthanides, light blue; oxygen, red; sulfur, light orange; carbon, black; hydrogen, grey)

Another heterometallic species is a mixed Nb(V)/Ta(V) complex, for which, the precursors used, have the type $(\text{gu})_3[\text{M}(\text{O}_2)_4]$ (M = Nb or Ta), where gu stands for guanidinium (CH_5N_3^+). These precursors were mixed prior to the synthesis with the tartaric acid (H_4tart) in a solution of distilled water and 35 wt % H_2O_2 .^[51] As revealed by single-crystal X-ray diffraction,

the structure remains the same as for the homometallic complexes with tantalum, but as for the two metal sites in the complex, there is one assigned to Nb(V) and a second one to Ta(V) (Figure I-21), leading to the anionic $[\text{NbTa}(\text{O}_2)_4(\text{tart})(\text{Htart})]^{5-}$ entity; with guanidinium (CH_5N_3^+) as counter cationic part.

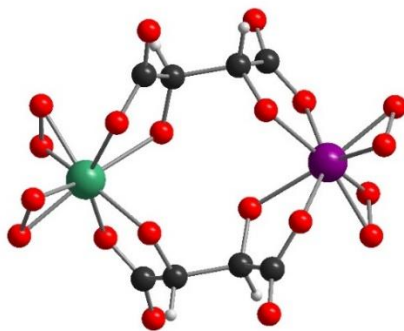


Figure I-21. Crystal structure of $[\text{NbTa}(\text{O}_2)_4(\text{tart})(\text{Htart})]^{5-}$ (color code: niobium, purple; tantalum, green; oxygen, red; carbon, black; hydrogen, grey).

During the same year (2005), K. H. Whitmire et al. reported the synthesis of heteroatomic molecular complexes consisting of Bi(III) and Nb(V) sites^[80]. Niobium(V)ethoxide and triphenyl bismuth were chosen as metal precursors, where salicylic acid (Hsal) was selected as linker. This mixture was suspended in a solution of toluene and refluxed for 1h. After cooling down, the mixture was left for 24h at room temperature and crystals of $\text{Bi}_2\text{Nb}_2(\mu\text{-O})(\text{sal})_4(\text{Hsal})_4(\text{OEt})_2$ appeared and characterized by single-crystal X-ray diffraction (Figure I-22). Heterocations are connected with each other by bridging oxo and carboxylate groups. The similar structure was also isolated with tantalum, starting from tantalum ethoxide.

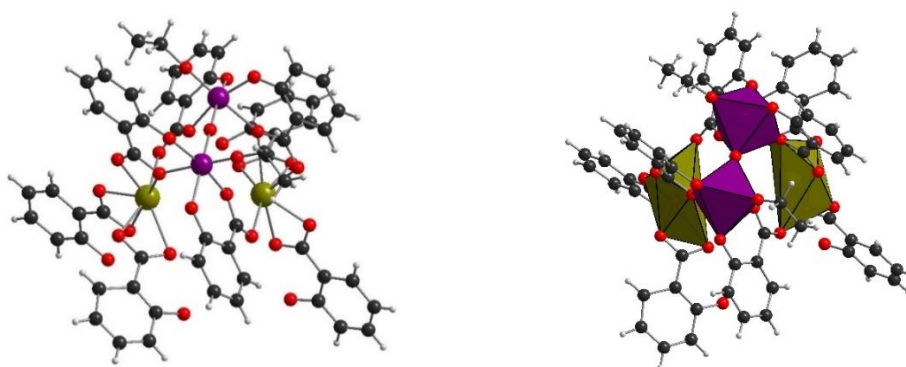


Figure I-22. Crystal structure of $\text{Bi}_2\text{Nb}_2(\mu\text{-O})(\text{sal})_4(\text{Hsal})_4(\text{OEt})_2$. (color code: niobium, purple; bismuth, military green; oxygen, red; carbon, black; hydrogen, grey)

When the same procedure is followed and 2-propanol is added as a solvent together with toluene, there is a substitution of ethoxy groups from isopropoxy ones. After 1h reflux and 14 days at room temperature crystals of $\text{BiNb}_4(\mu\text{-O})_4(\text{Hsal})_3(\text{sal})_4(\text{O}^i\text{Pr})_4$ appeared (Figure I-23)^[80]. The most probable explanation for the higher nuclearity of niobium sites is the extra alcohol added in the reaction mixture. The isopropanol, along with ethanol, reacts with the salicylic acid to produce water (through esterification process) and creates the oxo groups binding the four niobium sites in the $\{\text{Nb}_4\text{O}_4\}$ sub-unit.

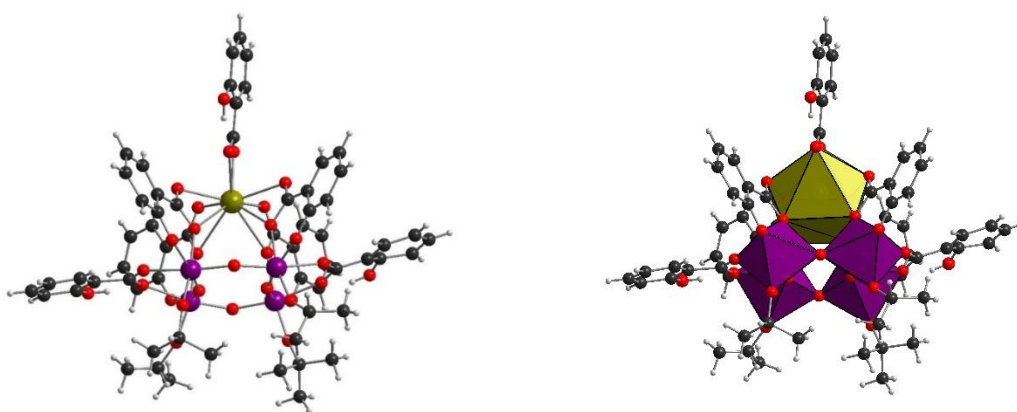


Figure I-23. Crystal structure of $\text{BiNb}_4(\mu\text{-O})_4(\text{Hsal})_3(\text{sal})_4(\text{O}^i\text{Pr})_4$. (color code: niobium, purple; bismuth, military green; oxygen, red; carbon, black; hydrogen, grey)

I.3 Towards niobium-containing multi-dimensional networks

These last couple of years, there are a few attempts reported in literature for the synthesis of Nb-based frameworks, in the pursuit of synthesizing new porous materials.^[14,19,21] Some of the few reported Nb(V) carboxylates were reported with semi coordinated oxalates, where the other half of oxalate was free to coordinate with other heterometals. Thus, in 2013, Pavica Planinic *et al.* reported a mixed Nb-Ba oxalate complex by adding $\text{Ba}(\text{NO}_3)_2$ into an aqueous solution of $(\text{NH}_4)_3[\text{NbO}(\text{C}_2\text{O}_4)_3]\cdot\text{H}_2\text{O}$ and leaving the solution in RT for 24h they obtained crystals of $\{\text{Ba}_2(\text{H}_2\text{O})_5[\text{NbO}(\text{C}_2\text{O}_4)_3]\text{HC}_2\text{O}_4\}\cdot\text{H}_2\text{O}$.^[69] The single-crystal X-ray diffraction revealed a central Nb(V) atom with seven-fold coordination in the form of a $[\text{NbO}(\text{C}_2\text{O}_4)_3]^{3-}$ anion, two Ba^{2+} cations and one HC_2O_4^- anion with six water molecules coordinated around an eleven-fold coordinated barium. The crystal packing revealed a 3D network through a layer of barium oxalates connected by niobium pillars (Figure I-24).

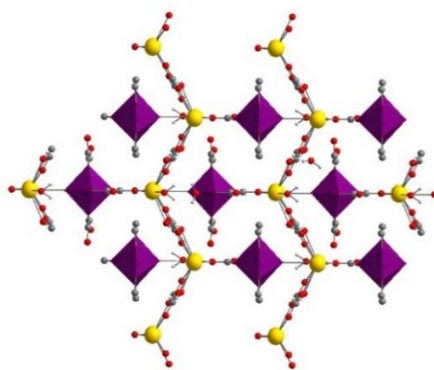


Figure I-24. Crystal packing of $\{Ba_2(H_2O)_5[NbO(C_2O_4)_3]HC_2O_4\} \cdot H_2O$ (color code: niobium, purple; barium, yellow; oxygen, red; carbon, black; hydrogen, grey)

Another significant report was the compound NbOFFIVE-1-Ni (KAUST-7) from M. Eddaoudi in 2016.^[11] A new Metal-Organic Framework structure is based on Ni(II) and bridged by pyrazine and oxyfluorinated $(NbOF_5)^{2-}$ species, resulting in a MOF-like structure as shown in Figure I-25. In this structure, there are two different building blocks consisting of a two dimensional square pillar of Ni-pyrazine motif in combination with a chain based on an oxyfluorinated $(NbOF_5)^{2-}$ basic unit, in order to result in a three-dimensional framework. This MOF compound containing the $(NbOF_5)^{2-}$ species as network nodes exhibits narrow pores of $4.752(1) \text{ \AA}$, and thus dedicated to the adsorption of small molecules. It was found numerous attractive separating applications as the removal of propyne and propadiene from propylene^[81], propylene from propane^[11], SO_2 ^[82] and CO_2 ^[83] from air. Moreover, it was used in the sensing of CO_2 and H_2O from air^[84] and proton conductivity performances.^[85]

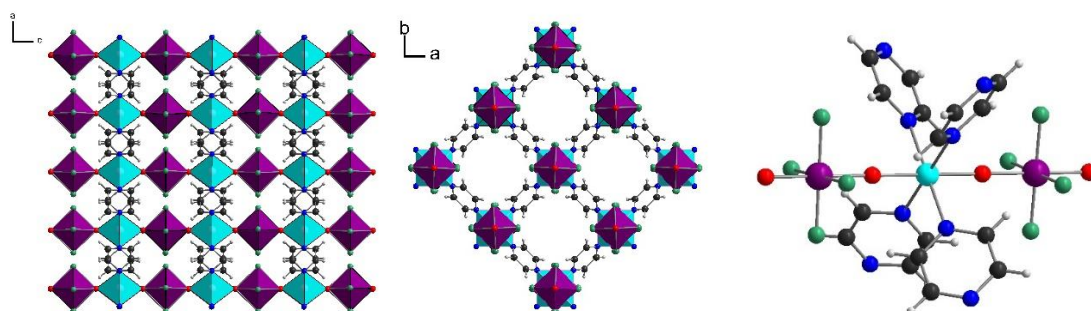


Figure I-25. Framework of $NiNbOF_5(pyr)_2 \cdot 2H_2O$ along b and c axis (left and middle). Crystal structure of $NiNbOF_5(pyr)_2 \cdot 2H_2O$ (right). (color code: niobium, purple; nickel, light blue; oxygen, red; nitrogen, blue; fluorine, green; carbon, black; hydrogen, grey)

In 2019, the group of M. Dinca, reported the successful incorporation of Nb(IV) and Nb(V) into a MOF-5(Zn) framework.^[86] Crystals of activated MOF-5 were soaked in a solution of $\text{NbCl}_4(\text{THF})_2$ in acetonitrile for 48 hours at room temperature to make a Nb(IV)-doped MOF-5 (noted Nb(IV)-MOF-5). By changing the solution into NbCl_5 , they obtained the MOF-5 structure incorporating Nb(V). The interesting point is the addition of a reduction agent ($(\text{TMS})_2\text{pyr}$) that could immediately induce the reduction of Nb(V)-MOF-5 to Nb(IV)-MOF-5. Their work was supported by density functional theory calculations (DFT), where they explored three possible models of the tetrameric MOF-5 cluster of $[\text{Zn}_4\text{O}]$, depending on the coordination around Nb site (Figure I-26). Between “ NbCl_2 ”, “ NbCl_4 ” and “ NbOCl_2 ” possibilities, the most likely one seemed to be a coordination mode of “ NbCl_4 ”. However, no X-ray diffraction analysis was performed and the Nb- Zn_4O local arrangement remains a suggested one. It seems that Zn is not entirely substituted by Nb atoms, so that we cannot talk about a pure Nb-MOF.

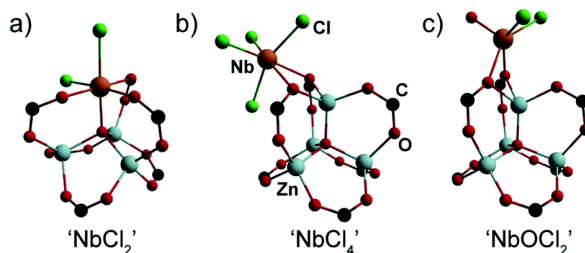


Figure I-26. Possible coordination modes of MOF-5 cluster based on DFT calculations.^[86] (color code: niobium, brown; zinc, light blue; oxygen, red; chlorine, green; carbon, black)

Another case of niobium doping in a well-known structure as UiO-66- NH_2 and MIL-125- NH_2 was also reported. The doping involved nd^0 transition metals at high oxidation state, like elements from the column V : V(V), Ta(V) and Nb(V).^[87] The existence of niobium is proven only by XPS and the structural data come from Density Functional Theory (DFT) calculations. However, the higher the percentage of doping, the lower the crystallinity as seen by Figure I-27.

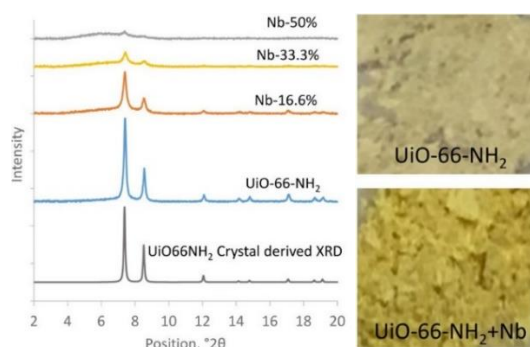


Figure I-27. Evolution of the powder-X-ray diffraction diagrams and SEM images of UiO-66-NH₂ and the Nb doping content in UiO-66-NH₂-Nb.^[87]

Another known MOF such as the CPO-27(Co) (Co 2,5-dihydroxyterephthalate), was impregnated with niobium, using ammonium niobium(V) oxalate as a precursor.^[88] This impregnated MOF can be used as a catalyst in order to enhance the performance of catalysis in the synthesis Fischer–Tropsch synthesis (FTS) of long chain hydrocarbons, which afterwards are fractured into smaller ones in the size of diesel (from 10 to 15 carbons) (Figure I-28).

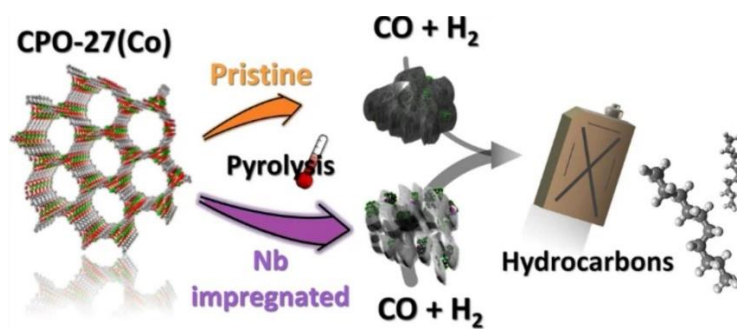


Figure I-28. Post-synthesis impregnation with niobium(V) oxalate precursor into CPO-27(Co) and its application in Fischer–Tropsch synthesis catalysis.^[88]

Another recent study is the one of O. K. Farha *et al.* in 2016, where they reported a supported NU-1000 with niobium(V) ions as a catalyst for cyclohexane oxidation (Figure I-29).^[89] The two post-synthetic methods used were vapor-phased atomic layer deposition (AIM) and the solution-phased (SIM). In this case, the occurrence of niobium(V) species was verified by inductively coupled plasma atomic emission spectroscopy (ICP-AES).

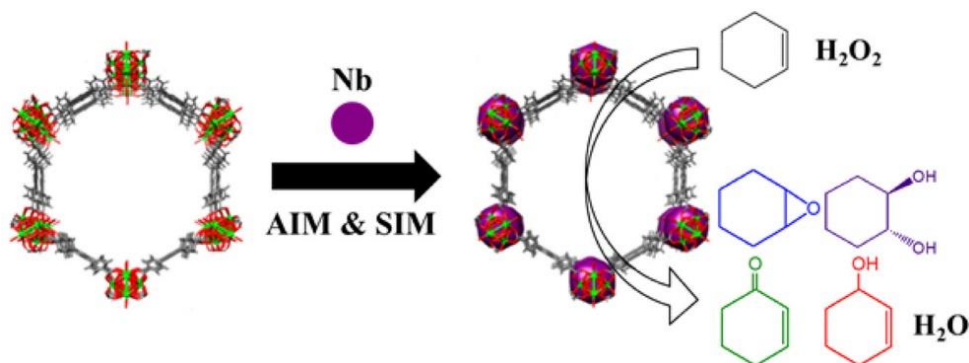


Figure I-29. Post-synthesis modifications in NU-100 with Nb(V) catalytic sites.^[89]

The latest example in literature is a two-dimensional metal-organic framework based in niobium(III) and molybdenum(III) reported in 2020 by Jeffrey Long *et al.*^[90] Under inert atmosphere (argon) in a glovebox $\text{NbCl}_3(\text{DME})$ (DME= 1,2-dimethoxyethane) and 5-dihydroxybenzoquinone were mixed in DMF and heated up at 120 °C for 18 hours. The powder obtained was indexed and refined (Le Bail refinement), generating the cell parameters $a = b = 13.743(6)$ Å and $c = 9.204(8)$ Å, which suggest a layered honeycomb structure in $P31m$ space group (157). The model of the structure presented in Figure I-30 has been generated based on the one of analogue molybdenum structure.

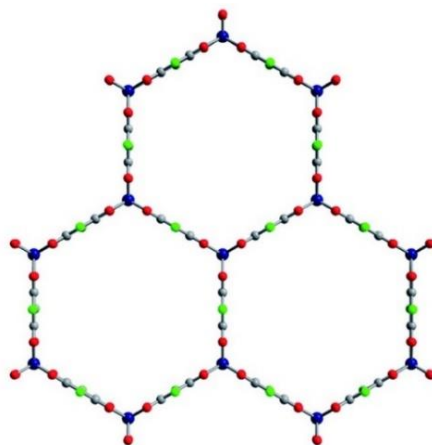


Figure I-30. Model structure for $(\text{H}_2\text{NMe}_2)_2\text{Nb}_2(\text{Cl}_2\text{dhbq})_3 \cdot 4.1\text{DMF}$.^[90] (color code: niobium, purple-blue; chlorine, green; oxygen, red; carbon, grey).

To conclude, the utilization of niobium poses a new field of investigation around tetravalent metals and not only, as even in the state of 3+ and 5+, very few structural arrangements have been reported in literature with carboxylate ligands. Indeed, the examination of the ionic radii of Nb(IV) and Zr(IV) or Hf(IV) shows quite close values (Zr^{4+} (0.98 Å) / Hf^{4+} (0.97 Å) versus Nb^{4+} (0.93 Å)) for the configuration of the eight-fold coordination

environments. Knowing the importance of the UiO-n family in the MOF community in terms of plethoric applications, the possibility to construct a niobium(IV)-based MOF could be envisaged. Indeed, the UiO-n is formed from a hexanuclear block $\{M_6O_4(OH)_4\}$ (M stands for tetravalent metal) stabilized by carboxylate ligands, and containing eight-fold coordinated Zr or Hf metallic centers (Figure I-31). Thus, the strategy to produce an identical network will be of significant interest since eight-fold coordinated niobium(IV) could be isolated in molecular complexes with different carboxylic acids^[36–38] as described in the paragraph I.2.3.

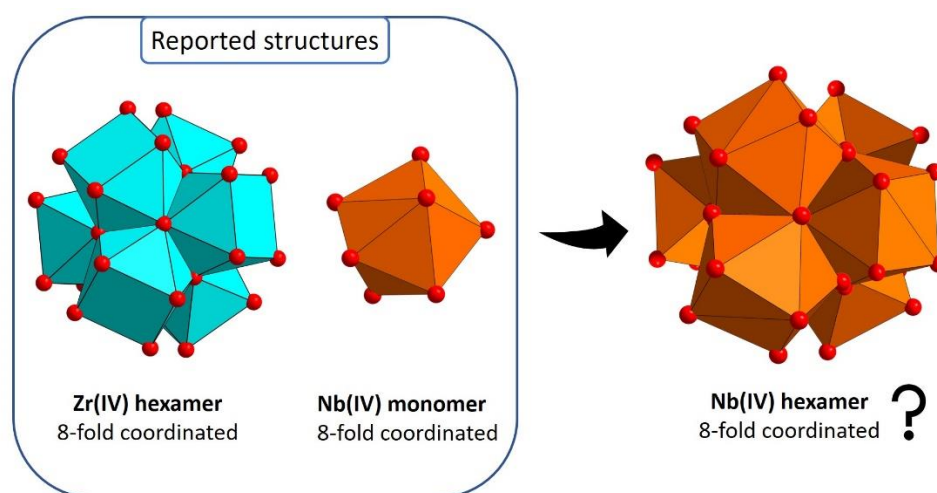


Figure I-31. Representation of the $\{Zr_6O_4(OH)_4\}$ building block (found in UiO-n series) and niobium(IV) mononuclear complex.^[91]

It is thus possible to explore the down limit for the formation of such a hexameric brick of $\{M_6O_4(OH)_4\}$ type, in term of ionic radii, with the use of niobium(IV) cation, for instance.

At the opposite, if we travel through the heaviest elements down to the periodic table, it was also reported the UiO-n series with the actinide series by using tetravalent cations from thorium(IV) up to plutonium(IV). Indeed, the formation of the hexameric brick of $\{M_6O_4(OH)_4\}$ type was now intensively investigated with such 5f elements. Therefore, unlikely the case of niobium, other tetravalent metals like U^{4+} and Th^{4+} , for which the MATHYB team at UCCS, has a deep experience, poses another field with plethora of structures, from clusters to porous multidimensional frameworks. This second axis of research is also investigated in the present thesis work and a brief overview of MOF-like compounds produced with tetravalent actinide will be described hereafter.

I.4 From actinide(IV) clusters to multidimensional networks using carboxylic acids as complexing linkers

Even though the hexavalent uranium is the most stable oxidation state of uranium under ambient air, the uranium dioxide (UO_2) with the tetravalent state, is the one commonly exploited in nuclear reactors for generating electricity. Its use gave rise to a lot of interests around the chemistry of tetravalent actinides, especially from Th(IV) to Pu(IV). Oxalic acid can be used as precipitating agent for recovering actinides from spent nuclear fuel (especially for Pu(IV) in the PUREX process). The first U(IV) carboxylates were reported back in 1964 by the reaction of uranium(IV) species with acetic acid^[92] and oxalic acid.^[93]

Recently, a lot of studies have reported the synthesis of oxo/polyoxo clusters by altering the synthetical conditions, in order to find ways to isolate well-defined clusters of higher nuclearities. The synthesis of these molecular assemblies is possible upon controlled hydrolysis rate, as shown in Figure I-32, either by pH variation, or the direct addition of a small amount of water in the synthesis, or by the addition of an alcohol and a carboxylic acid resulting in an esterification process to slowly generate water.^[94,95]

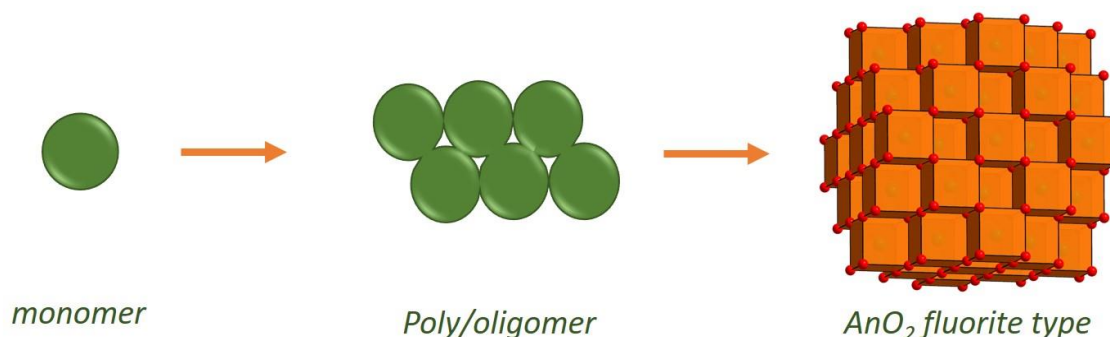


Figure I-32. Scheme of a hydrolysis process for actinide(IV).

The more water content exists in the system, the more oxo groups are generated and thus a higher nuclearity cluster is synthesized, as reported so far in species with a nuclearity that varies such as U_1 ^[96], U_3 ^[97], U_6 ^[98-101], U_{10} ^[102,103], U_{12} ^[100,103], U_{13} ^[103], U_{16} ^[101,102], U_{24} ^[103] and U_{38} ^[94,103] (Figure I-33), knowing that the ultimate product is the infinite network of UO_2 , viewed as U_∞ .

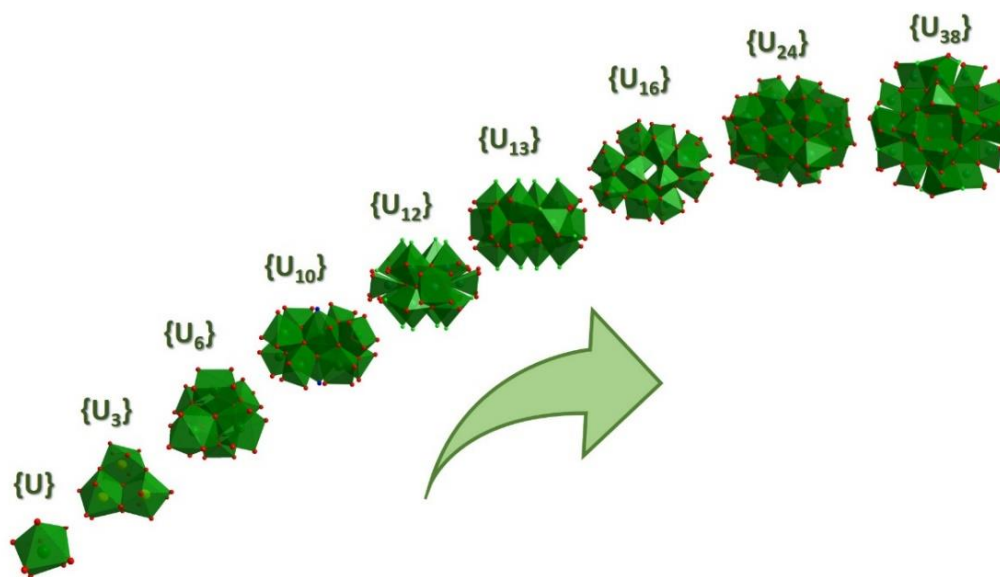


Figure I-33. Polyhedral representation of the different nuclearities of the U(IV) clusters.

In order to increase the nuclearity of polyoxo cluster, higher water content and higher temperature are often required. In general, there are three main approaches towards hydrolysis reaction.^[104] The first one is the addition of water in the organic system either direct in the solvent^[94] or indirect by combining an alcohol (specifically isopropanol) with the ligand (a carboxylic acid).^[95] That mixture gives an esterification reaction that produces water which is slowly diffused into the reaction mixture and provides a controlled hydrolysis. Another approach, where large assemblies are generated, is a system containing pyridine, potassium benzoate and traces of water.^[102] The last one, is the adjustment of pH, when working in an aqueous system.^[105]

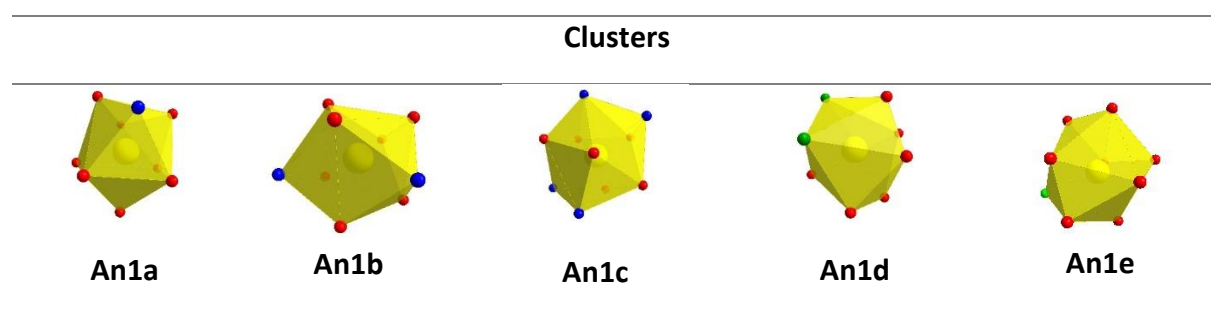
The hexanuclear brick (as found with Zr^{4+} in the UiO-n series), is the most well-studied one, reported for the first time in 1953 by Lundgren.^[106] It was isolated as $U_6O_4(OH)_4(SO_4)_6$ by heating at 200 °C a saturated solution of tetravalent uranium sulfate into H_2SO_4 (0.5 M). The structure consists of the inorganic core $[U_6O_4(OH)_4]^{12+}$, where the six U(IV) centers are all eight-fold coordinated to four μ_3 -hydroxo and four μ_3 -oxo sites for each thorium(IV) center, arranged in a way to adopt an octahedral geometry. The edges of the octahedron are triangular-shaped connected by the μ_3 -oxo, the μ_3 -hydroxo, carboxyl oxygen sites.

Since then, this type of brick has been reported many times^[99,100,102,107–114], stabilized by many organic molecules (benzoate, formate, acetate, 1,2-phenyldiphosphonate, tetraazacyclododecane-1,3,7,10-tetraacetate), notably the group of Takao stabilized it by

using formic acid.^[108] The first report of the incorporation of this uranium hexanuclear brick into a multi-dimensional framework (of UiO-66 type) was with ditopic ligands as fumarate, terephthalate, 4,4'-biphenyldicarboxylate and 2,6-naphthalenedicarboxylate.^[112] The same hexameric brick exists with other metals like thorium(IV)^[115] and transuranium metals like neptunium(IV)^[116,117] and plutonium(IV)^[117,118]. The UiO-type MOFs is a family of isostructural structures with the same topology (*Fm-3m* space group (225)) that contain the cationic motif $[U_6O_4(OH)_4]^{12+}$ surrounded often by twelve ditopic carboxylate ligands (*syn-syn* coordination mode) of different length sizes. The length of the ligand is typically in accordance with size of the pores, which form two different cages: one bigger with octahedral geometry and one smaller with tetrahedral geometry.

As seen from the Tables I-5, I-6 and I-7, most of the clusters that exist with U(IV) have been also reported with Th(IV), especially the hexanuclear brick^[98,119–121]. However the two biggest oxo/polyoxo cluster reported is an octamer $[Th_8(\mu_3-O)_4(\mu_2-OH)_8(H_2O)_{17}(SeO_4)_8 \cdot nH_2O]^{[122]}$ and a nonamer $Th_9(\mu_3-O)_4(\mu_2-OH)_8(H_2O)_{21}(SeO_4)_{10} \cdot nH_2O$.^[122] That could be explained as tetravalent thorium is a softest Lewis acid of the 5f series, and that decreases the equilibrium constant of condensation. The different actinide(IV) clusters vary from many monomers with different coordination numbers (seven to ten), to dimers with shared-edges, trimers, hexamers and few infinite chains. Many of those U(IV) and Th(IV) clusters, mostly the hexameric brick, were used afterwards as inorganic building blocks (Table I-5) in combination with multi-complexing ligands for the synthesis of Metal-Organic Frameworks (MOFs) that are summarized in Tables I-6 and I-7. It is logical that more examples exist with thorium, since Th(IV) is the main stable oxidation state and easier to manipulate under ambient atmosphere, whereas uranium(IV) is subjected to oxidation and needs specific handling with controlled atmosphere (e.g. glove box).

Table I-5. Summary of actinide(IV) building bricks existing in MOFs.



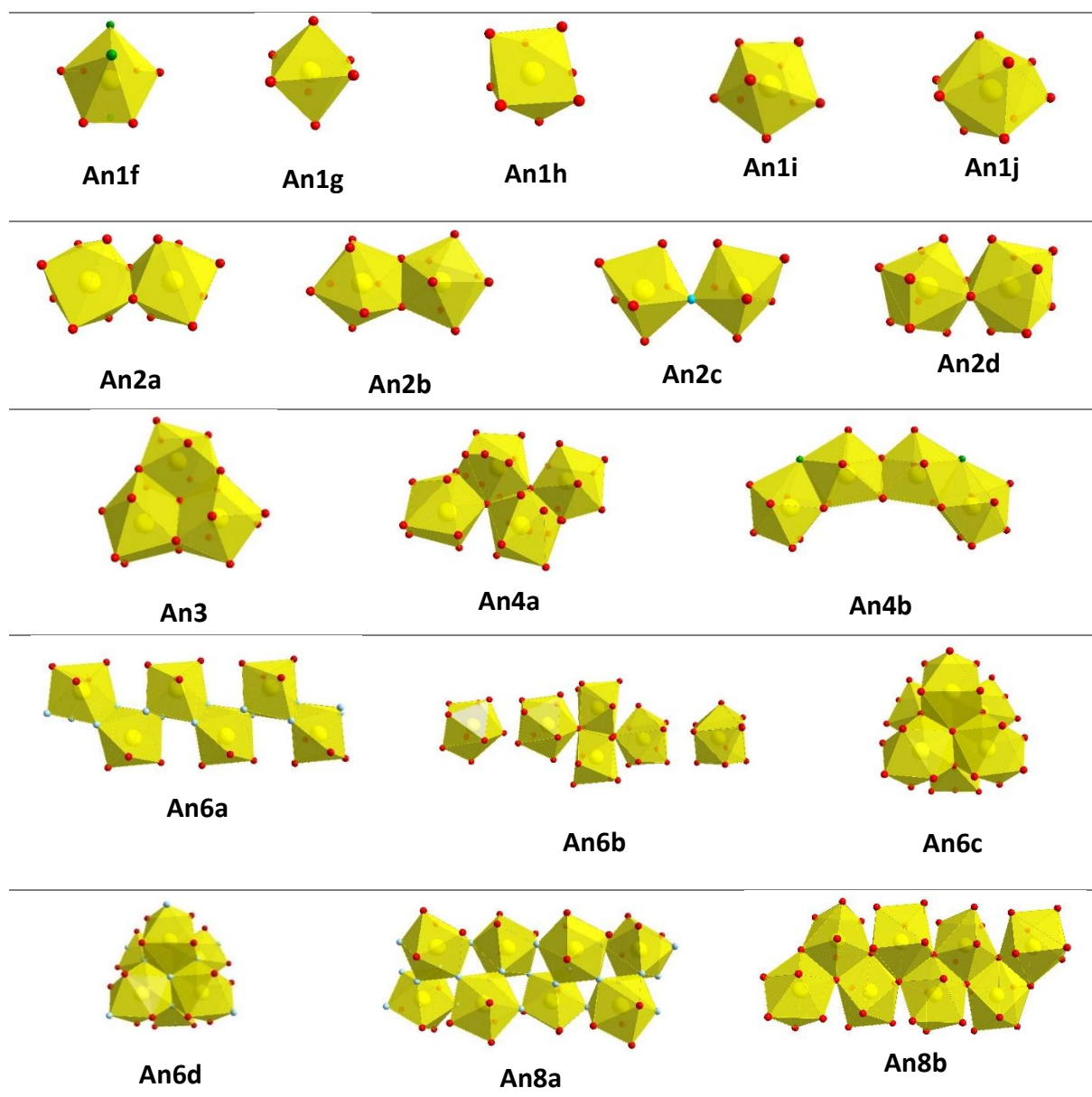


Table I-6. Summary of Th(IV)-MOFs.

Th-MOFs	Th(IV) cluster	Carboxylic acid	Ref
Th-2,3-PDC		Pyridine-3,5-dicarboxylic acid	[123]
Th-2,3-PZDC	An1b	Pyridine-4,6-dicarboxylic acid	[123]
Th-2,4-PDC		Pyridine-2,4-dicarboxylic acid	[123]
Th-EDTA		2,2',2'',2'''-(ethane-1,2-diylbis(azanetriyl))tetraacetic acid	[124]
Th-3,5-PYC	An1a	4,5-dihydro-1 <i>H</i> -pyrazole-3,5-dicarboxylic acid	[125]
Th-NTA		2,2',2''-nitrilotriacetic acid	[123]
Th-2,5-PZDC	An1c	Pyrazine-2,5-dicarboxylic acid	[123]
Th-BTB	An1f	5'-(4-carboxyphenyl)-[1,1' :3',1''-terphenyl]-4,4''-dicarboxylic acid	[126]
Th-TPO-2	An1d	4,4',4''-(oxo- λ^5 -phosphanetriyl)tribenzoic acid	[127]
Th-Q[10]	An4b	Cucurbit[10]uril	[128]
Th-BBP-1	An2c	1,4-phenylenebis(phosphonic acid)	[129]

TOF-3	An6d	2,2'-((1s,3s,5r,7r)-adamantane-1,3-diyl)diacetic acid	[130]
TOF-2	Structure unavailable	Benzene-1,3,5-tricarboxylic acid	[131]
Th-4-CPP	An6a	4-phosphobenzoic acid	[132]
TOF-1	An8a	Pyridine-2,5-dicarboxylic acid	[133]
Th-BBP-2	An1g	1,4-phenylenebis(phosphonic acid)	[129]
Th-BDC-2		Terephthalic acid	[134]
Th-2,6-NDC		Naphthalene-2,6-dicarboxylic acid	[135]
GWMOF-13	An1h	4,4'-oxydibenzoic acid	[136]
Th-BDC-4		Terephthalic acid	[137]
Th-BA		Benzoic acid	[138]
Th-BTC-5		Benzene-1,3,5-tricarboxylic acid	[139]
Th-3-FA	An1i	Furan-3-carboxylic acid	[140]
Th-2,5-FDC-2		Furan-2,5-dicarboxylic acid	[140]
Th-BTC-2			[139]
Th-BTC-3		Benzene-1,3,5-tricarboxylic acid	[139]
Th-BTC-4			[139]
Th-SINAP-4	An1i	Formic acid	[141]
Th-SINAP-5			[141]
Th-M3,4-PYC		1-methyl-1 <i>H</i> -pyrazole-3,4-dicarboxylic acid	[142]
Th-PAT		2-phosphonoacetic acid	[143]
Th-SINAP-6	An1i	Formic acid	[141]
Th-2-SB		2-sulfobenzoic acid	[144]
Th-NTB		4,4',4''-nitriлотribenzoic acid	[126]
ECUT-36	An1j		[145]
Th-BDC-1		Terephthalic acid	[134]
Th-L₁₃₅		5-(1,3-dioxo-1 <i>H</i> -benzo[<i>de</i>]isoquinolin-2(3 <i>H</i>)-yl)isophthalic acid	[146]
Th-IDA		2,2'-azanediyl diacetic acid	[124]
Th-OA-(2,3)	An1j	Oxalic acid	[147]
Th-TEDGA-OA		2,2'-oxybis(<i>N,N</i> -diethylacetamide)	[148]
SCU-11		4,4',4''-methanetriyltribenzoic acid	[149]
Th-BCPBA	An2a	1,1'-bis(4-carboxyphenyl)-[4,4'-bipyridine]-1,1'-diium	[137]
Th-M4,5-PYC	An2b	1-methyl-1 <i>H</i> -pyrazole-3,5-dicarboxylic acid	[142]
Th-BTC-6	An2b	Benzene-1,3,5-tricarboxylic acid	[139]
Th-TPO-1	An2d	Tri- <i>p</i> -tolylphosphine oxide	[127]
Th-BTC-1	An3	Benzene-1,3,5-tricarboxylic acid	[139]
SCU-8		[1,1'-biphenyl]-3,4',5-tricarboxylic acid	[150]
Th-NU-1011	An4a	3',6'-dibromo-4',5'-bis(4-carboxyphenyl)-[1,1':2',1''-terphenyl]-4,4''-dicarboxylic acid	[151]
Th-IHEP-5			[152]
Th-IHEP-6	An6b	4,4',4'',4''''-(porphyrin-5,10,15,20-tetrayl)tetrabenzoic acid	[152]
NU-905			[153]
Th-TATAB		4,4',4''-((1,3,5-triazine-2,4,6-triyl)tris(azanediyl))tribenzoic acid	[154]
Th-TTHA	An6c	2,2',2'',2''',2''''-((1,3,5-triazine-2,4,6-triyl)tris(azanetriyl))hexaacetic acid	[155]
Th-TCI		3,3',3''-(2,4,6-trioxo-1,3,5-triazinane-1,3,5-triyl)tripropionic acid	[156]

Th-BDC-3		Terephthalic acid	[134]
Th-SINAP-1		Formic acid	[141]
Th-SINAP-7		Naphthalene-1,4-dicarboxylic acid	[157]
Th-SINAP-8		Naphthalene-2,6-dicarboxylic acid	[157]
Th-SINAP-9			[158]
Th-SINAP-10		Teretphthalic acid	[158]
Th-SINAP-11		(E)-4-(2-carboxylvinyl)benzoic acid	[158]
Th-SINAP-12		(2E,2'E)-3,3'-(1,4-phenylene)diacrylic acid	[158]
Th-SINAP-13		[1,1'-biphenyl]-4,4'-dicarboxylic acid	[158]
Th-SINAP-14	An6c	(E)-4,4'-(diazene-1,2-dibenzoic acid	[158]
Th-SINAP-15		(Z)-4,4'-(ethene-1,2-diyl)dibenzoic acid	[158]
Th-NU-1008		3',6'-dibromo-4',5'-bis(4-carboxyphenyl)-[1,1':2',1''-terphenyl]-4,4''-dicarboxylic acid	[151]
TOF-16		2,2'-dihydroxy-[1,1'-binaphthalene]-5,5'-dicarboxylic acid	[159]
Th-UiO-66-R		2-(R)-benzene-1,4-dicarboxylic acid	[160]
Th ₆ -BPDC-12		[1,1'-biphenyl]-4,4'-dicarboxylic acid	[161]
Th-SINAP-2		Formic acid	[141]
Th ₆ -Me ₂ BPDC-8	An6c		[161]
Th ₆ -Me ₂ BPDC-NO ₃ -10		2,2'-dimehtyl-[1,1'-biphenyl]-4,4'-dicarboxylic acid	[161]
SINAP-23	An6c	2'-methyl-[1,1':4',1''-terphenyl]4,4''-dicarboxylic acid	[162]
SINAP-200		4',4''',4''''-nitriлотris([1,1'-biphenyl]-4-carboxylic acid	[163]

Table I-7. Summary of U(IV)-MOFs.

U-MOFs	U(IV) cluster	Ligand	Ref
U4-3, U4-4	An1g	Methylenebis(phosphonic acid)	[164]
U4-BTC-2		Benzene-1,3,5-tricarboxylic acid	[165]
U4-BDC-6	An1h	Terephthalic acid	[166]
U4-2-H ₂ O		Methylenebis(phosphonic acid)	[164]
U46-2		Methylenebis(phosphonic acid)	[164]
U4-2-FA-1	An1d	Furan-2-carboxylic acid	[167]
U4-BDC-(3,4)	An1e	Terephthalic acid	[168]
U4-BDC-5	An1j	Terephthalic acid	[168]
U4-Cl ₂ DHBQ		2,5-dichloro-3,6-dihydroxy-1λ ⁵ ,4λ ⁵ -benzene-1,4-dione	[169]
U4-5		Methylenebis(phosphonic acid)	[164]
U4-MEL	An2a	Benzene-1,2,3,4,5,6-hexacarboxylic acid	[170]
	An3	Benzene-1,3,5-tricarboxylic acid	[171]
U4-BTC-1			
U4-BDC-2	An4a	Terephthalic acid	[113]
U4-FA-2		Fumaric acid	[113]
U ₆ -Me ₂ BPDC-8	An6c	2,2'-dimethyl-[1,1'-biphenyl]4,4'-dicarboxylic acid	[161]
U ₆ -Me ₂ BPDC-TFA-10			[161]

U4-BPDC		[1,1'-biphenyl]-4,4'-dicarboxylic acid	[112]
U4-NDC		Naphthalene-2,6-dicarboxylic acid	[112]
U4-BDC-1	An6c	Terephthalic acid	[112]
U4-FA-1		Fumaric acid	[112]
U4-C5		Glutaric acid	[172]
U4-1,2-BDC	An8b	Phthalic acid	[170]

I.4.1 Mixed Th-U based carboxylates

Although, there are a lot of U(IV) and Th(IV) compounds (around 100), the production of mixed U(IV)-Th(IV) carboxylates is much less documented in literature.^[173] The interest that arises from these potential compounds is to obtain a mixed Th(IV)-U(IV) oxide from thermal decomposition that can be studied as a potential nuclear fuel in nuclear reactors as a model for U-Pu oxide (so-called MOX), that so far tend to use uranium(IV) dioxide (UO₂) only.

Mixed lanthanide(III)-actinide(IV) oxalates have been already reported in literature since 1963.^[174,175] However, the first actinide(III)-actinide(IV) oxalates, (NH₄)_{0.5}[Pu^{III}_{0.5}U^{IV}_{0.5}(C₂O₄)₂·H₂O]·nH₂O and (NH₄)_{2.7}Pu^{III}_{0.7}U^{IV}_{1.3}(C₂O₄)₅·nH₂O, were isolated only in 2013 (Figure I-34).^[176]

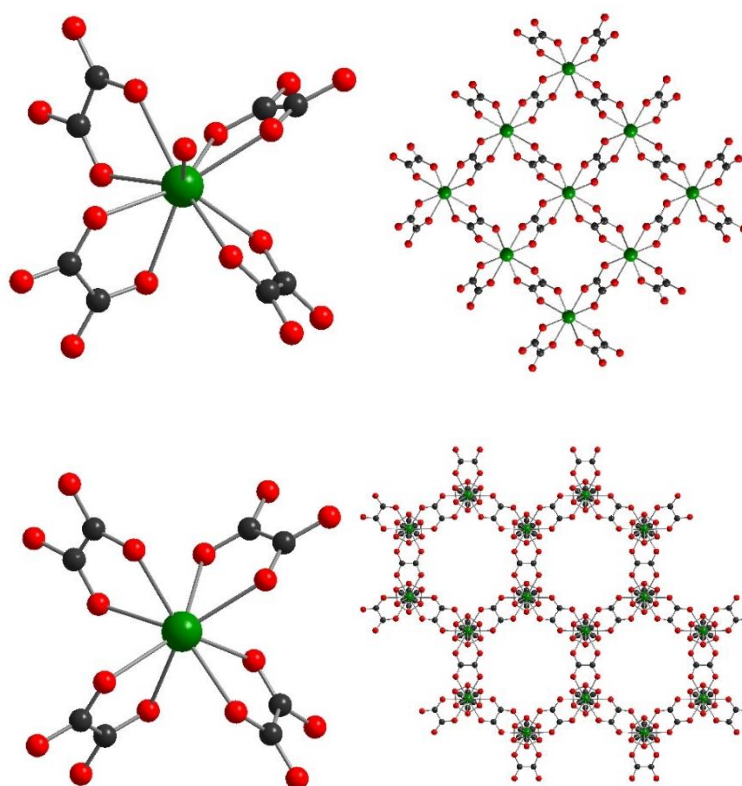


Figure I-34. $[An(C_2O_4)_4(H_2O)]$ entity and the two-dimensional framework of $(NH_4)_{0.5}[Pu^{III}_{0.5}U^{IV}_{0.5}(C_2O_4)_2 \cdot H_2O] \cdot nH_2O$ (top), $[An(C_2O_4)_4]$ entity and honeycomb-like two-dimensional framework of $(NH_4)_{2.7}Pu^{III}_{0.7}U^{IV}_{1.3}(C_2O_4)_5 \cdot nH_2O$ (bottom)

The synthetical procedure involved a diffusion cell with the use of membrane to separate the different compartments. This technique led to the simultaneous isolation of the two phases, each one in a different compartment of the diffusion cell, due to the difference of concentration between them. The strategy was then to study the thermal degradation of such U-Pu oxalates in order to generate a solid-state mixed oxide $(U,Pu)O_2$, which could be used as a fuel combustible, instead of using the “shake and bake” process (mixture of pure $UO_2 + PuO_2$ powders, and then heating for obtaining the mixed $(U,Pu)O_2$ solid), see Figure I-35. The “shake and bake” method consist of grinding and mixing two pots of UO_2 and PuO_2 , then heat and sinter to get the final for MOx (mixed oxide). The second route involves the solubilization of U^{4+} and Pu^{3+} salts into a solution of oxalates and precipitate them by means of oxalate complexing agent. These oxalates are then decomposed thermally in order to generate the mixed oxide.

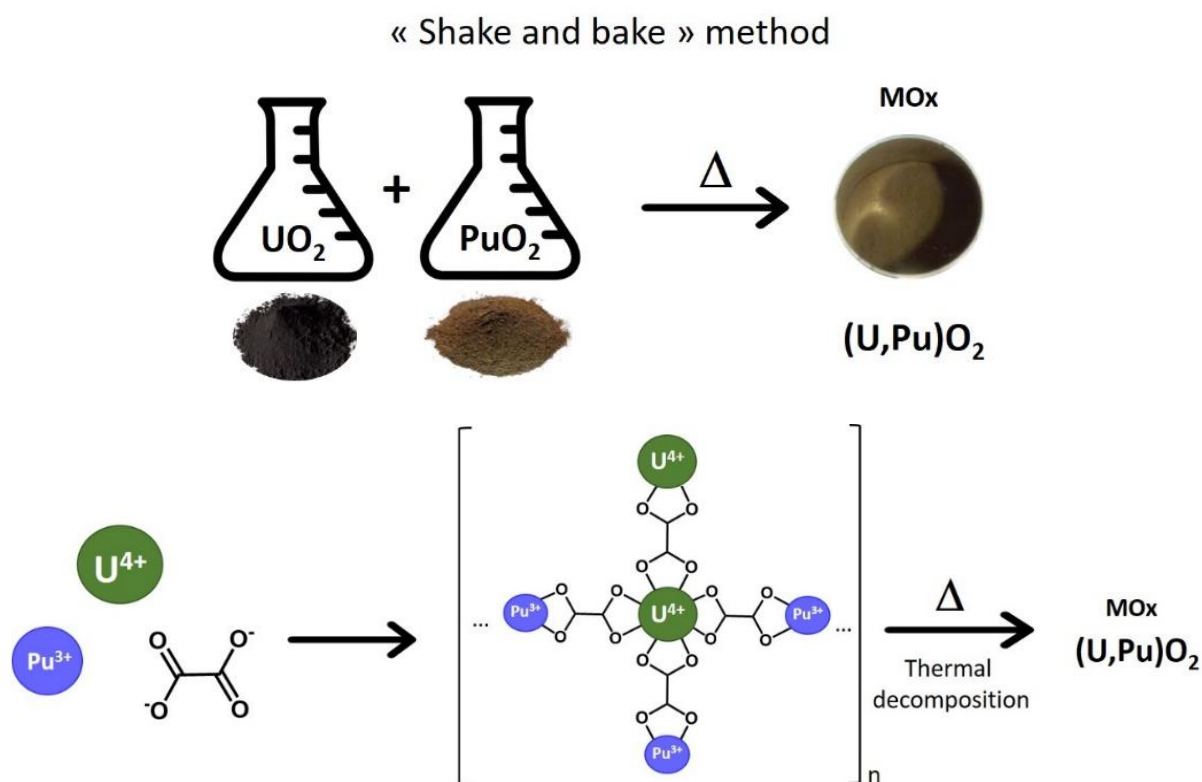


Figure I-35. “Shake and bake” method (top) and oxalate pathway (bottom) to produce mixed U,Pu oxides.

Few years later, the group of N. B. Shustova (South Carolina Univ., US), reported for the first time the metal node extension of uranyl (U^{6+}) into a Zr-based MOF (Zr_6-Me_2BPDC-

8)^[173] and a Th-based MOF (Th₆-Me₂BPDC-10) by adding the MOF solid into a DMF solution of UO₂(CH₃COO)₂ for 3 days at 75 °C (Figure I-36). The presence of the uranyl species was verified by infrared spectroscopy (U=O stretches at 913 and 866 cm⁻¹) and XPS spectroscopy. The resulting molar contribution Zr₆U_{0.87} has been calculated by integration of the XPS curves. However, the distribution of zirconium and uranium cations in the metal centers have not been studied in details.

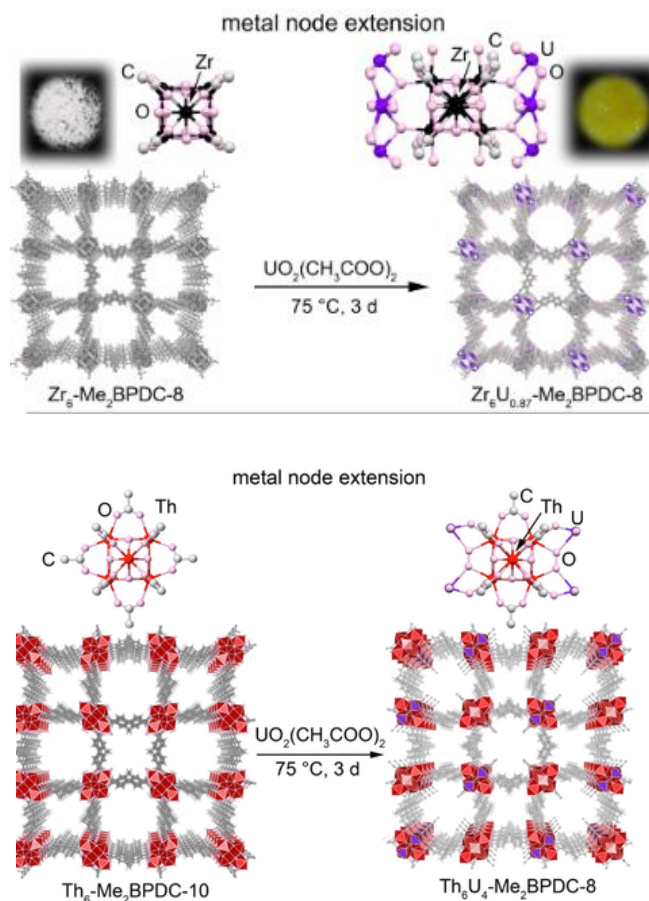


Figure I-36. Post-synthesis modifications in the metal node of Zr₆-Me₂BPDC-8 (top) and Th₆-Me₂BPDC-10 (bottom) with UO₂²⁺ treatment.^[173]

In the same study, trans-metalation process was applied in the case of Th₆-Me₂BPDC-10 by using the same conditions.¹⁰³ On the other side U₆-Me₂BPDC-8 was also doped with Th, by placing crystals in a solution of ThCl₄ in room temperature for 3 days (Figure I-37). The confirmation of this trans-metalation proved by ICP AES data and DFT calculations.

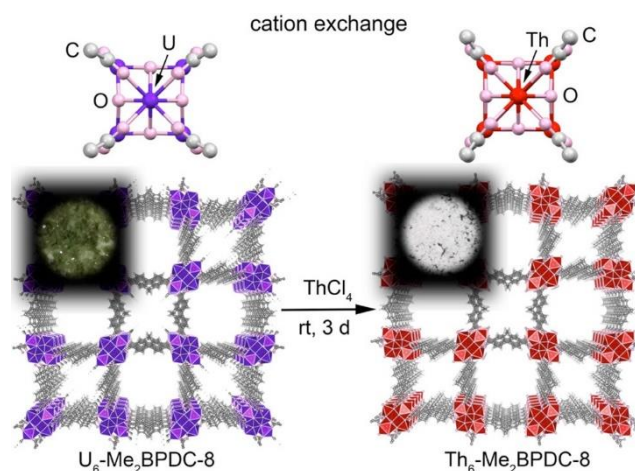


Figure I-37. Post-synthesis modifications in the cluster of $U_6\text{-Me}_2\text{BPDC-8}$ with ThCl_4 treatment.^[173]

This type of exchange is a post-synthesis modification and it seems efficient for demonstrate that cation exchange is possible. Whatsoever, regarding the huge amount of U(IV)-based and Th(IV)-based compounds reported (Tables I-6 and I-7), a whole new field of study opens, ready to be thoroughly explored.

I.5 Summary

The world of niobium carboxylates includes some molecular complexes, mostly mononuclear to tetranuclear entities, an hexamer and an hexadecamer. In these compounds, niobium cations are stabilized mostly by different monocarboxylic ligands and sometimes by dicarboxylic acids, as oxalic acid. However, even if dicarboxylic acids were used, they remain coordinated only by the one of the two carboxylic branches. This difficulty to create a network has led the studies to turn into synthesizing heterometallic compounds. This way, six bimetallic molecular complexes that combine niobium(V) with other metals (Fe^{2+} , Co^{2+} , Ni^{2+} , Cu^{2+} , Zn^{2+} , Bi^{3+} , La^{3+} , Ce^{3+} , Pr^{3+} , Nd^{3+} , Sm^{3+} , Eu^{3+} , Gd^{3+} , Tb^{3+} , Ta^{5+}) were reported. This incorporation of niobium is interesting as this element can potentially be used as a co-catalyst in catalytical applications and so, during the last years, some further studies in order to insert it in multidimensional networks were introduced. Well-known MOFs like HKAUST-7, MOF-5, UiO66-NH₂, MIL-125-NH₂, CPO-27(Co), and NU-1000 were doped with niobium(V) species (and also Nb(IV) species in the case of MOF-5). There is only one report of a two-dimensional niobium network linked with a derivative of benzoquinone (3,6-dichloro-2,5-dihydroxybenzoquinone). However, in this study, there is no evidence of niobium's oxidation state, no porosity measurement and the structure is a calculated model, according to another

well-known structure. Consequently, few advances have been done in the field of niobium carboxylates and that opens the way to explore a new crystal chemistry around this field, with the aim to isolate the first reported niobium-based porous framework.

On the other hand, the chemistry of tetravalent actinides like Th(IV) and U(IV) is more rich and already deeply explored. From molecular structures, with the hexanuclear cluster leaderliner stabilized by many monocarboxylic ligands, to more than one hundred porous structures have been already reported with a variety of both commercially available and homemade organic ligands. Although this list is already long, the chemical variety of possible ligands that can isolate new structures is even longer. Thus, investigating the use of new ligands towards new tetravalent actinide MOFs is still a field that can bring in interesting results. Moreover, regarding the vast amount of known structures, one may consider the formation of mixed Th(IV)-U(IV) carboxylate compounds. This aspect has been studied with the oxalate family (in the context of the PUREX process) or in the structures of UiO-n series via the incorporation of U(IV) into a Th(IV) structure and vice versa. For the latter, the general protocol is the soaking of crystals of a structure into a solution of the salt of the other metal. The strategy for the production of mixed actinides MOF like compounds is therefore not so investigated and would require further studies in order to propose other chemical systems that will be willing to the actinide exchange.

1.6 Purpose of the thesis

Based on the studies previously reported in literature, questions were raised about whether is it possible to generate the first niobium-based MOF. Niobium was chosen as its chemistry with carboxylates little have been yet explored and it exists in different oxidation state, so it can be involved in catalytical pathways. Thus, the goal of the present study is to explore the chemistry and reactivity of niobium towards different carboxylic acids ligands, in order to investigate the structural variety of the formation of infinite networks, through understanding of the complexation modes of Nb-O-C type. Starting by the isolation of a simple molecular carboxylate complex containing one or several niobium centers, we may hope to create a whole synthetical approach. By knowing the conditions that favor the complexation of carboxylic acids with niobium, the ultimate goal of being the first to isolate a porous niobium-based structure seems possible. Concerning the oxidation state of niobium, starting

by tetravalent niobium seemed us to be ideal since known MOF-like compounds have been isolated with various tetravalent metals as Zr^{4+} and Hf^{4+} , or Ti^{4+} . However, Nb^{4+} is not a stable oxidation state under ambient atmosphere, and the precursor of $NbCl_4$ is a black paste, difficult to handle, so the thesis project includes as well the chemistry around Nb^{5+} , the stable oxidation state of niobium. This field of coordination chemistry is really intriguing and innovative in a fundamental base, but it is also an exploratory field of high risk, as only a few niobium-bearing compounds have been reported at the molecular level only. Thus, we propose a strategy which will be based on the exploration of the reactivity of basic aromatic polycarboxylic acids such as terephthalic, trimesic acids, etc... with different sources of niobium(IV or V) reactants through diverse synthetic routes (hydro/solvothermal conditions, evaporation, etc..). This part constitutes the chapters II and III, related to the chemistry of niobium(IV) and niobium(V), respectively.

In parallel, we also extended the investigations for which the MATHYB group has a strong experience, on the crystal chemistry of actinides related to the MOF architectures. This part of the thesis is a continuation of the research works of two former Ph.D students (C. Falaise in 2014, N.P Martin in 2017) who focused their investigations on the synthesis of actinide-MOF materials. By taking a look at these heavier atoms than niobium in the periodical table, the 5f elements, as strong Lewis acids at oxidation state +4, are subject to hydrolysis process. When hydrolysis process is controlled, it is possible to monitor the condensation reaction and the size of the poly-oxo clusters of different nuclearities can be isolated. These clusters are stabilized by several monocarboxylic acids, which may stop their growth. They can be isolated as molecular compounds, are found to be incorporated in hybrid porous metal-organic frameworks (MOFs). Actinide-MOF compounds exist already in literature with commercially available commonly used ligands which are mainly related to rigid spacers composed of aromatic polydentate carboxylic acids (ex. terephthalic acid). The actual state of art in the MOF incorporating tetravalent actinide mentioned the use of large number of organic ditopic ligands (see tables 6 and 7), and we oriented our research on the reactivity of less studied dicarboxylic acids involving a central azo ($R-N=N-R'$) functionality, for which previous contributions reported the production of Zr-MOF solids.^[177] Thus the use of azobenzene-dicarboxylic acid derived molecules has been tested with thorium(IV) in the present thesis. The idea is how to create large pore architectures with long ditopic ligands

characterized by a limited freedom of flexibility. Here the azo functionality instead of alkyl chain, is hoped to bring some rigidities to the organic linker in order to promote highly porous system, preventing any interpenetrated networks.

The second aspect of this research field is the generation of mixed actinides coordination polymers, which have been rarely described in literature (see paragraph I.3.2). As mentioned previously (paragraph I.3.2), these mixed actinide compounds could be served as precursor to generate mixed actinide oxides, as potential nuclear combustibles, after the thermal decomposition and evacuation of the organic part, resulting in the formation the remaining actinide oxide. For this purpose, we propose to investigate the reactivity of different organic complexing agents, such as fumaric acid, replacing the usual oxalic acid. We also look for the formation of hexanuclear $\{(An1,An2)_6O_4(OH)_4\}$ building bricks (An1, An2 stands for two distinct tetravalent actinides), which can obtained either at the molecular level (with monotopic carboxylic acid), or involved in the 3D framework of UiO-n type (with ditopic carboxylic acid). For these studies, the chemical system Th(IV)-U(IV) was systemically investigated by controlling the substitution rate of Th(IV) by U(IV) in a solid-state solution. The parts related to the crystal chemistry of actinides are described in chapters IV and V.

At last, it should be noticed that a non-negligible part of the thesis time was impacted by the worldwide COVID lockdown and its consequences (stopping experiment periods, and/or difficulties characterization devices access), as well as several laboratory moves (due to building renovation works), which mainly prevented the easy access to the use of actinides reactants due to specific safety and administration rules.

I.7 References

- [1] C. Sanchez, K. J. Shea, S. Kitagawa, *Chem. Soc. Rev.* **2011**, *40*, 471–472.
- [2] M. Safaei, M. M. Foroughi, N. Ebrahimipour, S. Jahani, A. Omid, M. Khatami, *TrAC Trends Anal. Chem.* **2019**, *118*, 401–425.
- [3] M. Kalaj, K. C. Bentz, S. Ayala, J. M. Palomba, K. S. Barcus, Y. Katayama, S. M. Cohen, *Chem. Rev.* **2020**, *120*, 8267–8302.
- [4] S. Kitagawa, R. Kitaura, S. I. Noro, *Angew. Chemie Int. Ed.* **2004**, *43*, 2334–2375.
- [5] S. L. Griffin, N. R. Champness, *Coord. Chem. Rev.* **2020**, *414*, 213295.
- [6] P. Van Der Voort, K. Leus, Y. Y. Liu, M. Vandichel, V. Van Speybroeck, M. Waroquier, S. Biswas, *New J. Chem.* **2014**, *38*, 1853–1867.
- [7] K. Barthelet, J. Marrot, D. Riou, G. Férey, *Angew. Chem. Int. Ed.* **2002**, *41*.
- [8] K. Barthelet, J. Marrot, G. Férey, D. Riou, *Chem. Commun.* **2004**, *4*, 520–521.
- [9] K. Barthelet, K. Adil, F. Millange, C. Serre, D. Riou, G. Férey, *J. Mater. Chem.* **2003**, *13*, 2208–2212.
- [10] G. Sargazi, D. Afzali, A. Mostafavi, S. Y. Ebrahimipour, *J. Solid State Chem.* **2017**, *250*, 32–48.
- [11] A. Cadiau, K. Adil, P. M. Bhatt, Y. Belmabkhout, M. Eddaoudi, *Science (80-.)*. **2016**, *353*, 137–140.
- [12] B. J. Aylett, *Polyhedron* **1985**, *4*, 1799–1800.
- [13] J. K. Burdett, T. Hughbanks, *J. Am. Chem. Soc.* **1984**, *106*, 3101–3113.
- [14] I. Nowak, M. Ziolek, *Chem. Rev.* **1999**, *99*, 3603–3624.
- [15] R. D. Shannon, *Acta Crystallogr. Sect. A* **1976**, *32*, 751–767.
- [16] J. Winarta, B. Shan, S. M. McIntyre, L. Ye, C. Wang, J. Liu, B. Mu, *Cryst. Growth Des.* **2019**, *20*, 1347–1362.
- [17] M. Dan-Hardi, C. Serre, T. Frot, L. Rozes, G. Maurin, C. Sanchez, G. Férey, *J. Am. Chem. Soc.* **2009**, *131*, 10857–10859.
- [18] A. G. S. Prado, L. B. Bolzon, C. P. Pedroso, A. O. Moura, L. L. Costa, *Appl. Catal. B Environ.* **2008**, *82*, 219–224.
- [19] K. Tanabe, S. Okazaki, *Appl. Catal. A, Gen.* **1995**, *133*, 191–218.
- [20] B. M. Weckhuysen, D. E. Keller, *Catal. Today* **2003**, *78*, 25–46.
- [21] K. Tanabe, *Catal. Today* **2003**, *78*, 65–77.
- [22] K. Tanabe, *CHEMTECH; (United States)* **1991**, *21:10*.
- [23] K. Tanabe, *Mater. Chem. Phys.* **1987**, *17*, 217–225.
- [24] F. M. T. Mendes, C. A. Perez, R. R. Soares, F. B. Noronha, M. Schmal, *Catal. Today* **2003**, *78*, 449–458.
- [25] A. A. Shmakova, E. M. Glebov, V. V. Korolev, D. V. Stass, E. Benassi, P. A. Abramov, M. N. Sokolov, *Dalt. Trans.* **2018**, *47*, 2247–2255.
- [26] L. G. Hubert-Pfalzgraf, in *Encycl. Inorg. Bioinorg. Chem.*, American Cancer Society, **2011**.
- [27] F. A. Cotton, M. P. Diebold, W. J. Roth, *Inorg. Chem.* **1985**, *24*, 3509–3510.
- [28] F. Ott, *Elektrochem.Z.* **1912**, *18*.

- [29] F. Ott, G. W. Mellors, G. W. Mellors, S. Senderoff, U. Cohen, **1978**, 349, 1978–1979.
- [30] E. W. Golibersuch, R. C. Young, *J. Am. Chem. Soc.* **1949**, 71, 2402–2405.
- [31] A. Bino, *J. Am. Chem. Soc.* **1980**, 102, 7990–7991.
- [32] A. Bino, *Inorg. Chem.* **1982**, 21, 1917–1920.
- [33] F. A. Cotton, M. P. Diebold, M. Matusz, W. J. Roth, *Inorganica Chim. Acta* **1986**, 112, 147–152.
- [34] F. A. Cotton, S. A. Duraj, W. J. Roth, *J. Am. Chem. Soc.* **1984**, 106, 3527–3531.
- [35] F. A. Cotton, M. P. Diebold, R. Llusar, W. J. Roth, *J. Chem. Soc. Chem. Commun.* **1986**, 651, 1276–1278.
- [36] F. A. Cotton, M. P. Diebold, W. J. Roth, *Inorg. Chem.* **1987**, 26, 2889–2893.
- [37] P. B. Arimondo, F. Calderazzo, U. Englert, C. Maichle-Mössmer, G. Pampaloni, J. Strähle, *J. Chem. Soc. - Dalt. Trans.* **1996**, 311–319.
- [38] B. L. Ooi, Q. Xu, T. Shibahara, *Inorganica Chim. Acta* **1998**, 274, 103–107.
- [39] B. L. Ooi, G. Sakane, T. Shibahara, *Inorg. Chem.* **1996**, 35, 7452–7454.
- [40] A. Antiñolo, S. García-Yuste, I. López-Solera, A. Otero, J. C. Pérez-Flores, I. Del Hierro, L. Salvi, H. Cattey, Y. Mugnier, *J. Organomet. Chem.* **2005**, 690, 3134–3141.
- [41] B. L. Ooi, I. Sjøtofte, J. J. Vittal, *Inorganica Chim. Acta* **2004**, 357, 625–629.
- [42] B. L. Ooi, T. Shihabara, G. Sakane, K. F. Mok, *Inorganica Chim. Acta* **1997**, 266, 103–107.
- [43] R. A. D. Wentworth, C. H. Brubaker, *Inorg. Chem.* **1963**, 2, 1–4.
- [44] R. A. D. Wentworth, C. H. Brubaker, *Inorg. Chem.* **1964**, 3, 47–50.
- [45] A. Cotton, M. P. Diebold, W. J. Roth, **1987**, 4, 3319–3322.
- [46] F. Albert Cotton, M. P. Diebold, W. J. Roth, *Inorg. Chem.* **1988**, 27, 2347–2352.
- [47] F. Russ, *Prag, Dtsch. techn. Hochschule* **1902**.
- [48] G. Mathern, R. Weiss, *Acta Crystallogr. Sect. B* **1971**, 27, 1572–1581.
- [49] G. Mathern, R. Weiss, *Acta Crystallogr. Sect. B* **1971**, 6, 1582–1597.
- [50] D. Bayot, B. Tinant, B. Mathieu, J.-P. Declercq, M. Devillers, *Eur. J. Inorg. Chem.* **2003**, 2003, 737–743.
- [51] D. Bayot, A. Bernard Tinant, M. Devillers, *Inorg. Chem.* **2005**, 44, 1554–1562.
- [52] C. Djordjević, V. Katović, *J. Inorg. Nucl. Chem.* **1963**, 25, 1099–1109.
- [53] D. A. Brown, M. G. H. Wallbridge, N. W. Alcock, **1993**, 2037–2039.
- [54] D. A. Brown, M. G. H. Wallbridge, W. S. Li, M. McPartlin, *Polyhedron* **1994**, 13, 2265–2270.
- [55] D. A. Brown, M. G. H. Wallbridge, W. S. Li, M. McPartlin, I. J. Scowen, *Inorganica Chim. Acta* **1994**, 227, 99–104.
- [56] T. J. Boyle, T. M. Alam, D. Dimos, G. J. Moore, C. D. Buchheit, H. N. Al-shareef, E. R. Mechenbier, B. R. Bear, J. W. Ziller, **1997**, 2, 3187–3198.
- [57] N. Steunou, C. Bonhomme, C. Sanchez, J. Vaissermann, L. G. Hubert-Pfalzgraf, *Inorg. Chem.* **1998**, 37, 901–910.
- [58] L. G. Hubert-Pfalzgraf, V. Abada, S. Halut, J. Roziere, *Polyhedron* **1997**, 16, 581–585.
- [59] M. D. Korzyński, L. S. Xie, M. Dincă, *Helv. Chim. Acta* **2020**, 103, e2000186.

- [60] G. Mathern, R. Weiss, *Acta Crystallogr. Sect. B Struct. Crystallogr. Cryst. Chem.* **1971**, *27*, 1610–1618.
- [61] N. Galešić, N. Brničević, B. Matković, M. Herceg, B. Zelenko, M. Šljukić, B. Prelesnik, R. Herak, *J. Less-Common Met.* **1977**, *51*, 259–270.
- [62] L. Eriksson, G. Svensson, V. Tabachenko, J. Sjöblom, T. K. Thorsen, P. Coppens, O. Buchardt, *Acta Chem. Scand.* **1993**, *47*, 1038–1040.
- [63] B. Kojić-Prodić, R. Liminga, S. Ščavaničar, *Acta Crystallogr. Sect. B* **1973**, *29*, 864–869.
- [64] M. Šestan, B. Perić, G. Giester, P. Planinić, N. Brničević, *Struct. Chem.* **2005**, *16*, 409–414.
- [65] M. Jurić, P. Planinić, N. Brničević, D. Matković-Čalogović, *J. Mol. Struct.* **2008**, *888*, 266–276.
- [66] W. X. C. Oliveira, C. L. M. Pereira, C. B. Pinheiro, K. Krambrock, T. Grancha, N. Moliner, F. Lloret, M. Julve, *Polyhedron* **2016**, *117*, 710–717.
- [67] M. Jurić, B. Perić, N. Brničević, P. Planinić, D. Pajić, K. Zadro, G. Giester, B. Kaitner, *Dalt. Trans.* **2008**, 742–754.
- [68] C. N. Muniz, H. Patel, D. B. Fast, L. E. S. Rohwer, E. W. Reinheimer, M. Dolgos, M. W. Graham, M. Nyman, *J. Solid State Chem.* **2018**, *259*, 48–56.
- [69] M. Jurić, J. Popović, A. Šantić, K. Molčanov, N. Brničević, P. Planinić, *Inorg. Chem.* **2013**, *52*, 1832–1842.
- [70] D. Bayot, B. Tinant, M. Devillers, *Catal. Today* **2003**, *78*, 439–447.
- [71] M. A. Porai-Koshits, L. A. Aslanov, G. V Ivanova, T. N. Polynova, *Kristalloghim* **1985**, *19*, 79.
- [72] C. Sanchez, M. In, P. Toledano, P. Griesmar, *MRS Proc.* **1992**, *271*, 669.
- [73] N. Pajot, R. Papiernik, L. G. Hubert-pfalzgraf, J. Vaissermannb, **1995**, *83*, 1817–1819.
- [74] U. Schubert, E. Arpac, W. Glaubitt, A. Helmerich, C. Chaulb, F. Silicatforschung, D.- Würzburg, A. C. Der Universitat, D.- Würzburg, **1992**, 291–295.
- [75] D. C. Bradley, C. E. Holloway, *J. Chem. Soc. A Inorganic, Phys. Theor.* **1968**, 219–223.
- [76] T. J. Boyle, N. L. Andrews, T. M. Alam, M. A. Rodriguez, J. M. Santana, B. L. Scott, *Polyhedron* **2002**, *21*, 2333–2345.
- [77] D. C. Bradley, M. B. Hursthouse, P. F. Rodesiler, *Chem. Commun.* **1968**, 1112–1113.
- [78] M. Jurić, B. Perić, N. Brničević, P. Planinić, D. Pajić, K. Zadro, G. Giester, B. Kaitner, *J. Chem. Soc. Dalt. Trans.* **2007**, 742–754.
- [79] M. Jurić, P. Planinić, N. Brničević, D. Matković-Čalogović, *J. Mol. Struct.* **2008**, *888*, 266–276.
- [80] J. H. Thurston, K. H. Whitmire, *Inorg. Chem.* **2003**, *42*, 2014–2023.
- [81] L. Yang, X. Cui, Z. Zhang, Q. Yang, Z. Bao, Q. Ren, H. Xing, *Angew. Chemie* **2018**, *130*, 13329–13333.
- [82] M. R. Tchalala, P. M. Bhatt, K. N. Chappanda, S. R. Tavares, K. Adil, Y. Belmabkhout, A. Shkurenko, A. Cadiau, N. Heymans, G. De Weireld, G. Maurin, K. N. Salama, M. Eddaoudi, *Nat. Commun.* **2019**, *10*, 1–10.
- [83] P. M. Bhatt, Y. Belmabkhout, A. Cadiau, K. Adil, O. Shekhah, A. Shkurenko, L. J. Barbour, M. Eddaoudi, *J. Am. Chem. Soc.* **2016**, *138*, 9301–9307.
- [84] M. R. Tchalala, Y. Belmabkhout, K. Adil, K. N. Chappanda, A. Cadiau, P. M. Bhatt, K. N. Salama, M. Eddaoudi, *ACS Appl. Mater. Interfaces* **2019**, *11*, 1706–1712.
- [85] P. G. M. Mileo, K. Adil, L. Davis, A. Cadiau, Y. Belmabkhout, H. Aggarwal, G. Maurin, M. Eddaoudi, S. Devautour-Vinot, *J. Am. Chem. Soc.* **2018**, *140*, 13156–13160.

- [86] M. D. Korzyński, Luca Braglia, Elisa Borfecchia, K. A. Lomachenko, Amgalanbaatar Baldansuren, C. H. Hendon, Carlo Lamberti, Mircea Dincă, *Chem. Sci.* **2019**, *10*, 5906–5910.
- [87] M. A. Syzgantseva, C. P. Ireland, F. M. Ebrahim, B. Smit, O. A. Syzgantseva, *J. Am. Chem. Soc.* **2019**, *141*, 6271–6278.
- [88] M. Rivera-Torrente, C. Hernández Mejía, T. Hartman, K. P. de Jong, B. M. Weckhuysen, *Catal. Lett.* **2019**, *149*, 3279–3286.
- [89] S. Ahn, N. E. Thornburg, Z. Li, T. C. Wang, L. C. Gallington, K. W. Chapman, J. M. Notestein, J. T. Hupp, O. K. Farha, *Inorg. Chem.* **2016**, *55*, 11954–11961.
- [90] M. E. Ziebel, J. C. Ondry, J. R. Long, *Chem. Sci.* **2020**, *11*, 6690.
- [91] J. H. Cavka, S. Jakobsen, U. Olsbye, N. Guillou, C. Lamberti, S. Bordiga, K. P. Lillerud, *J. Am. Chem. Soc.* **2008**, *130*, 13850–13851.
- [92] I. Jelenid, D. Grdenid, A. Bezjak, *SHORT Commun. Acta Cryst* **1964**, *17*, 758.
- [93] R. C. Paul, J. S. Ghotra, M. S. Bains, *J. Inorg. Nucl. Chem.* **1965**, *27*, 265–266.
- [94] C. Falaise, C. Volkringer, J. F. Vigier, A. Beaurain, P. Roussel, P. Rabu, T. Loiseau, *J. Am. Chem. Soc.* **2013**, *135*, 15678–15681.
- [95] N. P. Martin, C. Volkringer, N. Henry, X. Trivelli, G. Stoclet, A. Ikeda-Ohno, T. Loiseau, *Chem. Sci.* **2018**, *9*, 5021–5032.
- [96] C. Falaise, J. Delille, C. Volkringer, T. Loiseau, *Eur. J. Inorg. Chem.* **2015**, *2015*, 2813–2821.
- [97] C. Volkringer, I. Mihalcea, J. F. Vigier, A. Beaurain, M. Visseaux, T. Loiseau, *Inorg. Chem.* **2011**, *50*, 11865–11867.
- [98] C. Hennig, S. Takao, K. Takao, S. Weiss, W. Kraus, F. Emmerling, M. Meyer, A. C. Scheinost, **2012**, *10*.
- [99] V. Mougel, B. Biswas, J. Pécaut, M. Mazzanti, *Chem. Commun.* **2010**, *46*, 8648–8650.
- [100] G. Nocton, F. Burdet, J. Pécaut, M. Mazzanti, *Angew. Chemie* **2007**, *119*, 7718–7722.
- [101] L. Chatelain, R. Faizova, F. Fadaei-Tirani, J. Pécaut, M. Mazzanti, *Angew. Chemie* **2019**, *131*, 3053–3058.
- [102] B. Biswas, V. Mougel, J. Pécaut, M. Mazzanti, *Angew. Chemie* **2011**, *123*, 5863–5866.
- [103] L. Chatelain, R. Faizova, F. Fadaei-Tirani, J. Pécaut, M. Mazzanti, *Angew. Chemie* **2019**, *131*, 3053–3058.
- [104] K. E. Knope, L. Soderholm, *Chem. Rev.* **2013**, *113*, 944–994.
- [105] K. E. Knope, R. E. Wilson, M. Vasiliu, D. A. Dixon, L. Soderholm, *Inorg. Chem.* **2011**, *50*, 9696–9704.
- [106] G. Lundgren, *Ark. Kemi* **1953**, *5*, 349–363.
- [107] J. Ling, H. Lu, Y. Wang, K. Johnson, S. Wang, *RSC Adv.* **2018**, *8*, 34947–34953.
- [108] S. Takao, K. Takao, W. Kraus, F. Emmerling, A. C. Scheinost, G. Bernhard, C. Hennig, *Eur. J. Inorg. Chem.* **2009**, *2009*, 4771–4775.
- [109] L. M. Mokry, N. S. Dean, C. J. Carrano, *Angew. Chemie Int. Ed. English* **1996**, *35*, 1497–1498.
- [110] J. C. Berthet, P. Thuéry, M. Ephritikhine, *Chem. Commun.* **2005**, 3415–3417.
- [111] J. C. Berthet, P. Thuéry, M. Ephritikhine, *Inorg. Chem.* **2010**, *49*, 8173–8177.
- [112] C. Falaise, C. Volkringer, J. F. Vigier, N. Henry, A. Beaurain, T. Loiseau, *Chem. – A Eur. J.* **2013**, *19*, 5324–5331.
- [113] C. Falaise, C. Volkringer, T. Loiseau, *Cryst. Growth Des.* **2013**, *13*, 3225–3231.

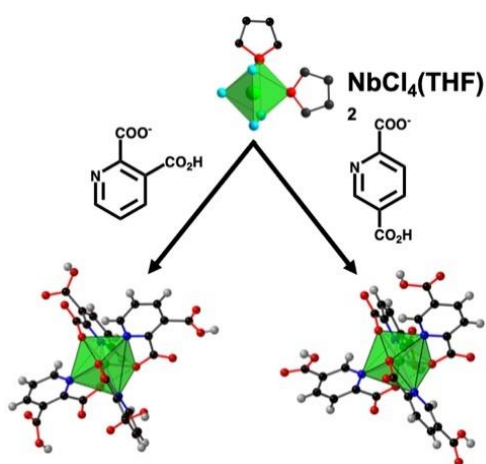
- [114] S. Duval, S. Sobanska, P. Roussel, T. Loiseau, *Dalt. Trans.* **2015**, *44*, 19772–19776.
- [115] C. Falaise, J. S. Charles, C. Volkringer, T. Loiseau, *Inorg. Chem.* **2015**, *54*, 2235–2242.
- [116] N. P. Martin, J. März, H. Feuchter, S. Duval, P. Roussel, N. Henry, A. Ikeda-Ohno, T. Loiseau, C. Volkringer, *Chem. Commun.* **2018**, *54*, 6979–6982.
- [117] K. Lv, C. Urbank, M. Patzschke, J. März, P. Kaden, S. Weiss, M. Schmidt, *J. Am. Chem. Soc.* **2022**, *144*, 2879–2884.
- [118] A. M. Hastings, D. Ray, W. Jeong, L. Gagliardi, O. K. Farha, A. E. Hixon, *J. Am. Chem. Soc.* **2020**, *142*, 9363–9371.
- [119] H. Lu, M. Xu, Z. Zheng, Q. Liu, J. Qian, Z.-H. Zhang, M.-Y. He, Y. Qian, J.-Q. Wang, J. Lin, *Inorg. Chem.* **2021**, *60*, 18629–18633.
- [120] C. Falaise, K. Kozma, M. Nyman, *Chem. – A Eur. J.* **2018**, *24*, 14226–14232.
- [121] M. Vasiliu, K. E. Knope, L. Soderholm, D. A. Dixon, *J. Phys. Chem. A* **2012**, *116*, 6917–6926.
- [122] K. E. Knope, M. Vasiliu, D. A. Dixon, L. Soderholm, *Inorg. Chem.* **2012**, *51*, 4239–4249.
- [123] M. Frisch, C. L. Cahill, *Cryst. Growth Des.* **2008**, *8*, 2921–2928.
- [124] P. Thuéry, *Inorg. Chem.* **2011**, *50*, 1898–1904.
- [125] K. L. Ziegelgruber, K. E. Knope, M. Frisch, C. L. Cahill, *J. Solid State Chem.* **2008**, *181*, 373–381.
- [126] Y. Li, Z. Weng, Y. Wang, L. Chen, D. Sheng, J. Diwu, Z. Chai, T. E. Albrecht-Schmitt, S. Wang, *Dalt. Trans.* **2016**, *45*, 918–921.
- [127] Y. Li, Z. Weng, Y. Wang, L. Chen, D. Sheng, Y. Liu, J. Diwu, Z. Chai, T. E. Albrecht-Schmitt, S. Wang, *Dalt. Trans.* **2015**, *44*, 20867–20873.
- [128] Y. Zhang, K. Lu, M. Liu, I. Karatchevtseva, Z. Tao, G. Wei, *Dalt. Trans.* **2020**, *49*, 404–410.
- [129] P. O. Adelani, T. E. Albrecht-Schmitt, **2012**, *192*, 377–384.
- [130] K. M. Ok, D. O’Hare, *Dalt. Trans.* **2008**, 5560–5562.
- [131] K. M. Ok, J. Sung, G. Hu, R. M. J. Jacobs, D. O’Hare, *J. Am. Chem. Soc.* **2008**, *130*, 3762–3763.
- [132] P. O. Adelani, T. E. Albrecht-Schmitt, *Inorg. Chem.* **2010**, *49*, 5701–5705.
- [133] J. Y. Kim, A. J. Norquist, D. O’Hare, *J. Am. Chem. Soc.* **2003**, *125*, 12688–12689.
- [134] C. Falaise, J. S. Charles, C. Volkringer, T. Loiseau, *Inorg. Chem.* **2015**, *54*, 2235–2242.
- [135] J. Andreo, E. Priola, G. Alberto, P. Benzi, D. Marabello, D. M. Proserpio, C. Lamberti, E. Diana, *J. Am. Chem. Soc.* **2018**, *140*, 14144–14149.
- [136] K. P. Carter, J. A. Ridenour, M. Kalaj, C. L. Cahill, *Chem. – A Eur. J.* **2019**, *25*, 7114–7118.
- [137] F. Chen, C. Wang, J. Lan, Y. Ji, Z. Chai, *Radiochim. Acta* **2017**, *105*, 531–539.
- [138] C. Falaise, C. Volkringer, T. Loiseau, *Inorg. Chem. Commun.* **2014**, *39*, 26–30.
- [139] N. P. Martin, C. Volkringer, C. Falaise, N. Henry, T. Loiseau, *Cryst. Growth Des.* **2016**, *16*, 1667–1678.
- [140] A. V. Murray, N. A. Vanagas, J. N. Wacker, J. A. Bertke, K. E. Knope, *Eur. J. Inorg. Chem.* **2020**, *2020*, 3287–3295.
- [141] Z. J. Li, S. Guo, H. Lu, Y. Xu, Z. Yue, L. Weng, X. Guo, J. Lin, J. Q. Wang, *Inorg. Chem. Front.* **2019**, *7*, 260–269.
- [142] K. P. Carter, A. T. Kerr, I. V. Taydakov, C. L. Cahill, *Solid State Sci.* **2018**, *76*, 20–32.

- [143] P. Ramaswamy, R. Prabhu, S. Natarajan, *Inorg. Chem.* **2010**, *49*, 7927–7934.
- [144] P. Thuéry, *Eur. J. Inorg. Chem.* **2014**, *2014*, 58–68.
- [145] L. J. Sun, Y. L. Fan, M. J. Yin, H. P. Zhang, H. Feng, L. J. Guo, F. Luo, *Cryst. Growth Des.* **2020**, *20*, 3605–3610.
- [146] D. L. Reger, A. P. Leitner, M. D. Smith, *Cryst. Growth Des.* **2016**, *16*, 527–536.
- [147] F. Blanchard, M. Rivenet, N. Vigier, I. Hablot, S. Grandjean, F. Abraham, *Cryst. Growth Des.* **2018**, *18*, 4593–4601.
- [148] P. Farger, B. Haidon, P. Roussel, B. Arab-Chapelet, M. Rivenet, *Inorg. Chem.* **2019**, *58*, 1267–1277.
- [149] Y. Wang, W. Liu, Z. Bai, T. Zheng, M. A. Silver, Y. Li, Y. Wang, X. Wang, J. Diwu, Z. Chai, S. Wang, *Angew. Chemie - Int. Ed.* **2018**, *57*, 5783–5787.
- [150] Y. Li, Z. Yang, Y. Wang, Z. Bai, T. Zheng, X. Dai, S. Liu, D. Gui, W. Liu, M. Chen, L. Chen, J. Diwu, L. Zhu, R. Zhou, Z. Chai, T. E. Albrecht-Schmitt, S. Wang, *Nat. Commun.* **2017**, *8*, 1–11.
- [151] P. Li, X. Wang, K. I. Otake, J. Lyu, S. L. Hanna, T. Islamoglu, O. K. Farha, *ACS Appl. Nano Mater.* **2019**, *2*, 2260–2265.
- [152] Z. W. Huang, K. Q. Hu, L. Mei, X. H. Kong, J. P. Yu, K. Liu, L. W. Zeng, Z. F. Chai, W. Q. Shi, *Dalt. Trans.* **2020**, *49*, 983–987.
- [153] P. Li, S. Goswami, K. I. Otake, X. Wang, Z. Chen, S. L. Hanna, O. K. Farha, *Inorg. Chem.* **2019**, *58*, 3586–3590.
- [154] N. Zhang, L. X. Sun, Y. H. Xing, F. Y. Bai, *Cryst. Growth Des.* **2019**, *19*, 5686–5695.
- [155] N. Zhang, L. X. Sun, F. Y. Bai, Y. H. Xing, *Inorg. Chem.* **2020**, *59*, 3964–3973.
- [156] L. Liang, R. Zhang, J. Zhao, C. Liu, N. S. Weng, *J. Solid State Chem.* **2016**, *243*, 50–56.
- [157] Z. J. Li, Z. Yue, Y. Ju, X. Wu, Y. Ren, S. Wang, Y. Li, Z. H. Zhang, X. Guo, J. Lin, J. Q. Wang, *Inorg. Chem.* **2020**, *59*, 4435–4442.
- [158] Z. J. Li, Y. Ju, Y. Ju, B. Yu, X. Wu, H. Lu, Y. Li, J. Zhou, X. Guo, Z. H. Zhang, J. Lin, J. Q. Wang, J. Q. Wang, S. Wang, *Chem. Commun.* **2020**, *56*, 6715–6718.
- [159] S. E. Gilson, M. Fairley, P. Julien, A. G. Oliver, S. L. Hanna, G. Arntz, O. K. Farha, J. A. Laverne, P. C. Burns, *J. Am. Chem. Soc.* **2020**, *142*, 13299–13304.
- [160] Z. J. Li, Y. Ju, H. Lu, X. Wu, X. Yu, Y. Li, X. Wu, Z. H. Zhang, J. Lin, Y. Qian, M. Y. He, J. Q. Wang, *Chem. – A Eur. J.* **2021**, *27*, 1286–1291.
- [161] O. A. Ejegbavwo, C. R. Martin, O. A. Olorunfemi, G. A. Leith, R. T. Ly, A. M. Rice, E. A. Dolgoplova, M. D. Smith, S. G. Karakalos, N. Birkner, B. A. Powell, S. Pandey, R. J. Koch, S. T. Misture, H. C. Zur Loye, S. R. Phillpot, K. S. Brinkman, N. B. Shustova, *J. Am. Chem. Soc.* **2019**, *141*, 11628–11640.
- [162] Z. J. Li, Y. Ju, Z. Zhang, H. Lu, Y. Li, N. Zhang, X. L. Du, X. Guo, Z. H. Zhang, Y. Qian, M. Y. He, J. Q. Wang, J. Lin, *Chem. – A Eur. J.* **2021**, *27*, 17586–17594.
- [163] Z.-J. Li, M. Lei, H. Bao, Y. Ju, H. Lu, Y. Li, Z.-H. Zhang, X. Guo, Y. Qian, M.-Y. He, J.-Q. Wang, W. Liu, J. Lin, *Chem. Sci.* **2021**, *12*, 15833–15842.
- [164] L. Chen, J. DiWu, D. Gui, Y. Wang, Z. Weng, Z. Chai, T. E. Albrecht-Schmitt, S. Wang, *Inorg. Chem.* **2017**, *56*, 6952–6964.
- [165] M. Dufaye, N. P. Martin, S. Duval, C. Volkringer, A. Ikeda-Ohno, T. Loiseau, *RSC Adv.* **2019**, *9*, 22795–22804.
- [166] D. P. Halter, R. A. Klein, M. A. Boreen, B. A. Trump, C. M. Brown, J. R. Long, *Chem. Sci.* **2020**, *11*, 6709–

- 6716.
- [167] N. A. Vanagas, R. F. Higgins, J. N. Wacker, D. R. C. Asuigui, E. Warzecha, S. A. Kozimor, S. L. Stoll, E. J. Schelter, J. A. Bertke, K. E. Knope, *Chem. – A Eur. J.* **2020**, *26*, 5872–5886.
- [168] C. Falaise, A. Assen, I. Mihalcea, C. Volkringer, A. Mesbah, N. Dacheux, T. Loiseau, *Dalt. Trans.* **2015**, *44*, 2639–2649.
- [169] V. E. Refn, M. Kubus, S. Mossin, R. W. Larsen, K. S. Pedersen, *ACS Omega* **2020**, *5*, 3462–3466.
- [170] N. P. Martin, J. März, C. Volkringer, N. Henry, C. Hennig, A. Ikeda-Ohno, T. Loiseau, *Inorg. Chem.* **2017**, *56*, 2902–2913.
- [171] C. Volkringer, I. Mihalcea, J. F. Vigier, A. Beaurain, M. Visseaux, T. Loiseau, *Inorg. Chem.* **2011**, *50*, 11865–11867.
- [172] R. A. Zehnder, J. M. Boncella, J. N. Cross, S. A. Kozimor, M. J. Monreal, H. S. La Pierre, B. L. Scott, A. M. Tondreau, M. Zeller, *Cryst. Growth Des.* **2017**, *17*, 5568–5582.
- [173] E. A. Dolgoplova, O. A. Ejegbavwo, C. R. Martin, M. D. Smith, W. Setyawan, S. G. Karakalos, C. H. Henager, H. C. Zur Loye, N. B. Shustova, *J. Am. Chem. Soc.* **2017**, *139*, 16852–16861.
- [174] F. Abraham, B. Arab-Chapelet, M. Rivenet, C. Tamain, S. Grandjean, *Coord. Chem. Rev.* **2014**, *266–267*, 28–68.
- [175] J. Block, L. Gordon, *Talanta* **1963**, *10*, 351–365.
- [176] C. Tamain, B. Arab Chapelet, M. Rivenet, F. Abraham, R. Caraballo, S. Grandjean, *Inorg. Chem.* **2013**, *52*, 4941–4949.
- [177] W. Y. Gao, T. Thiounn, L. Wojtas, Y. S. Chen, S. Ma, *Sci. China Chem.* **2016**, *59*, 980–983.

Chapter II

Niobium(IV) pyridine-carboxylate complexes



This chapter explored the crystal chemistry of niobium(IV) carboxylates. The reactivity of the 2,3-pyridine-dicarboxylic (known as quinolinic or H_2qui) acid and 2,5-pyridine-dicarboxylic (known as isocinchomeric or H_2icc) acid has been investigated as complexing agent toward the niobium(IV) tetrachloride precursor ($NbCl_4 \cdot 2THF$) in different organic solvent mixtures. It resulted in the isolation of four crystalline assemblies of mononuclear eight-fold coordinated coordination complexes.

CHAPTER II - Niobium(IV) pyridine-carboxylate complexes

The ultimate goal and inspiration for this study may be the isolation of the first niobium-based MOF mimicking the other well-known Zr(IV)/Hf(IV)/Ti(IV)-MOF solids. But, in order to arrive up to that point, there are many questions to be answered before. Metal-organic frameworks are hybrid porous crystalline structure that contain a metallic center and an organic chain, so a careful selection of precursors has to be made in advance. As it concerns the niobium(IV) precursor, the only commercially available source is a niobium(IV) tetrachloride tetrahydrofuran complex ($\text{NbCl}_4(\text{THF})_2$). That seems quite convenient, as chloride precursors are used to be selected for MOF synthesis, since they are soluble in many organic solvents and chloride anions could be easily replaced by other ligands. As it concerns the organic linker, it should contain carboxylic acids as functions to be complexed with the niobium(IV) centers. Our approach involves as a first step the use of monocarboxylic ligands, that will lead to the isolation of molecular complexes. This way, we could better understand deeply the complexation modes of niobium(IV) carboxylates and set the base for extending the approach the second step, where a second carboxylic function will be added to the monocarboxylate ligands that successfully reacted with niobium(IV) species. This second carboxylate functions could further react with a second niobium(IV) center and give rise, depending on the directions of the growth, from a one- to multi-dimensional framework.

By following the above strategy, $\text{NbCl}_4(\text{THF})_2$ was successfully dissolved in different organic solvents like dimethylformamide, tetrahydrofuran, ethanol, isopropanol, as well as mixtures of them. For all the different solvent combinations, different monocarboxylic acids like benzoic acid, 4-biphenyldicarboxylic acid, 1-naphthoic acid, 2-naphthoic acid, etc, were also added to the mixture in order to explore their reactivity towards niobium(IV) in solution. These solutions were either placed in room temperature or in an oven (80-180 °C). Unfortunately, no crystalline precipitate was isolated (formation of amorphous powder) and so tries were extended to dicarboxylic acids known to isolate Zr(IV) and Ti(IV) MOFs, like terephthalic acid, amino-terephthalic acid, 4,4'-biphenyldicarboxylic acid, 2,6-naphthoic acid, trimesic acid, pyromellitic acid, mellitic acid, etc. Like in the last case, this type of reaction only led to the formation of amorphous precipitate, without any observation of crystalline phases, either at room temperature, or by following a solvothermal route. An attempt to add small

amount of water in the system to induce a controlled hydrolysis was made as well, but even with the smallest addition (0.056 mmol H₂O / Nb) of water, niobium(IV)oxide (NbO₂) precipitated. Since all kinds of pure carboxylate ligands failed to react, partially replacing carboxylic acids with other complexing functions was an idea worth testing. Inspired by the reactivity of 2-pyridinecarboxylic acid towards niobium(IV)^[1], the interest was shifted to the pyridine-family ligands. Thus, ligands like the 2,3-pyridinedicarboxylic acid, 2,4-pyridinedicarboxylic acid, 2,5-pyridinedicarboxylic acid, 2,6-pyridinedicarboxylic acid and 3,5-pyridinedicarboxylic acid were tested. More specifically, the 2,3-pyridinedicarboxylic acid and 2,5-pyridinedicarboxylic acid successfully reacted with Nb(IV) centers of NbCl₄(THF)₂ giving rise to **four crystalline molecular carboxylate niobium(IV) complexes**. This chapter contains the structural description of these complexes and a characterization of this new series of Nb(IV) complexes.

II. 1 Synthesis of molecular mononuclear niobium(IV) carboxylate complexes

In this study, the pyridine-family ligands containing carboxylic groups found to have great reactivity with the commercially available complex NbCl₄(THF)₂ in organic solvents or a combination of them (acetonitrile, N,N'-dimethylformamide, pyridine, triethylamine) resulting to mononuclear Nb^{IV} complexes. The reactions occur after the mixing of the precursors in room temperature. In a few cases, a slight increase of the temperature up to 80 °C proved to help the crystallization. The synthesized compounds have been characterized by X-Ray diffraction techniques and infrared spectroscopy. The different results have recently been published in the october issue of *Inorganic Chemistry* (2022, 61, 39, 15346–15358) and are transcribed hereafter.^[2]

All manipulations with niobium(IV) were held inside a glove box (Jacomex, GP Campus) under an argon atmosphere in order to prevent the oxidation of Nb^{IV} to Nb^V. The niobium(IV) precursor is commercially available under the form of the tetrachloride NbCl₄(THF)₂. All synthesis protocols are summarized in the following Table II-1 and explained later in details.

Table II-1. Synthesis protocols for niobium carboxylates.

Metal source	Ligand	Solvent			T (°C)	Time	Yield (%Nb)
NbCl ₄ (THF) ₂ 12 mg 0.05 mmol	H ₂ qui 15 mg 0.1 mmol	Acetonitrile 1 mL 19 mmol			RT	3 h	62 %
NbCl ₄ (THF) ₂ 12 mg 0.05 mmol	H ₂ qui 15 mg 0.1 mmol	Acetonitrile 1 mL 19 mmol	Pyridine 0.5 mL 6.21 mmol		80 °C	24 h	14 %
NbCl ₄ (THF) ₂ 12 mg 0.05 mmol	H ₂ qui 15 mg 0.1 mmol	Acetonitrile 1 mL 19 mmol	Pyridine 0.5 mL 6.21 mmol	Triethylamine 20 µL 0.14 mmol	80 °C	24 h	12 %
NbCl ₄ (THF) ₂ 12 mg 0.05 mmol	H ₂ icc 15 mg 0.1 mmol	DMF 1 mL 13 mmol			RT	3 d	35 %

II. 1.1 Synthesis of [Nb(Hqui)₄·0.8(CH₃CN)] (Complex **Nb(IV)-1**)

Nb^{IV}(μ-O₂C₇H₄NO₂)₄·CH₃CN **Nb(IV)-1** has been synthesized after the addition of NbCl₄(THF)₂ (12 mg, 0.05 mmol) in a solution 1 mL of acetonitrile (19 mmol) with quinolinic acid (15 mg, 0.1 mmol) in a 2mL glass vial. Upon the addition, the reaction starts as the first brick-like brownish orange crystals are observed after 3 hours (Figure II-1). The vial was left sealed at room temperature. Parallelepiped-shape crystals (200-400 μm) with an X-Ray diffraction quality are observed after 3 days. Images of the crystals of **Nb(IV)-1** taken under the optical microscope are shown in Figure II-1a. Elemental chemical analysis: calculated C: 44.8%, H: 2.7%, N: 8.5%; experimental C: 44.7 %, H: 2.6 %, N: 8.0 %.

II. 1.2 Synthesis of [Nb(Hqui)₄·0.7CH₃CN·2pyr] (Complex **Nb(IV)-2**)

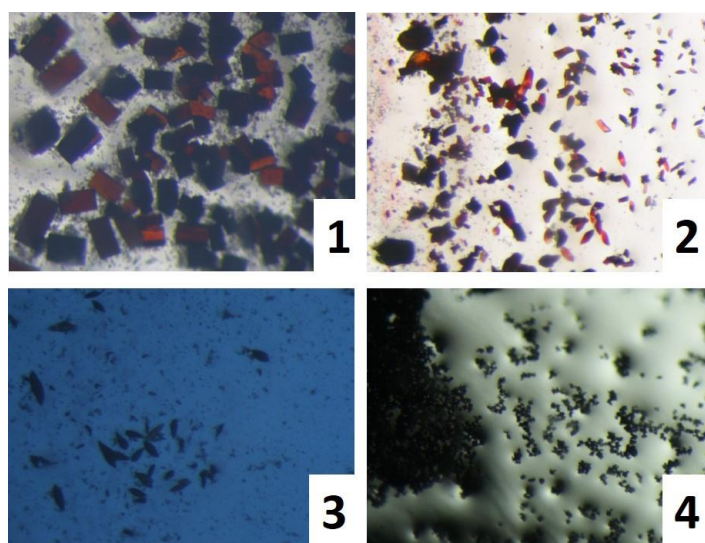
Nb^{IV}(μ-O₂C₇H₄NO₂)₄·CH₃CN·C₅H₅N (**Nb(IV)-2**) has been synthesized after the addition of NbCl₄(THF)₂ (12 mg, 0.05 mmol) in a solution of 1 mL of acetonitrile (19 mmol) and 0.5 mL pyridine (6.21 mmol) with quinolinic acid (15 mg, 0.1 mmol) in a 2 mL glass vial. Pyridine was added as an attempt to deprotonated the free carboxylic group of the quinolinate group existing in **Nb(IV)-1**. The first block-like brownish orange crystals are observed after heating for 24 hours at 80 °C (Figure II-1). Temperature was tentatively applied to support the deprotonation. Images of the crystals (30-180 μm) of **Nb(IV)-2** taken under the optical microscope are shown in Figure II-1b. Elemental chemical analysis: calculated C: 50.1%, H: 3.0%, N: 9.9%; experimental C: 48.9 %, H: 2.9 %, N: 8.6 %.

II. 1.3 Synthesis of $[\text{Nb}(\text{qui})(\text{Hqui})_3\cdot\text{Cl}\cdot\text{Hpyr}\cdot\text{HTEA}\cdot 1.5\text{H}_2\text{O}]$ (Complex **Nb(IV)-3**)

$[\text{Nb}(\text{qui})(\text{Hqui})_3\cdot\text{Cl}\cdot\text{Hpyr}\cdot\text{HTEA}\cdot 1.5\text{H}_2\text{O}]$ (**Nb(IV)-3**) has been synthesized after the addition of $\text{NbCl}_4(\text{THF})_2$ (12 mg, 0.05 mmol) in a solution of 1 mL of acetonitrile (19 mmol), 0.5 mL pyridine (6.21 mmol) and 20 μL triethylamine (0.14 mmol) with quinolinic acid (15 mg, 0.1 mmol) in a 2 mL glass vial. Triethylamine and pyridine were added as an attempt to deprotonate the free carboxylic group of the quinolinate group existing in **Nb(IV)-1**. The amount of triethylamine was chosen to be equimolar with ligand molecule. The block-like dark blue crystals are observed after heating for 24 hours at 80 °C (Figure II-1). Temperature was tentatively applied to support the deprotonation. Images of the crystals (30-50 μm) of **Nb(IV)-3** taken under the optical microscope are shown in Figure II-1c. In case of 5 acetonitrile molecules (not revealed by single-crystal XRD analysis, elemental chemical analysis is: calculated C: 48.0%, H: 4.0%, N: 10.8%; experimental C: 47.6 %, H: 3.8 %, N: 9.7 %.

II. 1.4 Synthesis of $[\text{Nb}(\text{Hicc})_4\cdot 6\text{DMF}]$ (Complex **Nb(IV)-4**)

$\text{Nb}^{\text{IV}}(\mu\text{-O}_2\text{C}_7\text{H}_4\text{NO}_2)_4\cdot 6\text{DMF}$ (**Nb(IV)-4**) has been synthesized after the addition of $\text{NbCl}_4(\text{THF})_2$ (12 mg, 0.05 mmol) in a solution of 1 mL of DMF (12.9 mmol) with 2,5-pyridine-dicarboxylic acid (isocinchomeric acid, 15 mg, 0.1 mmol) in a 2 mL glass vial. The reaction mixture was left in the sealed vial in RT and black octahedral-like crystals of **Nb(IV)-4** were isolated after 3 days (Figure II-1). Images of the crystals (20-30 μm) of **Nb(IV)-4** taken under the optical microscope are shown in Figure II-1d. Elemental chemical analysis: calculated C: 46.2 %, H: 4.8%, N: 11.7%; experimental C: 45.1 %, H: 4.5 %, N: 10.9 %.



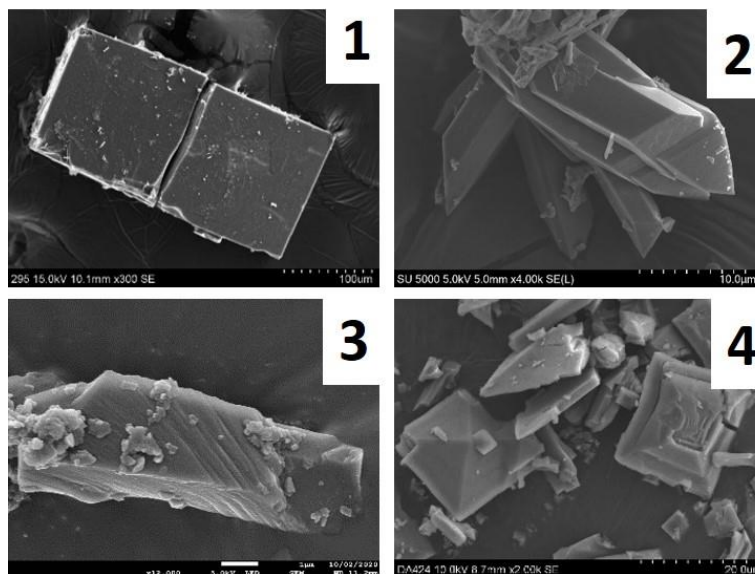


Figure II-1. (top) Crystals of **Nb(IV)-1-4** under optical microscope and (bottom) SEM images.

Powder X-ray diffraction assesses the homogeneity of the four complexes (Figure A2, paragraph A3, Appendix).

II. 1.5 Synthesis route discussion

The reactivity of two types of pyridine-based dicarboxylic acids (quinolinic acid or isocinchomeric acid) with niobium(IV) tetrachloride salt led to the isolation of four distinct crystalline compounds. These reactants are mixed in a glass vial by using either acetonitrile solvent (**Nb(IV)-(1-3)**) or N,N-dimethylformamide solvent (**Nb(IV)-4**), inside a glove box under inert atmosphere (argon) in order to prevent any oxidation of Nb(IV) to Nb(V). The organic solvents were chosen as both of them solubilized satisfyingly the pyridine-dicarboxylic acid derivate ligands and niobium(IV) precursor. Then, the vials are kept closed until crystallization, whether they are heated (at 80 °C for **Nb(IV)-2** and **Nb(IV)-3**, for one day) or not (room temperature crystallization for **Nb(IV)-1** and **Nb(IV)-4**, for three days).

In a first attempt, the strategy was to study the connection arrangement of the ditopic 2,3-pyridine-dicarboxylate ligand around the niobium(IV) center. It was observed (structure description section) that only one carboxylate arm and neighboring nitrogen atom of the pyridine ring was involved in the coordination sphere of the 4d metal (**Nb(IV)-1**).

Since the second carboxylate arm of the quinolinate ligand remains under its protonated state in **Nb(IV)-1**, we investigated the influence of the addition of an organic base in order to tentatively obtain the di-anionic form of the ditopic carboxylate ligand ($^{-}O_2C-C_5H_5N-CO_2^{-}$), with

the aim to further condense a second niobium(IV) center with this type of linker. For these attempts, we used pyridine ($pK_a = 5.23$) as additional solvent with acetonitrile (**Nb(IV)-2**) and a mixture of pyridine / triethylamine ($pK_a = 10.75$) together with acetonitrile (**Nb(IV)-3**). It is interesting to notice that the crystalline phases of **Nb(IV)-2** and **Nb(IV)-3** appeared only after a solvothermal treatment of the starting solution after heating at 80°C for 24 hours, but with lower reaction yields (in the range 12.-14 %, based on Nb) instead of 62-35% (based on Nb) for the **Nb(IV)-1** and **Nb(IV)-4**, synthesized at room temperature. Although the addition of organic bases (pyridine, triethylamine) in the reaction medium, a similar connection mode of the quinolate ligand with the niobium(IV) center was found together with a unreacted free carboxylic acid function.

In a last reaction, we study the reactivity of the parent pyridine-dicarboxylic acid, with the two carboxylate functionalities in 2,5 position (isocinchomeric acid) instead of 2,3 (quinolinic acid), assuming that opposite carboxylate groups may favor the connection of two different niobium(IV) centers (mimicking the 1,4-benzene dicarboxylate or terephthalate configuration, for instance), in order to generate infinite networks. When the isocinchomeric acid was used, we were able to isolate an analogous complex with niobium(IV), which crystallized in N,N-dimethylformamide solvent (**Nb(IV)-4**), since our attempts for the synthesis route with the acetonitrile solvent were found unsuccessful.

After synthesis, no by-product was observed for the four compounds **Nb(IV)-(1-4)**, and the remaining content of the non-crystallized niobium and pyridinedicarboxylic acid species remained in the supernatant solution. After long exposure to air for **Nb(IV)-2** and **Nb(IV)-3**, an amorphous powder is obtained without any trace of the original crystalline complexes. Some attempts were made to add small amounts of water to the chemical system in order to promote a controlled hydrolysis reaction toward niobium(IV) species, but were unsuccessful due to the systematic formation of crystalline NbO₂.

II. 2 Structural description

All the structures of compounds **Nb(IV)-(1-4)** are based on the same molecular assemblies containing one niobium(IV) center eight-fold coordinated by four bidentate pyridine-based dicarboxylate (2,3-pyridine-dicarboxylate (**Nb(IV)-1-3**), or 2,5-pyridine-dicarboxylate (**Nb(IV)-4**)) ligands through the carboxyl O and pyridyl N atoms, associated with

different solvent molecules. The geometry around the niobium(IV) atoms defines a triangulated dodecahedral environment (D_{2d} symmetry) as expected for eight-fold coordination system of $\{MA_4B_4\}$ unit for d^1 transition cations (Orgel concept^[3]). This series of four niobium-centered complexes are closely related to that observed in the niobium(IV) 2-pyridinedicarboxylate (known as picolinate = pic) moiety $[Nb(pic)_4 \cdot 2EtOH]$, previously described by Ooi *et al.*, in 1996.^[4] All the compounds **Nb(IV)-1** \rightarrow **Nb(IV)-4** have been characterized by single-crystal X-ray diffraction analysis. The summary of the crystallographic data is summarized in the following Table II-2.

Table II-2. Crystal data and structure refinements for compounds **Nb(IV)-(1 – 4)**.

	Nb(IV)-1	Nb(IV)-2	Nb(IV)-3	Nb(IV)-4
Formula	C _{29.66} H _{21.31} N _{4.83} NbO ₁₆	C _{39.4} H _{28.1} N _{6.7} NbO ₁₆	C ₇₈ H ₇₄ Cl ₂ N ₁₂ Nb ₂ O ₃₅	C ₄₆ H ₅₈ N ₁₀ NbO ₂₂
Formula weight	794.28	944.29	1996.21	1193.69
Temperature/K	103	100	100	100
Crystal type	brownish-orange block	brownish-orange octahedron	brown block	dark blue block
Crystal size/mm	0.41 x 0.27 x 0.17	0.27 x 0.20 x 0.18	0.11 x 0.09 x 0.04	0.2 x 0.1 x 0.1
Crystal system	tetragonal	Monoclinic	triclinic	tetragonal
Space group	<i>P4/ncc</i>	<i>C2/c</i>	<i>P-1</i>	<i>I4₁/a</i>
a/Å	14.5184(11)	19.2258(4)	13.6480(7)	17.3445(8)
b/Å	14.5184(11)	14.0993(3)	13.8277(7)	17.3445(8)
c/Å	14.2771(10)	16.0613(4)	14.5164(7)	18.4014(10)
α/°	90	90	93.994(3)	90
β/°	90	117.0518(9)	100.661(3)	90
γ/°	90	90	115.361(2)	90
Volume/Å³	3009.4(5)	3877.42(15)	2398.4(2)	5535.7(6)
Z, ρ_{calculated}/g.cm⁻³	4, 1.753	4, 1.618	1, 1.382	4, 1.432
μ/mm⁻¹	0.492	0.397	0.381	0.304
θ range/°	1.98 - 26.44	1.87 - 30.51	1.45 - 26.41	1.61 - 26.36
	-18 ≤ h ≤ 18	-27 ≤ h ≤ 25	-17 ≤ h ≤ 17	-21 ≤ h ≤ 19
Limiting indices	-18 ≤ k ≤ 18	-20 ≤ k ≤ 18	-16 ≤ k ≤ 17	-21 ≤ k ≤ 20
	-17 ≤ l ≤ 17	-22 ≤ l ≤ 20	-17 ≤ l ≤ 18	-22 ≤ l ≤ 22
Collected reflections	105224	32120	38119	34413
Unique reflections	1561	5916	9556	2835
	[R(int) = 0.0368]	[R(int) = 0.0221]	[R(int) = 0.0653]	[R(int) = 0.0333]
Parameters	188	327	584	198
Number of restraints	85	0	18	0
Goodness-of-fit on F²	1.052	1.083	1.025	1.063
Final R indices	R1 = 0.0552	R1 = 0.0358	R1 = 0.0753	R1 = 0.0290
[I > 2σ(I)]	wR2 = 0.1558	wR2 = 0.0950	wR2 = 0.1933	wR2 = 0.0722
R indices (all data)	R1 = 0.0704	R1 = 0.0384	R1 = 0.1136	R1 = 0.0338
	wR2 = 0.1822	wR2 = 0.0970	wR2 = 0.2154	wR2 = 0.0753
Largest diff. peak and hole/e.Å⁻³	1.35 and -0.74	0.76 and -0.68	1.25 and -1.57	0.437 and -0.279

II. 2.1 Complex 1 : $[Nb(Hqui)_4 \cdot 0.8(CH_3CN)]$

Crystal structure of compound $Nb(Hqui)_4 \cdot 0.8CH_3CN$ (**Nb(IV)-1**) possesses one crystallographically niobium site (Nb1). This site is sitting on the special position $4b$ (axis -4) and involved in a mononuclear complex with one crystallographical type of quinolate (2,3-

pyridine-dicarboxylate) ligands, located in general position 16*g*. The niobium center (Nb1) is coordinated by the nitrogen atom (N1) of the pyridine ring and one oxygen atom (O1) from the carboxylate group in position 2, from four quinolinate ligands (Figure II-2), leading to the environment $\{NbO_4N_4\}$. The corresponding bond lengths are 2.278(4) Å for Nb1-N1 (4x) and 2.085(3) Å for Nb1-O1 (4x). The dihedral angle between the two interpenetrating planes defined by the O...N...N...O sequence of connecting atoms to the central niobium cation is 90°, revealing the ideal D_{2d} dodecahedral geometry for the $\{NbO_4N_4\}$ unit.^[5,6] If the D_{4d} square antiprism geometry is considered, the dihedral angle value will be 77.4° instead. The interatomic Nb-O and Nb-N bond distances are in the range of those encountered in the niobium(IV) complex obtained with a parent pyridine-based monocarboxylate ligand such as the picolinic acid (2-pyridinecarboxylic acid). In that case, the Nb-O lengths varied from 2.092(2) up to 2.108(1) Å, and Nb-N lengths varied from 2.295(2) up to 2.310(2)(1) Å, from single-crystal XRD data collected at room temperature.^[4] The remaining free C1-O2 bond of the monodentate carboxylate group exhibits a length of 1.227(6) Å, revealing its non-protonated state, that will be confirmed later in this chapter by infrared spectroscopy. A part of the pyridine ring was found on two close positions, with a statistical disorder of 58/42 for the C3 → C7 atoms and the O atoms of the second carboxylate arm. For the latter, the bond C-O distances are slightly contrasted with a shorter one (C7B-O5 = 1.233(10) Å) and longer ones (C7B-O6 = 1.268(9) Å, C7A-O4 = 1.271(12) Å and C7A-O3 = 1.274(9)), indicated a typical protonated state.

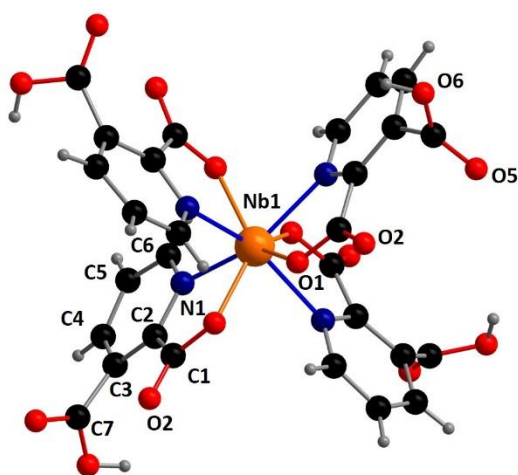


Figure II-2. Ball and stick representation of the mononuclear niobium(IV)-centered coordination complex of $Nb(Hqui)_4 \cdot 0.8CH_3CN$ (**Nb(IV)-1**). For clarity, the statistical disorder related to the C3, C4, C5, C6, C7, O5 and O6 atoms are not shown. Green circle: Nb; blue: N, red.

The monoprotonated quinolinate linker which is tetra-coordinated to one niobium(IV) center, ensures the electroneutrality of the complex. The supramolecular assembly is based on the stacking of the $[\text{Nb}(\text{Hqui})_4]$ species along the c axis, with a rotation of around 45° of the pyridine ring fragments between two adjacent niobium centers. It results in the formation of four-pointed star-like channels, in which free acetonitrile solvent resides (Figure II-3). This acetonitrile molecule is not well positioned as it seems to be disordered along its own linear axes, running parallel to the c axis. Thus, finally $C_{\text{CH}_3\text{CN}}$ and $N_{\text{CH}_3\text{CN}}$ occupancies were refined to the value close to 0.8 and 0.4, respectively, corresponding to a crystallographical ratio of $0.8\text{CH}_3\text{CN}$ for one $[\text{Nb}(\text{Hqui})_4]$ species. During the refinement calculations, the protons of methyl group of acetonitrile could not be located due to their free rotation around the linear C-C-N axis related to the tetragonal c axis. Within a layer in the (a,b) plane, each quinolinate molecule interacts to each other, via one terminal carboxylic acid arm pointing perpendicularly toward a neighboring pyridine ring fragment of a second ligand. The remaining free carboxylic acid functions are arranged around the acetonitrile solvent, with C \cdots N distances of 2.75(4) Å.

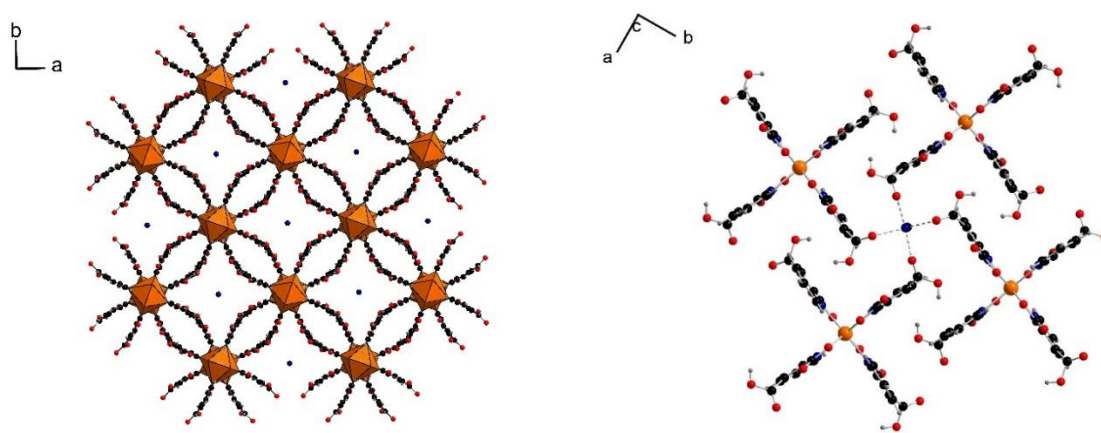


Figure II-3. (left) polyhedral view of the packing structure of the neutral $[\text{Nb}(\text{Hqui})_4]$ complex arranged around the acetonitrile solvent in compound **Nb(IV)-1**, along the c axis. (right) detailed view of the arrangement of $[\text{Nb}(\text{Hqui})_4]$ moieties in the (a,b) plane, showing the shortest interactions of the free non-bonded carboxylic acid functions of the quinolinate ligands with acetonitrile. Linear acetonitrile molecules are located along the $[001]$ direction, and only its nitrogen atom (blue circles) are shown. Orange polyhedron: Nb; blue circle: N; red: O; dark grey: C; light grey: H.

II. 2.2 Complex 2: $[\text{Nb}(\text{Hqui})_4 \cdot 0.7\text{CH}_3\text{CN} \cdot 2\text{pyr}]$

As observed in complex **Nb(IV)-1**, the dicarboxylate ligand is only mono-deprotonated. We therefore explored different synthetic routes in order to deprotonate the second arm of the carboxylic acid function of the quinolinate molecule, in order to have a second connecting group towards a niobium center. In this way we tried to increase the dimensionality of the

resulting complex from a molecular assembly to chain-like, layered or 3D network. Thus, we firstly attempted to add a mild organic base in the reaction. Adding pyridine resulted in complex **Nb(IV)-2** ($\text{Nb}(\text{Hqui})_4 \cdot 0.7\text{CH}_3\text{CN} \cdot 2\text{pyr}$), that exhibits a similar eight-fold coordination sphere around the niobium(IV) atom, as found in complex **Nb(IV)-1** (Figure II-4). The niobium cation is surrounded by two types of crystallographically independent quinolinate ligands, through four pyridyl nitrogen and four carboxyl oxygen atoms (in position 2), with Nb-O and Nb-N bonding lengths of 2.090(1)-2.104(1) Å, and 2.286(1)-2.287(1) Å, respectively. These Nb-O and Nb-N bond ranges were similar to those found in compound 1 and related Nb(IV)-picolinate complex.^[4] The resulting $[\text{NbO}_4\text{N}_4]$ polyhedron describes a distorted dodecahedral geometry as defined by the dihedral angle of 87.49(4)° between the two planes from obtained through the sequence of O···N···N···O atoms from the two sets of nearly perpendicular bidentate quinolinate molecules (Figure II-4). This angle value is in agreement with a dodecahedral environment around the niobium center^[6], even if it is slightly shifted from the ideal case of 90°. The remaining C-O bond is not protonated, with short C7-O3 and C14-O4 distances of 1.220(2) and 1.217(2) Å, respectively. The second carboxylate arm in position 3 is under its protonated form with the two specific contrasted C=O and C-OH bond lengths of 1.211(3)-1.229(2), and 1.276(3)-1.300(3) Å.

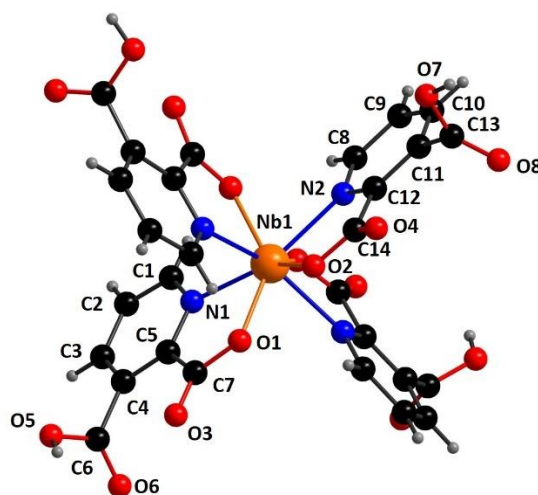


Figure II-4. Ball and stick representation of the mononuclear niobium(IV)-centered coordination complex of $\text{Nb}(\text{Hqui})_4 \cdot 0.7\text{CH}_3\text{CN} \cdot 2\text{pyr}$ (**Nb(IV)-2**). Orange circle: Nb; blue: N, red: O; dark grey: C, light grey: H.

The crystal packing is constructed from the molecular assembly of neutral $\text{Nb}(\text{Hqui})_4$ entities, which are arranged around pyridine and acetonitrile solvents species, trapped within triangular-shaped pseudo-channels along the $[-101]$ direction (Figure II-5). These molecules were found disordered on two positions: there exists an occupancy of 35/65 for pyridine,

related to a multiplicity twice related to the niobium center. For acetonitrile, the carbon atoms are also disordered on two positions, with the same occupancy 35/65, around the nitrogen atom, which has an occupancy factor refined to 70%. The interactions of these intercalated pyridine/acetonitrile species with the $\text{Nb}(\text{Hqui})_4$ entities, are rather weak, with interatomic distances greater than 3.2 Å regarding the C-OH bondings of the monoprotonated quinolate ligands. Thus, the organization of the $\text{Nb}(\text{Hqui})_4$ complexes differs from that observed in compound **Nb(IV)-1**, through the structuring role of the couple pyridine/acetonitrile in compound **Nb(IV)-2**, compared to only acetonitrile occurs in compound **Nb(IV)-1**. One notices preferential strong hydrogen interactions between the terminal carboxylic acid functions (through $\text{C-O7H}\cdots\text{O5} = 1.660(2)$ Å) of two adjacent $\text{Nb}(\text{Hqui})_4$ entities, generating chains along the [101] direction (Figure II-5).

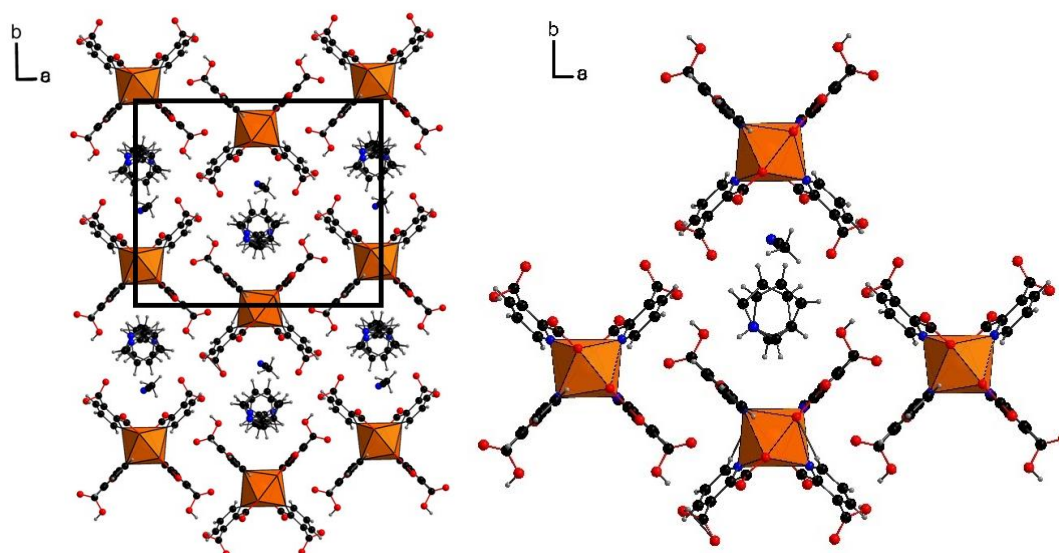


Figure II-5. (left) polyhedral view of the packing structure of the neutral $[\text{Nb}(\text{Hqui})_4]$ complex arranged around the acetonitrile and pyridine solvent in compound **Nb(IV)-2**, along the [-101] direction. (right) detailed view of the arrangement of $[\text{Nb}(\text{Hqui})_4]$ moieties, showing better the supramolecular arrangement.

II. 2.3 Complex 3: $[\text{Nb}(\text{qui})(\text{Hqui})_3\cdot\text{Cl}\cdot\text{Hpyr}\cdot\text{HTEA}\cdot 1.5\text{H}_2\text{O}]$

The crystal structure of compound of $\text{Nb}(\text{qui})(\text{Hqui})_3\cdot\text{Cl}\cdot\text{Hpyr}\cdot\text{HTEA}\cdot 1.5\text{H}_2\text{O}$ (**Nb(IV)-3**) consists of one niobium(IV) metal center, bound to four distinct crystallographically independent quinolate ligands (Figure II-6). As observed for the other complexes, the niobium atom is eight-fold coordinated to four pyridyl nitrogen atoms ($\text{Nb-N} = 2.283(5)$ - $2.296(4)$ Å) and four carboxyl oxygen ($\text{Nb-O} = 2.084(3)$ - $2.097(4)$ Å), which are comparable with the Nb-O and Nb-N bondings ($2.090(1)$ - $2.108(1)$ Å, and $2.295(2)$ - $2.310(2)$ Å) encountered

for the tetravalent oxidation state of Nb (see compounds **Nb(IV)-(1-2)**). The coordination sphere around the niobium(IV) cation defines a dodecahedral polyhedron, with dihedral angles between the planes formed by two sets of O···N···N···O atoms sequence from quinolinate linkers, of $89.3(1)^\circ$ (Figure II-6). This value reveals a very weak distortion to the ideal geometry.^[6] As for compounds **Nb(IV)-(1-2)**, the second C-O bonding from the monodentate carboxylate arm is terminal with relatively short C-O bond lengths (C-O = 1.217(6)-1.221(9) Å). For the other carboxylate arm in position, the situation differs, since we observe the protonation for three of the four connecting quinolinate ligands. The expected long C-OH and short C=O bond distances are found with the values of 1.306(10)-1.319(7) Å and 1.177(11)-1.205(7) Å, respectively. The fourth quinolinate molecule exhibits the two C5-O bondings from carboxylate arm in position 3, with the values of C5-O3 and C5-O4 of 1.253(6) and 1.258(7) Å, respectively, and indicating its non-protonated state.

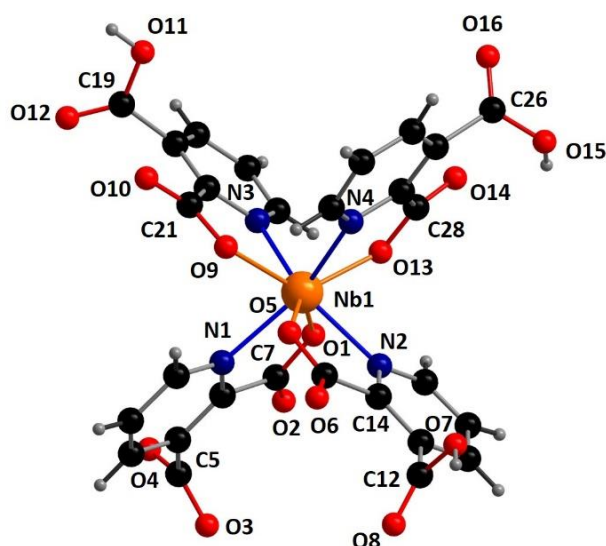


Figure II-6. Ball and stick representation of the mononuclear niobium(IV)-centered coordination complex of $\text{Nb(qui)(Hqui)}_3 \cdot \text{Cl} \cdot \text{Hpyr} \cdot \text{HTEA} \cdot 1.5\text{H}_2\text{O}$ (**Nb(IV)-3**). Orange circle: Nb; blue: N, red: O; dark grey: C, light grey: H.

The occurrence of unprotonated quinolinate ligands attached to niobium atoms results in a negatively charged $[\text{Nb(qui)(Hqui)}_3]^-$ entity, which is surrounded by distinct species such as triethylamine, pyridine, isolated chloride anions and water molecules (the latter coming from hydrated triethylamine precursor) (Figure II-7). The pyridine and triethylamine molecules were observed under their protonated form, which thus bring two positive charges, and compensated by the two negative charges from chloride and $[\text{Nb(qui)(Hqui)}_3]^-$ anions, ensuring the electroneutrality of the crystalline structure. But, the structure resolution did not

allow for identifying properly all the species within the crystal packing of compound **Nb(IV)-3**. SQUEZZE procedure was used to remove a calculated electronic density of 112 electrons on a void volume of 429 Å³. These electrons could be assigned to five unlocated acetonitrile molecules. Therefore, we tentatively propose a schematic view of the different interactions between the intercalated species. Indeed, preferential hydrogen bonds occur between the [Nb(qui)(Hqui)₃]⁻ entities themselves, through the oxygen atoms from deprotonated carboxylate and carboxylic acid group (O7-H...O3 = 2.075(6) Å and O11-H...O4 = 1.713(5) Å), resulting in the chain-like system, running along the [111] direction (Figure II-7). The protonated triethylamine molecule is hydrogen bonded via its central ammonium group to oxygen from deprotonated carboxylate arm, with N5-H...O3 = 1.875(5) Å. The free pyridinium anions preferentially interact through the non-bonded oxygen atom O2, from the carboxylate arm in position 2, belonging to the deprotonated quinolinate ligand (N6-H...O2 = 2.341(7) Å). The water molecule (OW17) is hydrogen bonded to the carboxylic acid function of one quinolinate ligand (O15-H...OW17 = 2.027(7) Å). Other species (Cl⁻, H₂O) are weakly interacting with the [Nb(qui)(Hqui)₃]⁻ units with bond distances greater than 2.8 Å.

Both compounds **Nb(IV)-2** and **Nb(IV)-3**, obtained in the presence of additional organic base, revealed that the similar connection mode of the quinolinate ligands with niobium(IV), leaving the second carboxylic acid arm under its protonated form.

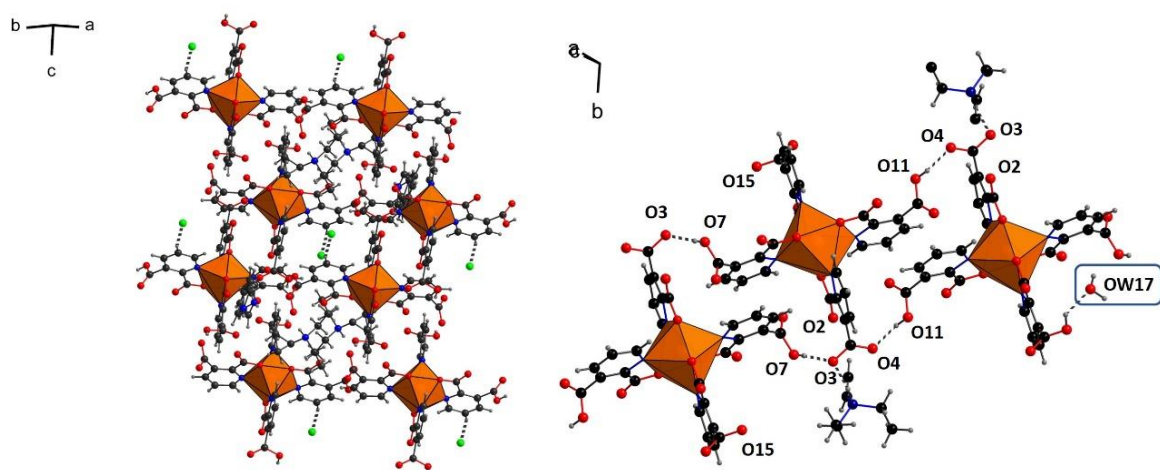


Figure II-7. (left) Polyhedral representation of the structure of compound Nb(qui)(Hqui)₃·Cl·Hpyr·HTEA·1.5H₂O (**Nb(IV)-3**) along the [110] direction. (right) Detailed view of the hydrogen bond interactions between [Nb(qui)(Hqui)₃]⁻ entities and with protonated pyridine and triethylamine, and water molecules, along the [111] direction (dotted lines: hydrogen bondings). Pyridine and one methyl group of triethylamine molecules were found to be disordered on two equivalent positions, and are not shown for clarity. Green circle: Nb; blue: N, red: O; dark grey: C, light grey: H; light green: Cl; orange: free water.

II. 2.4 Complex 4: $[\text{Nb}(\text{Hicc})_4 \cdot 6\text{DMF}]$

In a last reaction, we studied the reactivity of the parent pyridine-dicarboxylic acid, with the two carboxylate functionalities in 2,5 position instead of 2,3 (quinolinic acid). With the isocinchomeric acid, we were able to isolate an analogous complex with niobium(IV), which crystallized in N,N-dimethylformamide solvent. Its crystal structure $\text{Nb}(\text{Hicc})_4 \cdot 6\text{DMF}$ (**Nb(IV)-4**) is built up from one crystallographically unique niobium(IV) atom (Nb1), sitting on the special position 4*b* (axis -4) and linked through pyridinato nitrogen atoms and carboxyl oxygen atoms in position 2 of one crystallographical type of isocinchomeronate (2,5-pyridine-dicarboxylate) ligand, located in general position 16*f* (Figure II-8). The four isocinchomeronate linkers adopt a bidentate connection mode with the niobium(IV) center with Nb1-O1 bond distance of 2.1082(11) Å (x4) and Nb1-N1 bond distance of 2.266(2) Å (4x). As for compounds **Nb(IV)-(1-3)**, it was observed an ideal dodecahedral geometry for the $[\text{NbO}_4\text{N}_4]$ unit, since the dihedral angle between the two interpenetrating planes is defined by the O...N...N...O sequence is 90°. [6] The Nb-O and Nb-N bond lengths are in the same range (2.090(1) - 2.108(1) Å, and 2.295(2) - 2.310(2) Å) as found in the other compounds **Nb(IV)-(1-3)**, for an eight-fold coordinated niobium atom at the tetravalent oxidation state. The second carboxyl oxygen atom of the monodentate carboxylate arm is free, with a rather short C1=O2 distance of 1.224(2) Å, reflecting its expected non-protonated state. The second carboxylic acid function in position 5 is observed as its protonated state, with two typical distinct C7-O4H and C7=O3 bond distances of 1.319(3) Å and 1.205(2) Å, respectively.

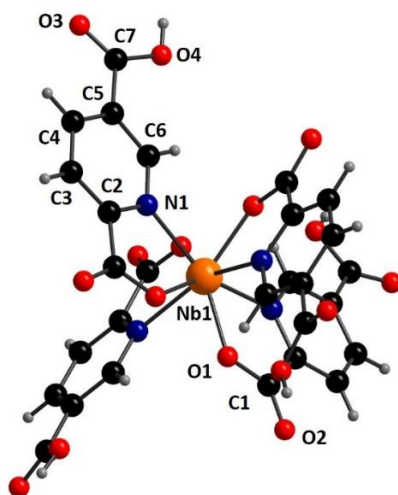


Figure II-8. Ball and stick representation of the complex $\text{Nb}(\text{Hicc})_4 \cdot 6\text{DMF}$ (**Nb(IV)-4**) showing the eight-fold coordinated niobium(IV) center. Orange circle: Nb; blue: N, red: O; dark grey: C, light grey: H.

The molecular assembly of the neutral $[\text{Nb}(\text{Hicc})_4]$ moieties are arranged along a square net in the ab plane, with intercalated DMF solvent molecules (Figure II-9). Two types of DMF species are observed in the crystal packing with different multiplicities: one (noted A in Figure II-9) strongly interacts with the free carboxylic acid proton of the isocinchomeronate ligand ($\text{CO-H}\cdots\text{O}_{\text{DMF(A)}} = 1.728(2) \text{ \AA}$), with the same molar ratio (1 Hicc / 1 DMF(A)). The second DMF molecule (noted B in Figure II-9) has a half multiplicity and is inserted in pseudo-channel defines by the packing of the $[\text{Nb}(\text{Hicc})_4\cdots 4\text{DMF(A)}]$ entities, with weaker interactions (ex: $\text{O}_{\text{DMF(B)}}\cdots\text{O}_{2\text{icc}} > 3.687(4) \text{ \AA}$). The latter is found disordered on two equivalent positions for the carbonyl oxygen and one methyl group.

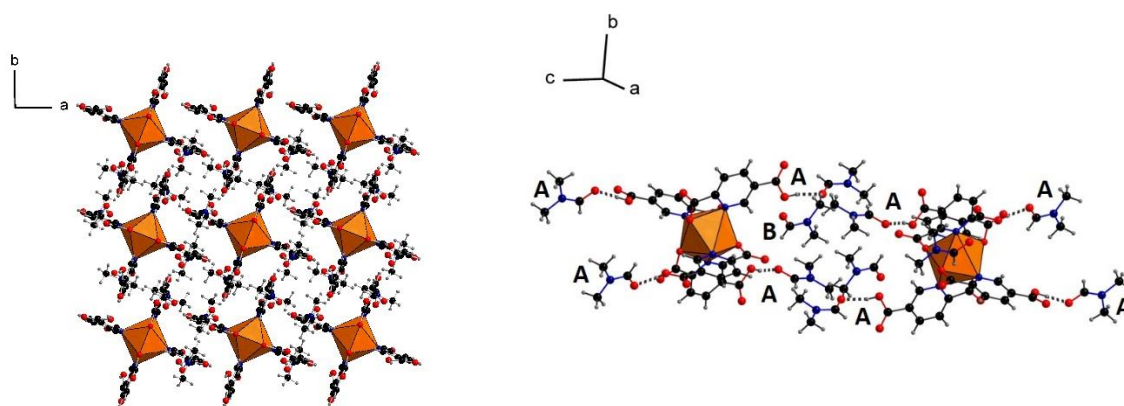


Figure II-9. (left) polyhedral view of the packing arrangement of the $[\text{Nb}(\text{Hicc})_4]$ moieties intercalated by DMF solvent molecules, in compound **Nb(IV)-4**, along the c axis. (right) detailed representation of the two distinct types of DMF solvent molecules: DMF molecules type A are strongly hydrogen-bonded linked to the proton from free carboxylic acid function of isocinchomeronate ligand, forming the entity $[\text{Nb}(\text{Hicc})_4\cdots 4\text{DMF(A)}]$; DMF molecules type B exhibit a disorder for the carbonyl/C-H groups as well as disorder methyl proton. For clarity, only disorder is not shown for this DMF species. Green polyhedron: Nb; blue circle: N, red: O; dark grey: C, light grey: H., dotted line: hydrogen bond between isocinchomeronate ligand and DMF(A) molecules.

II. 3 Infrared spectroscopy in Nb(IV) carboxylate complexes

All four niobium(IV) carboxylate complexes **Nb(IV)-(1-4)** were investigated by infrared spectroscopy (Figures A6-A9, paragraph A4, Appendix) and compared with the organic pyridine-dicarboxylic acid precursor used for their synthesis.

All the attributed peaks are summarized in Table II-3, where a comparison between the values in the four different complexes can be done. Since the coordination sphere remains the same in all four complexes, no big differences are expected for the $\nu_{\text{asym}}(\text{COO})$ and $\nu_{\text{sym}}(\text{COO})$. Indeed, these values vary between $1674\text{-}1685 \text{ cm}^{-1}$ and $1399\text{-}1438 \text{ cm}^{-1}$ respectively. Another type of vibration that exist for all compounds is the $\nu(\text{C-H})_{\text{ar}}$ and $\nu(\text{C=N})_{\text{ar}}$, where values vary between $3081\text{-}3105 \text{ cm}^{-1}$ and $1547\text{-}1590 \text{ cm}^{-1}$ respectively. There are also some vibrations that

exist only for some complexes and arise from the hydrogen bonding between the complex and the solvent molecules around them. The $\nu(\text{N-H})$ stretches in **Nb(IV)-2** and **Nb(IV)-3** come from pyridine molecules and are centered at 3444 and 3424 cm^{-1} respectively. It is noticed that no vibration peak in the region 2200-2280 cm^{-1} related to the $\nu(\text{C}\equiv\text{N})$ stretching is visible, although the acetonitrile ($\text{CH}_3\text{C}\equiv\text{N}$) molecule has been identified by single-crystal XRD analysis in compounds **Nb(IV)-1** and **Nb(IV)-2**, and assumed to be present as disordered manner in compounds **Nb(IV)-3**.

Table II-3. Infrared wavenumbers (cm^{-1}) of the assigned bands for compounds **Nb(IV)-(1-3)** (with 2,3-pyridinedicarboxylate) and **Nb(IV)-4** (with 2,5-pyridinedicarboxylate).

	carboxylate group $\nu_{\text{asym}}(\text{COO})$	carboxylate group $\nu_{\text{sym}}(\text{COO})$	free carboxylic group $\nu(\text{C=O})_{\text{acid}}$	$\nu(\text{C-H})_{\text{ar}}$	$\nu(\text{C=N})_{\text{ar}}$	$\nu(\text{N-H})$
2,3- pyridinedicarboxylic acid	-	-	1717	3101	1578	-
Nb(IV)-1	1682	1435	1741	3105	1547	-
Nb(IV)-2	1678	1438	1734	3105	1547	3444
Nb(IV)-3	1674	1435	1722	3081	1547	3424
2,5- pyridinedicarboxylic acid	-	-	1722	3093	1590	-
Nb(IV)-4	1685	1399	1729	3084	1578	-

II. 4 Magnetism in Nb(IV) carboxylate complexes

Due to the $4d^1$ electronic configuration for niobium(IV), we investigated the magnetic behavior of the series of the four molecular compounds **Nb(IV)-(1-4)**. Indeed, the magnetic characterization has been rarely reported in literature^[1,7-10] for such eight-fold coordinated niobium(IV) centers with well-defined geometrical environment (Table II-4). The magnetic susceptibility $\chi(T)$ has been measured as a function of the temperature in the range 2-300 K (Figure II-10). The thermal dependence has been fitted classically from the Curie-Weiss law $\chi(T) = C/(T-\theta)$, where T is the temperature, C is the Curie constant and θ is the Weiss constant.

The effective magnetic moment has been extracted from the slope of the linear plot of $\chi^{-1}T$ versus T in the range 15-150 K for complex **Nb(IV)-1**, 50-200 K for complex **Nb(IV)-2**, 75-200 K for complex **Nb(IV)-3** and 50-150 K for complex **Nb(IV)-4**. The experimental effective magnetic moment values, μ_{eff} for the complexes **Nb(IV)-(1-4)** were 1.61, 1.47, 1.50 and 1.58 μ_B (Bohr Magnetons), respectively (Figure II-10). These values are ranging around the

theoretical one ($\mu_{\text{eff}} = 1.73 \mu_{\text{B}}$), which correspond to a spin-only system, expected for a single unpaired electron with a d^1 electronic configuration, as it occurs with niobium(IV).^[11]

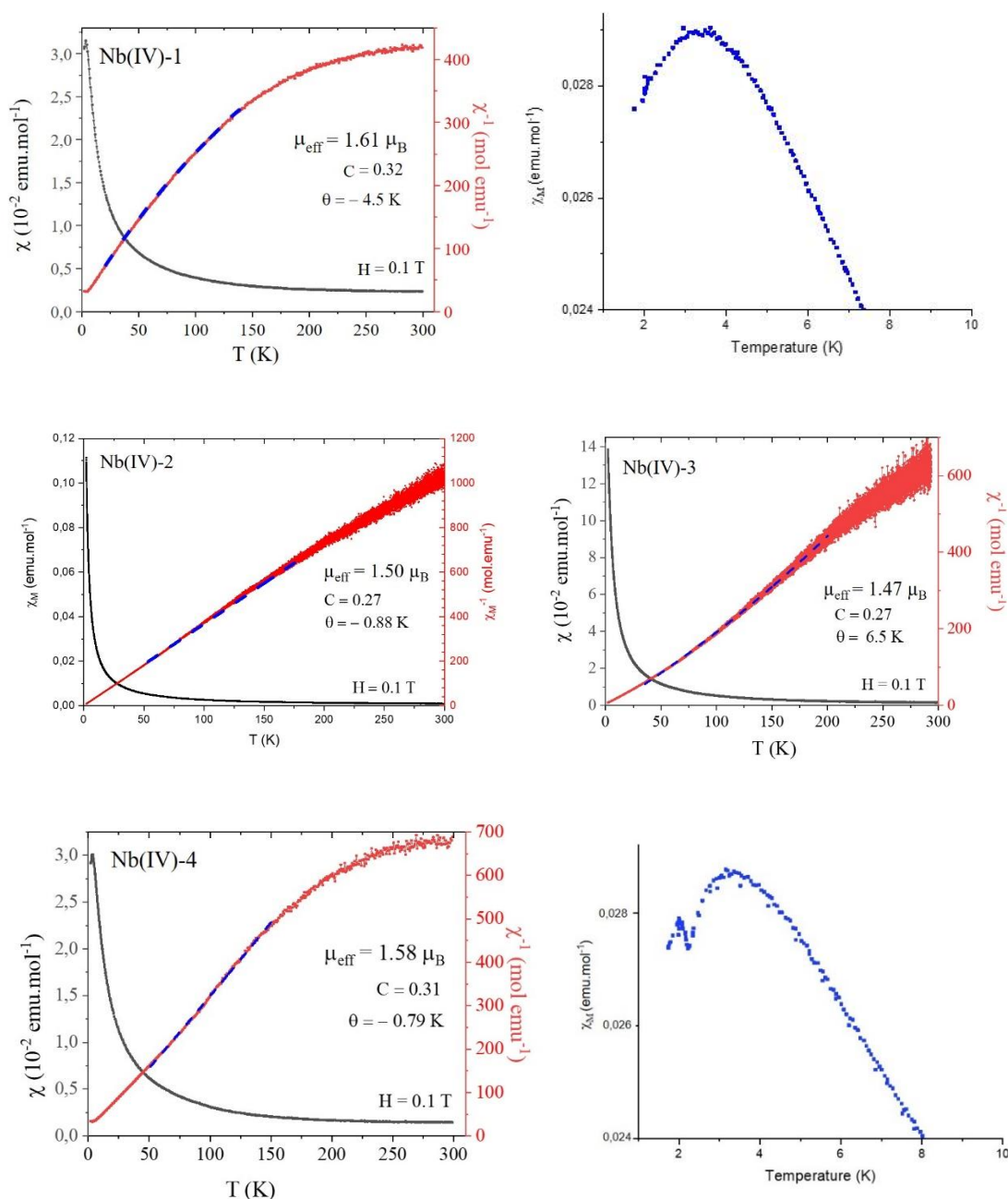


Figure II-10. Magnetic susceptibility (χ , ordinate scale in the left, black circles), inverse susceptibility (χ^{-1} , ordinate scale in the right, red circles) curves as a function of temperature for the powdered **Nb(IV)-1** and linear plot range (dashed blue line) for the estimation of the experimental $\mu_{\text{eff}} = 1.61 \mu_{\text{B}}$ (top left). Zoom at the range 2-10 K highlights the transition observed at 3.6 K (top right). Magnetic susceptibility (χ , ordinate scale in the left, black circles), inverse susceptibility (χ^{-1} , ordinate scale in the right, red circles) curves as a function of temperature for the powdered **Nb(IV)-2** (middle left) and **Nb(IV)-3** (middle right) and linear plot range (dashed blue line) for the estimation of the experimental $\mu_{\text{eff}} = 1.50$ and $1.47 \mu_{\text{B}}$ respectively. Magnetic susceptibility (χ , ordinate scale in the left, black circles), inverse susceptibility (χ^{-1} , ordinate scale in the right, red circles) curves as a function of temperature for the powdered **Nb(IV)-4** and linear plot range (dashed blue line) for the estimation of the experimental $\mu_{\text{eff}} = 1.61 \mu_{\text{B}}$ (bottom left). Zoom at the range 2-10 K for the transition observed at 3.3 K (bottom right).

Table II-4. Magnetic moments of eight-fold coordinated niobium(IV) centers in complexes with O and/or N-donor ligand at room temperature.

Compound	Coordination environment	Geometry	Effective magnetic moment μ_B	Reference
Nb(IV)-1	[NbO ₄ N ₄]	dodecahedron	1.61	our work
Nb(IV)-2	[NbO ₄ N ₄]	dodecahedron	1.50	our work
Nb(IV)-3	[NbO ₄ N ₄]	dodecahedron	1.47*	our work
Nb(IV)-4	[NbO ₄ N ₄]	dodecahedron	1.58	our work
Nb(pyc)₄·2EtOH^a	[NbO ₄ N ₄]	dodecahedron	1.44	[1]
Nb(O₂CNEt₂)₄	[NbO ₈]	dodecahedron	1.55	[7]
Nb(acac)₄^b	[NbO ₈]	not reported	1.47	[8]
Nb(hfacac)₄^c	[NbO ₈]	square antiprism	1.54	[9]
(Pc₂Nb)·CINP^d	[NbN ₈]	square antiprism	1.69	[10]

^apyc= 2-pyridinecarboxylate ; ^bacetylacetonate ; ^chexafluoroacetylacetonate ; ^dPc = phthalocyaninate, CINP = 1-chloronaphthalene.

*this μ_{eff} value has been estimated from the chemical formula obtained by single-crystal XRD analysis, without taking into account the non-revealed intercalated molecular species due to the use of SQUEEZE procedure. If five acetonitrile molecules are present in the structure as suggested the number of remaining electrons, it is estimated a value of $\mu_{eff} = 1.52 \mu_B$.

For two of the complexes (**Nb(IV)-1** and **Nb(IV)-4**), it is observed a curvature change a very low temperature on the $\chi(T)$ versus T plot, with T = 3.6 and 3.3 K, respectively (Figure II-10), and typically related to an antiferromagnetic transition. However, this magnetic susceptibility variation was not visible for the two other complexes **Nb(IV)-2** and **Nb(IV)-3**. This magnetic behavior might be correlated to the different supramolecular Nb···Nb distances in each complex (Figure II-11).

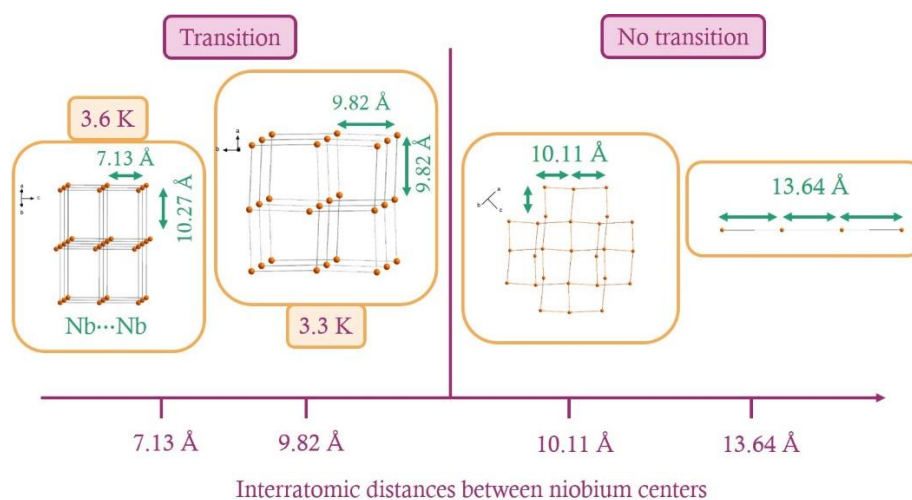


Figure II-11. Extraction of antiferromagnetic transition temperature related to the interatomic distances between niobium centers.

Regarding the shortest distances within a regular or distorted square net of niobium(IV) nodes, we noticed two interatomic length values lower than 10 Å for complexes **Nb(IV)-1** and **Nb(IV)-4** and two others greater than 10 Å for complexes **Nb(IV)-2** and **Nb(IV)-3** (Table II-5). It results that a Nb...Nb distance value greater than 10 Å does not give rise to such antiferromagnetic transition, whereas it exists at lower Nb...Nb distance, with a transition temperature increase inversely to the interatomic length.

Table II-5. List of the shortest interatomic Nb...Nb distances and antiferromagnetic transition temperature in complexes **Nb(IV)-(1-4)**.

	shortest Nb...Nb distances (Å)	transition temperature (K)
Nb(IV)-1	7.1385(5)	3.6
Nb(IV)-2	10.1153(16)	none
Nb(IV)-3	13.6479(14)	none
Nb(IV)-4	9.8169(4)	3.3

This behavior is supported also by magnetization experiments, where magnetization (M) is plotted against the magnetic field (H) (Figures 12). For complexes **Nb(IV)-1** and **Nb(IV)-4**, where interatomic niobium atoms see each other, magnetization is harder to achieve and needs a higher magnetic field value. Whereas, for complexes **Nb(IV)-2** and **Nb(IV)-3**, magnetization is easier and with lower values of magnetic field.

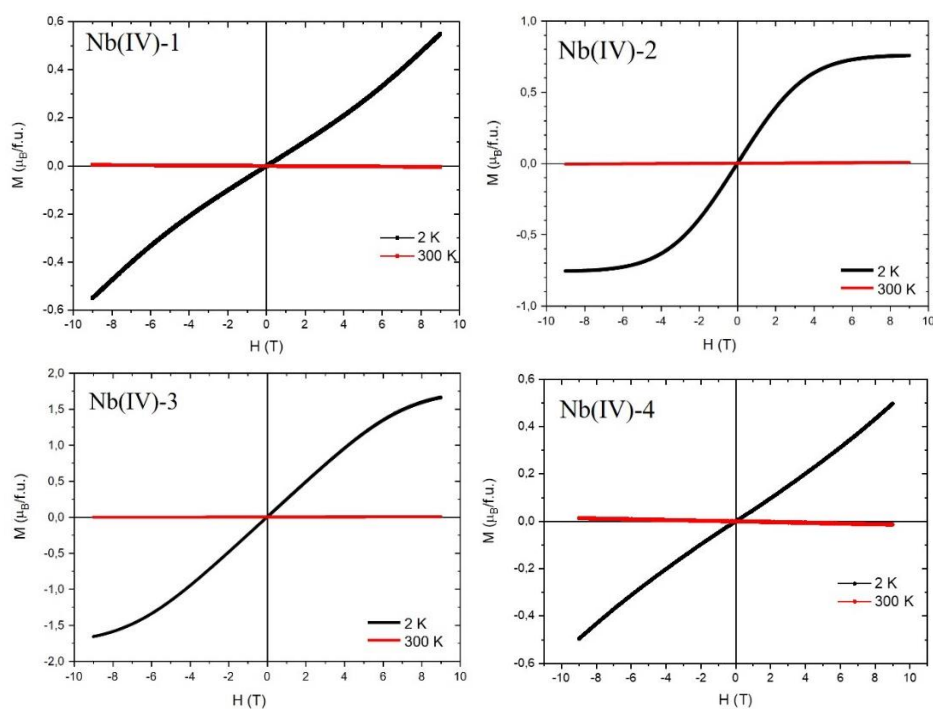


Figure II-12. Magnetization curves of complexes **Nb(IV)-1** (a), **Nb(IV)-2** (b), **Nb(IV)-3** (c) and **Nb(IV)-4** (d) at different temperatures as a function of the magnetic field.

II. 5 Electron Paramagnetic Resonance in Nb(IV) carboxylate complexes

In the series of Nb(IV)-containing complexes (**Nb(IV)-(1-4)**), the electronic configuration of Nb(IV) is [Kr] 4d⁴ 5s¹ leaving niobium with an unpaired electron and permits further analysis by Electron Paramagnetic Resonance (EPR).

For the three compounds, from the first derivative EPR spectra display in Figure II-13, show an EPR signal with a g factor of 1.970 (1), 1.968 (2) and 1.965 (3), which verifies the *d* character of electron, even if no hyperfine structure of the nuclear spin $I=9/2$ of niobium are observed. Such result indicates that the electron is no fully localized at room temperature.

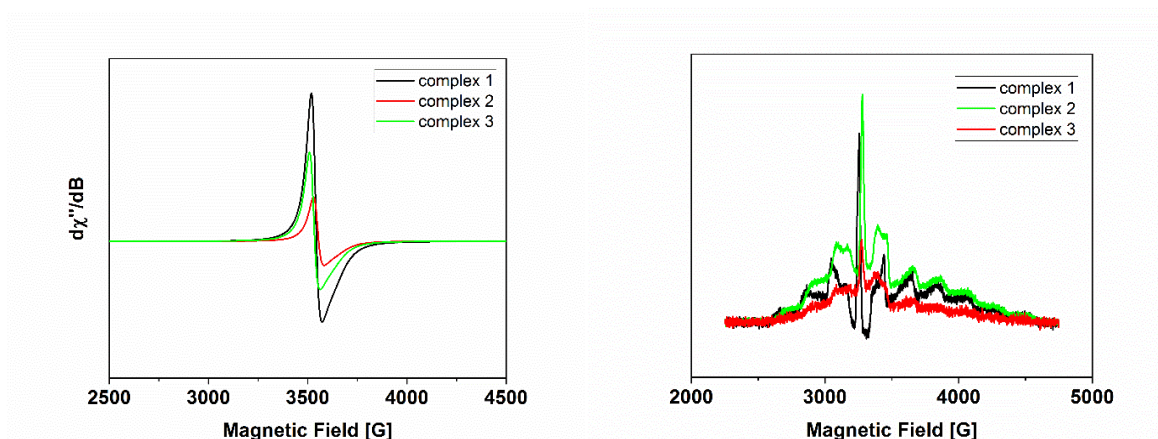


Figure II-13. CW-EPR spectra of compounds **Nb(IV)-1**, **Nb(IV)-2** and **Nb(IV)-3** recorded at room temperature (right) and echo field sweep experiments for complexes **Nb(IV)-(1-3)** (left).

Thus, we have performed pulsed EPR experiments a low temperature (5K) using pulse scheme excitation and detection using 2 pulses Hahn echo sequence as a function of field sweep. Such an experiment reveals the overlap of two signals respectively related to Nb(IV) and oxygen dangling bond (Figure II-14). The signal observed is isotropic with 9 lines observed with a hyperfine coupling of 205 G resulting in 70 % of fraction of the electron in niobium *d* orbitals. We can also observe the hyperfine coupling of niobium(IV) (Figure II-13), values close to the ones in literature.^[12] The intense absorption peak, corresponds to the signal of an oxo group, verifying the existence of a Nb-O bond, in which the electron is delocalized and there is an equilibrium between Nb[•]-O and Nb-O[•].

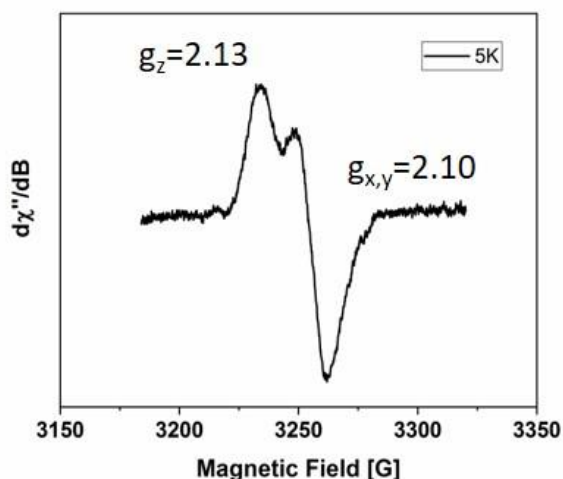


Figure II-14. Pseudo modulated spectra for the region $g=2$.

By performing Q-band experiments, we can observe a weak anisotropy of the g factor indicating that the symmetry is higher (Figure II-15). On the other side, we can assume that there is a weak coupling with nitrogen.

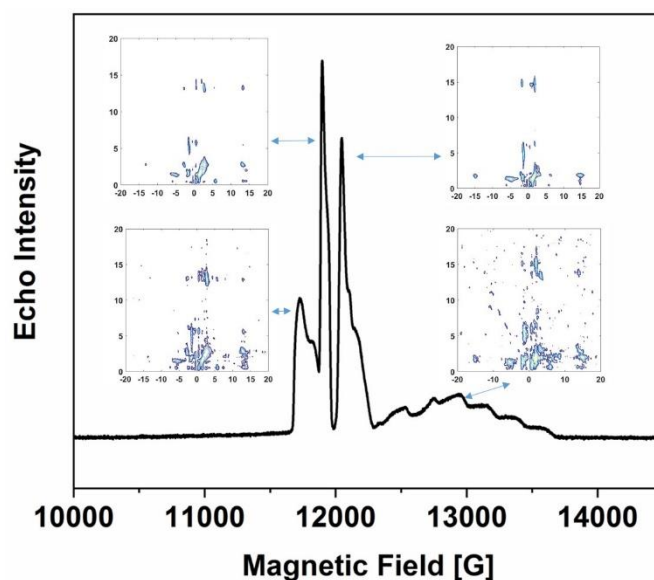


Figure II-15. Echo fieldsweep spectrum and 2D-HYSCORE spectra recorded at fourth EPR transition for **Nb(IV)-1**. Spectra were recorded at 6K.

To confirm this hypothesis, we performed 2D-HYSCORE experiments, which consist in transferring the electron magnetization to nuclear spin of surrounding nuclei in the structure. The results displayed in Figure II-16, shows that in the $(-,+)$ quadrant (strong coupling regime i.e. isotropic coupling constant $A_{iso} > 2\nu_i$, ν_i standing for the frequency of a given nuclei), we can observe a pattern arising from ^{14}N coupling with the observation of single quantum (sq)

and double quantum (dq) transitions with an isotropic coupling constant A_{iso} of 6.1 MHz (calculated at the sq cross peaks position, here at ≈ 3.05 MHz). Additionally in the (+,+) quadrant (weak coupling regime i.e. $A_{\text{iso}} < 2\nu_i$) we can observe an anti-diagonal cross peak centered at 3.6 MHz and coming from Nb coupling with a maximum coupling of 4.1 MHz.

Complexes **Nb(IV)-1** and **Nb(IV)-3** exhibit the same HYSCORE pattern whereas for **Nb(IV)-2**, ^1H nuclear frequency (at 14.5 MHz, Figure II-16-middle) is observed coming from ^1H of pyridine molecules. Oxygen is not present due to its low physical occurrence, due to its measured ^{17}O isotope. The nuclei coupling pattern observed at X band was confirmed also at Q-band by recording 2D HYSCORE spectra for oxygen transition and Nb(IV) ones (Figure II-16). For the Q-band experiment; we increase the frequency up to 34 GHz (instead of 9 GHz for X-band) resulting in the splitting of the different transitions, and were able to separate the oxygen component from the niobium(IV) ones. Same experiments also were conducted for **Nb(IV)-4**, but, the EPR experiment did not surprisingly give any signal. That led us to assume that the exchange of the electron between the d orbital of niobium and the p orbital of oxygen happens so quickly that cannot be detected in the frequencies of EPR. It would seem that the electron is more localized in the p orbital of oxygen than the d of niobium.

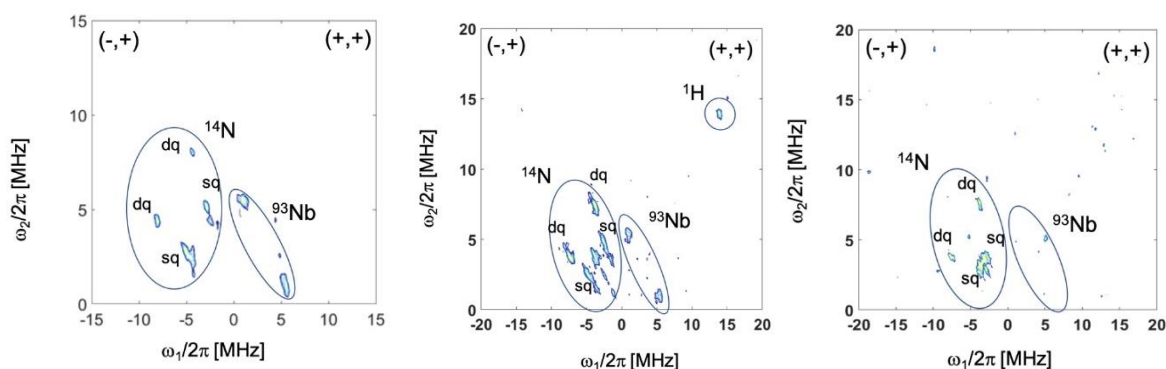


Figure II-16. 2D-HYSCORE EPR experiments for Complexes **Nb(IV)-1**, **Nb(IV)-2** and **Nb(IV)-3** EPR recorded at 5K.

II. 6 X-Ray Photoelectron Spectrometry in Nb(IV) carboxylate complexes

Due to the unexpected absence of EPR signal related to the niobium(IV) oxidation state in complex **Nb(IV)-4**, we carried out an XPS analysis in order to further investigate its Nb $4d$ electron configuration. We thus compared the XPS spectrum of compound **Nb(IV)-4**, with that of compound **Nb(IV)-1** (for which a EPR signature was typically observed due to Nb d^1 state, g

= 1.97), and with that of Nb_2O_5 , as a reference for niobium(V). Figure II-17 displays the Nb 3d spectra for the complexes **Nb(IV)-1** and **Nb(IV)-4** and the Nb_2O_5 reference.

The Nb_2O_5 spectrum is characteristic for Nb(V) species, with a doublet peak corresponding to Nb $3d^{5/2}$ and Nb $3d^{3/2}$ with the binding energy (BE) values of 207.2 eV and 209.9 eV, respectively (energy splitting of 2.72 eV).^[13] Complex **Nb(IV)-1** spectrum is composed of a doublet peak, shifted towards lower BE values as compared to Nb_2O_5 reference. The Nb $3d^{5/2}$ peak is localized at 206.4 eV and the spin-orbit splitting is 2.72 eV, which is characteristic of tetravalent state of Nb(IV) species.^[14,15] This result is consistent with all the above characterization techniques (magnetism, EPR).

Regarding the Nb 3d spectrum for the complex **Nb(IV)-4**, it is as well composed of a doublet peak with the Nb $3d^{5/2}$ component localized at 206.4 eV and a spin-orbit splitting of 2.72 eV, which matches with the values observed for the complex **Nb(IV)-1**. We can thus confirm that complex **Nb(IV)-4** consists of Nb(IV) centers, so we can confirm that we have a series of Nb(IV) complexes.

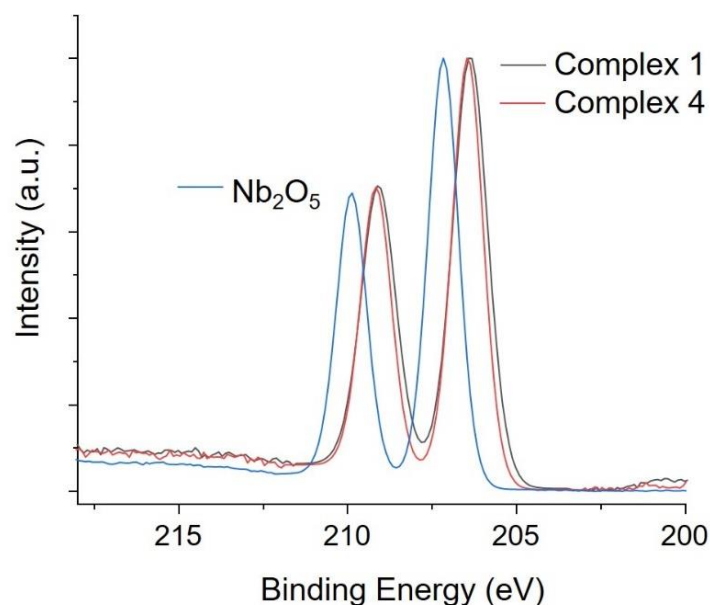


Figure II-17. Room temperature XPS spectra of the complex **Nb(IV)-1** (red line), **Nb(IV)-4** (blue line) and Nb_2O_5 (black line) at the Nb 3d edge.

II. 7 Conclusions

This chapter dealt with the synthesis and the deep characterization of four new molecular coordination niobium(IV) complexes (**Nb(IV)-(1-4)**) using pyridine-based ligands with carboxylic functions, as 2,3-pyridinedicarboxylic or 2,5-pyridinedicarboxylic acid. All

complexes were analyzed by single crystal X-ray diffraction and the tetravalent oxidation state has been confirmed by magnetism measurements and XPS, from which the d^1 electronic configuration for Nb(IV) sites is observed. EPR spectroscopy however, shows that at room temperature this d^1 electron is delocalized between the d orbital of niobium and the p orbital of oxygen. It is possible to localize the electron in the d orbital of niobium(IV) centers only in low temperature (5 K), where the hyperfine coupling of niobium(IV) is revealed. In all complexes **Nb(IV)-(1-4)**, niobium(IV) centers exhibit a similar coordination sphere, showing an eight-fold dodecahedral environment, with a $[\text{Nb}^{\text{IV}}\text{O}_4\text{N}_4]$ configuration, with four oxygen atoms deriving from the monodentate carboxylate group and four neighboring nitrogen atoms from the pyridine ring, adopting this way a triangulated dodecahedral geometry. This specific structural eight-fold coordination with a triangulated geometry around the niobium(IV) follows the Orgel concept^[3], previously reported in the niobium(IV) picolinate (2-pyridinecarboxylate).^[1] In this coordination sphere, carboxylate oxygens are considered as π -donor and nitrogens π -acceptor ligands. This Nb-O and Nb-N interatomic bond lengths are characterized by shorter (2.084(3)-2.1084(11) Å) and longer (2.266(4)-2.296(4) Å) distances, respectively. Indeed, this configuration around niobium(IV) sites is observed to be favorable by this mixed N,O ligands, where the carboxylate function involved in the coordination sphere is located in a para position compared to the nitrogen of the pyridine ring. This carboxylate, as a monodentate carboxylate group, exhibits a second free oxygen atom that in each complex that forms hydrogen bonding with the different solvent species of each preparation. These hydrogen bonds result into a unique supramolecular structure for each complex and the generation of different types of pseudo channels. The second carboxylic acid remains also free and protonated, whatever its position (either in ortho or para position with respect to the other carboxylic function) and is not complexed in the final structure. Despite the addition of different organic bases with the aim to favor the deprotonation of the carboxylic acid function, our efforts to deprotonate and link the second carboxylic function with other niobium(IV) centers through was not successful. A summarized schema of these reactions that took place in this chapter is available in Figure II-18.

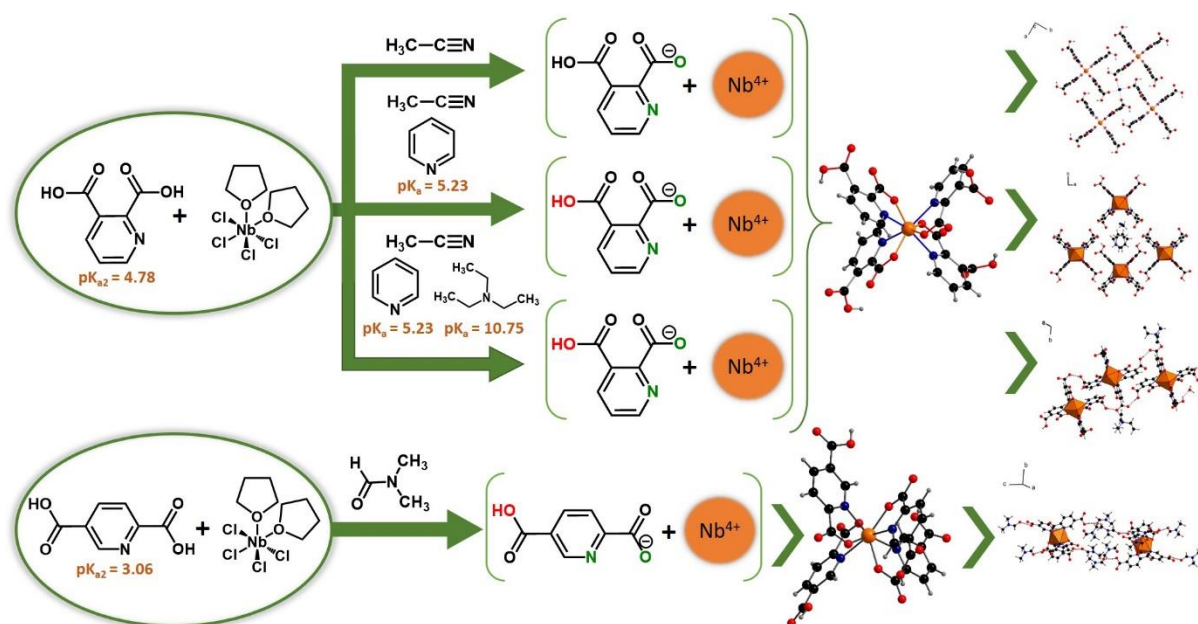


Figure II-18. Schematic representation of reaction pathways in this chapter.

As a next step, we will be focused on the use of polytopic organic linkers incorporating both N-acceptor and O-donor groups, in order to tentatively develop a niobium-based multidimensional coordination network. This work could be also extended to other tetravalent transition metals, with an ionic radius close to Nb(IV), as for Ti(IV) (Table II-6). The ionic radius of Ti(IV) is close to the one of Nb(IV) and it is a well-studied metal with which many MOFs have been reported up to date.^[16,17] Therefore, pyridine polycarboxylate ligands may present a new opportunity to isolate new Ti(IV) metal-organic frameworks with a coordination sphere of $[M^{IV}O_4N_4]$.

Table II-6. Ionic radius of Nb(IV), Sn(IV) and Ti(IV) depending on the coordination number.^[18]

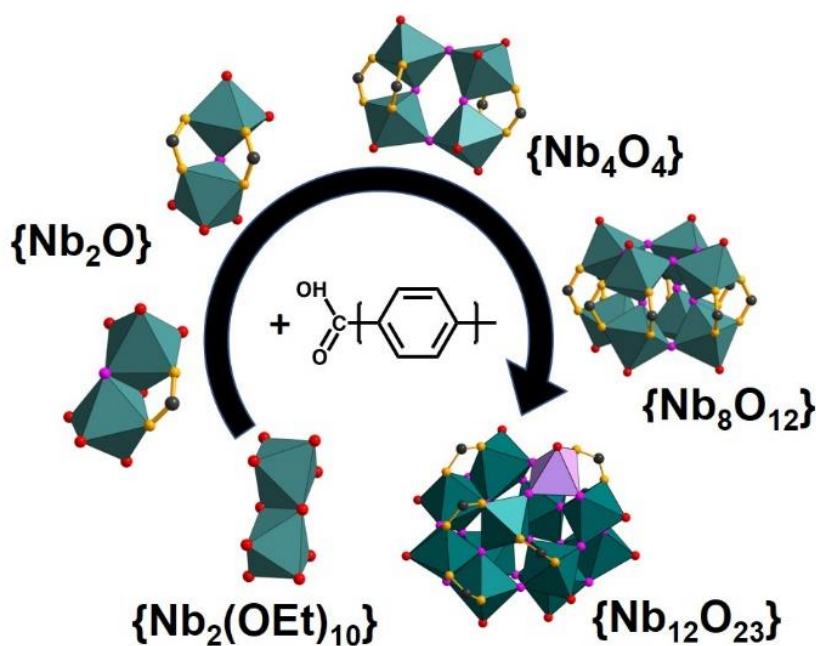
Tetravalent cation	Coordination	Ionic radius (pm)
Nb⁴⁺	6	82
	8	93
Ti⁴⁺	6	74.5
	8	88

II. 8 References

- [1] B. L. Ooi, G. Sakane, T. Shibahara, *Inorg. Chem.* **1996**, *35*, 7452–7454.
- [2] D. Andriotou, S. Duval, C. Volkringer, A. M. Arevalo-Lopez, P. Simon, H. Vezin, T. Loiseau, *Inorg. Chem.* **2022**, *61*, 15346–15358.
- [3] L. E. Orgel, *J. Inorg. Nucl. Chem.* **1960**, *14*, 136–138.
- [4] B.-L. Ooi, A. Genta Sakane, T. Shibahara, *Inorg. Chem.* **1996**, *35*, 7452–7454.
- [5] E. J. Peterson, R. B. Von Oreele, T. M. Brown, *Inorg. Chem.* **1976**, *15*, 309–315.
- [6] S. J. Lippard, B. J. Russ, *Inorg. Chem.* **1968**, *7*, 1686–1688.
- [7] P. B. Arimondo, F. Calderazzo, U. Englert, C. Maichle-Mössmer, G. Pampaloni, J. Strähle, *J. Chem. Soc. Dalton Trans.* **1996**, 311–319.
- [8] R. L. Deutscher, D. L. Kepert, *Inorganica Chim. Acta* **1970**, *4*, 645–650.
- [9] F. Calderazzo, U. Englert, C. Maichle-Mössmer, F. Marchetti, G. Pampaloni, D. Petroni, C. Pinzino, J. Strähle, G. Tripepi, *Inorganica Chim. Acta* **1998**, *270*, 177–188.
- [10] N. Steunou, C. Bonhomme, C. Sanchez, J. Vaissermann, L. G. Hubert-Pfalzgraf, *Inorg. Chem.* **1998**, *37*, 901–910.
- [11] P. W. Selwood, in *Magnetochemistry*, Interscience Publishers, New York, **1956**.
- [12] M. D. Korzyński, L. Braglia, E. Borfecchia, K. A. Lomachenko, A. Baldansuren, C. H. Hendon, C. Lamberti, M. Dincă, *Chem. Sci.* **2019**, *10*, 5906–5910.
- [13] N. Özer, D. G. Chen, C. M. Lampert, *Thin Solid Films* **1996**, *277*, 162–168.
- [14] R. Fontaine, R. Caillat, L. Feve, M. J. Guittet, *J. Electron Spectros. Relat. Phenomena* **1977**, *10*, 349–357.
- [15] Z. Weibin, W. Weidong, W. Xueming, C. Xinlu, Y. Dawei, S. Changle, P. Liping, W. Yuying, B. Li, *Surf. Interface Anal.* **2013**, *45*, 1206–1210.
- [16] X. Chen, X. Peng, L. Jiang, X. Yuan, H. Yu, H. Wang, J. Zhang, Q. Xia, *Chem. Eng. J.* **2020**, *395*, 125080.
- [17] B. M. Lee, K. J. Loh, H. L. Nguyen, *J. Phys. Energy* **2021**, *3*, 021003.
- [18] R. D. Shannon, *Acta Crystallogr. Sect. A* **1976**, *32*, 751–767.

Chapter III

Pentavalent niobium carboxylate poly-oxo clusters



In this chapter, the reactivity of a series of aryl monocarboxylic acids (benzoic, 1- or 2-naphtic, 4'-methylbiphenyl-4-carboxylic and anthracene-9-carboxylic acids), as well as di- and poly-carboxylic acids (pyromellitic acid, 4,4'-azobenzenedicarboxylic acid and 3,3',5,5'-dicarboxylic acid) has been investigated as complexing agent toward the pentavalent ethoxide niobium(V) (Nb(OEt)_5) precursor by considering the hydrolysis rate. A total of twelve crystalline molecular coordination complexes has been isolated with distinct niobium(V) nuclearities, as well as carboxylates complexation states.

CHAPTER III - Pentavalent niobium carboxylate poly-oxo clusters

This chapter focuses on the chemistry and reactivity of pentavalent niobium with carboxylates ligands. Tetravalent niobium (Chapter II) was found to be an unstable oxidation state of niobium and its handling is relatively difficult. These restrictions made us thinking of switching to the stable oxidation state of niobium, Nb(V). The high valence Nb(V) cations drawn our attention as few reports has been related to the generation of Metal-Organic Frameworks. The studies that exist in literature usually involve the incorporation of Nb(V) species into known MOF containing other metals (Chapter I, paragraph I.3), like UiO-66(Zr)-NH₂^[1], MIL-125(Ti)-NH₂^[1], NU(Zr)-1000^[2] and CPO(Co)-27^[3]. It has also been reported as a building brick of (NbOF₅)²⁻ pillars in KAUST-7^[4] among a Nb-Ni network and as a mononuclear niobium sites into a Nb-Mo network, forming a layered honeycomb lattice with 3,6-dichloro 2,5-dihydroxybenzoquinone ligand.^[5] Apart from these approaches, Nb(V) has been also reported to react with carboxylates, usually coming from oxalate precursors.^[6-10]

Herein, we will extend this study and try to control the hydrolysis process in order to isolate niobium(V) poly-oxo clusters with different nuclearities stabilized by different aromatic monocarboxylic acids. There are two commercially available precursors for Nb(V); the niobium(V) pentachloride (NbCl₅) and the niobium(V)pentaethoxide (NbOEt₅). As for Nb(IV), the chloride precursor was chosen in the first place. However, NbCl₅ found to be difficult to fully solubilize in various organic solvents (DMF, DMA, DEF, Acetonitrile, THF, ethanol, isopropanol) and to crystallize upon reaction with aromatic monocarboxylic acids (benzoic acid, naphthoic acid, 4-biphenyldicarboxylic acid, etc...). After many tries, our interest turned to the alkoxide precursor (NbOEt₅). Alkoxides are subject to hydrolysis and so all the handlings with Nb(V)ethoxide were made in a glove box under inert (argon) atmosphere. Alkoxides are also not thermally stable, so their heating up to more than 100 °C a preparation was avoided. Niobium(V)ethoxide is a pale yellowish viscous liquid (density of 1.258 g.cm⁻³) that typically adopts a monomeric structure but in solution aggregates as dimer, leading to an equilibrium between the two species (Figure III-1).^[11]

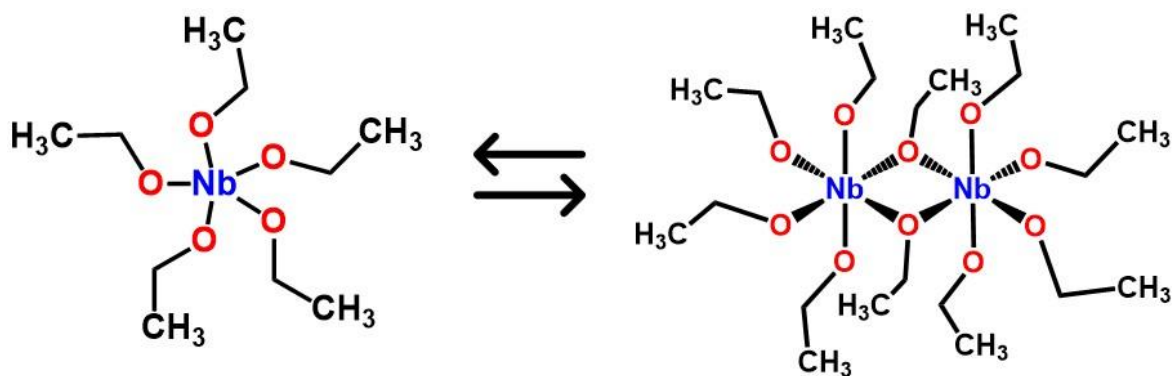


Figure III-1. Equilibrium between $Nb(OEt)_5$ and $Nb_2(OEt)_{10}$.

As $Nb(OEt)_5$ is already in liquid state, a synthetical strategy was to not use any solvent and just dilute the carboxylic acids into $Nb(V)$ ethoxide. Although solubilization is possible, the solubility is highly variable depending on the ligand selected (few minutes for benzoic and naphthoic acid to some days for pyromellitic and 3,3',5,5'-azobenzene tetracarboxylic acid). However, the addition of a co-solvent was also tested (ethanol, isopropanol, acetonitrile), but most of these systems did not lead to the production of crystallized compounds. Only isopropanol and acetonitrile proved to help the crystallization, when anthracene-9-carboxylic acid was used as carboxylate source. In this chapter we developed three different synthetical routes, according to the amount of water added to the system. The first one is the crystallization at room temperature in a closed cell system. The second one involves the use of a desiccator that contains a beaker filled with saturated solution of Na_2CO_3 to create 55 % humidity in the atmosphere. After 24 hours of exposure into the desiccator, the vial is closed and placed in an oven at 50 °C for three weeks (addition of water by exposure to humid atmosphere). The last one utilizes acetonitrile as a solvent, which one is decomposed under heating to give acetic acid and ammonia.^[12] In addition to monocarboxylic acids, di- and polycarboxylic acids were tested as well. Finally, this chapter contains the structural description of **nine Nb(V) poly-oxo clusters stabilized by monocarboxylates** (first part) and **three Nb(V) polyoxo clusters stabilized by polycarboxylates** (second part). A last part includes the study of most of these $Nb(V)$ polyoxo clusters by ^{93}Nb solid state NMR.

III. 1 Nb(V) monocarboxylate poly-oxo clusters

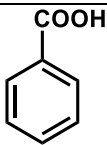
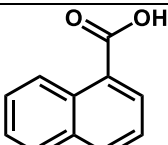
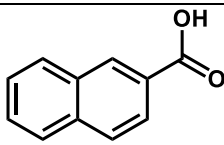
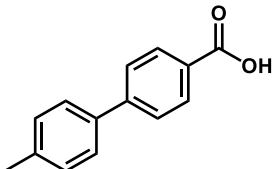
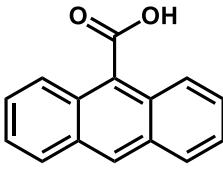
This part has been mainly just published in an october issue of Chem. Eur J. (2022, e202201464).^[13] Only the data related to the **Nb(V)-9** compound has been added and updated compared to the article.

III. 1.1 Synthesis of Nb(V) monocarboxylate complexes

In this study, different monocarboxylic acid ligands found to have great reactivity with the commercially available ethoxide complex Nb(OEt)₅ with isopropanol or acetonitrile, or without the presence of additional organic solvent resulting to dinuclear and polynuclear Nb(V) complexes. The reactions occur after the mixing of the precursors at room temperature in a closed vial. X-ray diffraction quality crystals can be collected after leaving the reaction vial at room temperature from some days to some months. In some cases, and in order to obtain the polynuclear entities, the synthetical protocol is changed with an increase of the temperature up to 120 °C. The synthesized compounds have been characterized by X-ray diffraction techniques (powder and single-crystal analysis), infrared spectroscopy, liquid NMR and solid state nuclear magnetic resonance.

We were able to isolate nine molecular poly-oxo clusters by using the different monocarboxylic acids shown in Table III-1.

Table III-1. Monocarboxylic acids used in synthesis to isolate nine Nb(V) poly-oxo clusters.

Ligands		
		
benzoic acid	1-naphthoic acid	2-naphthoic acid
		
4'-methyl-[1,1'-biphenyl]-4-carboxylic acid		anthracene-9-carboxylic acid

All synthesis protocols are summarized in the following Table III-2 and explained later in details.

Table III-2. Synthetical protocols for **Nb(V)-(1-9)**.

	Metal source	Ligand	Solvent	T	Time	Yield
Nb(V)-1	Nb(OEt) ₅ 0.75 mL 3 mmol	Benzoic acid 756.4 mg 6.2 mmol	-	RT	1 m	24.5 %
Nb(V)-2	Nb(OEt) ₅ 0.75 mL 3 mmol	2-naphthoic acid 1033 mg 6 mmol	-	RT	5 d	6.1 %
Nb(V)-3	Nb(OEt) ₅ 0.75 mL 3 mmol	1-naphthoic acid 1033 mg 6 mmol	-	RT	6 m	2.4 %
Nb(V)-4	Nb(OEt) ₅ 0.75 mL 3 mmol	4'-methylbiphenyl-4-carboxylic acid 1273 mg 6mmol	-	RT	3 w	19.1 %
Nb(V)-5	Nb(OEt) ₅ 0.75 mL 3 mmol	anthracene-9-carboxylic acid 222.2 mg 1 mmol	-	RT	2 w	13.1 %
Nb(V)-6	Nb(OEt) ₅ 0.2 mL 0.8 mmol	anthracene-9-carboxylic acid 85.3 mg 0.3 mmol	Isopropanol 1 mL 13.1 mmol	RT	2 w	4.8 %
Nb(V)-7	Nb(OEt) ₅ 0.2 mL 0.8 mmol	2-naphthoic acid 145 mg 0.85 mmol	-	50 °C	3 w	9.7 %
Nb(V)-8	Nb(OEt) ₅ 60 µL 0.24 mmol	2-naphthoic acid 460 mg 2.7 mmol	Acetonitrile 1 mL 19.1 mmol	100 °C	4 d	11.6 %
Nb(V)-9	NbCl ₄ (THF) ₂ 12 mg 0.05 mmol	anthracene-9-carboxylic acid 85.3 mg 0.3 mmol	Isopropanol 1 mL 13.1 mmol	120 °C	5 d	2.2 %

Compound Nb(V)-1 [Nb₄(μ₂-O)₄(C₇H₅O₂)₄(OEt)₈]: A mixture of 0.75 mL (3 mmol) Nb(OCH₂CH₃)₅ and 756.4 mg (6.2 mmol) benzoic acid was placed in a 2 mL glass tube, sealed with a phenolic cap, and left at room temperature. The formation of brick-like colorless crystals, was observed after one month. Compound **Nb(V)-1** was analyzed by optical microscope showing large elongated parallelepiped-shape crystals up to 1 mm size. The resulting colorless crystals filtered off, washed with ethanol and dried at room temperature. Crystallization yield was 24.5 %_{Nb}. (Figure III-2).

Compound Nb(V)-2 [Nb₂(μ₂-O)(C₁₁H₇O₂)₂(OEt)₆]: A mixture of 0.75 mL (3 mmol) Nb(OCH₂CH₃)₅ and 1.033 mg (6 mmol) 2-naphthoic acid was placed in a 2 mL glass tube, sealed with a phenolic cap, and left at room temperature. Baguette-like transparent crystals appeared after 5 days. Compound **Nb(V)-2** was analyzed by optical microscope showing large

elongated parallelepiped-shape crystals up to 300 μm size. The resulting colorless crystals filtered off, washed with ethanol and dried at room temperature. Crystallization yield was 6.1 %_{Nb}. (Figure III-2).

Compound Nb(V)-3 $[\text{Nb}_2(\mu_2\text{-O})(\mu_2\text{-OEt})(\text{C}_{11}\text{H}_7\text{O}_2)(\text{OEt})_6]$: A mixture of 0.75 mL (3 mmol) $\text{Nb}(\text{OCH}_2\text{CH}_3)_5$ and 1.033 mg (6 mmol) 1-naphthoic acid was placed in a 2 mL glass tube, sealed with a phenolic cap, and left at room temperature. Baguette-like transparent crystals appeared after 6 months. Compound **Nb(V)-3** was analyzed by optical microscope showing large elongated parallelepiped-shape crystals up to 300 μm size. The resulting colorless crystals filtered off, washed with ethanol and dried at room temperature. Crystallization yield was 2.4 %_{Nb}. (Figure III-2).

Compound Nb(V)-4 $[\text{Nb}_2(\mu_2\text{-O})(\text{C}_{14}\text{H}_{11}\text{O}_2)_2(\text{OEt})_6]$: A mixture of 0.75 mL (3 mmol) $\text{Nb}(\text{OCH}_2\text{CH}_3)_5$ and 1.273 mg (6 mmol) 4'-methylbiphenyl-4-carboxylic acid was placed in a 2 mL glass tube, sealed with a phenolic cap, and left at room temperature. Plate-like crystals appeared after 3 weeks. Compound **Nb(V)-4** was analyzed by optical showing elongated parallelepiped-shape crystals up to 40 μm size. The resulting colorless crystals filtered off, washed with ethanol and dried at room temperature. Crystallization yield was 19.1 %_{Nb}. (Figure III-2).

Compound Nb(V)-5 $[\text{Nb}_2(\mu_2\text{-O})(\mu_2\text{-OEt})(\text{C}_{15}\text{H}_9\text{O}_2)(\text{OEt})_6]_2$: A mixture of 0.75 mL (3 mmol) $\text{Nb}(\text{OCH}_2\text{CH}_3)_5$ and 222.24 mg (1 mmol) anthracene-9-carboxylic acid was placed in a 2 mL glass tube, sealed with a phenolic cap, and left at room temperature. Brick-like crystals appeared after 2 weeks. Compound **Nb(V)-5** was analyzed by optical microscope showing block-shape crystals up to 30 μm size. The resulting pale yellowish crystals filtered off, washed with ethanol and dried at room temperature. Crystallization yield was 13.1 %_{Nb}. (Figure III-2).

Compound Nb(V)-6 $[\text{Nb}_2(\mu_2\text{-O})(\text{C}_{15}\text{H}_9\text{O}_2)_2(\text{O}^i\text{Pr})_6]$: A mixture of 0.2 mL (0.8 mmol) $\text{Nb}(\text{OCH}_2\text{CH}_3)_5$ and 85.3 mg (0.3 mmol) anthracene-9-carboxylic acid, isopropanol 1 mL (13.1 mmol) was placed in a 2 mL glass tube, sealed with a phenolic cap, and left at room temperature. Brick-like transparent crystals appeared after 2 weeks. Compound **Nb(V)-6** was analyzed by optical microscope showing large block-shape crystals up to 50 μm size. The resulting colorless crystals filtered off, washed with ethanol and dried at room temperature. Crystallization yield was 4.8 %_{Nb}. (Figure III-2).

Compound Nb(V)-7 $[\text{Nb}_4(\mu_2\text{-O})_4(\text{C}_{11}\text{H}_7\text{O}_2)_4(\text{OEt})_8]$: A mixture of 0.2 mL (0.8 mmol) $\text{Nb}(\text{OCH}_2\text{CH}_3)_5$ and 145 mg (0.85 mmol) 2-naphthoic acid was placed in a 2 mL glass tube, sealed with a phenolic cap in inert atmosphere. The vial was placed in a desiccator with a saturated solution of Na_2CO_3 (55 % humidity) with an open cap and after 24 hours was closed and the vial was placed in the oven at 50°C. Only a powdered sample is obtained, in which needle-like transparent crystals are observed after 3 weeks. Compound **Nb(V)-7** was analyzed by optical microscope showing large elongated parallelepiped-shape crystals up to 150 μm size. The resulting colorless crystals filtered off, washed with ethanol and dried at room temperature. Crystallization yield was 9.7 %_{Nb} (Figure III-2).

Compound Nb(V)-8 $[\text{Nb}_8(\mu_2\text{-O})_{12}(\text{C}_{11}\text{H}_7\text{O}_2)_8(\eta_1\text{-C}_{11}\text{H}_7\text{O}_2)_4(\text{OEt})_4] \cdot [\text{Nb}_8(\mu_2\text{-O})_{12}(\text{C}_{11}\text{H}_7\text{O}_2)_8(\eta_1\text{-C}_{11}\text{H}_7\text{O}_2)_2(\text{OEt})_6]$: A mixture of 60 μL (0.24 mmol) $\text{Nb}(\text{OCH}_2\text{CH}_3)_5$, 460 mg (2.7 mmol) 2-naphthoic acid and acetonitrile (1 mL, 19.1 mmol) was placed in a 2 mL glass tube, sealed with a phenolic cap, and placed in an oven at 100 °C. After 4 days, dark red parallelepiped blocks appeared and as the temperature decreases we observe the recrystallisation of 2-naphthoic acid and finally no supernatant is obtained. Compound **Nb(V)-8** was analyzed by optical microscope showing large parallelepiped-shape crystals up to 40 μm size. The resulting dark red crystals filtered off, washed with acetonitrile and dried at room temperature. Crystallization yield was 11.6 %_{Nb}. (Figure III-2).

Compound Nb(V)-9 $[\text{Nb}_{12}(\mu_2\text{-O})_{20}(\mu_3\text{-O})_2(\text{C}_{15}\text{H}_9\text{O}_2)_8(\text{Pr}^i\text{OH})_5]$: A mixture of 12 mg (0.05 mmol) $\text{NbCl}_4(\text{THF})_2$, 50 mg (0.23 mmol) anthracene-9-carboxylic acid and isopropanol (1 mL, 13.1 mmol) was placed in a 2 mL glass tube, sealed with a phenolic cap, and placed in an oven at 120 °C. After 5 days orange parallelepiped blocks appeared. Compound **Nb(V)-9** was analyzed by optical microscope showing large parallelepiped-shape crystals up to 100 μm size. The resulting orange crystals filtered off, washed with isopropanol and dried at room temperature. Crystallization yield was 4.2 %_{Nb}. (Figure III-2).

All niobium-based coordination monocarboxylate complexes **Nb(V)-(1-9)** were found to be stable under air for several weeks and manipulated without any specific precaution. The purity of all nine complexes have been evaluated by powder X-ray diffraction (Figure A3, paragraph A3, Appendix).

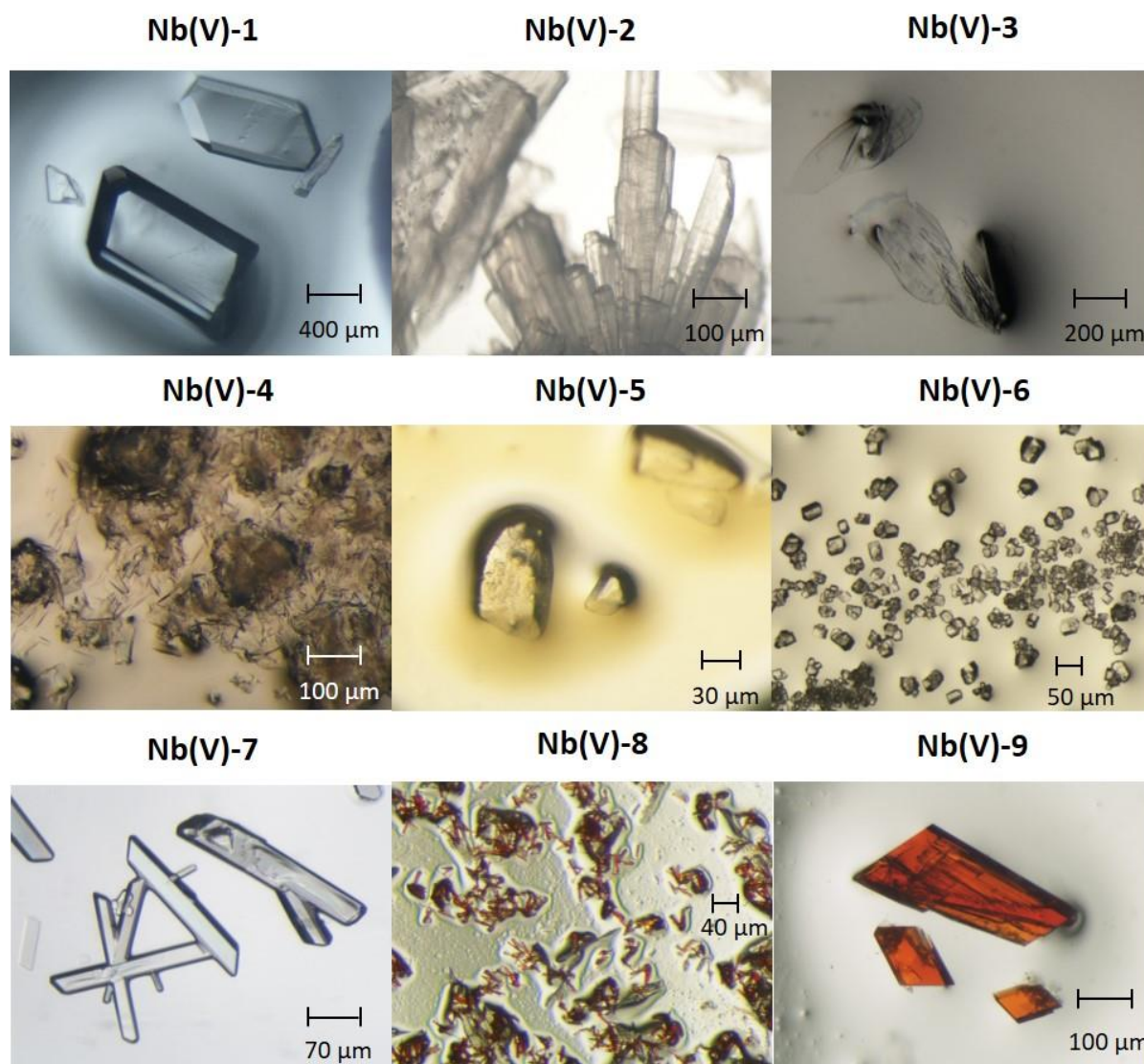


Figure III-2. Crystals of compounds **Nb(V)**-(1-9) from top left to bottom right under optical microscope.

III. 1.1.2 Synthesis route discussion

The systematic reaction of the niobium ethoxide precursor with different benzene-based monocarboxylic acids gave rise to the identification of nine distinct coordination complexes, with nuclearities rising from 2 to 8. Beside the carboxylate complexation, the common feature is the occurrence of one or several μ_2 -oxo groups bridging two adjacent niobium centers. Indeed, this bridging oxygen atom is not present in the initial niobium ethoxide source $\text{Nb}(\text{OEt})_5$, but the latter is able to undergo dimerization reaction, generating a dinuclear niobium precursor, and still without any μ_2 -oxo bridge. The niobium centers of this precursor are present as one or multiple Nb-pairs in these molecular species (1 x Nb_2 (**Nb(V)**-(2-6)), 2 x Nb_2 (**Nb(V)**-1 and **Nb(V)**-7), 4 x Nb_2 (**Nb(V)**-8)) (except for **Nb(V)**-9, for which $\text{NbCl}_4(\text{THF})_2$ was used as a metallic precursor instead). These moieties correspond to dinuclear

{Nb₂O}, tetranuclear {Nb₄O₄} or octanuclear {Nb₈O₁₂} niobium(V)-centered poly-oxo clusters related to different hydrolysis rate. Hydrolysis process was controlled by temperature, as heating up favorize hydrolysis. For example, in the case of Nb(V)-naphthoates (**Nb(V)-2**, **Nb(V)-7** and **Nb(V)-8**), **Nb(V)-2** is crystallizing in room temperature, **Nb(V)-7** at 50 °C and **Nb(V)-8** at 100 °C. Adding a solvent in the reaction mixture proved helpful for solubilize more ligand and increase the nuclearity (**Nb(V)-6** and **Nb(V)-8**). However, for synthesizing **Nb(V)-9** the strategy was to keep the same synthetical conditions as **Nb(V)-6** and only change to a more familiar precursor, niobium(IV) chloride (NbCl₄(THF)₂) (see chapter II), and was found to unexpectedly oxidized in Nb(V). Thus, we were able to isolate a dodecameric Nb(V) poly-oxo cluster.

III. 1.2 Structural description

All the compounds **Nb(V)-1** → **Nb(V)-9** have been characterized by single-crystal X-ray diffraction analysis. The summary of the crystallographic data is summarized in the following Table III-3.

Chapter III : Pentavalent niobium carboxylate poly-oxo clusters

Table III-3. Crystal data and structure refinements for compounds Nb(V)-(1 – 9).

	Nb(V)-1	Nb(V)-2	Nb(V)-3	Nb(V)-4	Nb(V)-5	Nb(V)-6	Nb(V)-7	Nb(V)-8	Nb(V)-9
Formula	C ₁₁ H ₁₅ NbO ₅	C ₃₄ H ₄₄ Nb ₂ O ₁₁	C ₂₅ H ₄₂ Nb ₂ O ₁₀	C ₄₀ H ₅₂ Nb ₂ O ₁₁	C ₅₈ H ₈₈ Nb ₄ O ₂₀	C ₁₉₂ H _{236.5} Nb ₈ O ₄₄	C ₆₀ H ₆₈ Nb ₄ O ₂₀	C ₂₆₂ H ₂₀₄ Nb ₁₆ O ₇₈	C ₃₀₀ H ₂₈₄ Nb ₂₄ O ₉₄
Formula weight	320.14	814.51	688.4	894.64	1476.92	3991.58	1214.54	6086.80	7623.09
Temperature/K	296	102	100	100	100	100	100	100	99.98
Crystal type	colorless parallelepiped	colorless parallelepiped	colorless parallelepiped	colorless parallelepiped	colorless parallelepiped	yellowish plate	colorless needle	colorless needle	orange parallelepiped
Crystal size/mm	0.20 x 0.19 x 0.13	0.99 x 0.66 x 0.30	0.58 x 0.26 x 0.10	0.13 x 0.12 x 0.11	0.31 x 0.26 x 0.13	0.28 x 0.16 x 0.10	0.42 x 0.10 x 0.09	0.02 x 0.02 x 0.01	0.04 x 0.015 x 0.015
Crystal system	triclinic	monoclinic	orthorhombic	monoclinic	triclinic	monoclinic	monoclinic	monoclinic	triclinic
Space group	<i>P</i> -1	<i>P</i> 2 ₁ / <i>c</i>	<i>P</i> 2 ₁ 2 ₁ 2 ₁	<i>C</i> 2/ <i>c</i>	<i>P</i> -1	<i>C</i> 2/ <i>c</i>	<i>P</i> 2 ₁ / <i>c</i>	<i>C</i> 2/ <i>c</i>	<i>P</i> -1
<i>a</i>/Å	10.8589(6)	20.228(2)	8.1182(14)	25.4759(7)	11.7194(6)	21.839(2)	10.9286(10)	67.5185(14)	18.9105(8)
<i>b</i>/Å	11.9022(6)	8.5199(8)	19.040(3)	9.0694(3)	14.1832(7)	9.9717(11)	20.1535(15)	10.7915(2)	30.3622(13)
<i>c</i>/Å	12.4716(6)	20.738(2)	19.081(3)	17.9087(4)	20.3412(10)	21.376(2)	16.3901(13)	47.1089(9)	31.0424(14)
α/°	72.281(2)	90	90	90	102.816(3)	90	90	90	111.3772(16)
β/°	70.918(2)	97.487(3)	90	101.834(1)	95.187(2)	95.901(3)	120.679(3)	134.142(1)	97.6406(17)
γ/°	67.815(2)	90	90	90	99.809(3)	90	90	90	103.9729(17)
Volume/Å³	1380.08(13)	3543.5(6)	2946.4(9)	4049.9(2)	3219.6(3)	4630.6(8)	3104.7(5)	24595.5(9)	15617.1(12)
Z	4, 1.541	4, 1.527	4, 1.550	4, 1.467	2, 1.523	1, 1.431	2, 1.584	4, 1.644	2, 1.621
ρ_{calculated}/g.cm⁻³	0.878	0.704	0.827	0.623	0.764	0.553	0.793	1.114	0.993
μ/mm⁻¹	0.878	0.704	0.827	0.623	0.764	0.553	0.793	1.114	0.993
θ range/°	1.77 - 26.40	2.11 - 30.53	1.51 - 26.42	1.63 - 26.39	1.50 - 30.53	1.92 - 26.42	1.76 - 26.39	0.92 - 25.00	1.49 - 55.492
Limiting indices	-13 ≤ <i>h</i> ≤ 13 -14 ≤ <i>k</i> ≤ 14 -15 ≤ <i>l</i> ≤ 15	-28 ≤ <i>h</i> ≤ 28 -12 ≤ <i>k</i> ≤ 10 -21 ≤ <i>l</i> ≤ 29	-9 ≤ <i>h</i> ≤ 10 -23 ≤ <i>k</i> ≤ 22 -23 ≤ <i>l</i> ≤ 23	-31 ≤ <i>h</i> ≤ 31 -11 ≤ <i>k</i> ≤ 11 -22 ≤ <i>l</i> ≤ 19	-16 ≤ <i>h</i> ≤ 16 -16 ≤ <i>k</i> ≤ 20 -29 ≤ <i>l</i> ≤ 29	-27 ≤ <i>h</i> ≤ 27 -12 ≤ <i>k</i> ≤ 12 -26 ≤ <i>l</i> ≤ 26	-13 ≤ <i>h</i> ≤ 13 -23 ≤ <i>k</i> ≤ 25 -18 ≤ <i>l</i> ≤ 20	-77 ≤ <i>h</i> ≤ 76 -10 ≤ <i>k</i> ≤ 10 -55 ≤ <i>l</i> ≤ 55	-22 ≤ <i>h</i> ≤ 22 -33 ≤ <i>k</i> ≤ 33 -32 ≤ <i>l</i> ≤ 34
Collected reflections	36059	60031	20882	30431	8430	36900	24721	84196	150210
Unique reflections	5642 [R(int) = 0.0245]	10808 [R(int) = 0.0267]	5810 [R(int) = 0.0581]	4132 [R(int) = 0.0396]	19179 [R(int) = 0.0259]	4753 [R(int) = 0.0287]	6330 [R(int) = 0.0964]	10386 [R(int) = 0.0506]	47641 [R(int) = 0.0409]
Parameters	301	466	342	254	814	303	383	1296	3443
Goodness-of-fit on F²	1.080	1.044	1.053	1.048	1.067	1.046	1.007	1.107	1.084
Final R indices [I>2σ(I)]	R1 = 0.0430 wR2 = 0.1193	R1 = 0.0332 wR2 = 0.0772	R1 = 0.0387 wR2 = 0.0661	R1 = 0.0272 wR2 = 0.0647	R1 = 0.0319 wR2 = 0.0780	R1 = 0.0292 wR2 = 0.0695	R1 = 0.0539 wR2 = 0.1081	R1 = 0.1008 wR2 = 0.3164	R1 = 0.0772 wR2 = 0.2555
R indices (all data)	R1 = 0.0563 wR2 = 0.1364	R1 = 0.0360 wR2 = 0.0799	R1 = 0.0504 wR2 = 0.0691	R1 = 0.0366 wR2 = 0.0687	R1 = 0.0393 wR2 = 0.0820	R1 = 0.0325 wR2 = 0.07151	R1 = 0.1072 wR2 = 0.1292	R1 = 0.1280 wR2 = 0.3328	R1 = 0.0881 wR2 = 0.2699
Largest diff. peak and hole/e.Å⁻³	1.48 and -0.97	1.58 and -3.39	0.77 and -0.68	0.41 and -0.42	1.57 and -1.14	0.93 and -0.54	0.71 and -1.17	1.38 and -0.94	1.61 and -1.45

Compound Nb(V)-1 [$\text{Nb}_4(\mu_2\text{-O})_4(\text{C}_7\text{H}_5\text{O}_2)_4(\text{OEt})_8$]

The crystal structure of compound **Nb(V)-1** is described from a centrosymmetric molecular tetranuclear core (Figure III-3) bearing two crystallographically independent niobium atoms (Nb1 and Nb2). Both cationic centers are six-fold coordinated with two μ_2 -oxo groups (Nb1-O3 = 1.913(3) Å; Nb1-O4 = 1.899(3) Å; Nb2-O3 = 1.918(3); Nb2-O4 = 1.885(3) Å), two carboxyl oxygen atoms from benzoate ligands (Nb1-O_c = 2.172(3)-2.176(3) Å; Nb2-O_c = 2.154(3)-2.178(3) Å) and two oxygen atoms from ethoxy groups (Nb1-O_{Et} = 1.833(4)-1.888(3) Å; Nb2-O_{Et} = 1.850(4)-1.883(3) Å). The presence of the bridging μ_2 -oxo group agrees well with bond valence calculations 1.976 for O3; 2.106 for O4)^[14]. The μ_2 -oxo groups are bridging two adjacent niobium atoms and are located in *cis* position in the {NbO₆} octahedra, resulting in a square ring of Nb1-O-Nb2 bondings within the tetrameric brick. The Nb1...Nb2 bond lengths are in the range 3.649(5)-3.664(4) Å, with Nb-O-Nb angles of 146.0(2)° (concave bending of Nb1-O3-Nb2 bond) and 149.3(2)° (convex bending of Nb1-O4-Nb2 bond). For one Nb1-O3-Nb2 sub-unit, the carboxylate arms from the benzoate molecule occupy a *cis* position, leading to one benzene group located along the Nb1-O3-Nb2 square plane, and a second benzene group placed either up or down perpendicularly to Nb1-O3-Nb2 square plane. The carboxylate group adopts a *syn-syn* bidentate bridging fashion with two neighboring niobium centers Nb1 and Nb2, linked through the μ_2 -O3 groups only. The neutral tetranuclear core is decorated by ethoxy groups attached to the niobium atoms. One of them (O8) linked to Nb1, is found to be disordered on two crystallographic positions. This tetrameric building block {Nb₄O₄} can be seen as the association of two dinuclear sub-units of type [Nb₂(μ_2 -O)(C₇H₅O₂)₂(OEt)₆], closely structurally related to that of coordination complexes **Nb(V)-(2-3)** (see hereafter). For those, two sets of two ethoxy groups has been formally substituted by one additional μ_2 -oxo group (here O4) in order to generate the Nb-O-Nb linkage within the square ring system. It is the fourth example of such a brick with niobium(V) synthesized in the presence of carboxylic acids. Previous studies reported a similar core, with different monocarboxylate linkers, such as methacrylate^[15], acetate^[16] and tertbutylacetate^[17]. A related tetranuclear coordination complex was also described with salicylate groups associated with bismuth^[18]. Due to the presence of bismuth, the off-planar benzene rings of the salicylate molecules are all located in one side of the tetranuclear core, and the alkoxy molecules (isopropanol) are located on the opposite side. At last, this tetramer {Nb₄O₄} is suggested in the work reported by Brown

et al. as a possible analog of the parent tantalum(V) benzoate derivatives (benzoate, para-methoxybenzoate and para-fluorobenzoate).^[19]

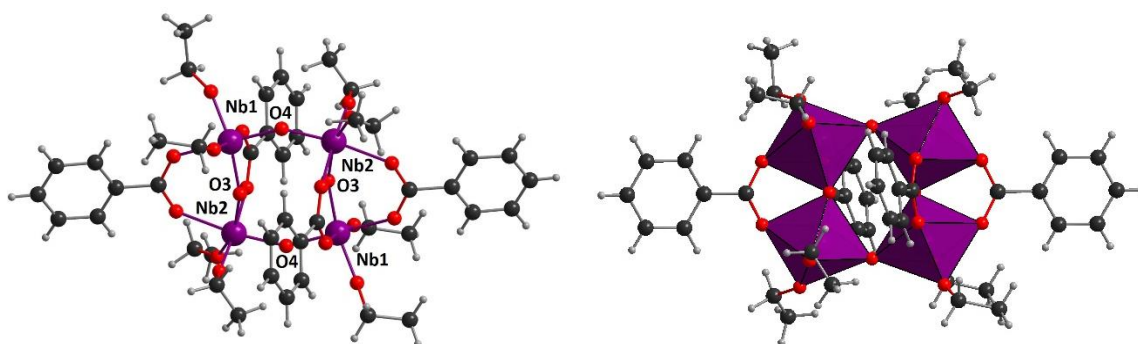


Figure III-3. Ball and stick (left) and polyhedral (right) representations of the molecular tetranuclear coordination complex **Nb(V)-1**. One of the ethoxy groups linked to Nb1 site (through Nb1-O8 bonding) is disordered on two equivalent positions. Only one of these ethoxy groups is shown for clarity.

Compound **Nb(V)-2** $[\text{Nb}_2(\mu_2\text{-O})(\text{C}_{11}\text{H}_7\text{O}_2)_2(\text{OEt})_6]$

The crystal structure of compound **Nb(V)-2** is built up from one neutral molecular dinuclear species, containing two different crystallographically independent niobium(V) centers (Nb1 and Nb2), with a distorted octahedral geometry (Figure III-4). Each of them is coordinated with the same configuration, three oxo groups from ethoxy molecules (Nb1-O_{Et} in the range 1.873(1)-1.880(1) Å; Nb2-O_{Et} in the range 1.865(2)-1.908(2) Å), two oxo groups from the carboxylate arm of the 2-naphtoate ligand (Nb1-O_c in the range 2.179(1)-2.195(1) Å; Nb2-O_c in the range 2.137(2)-2.156(1) Å) and one bridging μ_2 -oxo groups with Nb1-O5 bond length of 1.930(1) Å and Nb2-O5 bond length of 1.908(1) Å. The occurrence of bridging μ_2 -oxo species agrees well with bond valence calculations (1.958 for expected value of 2 for oxo)^[14]. Within the dinuclear core, the niobium-centered octahedral polyhedra are sharing one corner, with a Nb1...Nb2 distance of 3.667(4) Å. The niobium atoms are further linked to each other through two bidentate carboxylate arms of the two distinct 2-naphtoate ligands, with a *syn-syn* bridging mode. The two 2-naphtoate molecules are located in a *cis* position, creating a tilting angle 145.7(8)° for the Nb1-O5-Nb2 bonding. This arrangement is closely related to those encountered in the niobium(V) oxo-chloride $[\{\text{NbCl}_3(\text{C}_7\text{H}_5\text{O}_2)\}_2(\mu_2\text{-O})]$ stabilized by two benzoate ligands^[19] or in the niobium oxo-neopentyl alcohol $[\{\text{Nb}(\text{ONep})_3(\text{C}_5\text{H}_{10}\text{O}_2)\}_2(\mu_2\text{-O})]$ stabilized by two pivalate ligands^[17]. Both monocarboxylate linkers adopt a similar bidentate bridging *cis* fashion: for the benzoate case, the Nb-O-Nb bridge was found to be bent with an angle of 143.2°, since it is 144.0(4)° for the pivalate case.

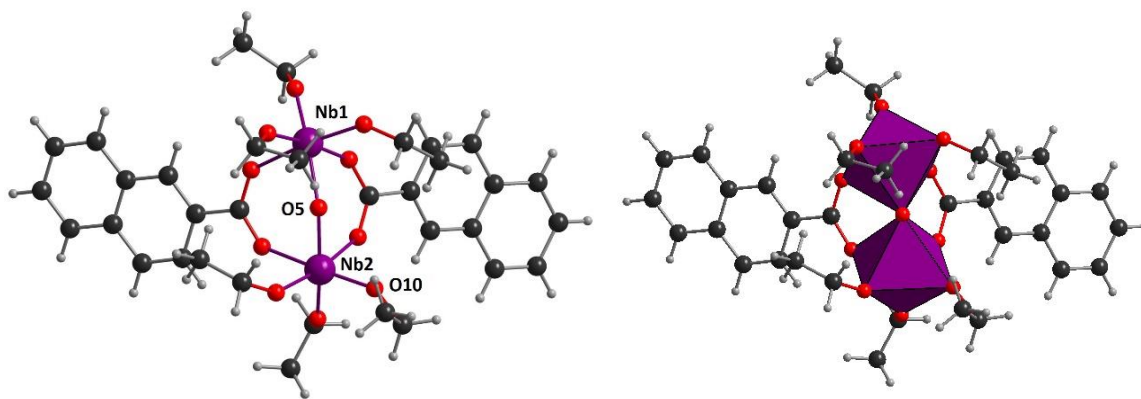


Figure III-4. Ball and stick (left) and polyhedral (right) representations of the molecular dinuclear coordination complex **Nb(V)-2**. One of the ethoxy groups linked to Nb2 site (through Nb2-O10 bonding) is disordered on two equivalent positions. Only one of these ethoxy groups is shown for clarity.

Compound **Nb(V)-3** [$\text{Nb}_2(\mu_2\text{-O})(\mu_2\text{-OEt})(\text{C}_{11}\text{H}_7\text{O}_2)(\text{OEt})_6$]

The compound **Nb(V)-3** crystallizes in a non-centric space group $P2_12_12_1$, and exhibits a structure built up from two crystallographically independent niobium(V) centers (Nb1 and Nb2) (Figure III-5). Both cations are octahedrally coordinated with three oxo groups from ethoxy molecules (Nb1-O_{Et} in the range 1.848(3)-1.903(4) Å; Nb2-O_{Et} in the range 1.878(4)-1.901(4) Å), one oxo groups from the carboxylate arm of the 1-naphthoate ligand (Nb1-O1_c = 2.216(3) Å; Nb2-O2_c = 2.204(2) Å), one bridging μ_2 -ethoxy group with Nb1-O6 bond length of 2.130(4) Å and Nb2-O6 bond length of 2.128(4) Å, and one bridging μ_2 -oxo groups with Nb1-O10 bond length of 1.952(4) Å and Nb2-O10 bond length of 1.918(5) Å. The bond valence of the μ_2 -oxo species is 1.72, close to that of 2 expected for such species^[14]. In this coordination complex, only one 1-naphthoate molecule is found and the carboxylate arm adopts a *syn-syn* bidentate bridging connecting mode with the two distinct niobium atoms Nb1 and Nb2. This configuration differs from the previous complex **Nb(V)-2**, for which two 1-naphthoate ligands were observed in *cis* position. The occurrence of the single carboxylate bridge together with the bridging μ_2 -ethoxy group induces a shortening of the Nb1...Nb2 distance, which is 3.2277(10) Å, instead of 3.667(4) Å in the dinuclear core of compound **Nb(V)-2**, and resulting in a tilting angle 113.0(2)° for the Nb1-O10-Nb2 bonding. The niobium-centered octahedral polyhedra are therefore linked through an edge-sharing mode via the μ_2 -oxo and μ_2 -ethoxy groups. The metric values of Nb...Nb lengths are smaller than those observed in the niobium-based dimeric moieties bearing two bridging alkoxides species, such as a μ_2 -methoxy bridge (Nb...Nb = 3.493 Å^[20]; Nb...Nb = 3.450 Å^[21] or a μ_2 -ethoxy bridge (Nb...Nb = 3.518 Å^[22]). Indeed,

the occurrence of the bridging μ_2 -oxo group with smaller Nb-O bond distance decreases the Nb \cdots Nb lengths in compound **Nb(V)-3**, when an additional bridging μ_2 -ethoxy group is present. At the opposite, the Nb \cdots Nb lengths are increased when lacking the μ_2 -ethoxy group, which are substituted by a second carboxylate pincer as found in the compound **Nb(V)-2**. One may also notice that the Nb \cdots Nb distance from edge-sharing $\{\text{NbO}_6\}$ octahedra in the dense purely inorganic B form of Nb_2O_5 ^[23], is 3.404 Å, and close to the value reported in the dimeric niobium alkoxides. It is interesting to notice that the position of carboxylate arm on the naphthalene group induces either a monocarboxylate coordination complex in compound **Nb(V)-3** (position 1) or a dicarboxylate coordination complex in compound **Nb(V)-2** (position 2).

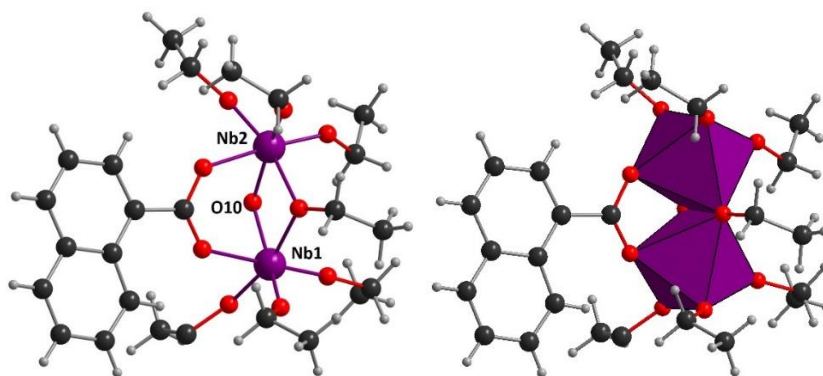


Figure III-5. Ball and stick (left) and polyhedral (right) representations of the molecular dinuclear coordination complex **Nb(V)-3**.

Compound **Nb(V)-4** [$\text{Nb}_2(\mu_2\text{-O})(\text{C}_{14}\text{H}_{11}\text{O}_2)_2(\text{OEt})_6$]

The crystal structure of compound **Nb(V)-4** exhibits the same dinuclear motif (Figure III-6) as found for compound **Nb(V)-2**, except that the centrosymmetric molecular moiety results in only one crystallographically independent niobium(V) center (Nb1). The latter is octahedrally coordinated through three oxo groups from ethoxy molecules, with Nb1-O_{Et} bond distances varying from 1.868(2) Å to 1.887(2) Å, two oxo groups from carboxylate arms (Nb1-O1_c = 2.167(2) Å and Nb1-O2_c = 2.169(2) Å), and one bridging μ_2 -oxo group (Nb1-O3 = 1.914(1) Å). The bond valence calculation for this oxygen O3 atom gives the value of 1.984, in agreement with the occurrence of an oxo group^[14]. The oxygen O3 atom sits on the special position 4e (axis 2 point symmetry), resulting in two equivalent niobium atoms forming the dimeric unit, in which the Nb1 \cdots Nb1 distance is 3.645(2) Å, related to the tilting angle of 144.42(2)° for the Nb1-O3-Nb1 bonding. As for compound **Nb(V)-2**, two carboxylate groups

from two distinct 4-methyl-biphenylmonocarboxylate ligands are linked to the two adjacent niobium (Nb1) centers, in a *syn-syn* bidentate bridging fashion, and adopting a *cis* position.

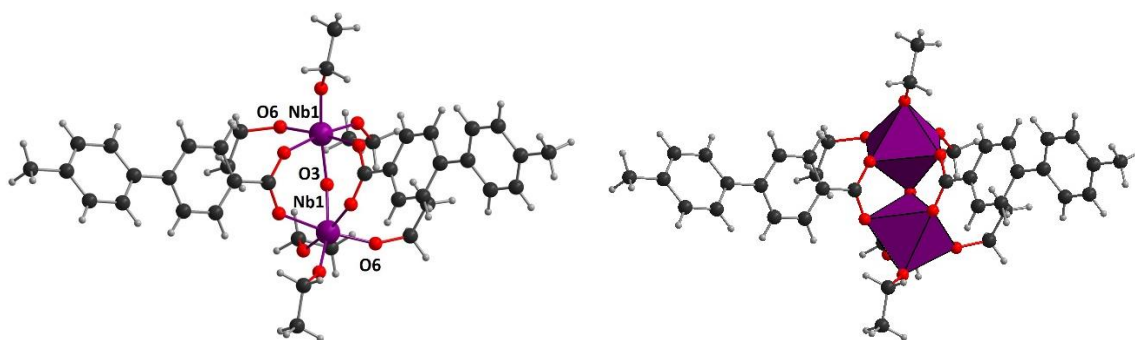


Figure III-6. Ball and stick (left) and polyhedral (right) representations of the molecular dinuclear coordination complex **Nb(V)-4**. One of the ethoxy groups linked to Nb1 site (through Nb1-O6 bonding) is disordered on two equivalent positions. Only one of these ethoxy groups is shown for clarity.

Compound **Nb(V)-5** $[\text{Nb}_2(\mu_2\text{-O})(\mu_2\text{-OEt})(\text{C}_{15}\text{H}_9\text{O}_2)(\text{OEt})_6]_2$

The crystal structure of compound **Nb(V)-5** is built up from two crystallographically independent motifs containing two distinct niobium(V) sites (Nb1 and Nb2 and Nb3 and Nb4), linked to each other through one μ_2 -oxo and one μ_2 -ethoxy groups, and one carboxylate arm of the 9-anthracenecarboxylate ligand (Figure III-7). The existence of only one carboxylate molecule within such a dinuclear niobium core is similar to that encountered in compound **Nb(V)-3**, obtained with 1-naphthoic acid. The 9-anthracenecarboxylate ligand acts as *syn-syn* bidentate linker with two adjacent niobium atoms (either Nb1 & Nb2 or Nb3 & Nb4). The four niobium centers are typically octahedrally coordinated with an identical geometrical environment. They are bound to one μ_2 -oxo group (Nb1-O3 = 1.934(1) Å; Nb2-O3 = 1.937(1) Å; Nb3-O13 = 1.939(2) Å; Nb4-O13 = 1.936(2) Å), one bridging μ_2 -ethoxy group (Nb1-O4_{Et} = 2.128(1) Å; Nb2-O4_{Et} = 2.121(1) Å; Nb3-O14_{Et} = 2.126(1) Å; Nb4-O14_{Et} = 2.1148(1) Å), one oxo group from the carboxylate arm of the 9-anthracenecarboxylate ligand (Nb1-O1_c = 2.196(1) Å; Nb2-O2_c = 2.181(1) Å; Nb3-O12_c = 2.205(1) Å; Nb4-O11_c = 2.191(1) Å), and three oxo groups from ethoxy molecules (Nb-O_{Et} in the range 1.855(2)-1.917(2) Å). The calculated bond valences of the μ_2 -oxo group bridging the two niobium centers are 1.872 for O3 and 1.862 for O13, in agreement with the occurrence of an oxo group^[14]. As observed in the dinuclear unit in compound **Nb(V)-3**, we observe that the niobium atoms are connected through only one carboxylate pincer in compound **Nb(V)-5**, resulting in an additional bridging μ_2 -ethoxy group. In compounds **Nb(V)-(2-4)**, this μ_2 -ethoxy group was not present and substituted by a second

carboxylate bridge from a second organic linker. For **Nb(V)-5**, the niobium-centered octahedral polyhedra are therefore linked through an edge-sharing mode via the two μ_2 -oxo ligands (oxo and ethoxy), corresponding to a shorter Nb1...Nb2 and Nb3...Nb4 distances of 3.2283(3) Å and 3.2561(3) Å, respectively. Related Nb-O-Nb bond angles are also lower, with value of 113.01(7)° and 114.37(8)° for the set Nb1-Nb2 and Nb3-Nb4, respectively. Similar metric values were observed in compound **Nb(V)-3**. The crystal structure packing of compound **Nb(V)-5** results from the molecular assemblies of two neutral dinuclear units with 9-anthracenecarboxylate, which differ only by the disorder of some ethoxy groups linked to the niobium centers. There exist one disordered ethoxy group for the Nb1-Nb2 set whereas there are three disordered ethoxy groups for the Nb3-Nb4 set.

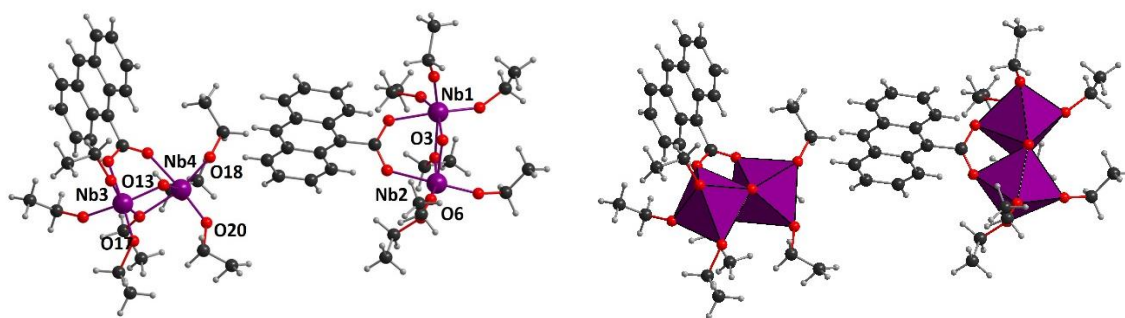


Figure III-7. Ball and stick (left) and polyhedral (right) representations of the molecular coordination complex **Nb(V)-5**. For one molecule, one of the ethoxy groups linked to Nb2 site (through Nb2-O6 bonding) is disordered on two equivalent positions. The same configuration occurs for the Nb3 and Nb4 sites of the second molecule with three disordered ethoxy groups (through Nb3-O17, Nb4-O18 and Nb4-O20 bondings). Only one of these ethoxy groups is shown for clarity.

Compound **Nb(V)-6** $[\text{Nb}_2(\mu_2\text{-O})(\text{C}_{15}\text{H}_9\text{O}_2)_2(\text{O}^i\text{Pr})_6]_2$

With the 9-anthracenecarboxylic acid (starting molar ratio of 0.375 carboxylic acid ligand for 1 niobium precursor instead of 0.333 carboxylic acid for 1 niobium in compound **Nb(V)-5**), a new type of crystalline product appeared, when adding isopropanol as solvent in the reaction medium. Crystal structure of **Nb(V)-6** is closely related to those observed in compounds **Nb(V)-2** and **Nb(V)-4**, and contains a centrosymmetric dinuclear core with one crystallographic unique niobium(V) atom (Nb1) and two bridging 9-anthracenecarboxylate species (Figure III-8). This cation is octahedrally coordinated with three oxo groups from isopropoxy molecules, with Nb1-O_{Pr} bond distances varying from 1.863(2) Å to 1.880(2) Å, two oxo groups from carboxylate arms (Nb1-O1_c = 2.175(2) Å and Nb1-O2_c = 2.219(2) Å), and one bridging μ_2 -oxo group (Nb1-O3 = 1.9103(6) Å). The bond valence calculation for this oxygen O3 atom gives the value of 2.038, in agreement with the occurrence of an oxo group^[14]. Within

the dinuclear core, two niobium centers are linked through two carboxylate arms from two distinct 9-anthracenecarboxylate ligands and one bridging μ_2 -oxo group (on special position 4e), generating a Nb1...Nb1 distance of 3.664(5) Å and a tilting Nb1-O3-Nb1 angle of 147.1(1)°, as found in the similar coordination complexes **Nb(V)-2** and **Nb(V)-4**. The two 9-anthracenecarboxylate ligands bridge two niobium atoms as *syn-syn* bidentating fashion. However, the terminal ethoxy groups occurring the compounds **Nb(V)-(1-5)** have been substituted by isopropoxy ligands, some of which occupy two disordering positions (through O6 atom; Figure III-8).

From the observation in compound **Nb(V)-6**, we were able to synthesize different coordination complexes with a dinuclear niobium core associating bulky anthracene moiety, with two distinct Nb/Ligand ratio of 2/1 and 2/2 by playing on the addition of alcohol solvent. These results seem to indicate that the Nb/Ligand ratio would be controlled by the initial carboxylic acid content rather than its steric hindrance.

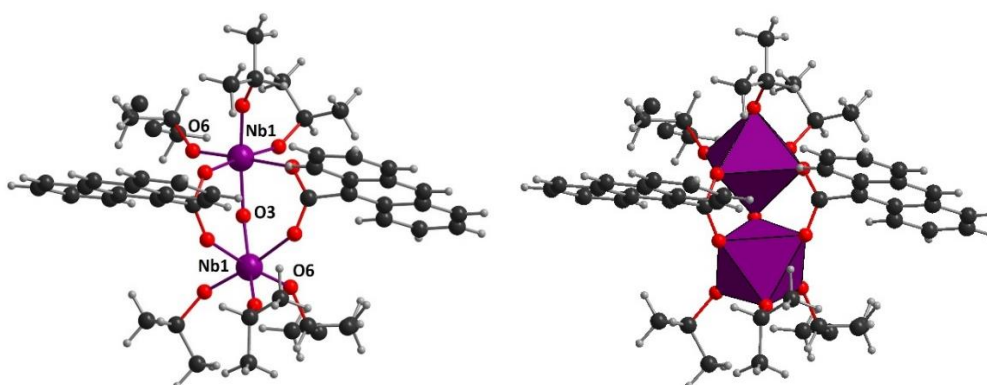


Figure III-8. Ball and stick (left) and polyhedral (right) representations of the molecular dinuclear coordination complex **Nb(V)-6**. One of the isopropoxy groups linked to Nb1 site (through Nb1-O6 bonding) is disordered on two equivalent positions. For them, the methyl groups are located on two close equivalent positions with occupancy 53/47. Only two of the four methyl groups are shown for clarity.

Compound **Nb(V)-7** [$\text{Nb}_4(\mu_2\text{-O})_4(\text{C}_{11}\text{H}_7\text{O}_2)_4(\text{OEt})_8$]

Compound **Nb(V)-7** is the second complex synthesized with the 2-naphthoic acid (see compound **Nb(V)-2**). Its crystal structure is closely related to that of the tetranuclear niobium(V)-centered $\{\text{Nb}_4\text{O}_4\}$ motif stabilized by benzoates species (**Nb(V)-2**), except that the latter ligand is substituted by the 2-naphthoate molecules (Figure III-9). It is built up from two inequivalent niobium(V) atoms (Nb1 & Nb2) linked to each other via μ_2 -oxo groups (O7 and O8), within a square-ring unit. Each niobium center is octahedrally coordinated by two μ_2 -oxo groups (Nb1-O7 = 1.908(4) Å, Nb1-O8 = 1.919(4) Å; Nb2-O7 = 1.895(4) Å, Nb2-O8 = 1.921(3)

Å), two oxygen atoms from ethoxyl groups ($\text{Nb1-O}_{\text{Et}} = 1.858(4)\text{-}1.879(4)$ Å; $\text{Nb2-O}_{\text{Et}} = 1.869(4)\text{-}1.885(3)$ Å), and two carboxyl oxygen atoms belonging to the 2-naphthoate ligand ($\text{Nb1-O}_{\text{c}} = 2.157(3)\text{-}2.163(4)$ Å; $\text{Nb2-O}_{\text{c}} = 2.167(4)\text{-}2.176(4)$ Å). The bond valence calculation for the μ_2 -oxygen atoms O7 and O8 gives the value of 1.987 and 2.017, respectively, in agreement with the occurrence of an oxo group^[14]. There occur two types of 2-naphthoate molecules acting through the carboxylate arm as a *syn-syn* bidentate bridging connecting mode with the two distinct niobium atoms Nb1 and Nb2. They are located in *cis* position related to the Nb1-O8-Nb2 linkage, which is characterized by a bonding angle of $145.9(2)^\circ$. The other Nb1-O7-Nb2 bond angle is slightly larger with a value of $152.5(2)^\circ$. These metric values are similar to those found the other tetrameric brick observed with benzoate ligands (**Nb(V)-1**), with the same alternation of concave and convex bending of Nb1-(μ_2 -O)-Nb2 bondings. Within the tetramer, the Nb1...Nb2 bond lengths are in the range $3.672(2)\text{-}3.694(1)$ Å. The dihedral angle of the two naphthalene rings is nearly perpendicular, with a value of $89.7(2)^\circ$, with one naphthalene pointing toward along the $\{\text{Nb}_4\text{O}_4\}$ tetramer plane and the second one upward and downward to this $\{\text{Nb}_4\text{O}_4\}$ plane. In this series, this value is the lowest one, since all other complexes involving dinuclear niobium-centered units with two carboxylate ligands, or tetranuclear niobium-centered units, exhibit an angle ranging from $100.92(4)^\circ$ (**Nb(V)-4**) up to $118.92(5)^\circ$ (**Nb(V)-2**), indicating a more opened angle for *cis* conformation of the carboxylate linkers. Indeed, this dihedral value is much lower that reported in the tetramer (112.8°) with benzoate ligands (**Nb(V)-1**). The $\{\text{Nb}_4\text{O}_4\}$ motif is then further decorated with eight ethoxyl groups pointing perpendicularly to the plane formed by the naphthalene groups.

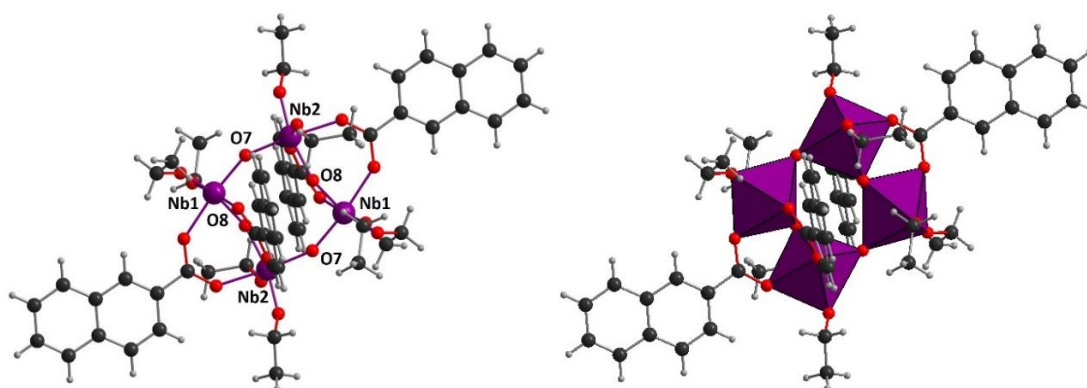
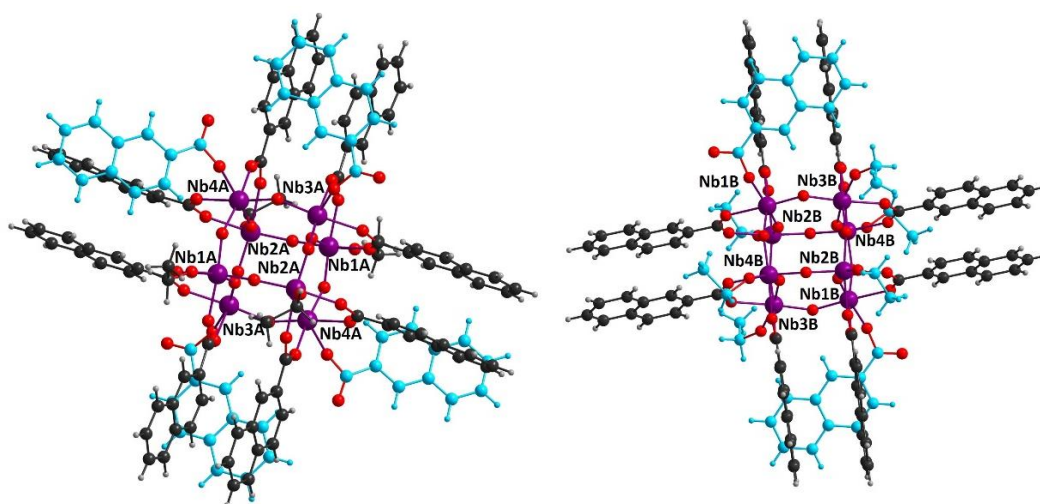


Figure III-9. Ball and stick (left) and polyhedral (right) representations of the molecular tetranuclear coordination complex **Nb(V)-7**. One of the ethoxy groups linked to Nb1 site (through Nb1-O10 bonding) and Nb2 site (through Nb2-O7 bonding), is disordered on two equivalent positions. Only one of these ethoxy groups is shown for clarity.

Compound **Nb(V)-8** $[\text{Nb}_8(\mu_2\text{-O})_{12}(\text{C}_{11}\text{H}_7\text{O}_2)_8(\eta_1\text{-C}_{11}\text{H}_7\text{O}_2)_4(\text{OEt})_4] \cdot [\text{Nb}_8(\mu_2\text{-O})_{12}(\text{C}_{11}\text{H}_7\text{O}_2)_8(\eta_1\text{-C}_{11}\text{H}_7\text{O}_2)_2\text{-}(\text{OEt})_6]$

Compound **Nb(V)-8** is the third niobium-centered complex isolated by means of the 2-naphthoate ligand (see compounds **Nb(V)-2** and **Nb(V)-7**). Its crystal structure is built up from two distinct neutral molecular entities (noted A and B), containing both eight niobium centers, with similar connection modes consisting of twelve bridging μ_2 -oxo groups (Figure III-10). The two arrangements can be viewed as the condensation of two niobium-centered tetranuclear bricks (related to those encountered in compounds **Nb(V)-7** and **Nb(V)-1**) through four additional μ_2 -oxo groups, located perpendicularly to its square plane of Nb-O-Nb bondings. It results in a cubic octanuclear core $\{\text{Nb}_8\text{O}_{12}\}$, where the niobium atoms occupy the eight corners, and the bridging μ_2 -oxo groups are located nearby the twelve edges. For each octameric entities A and B, there exist four crystallographic inequivalent niobium atoms, which are octahedrally coordinated to three μ_2 -oxo groups, two carboxyl oxygen atoms belonging to the 2-naphthoate ligand (in bidentate *syn-syn* bridging mode between two adjacent Nb) and one remaining oxygen atoms from either ethoxy groups or monodentate 2-naphthoate ligand. The Nb-O_{oxo} bond distances are in the range 1.825(9) - 1.967(9) Å for core A and 1.835(7) - 1.969(6) Å for core B, whereas the Nb-O_c (from the bidentate 2-naphthoate ligand) are in the range 2.092(7) - 2.196(10) Å for core A and 2.132(8) - 2.175(11) Å for core B. The bond valence calculations for the twelve μ_2 -oxygen atoms O1A-O6A and O1B-O6B, from the molecules A and B, corresponds to the values range of 2.022 - 2.122 and 1.979-2.083, respectively, in agreement with the occurrence of an oxo group^[14]. The last Nb-O bond lengths related to the ethoxy or monodentate naphthoate (η_1) ligands are observed in the range 1.941(14)-2.009(15) Å for core A and 1.927(7) - 2.022(13) Å for core B. For molecule A, the Nb-O-Nb bonding angles vary from 143.5(4)° to 147.7(4)°, whereas they vary from 142.6(4)° to 150.6(4)° for molecule B. Within the octamer A, the Nb...Nb bond distances are in the range 3.672(2)-3.694(1) Å and they are in the range 3.672(2)-3.694(1) Å for the octamer B. For the bidentate 2-naphthoate ligands, we observe dihedral angles between the naphthalene rings, nearly perpendicular, with values 85.2(6)-86.6(6)° for molecule A and 84.1(2)-86.3(4)° for molecule B. It results that the naphthalene rings pointed out in the (*a,c*) plane, with pairs of adjacent aromatic molecules, which exhibit typical π - π interactions, as reveal the C_{ar}...C_{ar} (C_{ar} = aromatic carbon) distances close to 3.6-3.7 Å. Moreover, weaker π - π interactions also occur

between the naphthalene rings ($C_{ar}\cdots C_{ar}$ of 3.7-4.0 Å length) belonging to two distinct neighboring octanuclear cores, which ensure the structural cohesion in the [100] and [001] directions. The two entities A and B only differ by the nature of terminal ligands via oxo groups attached to niobium centers, which are four ethoxy groups and four monodentate 2-naphthoate groups for A, and six ethoxy groups and two monodentate 2-naphthoate groups for A. These naphthalene monocarboxyl species exist under its non-protonated form, with short non-bonded C-O distances in the range $\approx 1.16(3)$ - $1.24(2)$ Å, relating to the C=O linkage. An infrared vibration band at 1670 cm^{-1} (Table III-2, Figures A17, paragraph A4, Appendix) is visible and attributed to such configuration of monodentate naphthoate linker. Indeed, it is the first example in our work of the substitution of ethoxy groups by monodentate carboxylic acids, with variable contents (either 4 EtO / 4 naphthoate or 6 EtO / 2 naphthoate), leading to a complex molecular assembly of octanuclear niobium cores. The other originality of this polynuclear niobium(V) brick is the number of the eight metallic $4d$ centers, engaged in a cubic configuration, which has not previously been reported in literature. Only a closely related octanuclear building block was described with the parent pentavalent tantalum(V), in the complex $[Ta_8(O)_{12}(O_2CNEt)_2]_{16}$.^[24] The latter brick is stabilized by the 16 *N,N*-diethylcarbamato ligands which act either as monodentate and bridging bidentate connection mode.



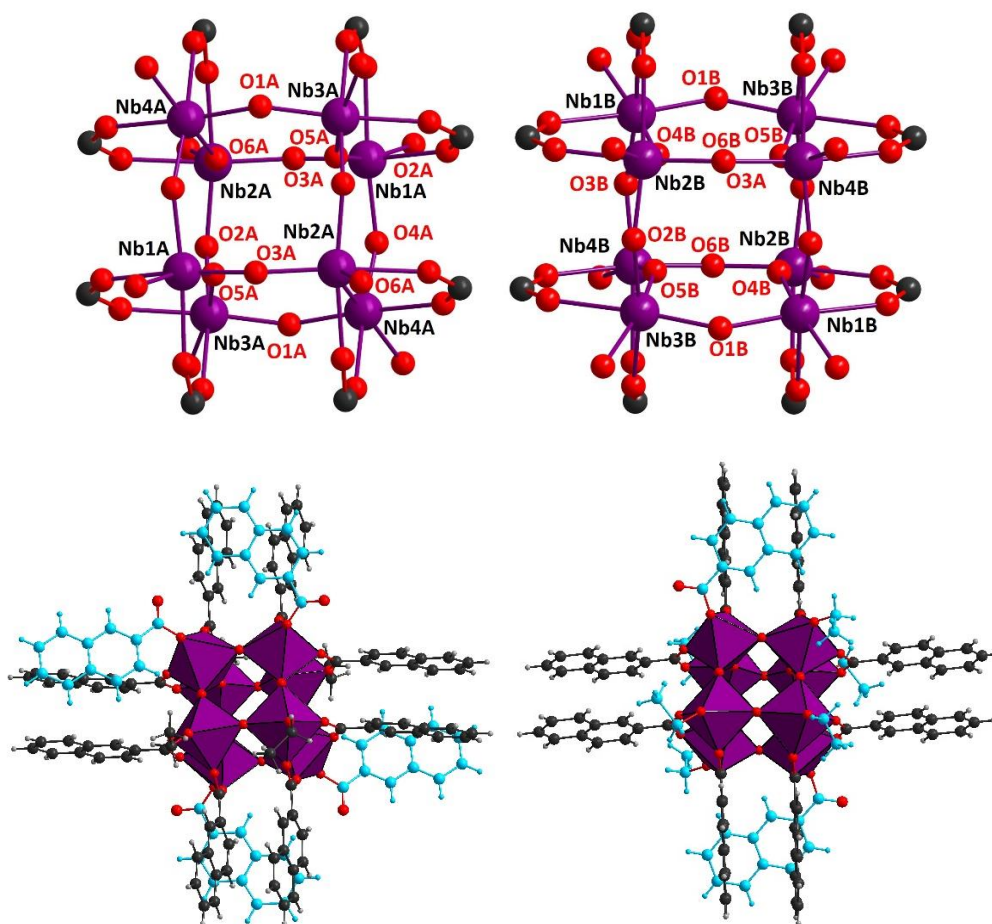


Figure III-10. Ball and stick (left) and polyhedral (right) representations of the molecular octanuclear coordination complex **Nb(V)-8**. The latter consists of two distinct inequivalent entities which contains either 4 ethoxy groups / 4 monodentate 2-naphthoate groups (Molecule A - left) or 6 ethoxy groups / 2 monodentate 2-naphthoate groups (Molecule B - right). These terminal ethoxy or monodentate 2-naphthoate groups are indicated in blue, for a better clarity of the representation.

Compound **Nb(V)-9** $[\text{Nb}_{12}(\mu_2\text{-O})_{20}(\mu_3\text{-O})_2(\text{C}_{15}\text{H}_9\text{O}_2)_8(\text{O}^i\text{Pr})_5]$

Nb(V)-9 is the third compound stabilized with anthracenoate molecules. Its crystal structure is built up by two crystallographically independent motifs (A and B) containing two distinct niobium(V) sites (Figure III-11, bottom). In each motif, the niobium centers are connected with each other with $\mu_2\text{-O}$ and $\mu_3\text{-O}$ bridging oxygens and each niobium core is surrounded by eight anthracenoates and ten isopropoxy groups. Each site has twelve niobium centers, from which eleven adopt a 6-fold coordination with distorted octahedral geometry (blue polyhedral) and one 5-fold coordinate niobium with a distorted square pyramidal geometry (purple octahedra). 5-fold coordination is not a common environment for niobium species. In literature, there are only two examples of a 5-fold coordinated niobium sites. The first was a cationic Nb^{I} complex surrounded with five acetonitrile molecules.^[25] The second one, was reported in the $\text{Ba}_4\text{Nb}_2\text{O}_9$, where niobium forms 4-, 5- and 6-coordinate niobium

sites.^[26] It was observed that the higher the coordination site, the longer the N-O bonds are. For example, in a 5-coordinate niobium(V), Nb-O_{oxo} bonds are 1.973(6)-1.977(6) Å, whereas for 6-coordinate niobium(V), Nb-O_{oxo} bonds are longer (2.067(5)-2.254(5) Å).^[26] In **Nb(V)-9**, a similar trend is observed for Nb-O_{oxo} bonds in the 5-coordinate niobium center with bond lengths of 1.847(5)-1.891(6) Å for motif A and 1.81(1)-1.846(7) Å for motif B. For both motifs we have a {Nb₁₂O₂₁} core, but oxo groups in motif A exist as three (μ₃-O) and eighteen (μ₂-O), whereas two (μ₃-O) and nineteen (μ₂-O) in motif B. Later, in {Nb₈O₁₆} (**Nb(V)-8**), the ratio O/Nb was at 2 and close to the one of the Nb₂O₅ oxide which is at 2.5. In the case of **Nb(V)-9**, the core {Nb₁₂O₂₁} has a lower content of oxo groups and results in an O/Nb ratio of 1.75. However, except of oxo corner sharing oxygen atoms, each motif has three oxo edge-sharing oxygen atoms, like it happens in the dense Nb₂O₅ phase. The anthracenoates of A and B entities are interacting with other by π-π stacking (3.63(1) Å) between C88 and C234 (Figure III-11, top).

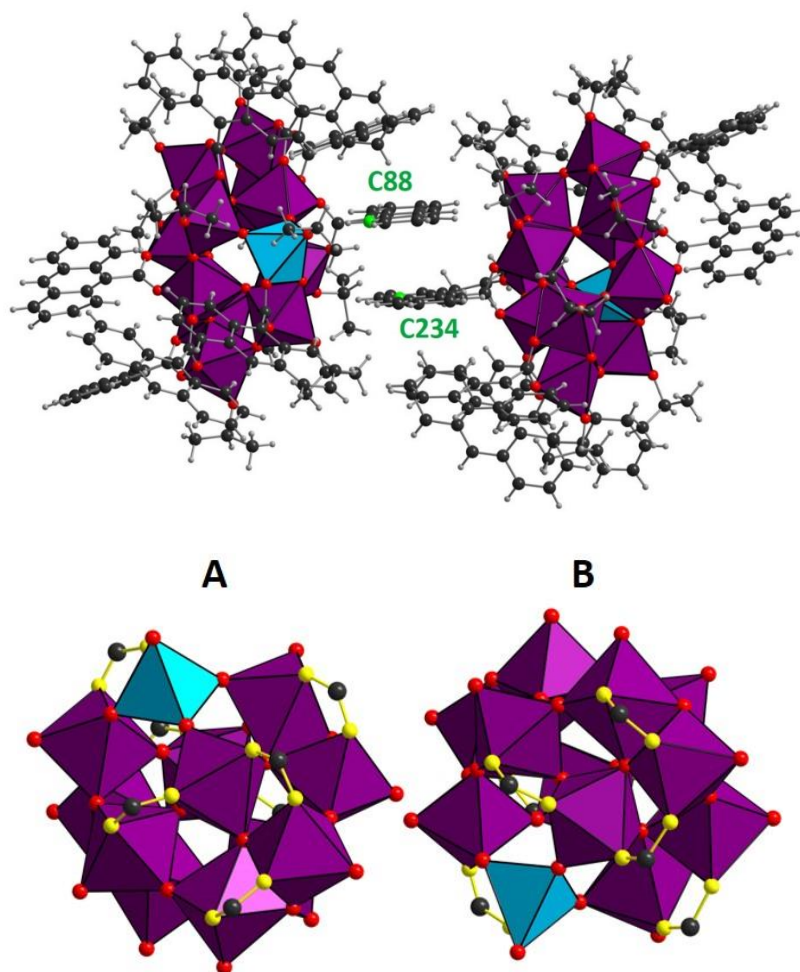


Figure III-11. Polyhedral representations of **Nb(V)-9** (top) and its A and B entities (bottom).

II.1.3 Infrared study in Nb(V) monocarboxylate complexes

We investigated the different niobium(V) ethoxide – carboxylic acid systems by infrared spectroscopy, in order to characterize the crystallization of the complexes **Nb(V)-(1-9)**. After the thermal treatment for the formation of complexes **Nb(V)-7** and **Nb(V)-8**, no supernatant was obtained due to the large amount of organic ligand that recrystallized after cooling. For each batch (except for compounds **Nb(V)-7** and **Nb(V)-8**, for which no supernatant is obtained at the end of the synthesis), the supernatant solutions have been studied just after the starting reactants mixing at $t = 1\text{h}$ at room temperature, and then after crystallization of the compounds (variable times depending on the crystallization duration for a given complex). Distinct zones are of interest are attributed to the ethoxide (or isopropoxide for complex **Nb(V)-5**) group^[27]. The 3050-2750 cm^{-1} range is of interest and related to the $\nu(\text{C-H})$ stretching vibrations of the ethyl groups (with typical bands at $\approx 2970_{(\text{asym})}$ and $\approx 2860_{(\text{sym})}$ cm^{-1}), and the 1480-1370 cm^{-1} zone related to the $\nu(\text{C-H})$ bending vibrations of the methyl groups (with typical bands at 1470-1404 and 1375 cm^{-1}). The bands at around 1200-1000 cm^{-1} are assigned to the $\nu(\text{C-O})$ vibrations coming from the ethoxide group linked to niobium center, via Nb-O-C_{Et} linkage: typical peaks are found at 1100-1090 cm^{-1} and 1060-1050 cm^{-1} . The broad peak at around 573-529 cm^{-1} are related to $\nu(\text{Nb-O})$ stretching modes^[28]. These different signatures are observed either in the supernatant solution or in crystallized niobium complexes, as expected.

For our interest in the formation of niobium carboxylate complexes, we focused our attention on the 1750-1550 cm^{-1} region, where free carboxylic acid $\nu(\text{C=O})$, and bonded carboxylate $\nu_{\text{asym}}(\text{COO})$ and $\nu_{\text{sym}}(\text{COO})$ stretching vibrations are typically found.

For the complexes **Nb(V)-(2-9)** (and **Nb(V)-7** for only before thermal treatment), we observed the same trends (Figures A11-A18, paragraph A4, Appendix), since unprotonated carboxylate ligands are always visible in the supernatant solutions after mixing the chemical reactants (Table III-4). Indeed, for complex **Nb(V)-2** system, the band at 1683 cm^{-1} , is related to the $\nu(\text{C=O})$ stretching from 2-naphtoic acid, but disappears when it is mixed with the niobium ethoxide solution. The corresponding vibration stretching is shifted to 1599 cm^{-1} and 1551 cm^{-1} , related to the $\nu_{\text{asym}}(\text{COO})$ and $\nu_{\text{sym}}(\text{COO})$, respectively, revealing the bonding between carboxylate group and niobium centers^[16] in supernatant solution, just after 1h mixing. This observation indicates the relative rapid complexation of the starting niobium

ethoxide by the carboxylate group occurring at room temperature in less than an hour, and therefore the presence of niobium-ethoxide-carboxylate in solution. This group of two peaks are also found in the solid-state form of the crystalline coordination complex of **Nb(V)-2** (at 1598 cm^{-1} and 1560 cm^{-1}). This reactivity of the carboxylic acid toward the niobium ethoxide is observed for the different crystallization processes for complexes **Nb(V)-(2-9)**. However, infrared signatures differ for some supernatant solution samples after crystallization, since some of them only show very weak bands related to $\nu(\text{C=OO})$ vibrations, corresponding to a smaller content of niobium carboxylate complex in the final solution. This evolution is attributed to the transfer of “soluble” niobium-ethoxide-carboxylate complex into the solid crystalline form. This is clearly the case for the crystallization of complex **Nb(V)-3** (with 1-naphthoic acid, after 6 months), or in a less extend, for complexes **Nb(V)-4** (with 4-methylbiphenylcarboxylic acid, after 3 weeks) and **Nb(V)-5** (with anthracene-9-carboxylic acid, after 2 weeks), for instance.

The formation of the complex **Nb(V)-1** with benzoic acid, shows the same behavior, with the band of the carboxylic function at 1680 cm^{-1} ($\nu(\text{C=O})$) shifting to 1598 and $1560\text{-}1556\text{ cm}^{-1}$ ($\nu(\text{COO})$) when mixed with the niobium ethoxide precursor. It is related to its unprotonated state, either in supernatant solution and solid-state crystallized form, indicating the carboxylate complexation with niobium cations. However, a new group of bands is appeared in the range $1722\text{-}1698\text{ cm}^{-1}$ in the supernatant solution (Figure A10, paragraph A4, Appendix), either after 1h mixing or 1-month crystallization, and is assigned to the $\nu(\text{C=O})$ coming from the formation of ethyl-benzoate ester. Similar reaction has been previously described for the synthesis of the tetranuclear niobium acetate complex^[16]. The formation of such basic ester organic molecule is expected in such a mixture involving the reaction between a carboxylic acid and an alcohol. The latter will come from proton exchange between the benzoic acid and the attached ethoxide group from niobium alkoxide precursor. This results in the complexation of benzoate with niobium (as indicated by the IR bands of the $\nu(\text{COO})$ vibrations) and a leaving group of ethanol species, which further react with benzoic acid, present in excess in the starting mixture. It is noticed that the bands attributed to the ethylbenzoate ester are not visible for the crystalline complex **Nb(V)-1**, and occurs only in the solution. The propylanthracenoate ester is also observed in solution for complex **Nb(V)-9** (Figure A18, paragraph A4, Appendix), at 1695 cm^{-1} . However, such ester molecules have not been

detected in the other niobium-carboxylic acid system, which could be due the sensitivity of the IR technique. Thus, the formation of the ester molecules with the systems involving other carboxylic acids has been then investigated by liquid ^1H NMR of the supernatant solution.

Table III-4. Comparison of the $\nu(\text{C}=\text{O})$ vibrations (from carboxylic acid function) and $\nu(\text{COO})$ vibrations (from carboxylate function) for the complexes **Nb(V)-(1-8)** (in cm^{-1}).

		$\nu(\text{C}=\text{O})_{\text{acid}}$	$\nu_{\text{asym}}(\text{COO})$	$\nu_{\text{sym}}(\text{COO})$
Nb(V)-1	benzoic acid	1680	/	/
	supernatant (1 hour)	/	1598	1556
	supernatant (1 month)	/	1599	1560
	crystalline product	/	1598	1560
Nb(V)-2	2-naphtic acid	1683	/	/
	supernatant (1 hour)	/	1599	1551
	supernatant (5 days)	/	1600-1587	1560
	crystalline product	/	1598	1560
Nb(V)-3	1-naphtic acid	1670	/	/
	supernatant (1hour)	/	1596	1543
	supernatant (1 months)	/	n.o. ^[a]	n.o. ^[a]
	crystalline product	/	1597	1537
Nb(V)-4	4-methylbiphenylcarboxylic acid	1678	/	/
	supernatant (1 hour)	/	1592	1537
	supernatant (3 weeks)	/	1591 (weak)	1535 (weak)
	crystalline product	/	1598	1561
Nb(V)-5	anthracene-9-carboxylic acid	1678	/	/
	supernatant (1 hour)	/	1594	1540
	supernatant (2 weeks)	/	n.o. ^[a]	n.o. ^[a]
	crystalline product	/	1597	1561
Nb(V)-6	anthracene-9-carboxylic acid	1682	/	/
	supernatant (1 hour)	/	1554	n.o. ^[a]
	supernatant (2 weeks)	/	1557 (weak)	n.o. ^[a]
	crystalline product	/	1584	1527
Nb(V)-7	2-naphtic acid	1683	/	/
	supernatant (1 hour)	/	1597	1550
	crystalline product	/	1598	1557
Nb(V)-8	2-naphtic acid	1683	/	/
	crystalline product	/	1670 ^[b] & 1586	1548
Nb(V)-9	anthracene-9-carboxylic acid	1678	/	/
	supernatant (1 hour)	/	n.o. ^[a]	n.o. ^[a]
	supernatant (5 days)	/	n.o. ^[a]	n.o. ^[a]
	crystalline product	/	1624	1538

^[a]n.o. : not observed. ^[b] from monodentate naphthoate species.

II.1.4 Liquid NMR ^1H (and 2D ^{13}C - ^1H) of supernatants for **Nb(V)-1**, **Nb(V)-2** and **Nb(V)-4**

Nuclear magnetic resonance was chosen in order to investigate the presence of the ester in the supernatant of each reaction batch. As mentioned before, the presence of these ester functions is a condition to form in-situ water molecules able to condense, in a controlled way, the niobium cations to each other through bridging oxo ligands, and form polynuclear species. Since the niobium precursor $\{\text{Nb}(\text{OEt})_5\}$ is a liquid, its ^1H -NMR spectrum has been recorded too, revealing a quartet centered at 5.035 ppm which is attributed to the two protons of $-\text{CH}_2-$ and a triplet at 1.83 ppm attributed to the three protons of $-\text{CH}_3$ (Figure III-12). At 4.82 ppm another broad peak is observed which can derive from the existence of two different $-\text{CH}_2-$ groups, either terminal or bridging in the dimeric $\{\text{Nb}_2(\mu^2\text{-OEt})_2(\text{OEt})_8\}$ precursor. Indeed, the integration matches with this hypothesis and we can assume that the 8 terminal $-\text{CH}_2-$ give the quartet at 5.035 ppm and the 2 bridging ones the broad signal at 4.82 ppm. However, in the case of $-\text{CH}_3$ groups belonging to the bridging ethoxy ligand, a signal is not clearly observed. One can assume that, due to the higher distances of the $-\text{CH}_3$ groups from the niobium centers, there are no significant differences in the chemical shifts those belonging to terminal and bridging ethoxy ligand, so that both signals appear overlapped.

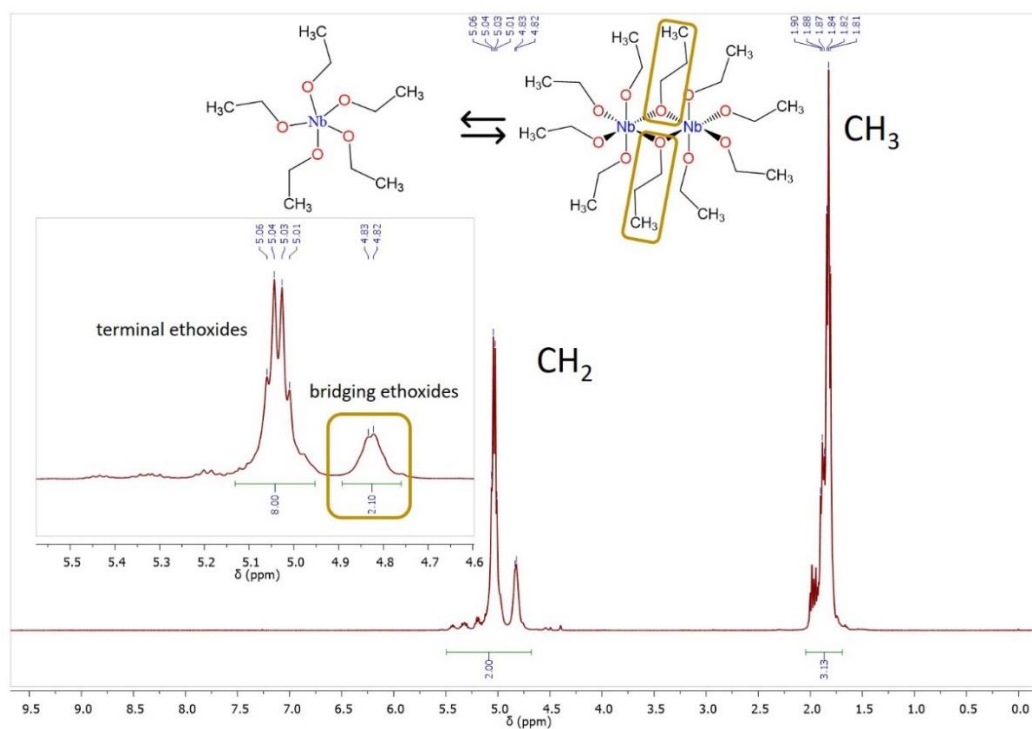


Figure III-12. ^1H NMR spectra for $\text{Nb}(\text{OEt})_5$.

Among the eight systems giving rise to crystalline products, we selected three of them (**Nb(V)-1**, **Nb(V)-2** and **Nb(V)-4**), for which clear liquid ^1H NMR signatures can be extracted from the supernatant solution, without significant perturbation of overlapping peaks due to the complexity of some carboxylic acid ligands in the aromatic region (such as in the case of anthracene-9-carboxylic acid). For each reaction leading to the compounds **Nb(V)-1**, **Nb(V)-2** and **Nb(V)-4**, supernatant ^1H -NMR experiments were conducted before and after the crystallization process to follow the formation of the ethyl ester species. As “before crystallization” we define the time for which the ligand solubilizes totally into the niobium(V)ethoxide precursor (approximately 1 hour) and as “after crystallization”, we define the time after the appearance of crystals (reaction time ranging from 5 days (**Nb(V)-2**), 7 days (**Nb(V)-4**) and 1 month (**Nb(V)-1**)).

We first describe in detail the results for compound **Nb(V)-2** (involving 2-naphthoic acid) as the best resolved system. Before crystallization, we observe expected ^1H NMR signals located in the aromatic region (from 7 to 9 ppm), and the aliphatic region (from 0 to 5 ppm; Figure III-13). For the for 2-naphthoic acid, the protons H1 and H2 show a singlet at 9.20 ppm and a doublet at 8.70 ppm respectively. The rest of the aromatic protons resonates at 8.46 ppm (doublet, H3), 8.40 ppm (multiplet, H4 and H7) and at 8.07 ppm (multiplet, H5 and H6). The signature of the ethoxy group of the niobium ethoxide precursor, appears with a weak shielding of the chemical shifts (at 4.98 ppm for $-\text{CH}_2-$ groups and 1.77 ppm for $-\text{CH}_3$ groups), compared to the free niobium ethoxide precursor (Figure III-12). It is worth noting that we still observed the presence of the terminal and bridging ethoxide groups generating the broad signal at 4.98 ppm and 4.76 ppm, respectively.

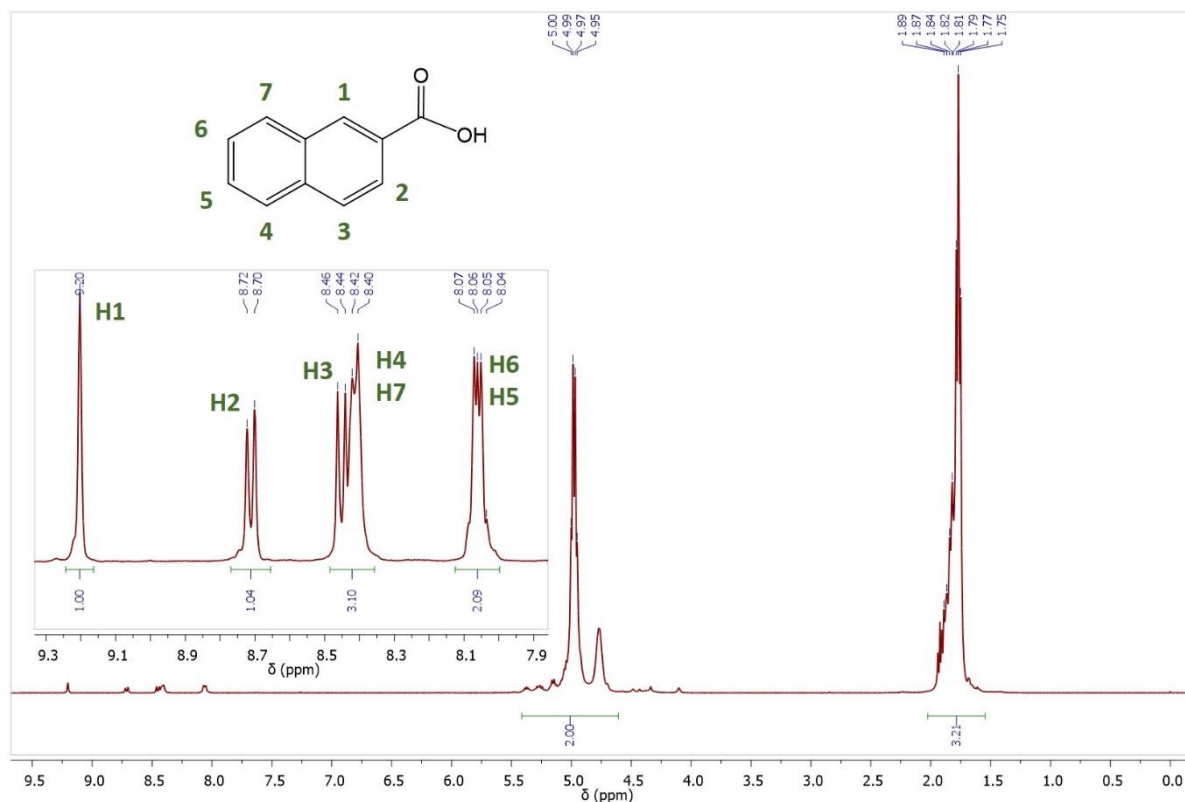


Figure III-13. ^1H NMR spectrum focused in the aromatic region for the supernatant of complex **Nb(V)-2** before crystallization.

After the crystallization (Figure III-14), the ^1H -NMR spectrum of supernatant is more complex, indicating that a reaction occurred between the 2-naphthoic ligand and the niobium ethoxide precursor (see Figure III-12). It was clearly observed a mixture of 2-naphthoic acid species (noted A), an ethyl-naphthoate ester form (noted B) and likely naphthoate ligand interacting with niobium centers prior to their crystallization (noted C). For these three species, the aromatic part of the ligand remains unchanged and should generate an identical number of ^1H signals, but different chemical shifts are observed due to the different chemical configurations. In the aromatic region, the H1 atom is firstly considered as isolated (one singlet for the starting solution (Figure III-13), but it is seen as three singlet signals corresponding to the three different configurations of naphthoates species, A, B and C (Figure III-14).

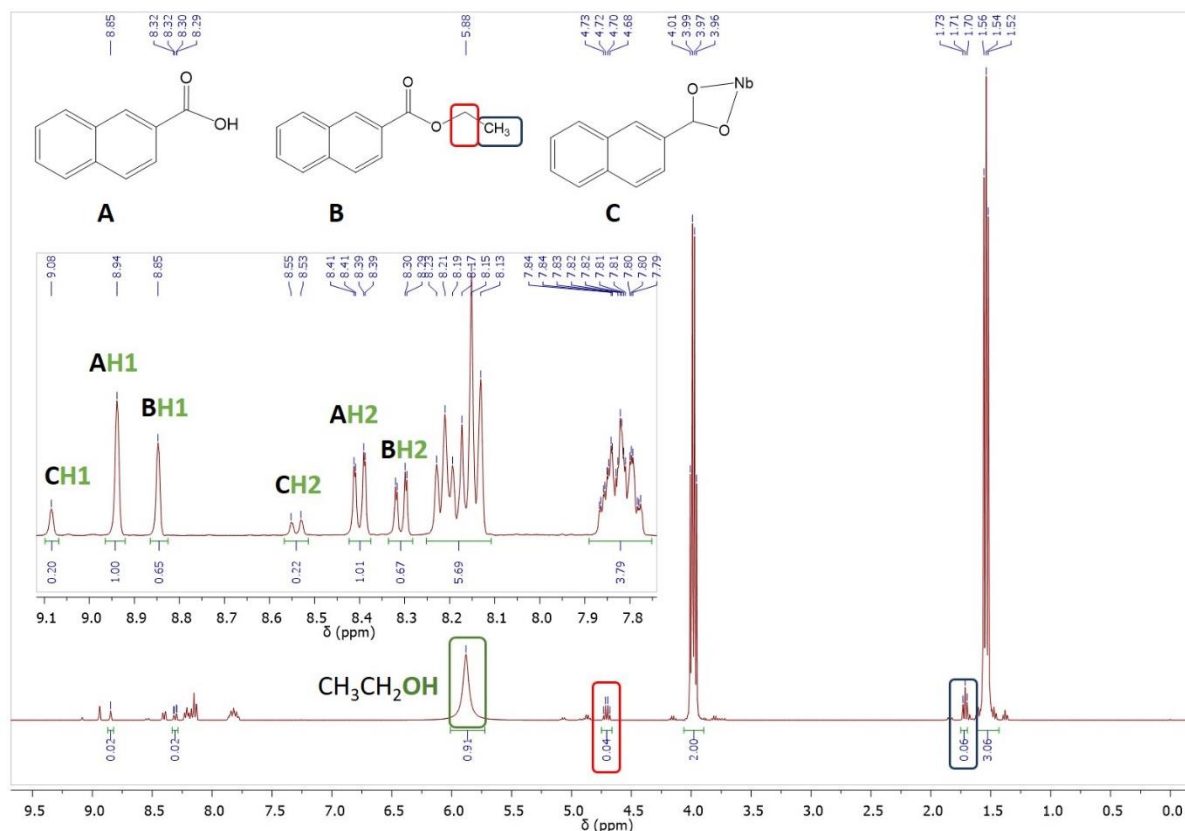


Figure III-14. ^1H NMR spectrum for the supernatant of **Nb(V)-2** after crystallization with a focus in the aromatic region. (green box; hydroxylic proton of ethanol, red box; $-\text{CH}_2-$ group of ester form B, blue box; $-\text{CH}_3$ group of ester form B)

To discriminate them, a ^{13}C - ^1H HMBC (Heteronuclear Multiple Bond Correlation) 2D experiment was performed (Figure III-15). This method gives correlations between carbons and protons that are separated by two, three, and, sometimes in conjugated systems, four bonds. From this analysis, we assign the signal located at 8.85 ppm to the ester form (B) as it is correlated to the carbon atom C1_B (carbon in 1 position for the naphthalene part of molecule B) bearing the H1_B proton with the $-\text{CH}_2-$ group of the ethyl group, centered at 4.71 ppm. The two remaining singlet signals correspond to the naphthoic acid, H1_A at 8.94 ppm and H1_C at 9.06 ppm, respectively. The latter has a weaker intensity because it is involved during the solid-state crystal growth of complex **Nb(V)-2**, and thus a lower concentration in supernatant solution.

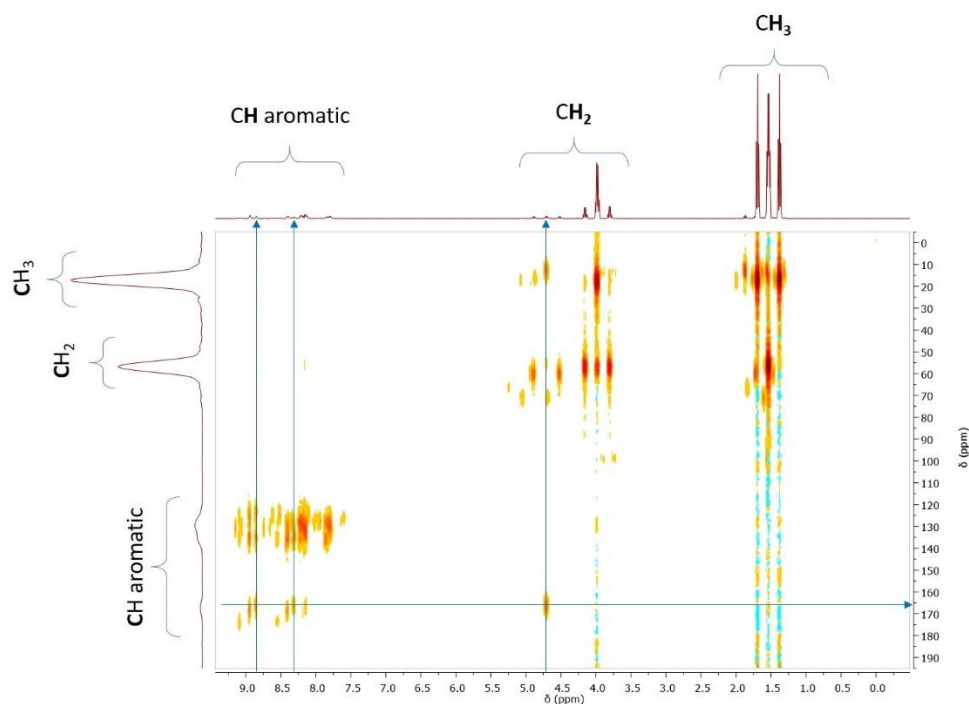


Figure III-15. ^{13}C -HMBC spectrum for the supernatant of compound **Nb(V)-2**.

This observation regarding the differentiation between A and C species is confirmed by a DOSY experiment performed on the supernatant after crystallization (Figure III-16). For the aromatic region of the spectrum, we clearly see the presence of the three different forms with diffusion values of $4.95 \times 10^{-10} \text{ m}^2/\text{s}$, $6.27 \times 10^{-10} \text{ m}^2/\text{s}$ and $2.55 \times 10^{-10} \text{ m}^2/\text{s}$ related to species A, B and C, respectively. As diffusion parameter is related to the size of a given molecule in solution, the lower diffusion value ($2.55 \times 10^{-10} \text{ m}^2/\text{s}$) is related to the naphthoate ligand interacting with the niobium centers (C). The remaining naphthoic acid (A) has thus a diffusion value of $4.95 \times 10^{-10} \text{ m}^2/\text{s}$. The latter appears to be smaller than the ester form (B) probably because of dimerization by $\text{COOH}\cdots\text{HOOC}$ interactions in the supernatant, resulting in a bigger hindrance for the (A) form than that of ester form (B).

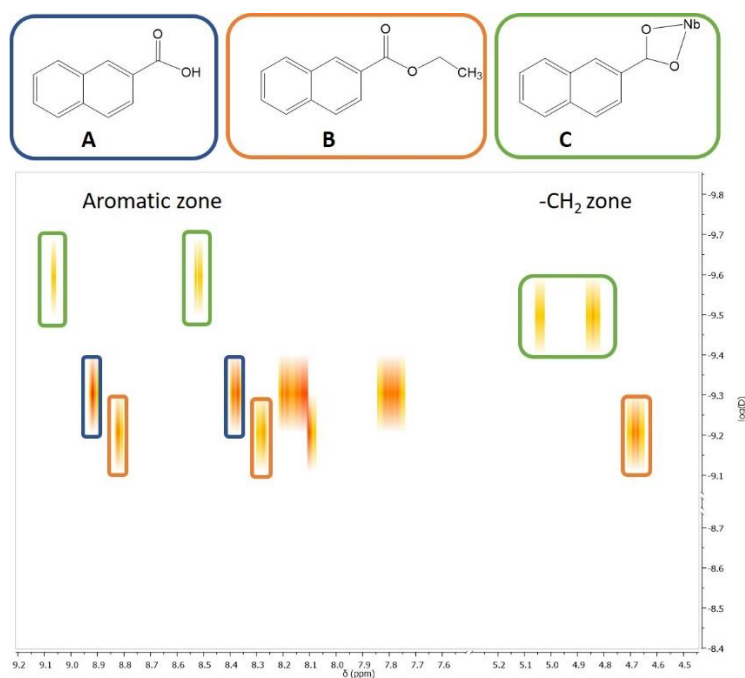


Figure III-16. DOSY spectrum of **Nb(V)-2** mixture after crystallization.

The second set of signals between 8.25 ppm and 8.6 ppm appears as three doublets standing for the H2 hydrogen atom. Accordingly, with the determination of the three-singlets H1, the three H2 doublet signals centered at 8.29 ppm, 8.40 ppm and 8.54 ppm are attributed to H2_B, H2_A and H2_C, with the same C, A, B order, respectively. H2_B is further confirmed by the ¹³C-¹H HMBC measurement (Figure III-15), as it interacts with the -CH₂- ethyl signal located at 4.71 ppm. The signals corresponding to the other protons (H3-H7) are heavily overlapped and resonate as two multiplets centered at 8.18 ppm and 7.81 ppm. It may be caused by their location, far from the carboxylate function. No HMBC correlation is observed for these protons. The free niobium ethoxide precursor resonates at 5.88 ppm, 3.98 ppm and 1.54 ppm.

For the aliphatic region, signals of the protons of the 2-ethylnaphthoate ester (B), -CH₂- that resonate at 4.72 ppm (quartet circled in red) and -CH₃- that resonate at 1.71 ppm (triplet circled in blue), belong also to the 2-ethylnaphthoate ester form (B). Moreover, we observe a broad singlet deriving at 5.88 ppm coming from the released ethanol molecules (green box on Figure III-14).

The same procedure was tentatively followed for the systems **Nb(V)-1** (involving benzoic acid) and **Nb(V)-4** (involving 4'-methylbiphenyl-4-carboxylic acid).

The benzoic ligand in system **Nb(V)-1** appears to be more reactive than the naphthoic ligand in system **Nb(V)-2**. This is probably due to the solubility of each ligand into Nb(V)ethoxide, as benzoic acid dissolves faster than naphthoic acid. Indeed, even prior to crystallization, several intense signals are already visible on the ^1H NMR spectrum. These signals are quite different and much less resolved than the free ligand spectrum in CDCl_3 (Figure III-17, left). In the aromatic region, three main signals (P1, P2 and P3) centered at 7.53 ppm, 8.26 ppm and 8.35 ppm, respectively, are visible and two very small signals (P4 and P5) centered at 8.55 ppm and 8.1 ppm are present, respectively. In the aliphatic region, several peaks (labelled E1 to E4) centered at 4.22 ppm, 4.60 ppm, 4.75 ppm, 4.36 ppm respectively, and corresponding to $-\text{CH}_2-$ groups of esters compounds are observed (Figure III-17, right).

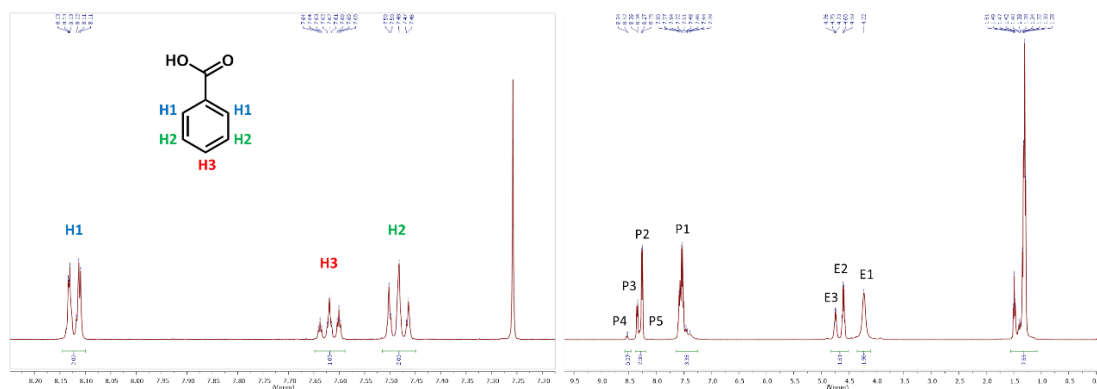


Figure III-17. ^1H NMR spectra of the benzoic acid in CDCl_3 (left) and ^1H NMR spectra focused in the aromatic region for the supernatant of **Nb(V)-1** before crystallization (right).

It is difficult to assign these signals to the molecules occurring in the supernatant. To get more information on the size of the various components of the mixture and based on our interpretation on the diffusion values, we have performed a DOSY measurement (Figure III-18 left). The E1 signal possesses a high diffusion value (compared to other systems; see Figure III-18 right) indicating that it is a small molecule and could therefore be interpreted as being an ethanol or ethanolate molecule. It is more probably assign to a species in equilibrium between these two forms causing the broadening of the E1 signal. This ethanol/ethanolate moiety comes from the niobium ethoxide precursor after the first complexation by a benzoic acid ligand. The acid ligand exchanges its proton with the ethanolate to form the ethanol and consequently, the benzoate ligand starts to complex the niobium centers. DOSY experiments also show that the E2 and E3 signals correspond to bigger molecules in solution, probably the unreacted niobium ethoxide precursor or benzoate ligand coordinated to the niobium

centers. P4 and E3 signals diffuse at the same speed on the DOSY spectrum (Figure III-18, left). Diffusion values of the P2, P3 and P1 signals suggest that the associated molecules are relatively large and could correspond to benzoate ligands linked to niobium centers.

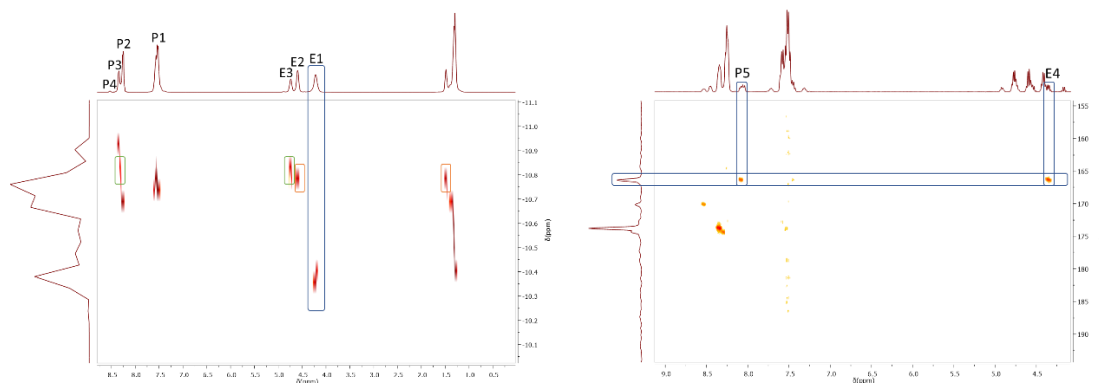


Figure III-18. DOSY spectrum of **Nb(V)-1** mixture before crystallization (left) and ^{13}C -HMBC spectrum of **Nb(V)-1** supernatant before crystallization in the aromatic and $-\text{CH}_2-$ aliphatic region (right).

After crystallization, the signals are well defined and can be interpreted by following the same way as we found for system **Nb(V)-2**. For the aromatic region, the signals are visible for the H1 and H5 protons of the benzoate groups. They correspond to the acid form (noted A), the ethyl ester form (noted B) and the complex form (noted C) (Figure III-19 left). The HMBC 2D measurement confirms that the B signals corresponds to an ethyl ester form as correlations exist between H1_B/H5_B with the $-\text{CH}_2-$ groups of the ethyl ester (Figure III-19 right). Based on the observation made with system **Nb(V)-2**, the two remaining signals centered at 8.03 ppm and 8.14 ppm should correspond to free benzoic acid (A) and complex ligand (B), respectively.

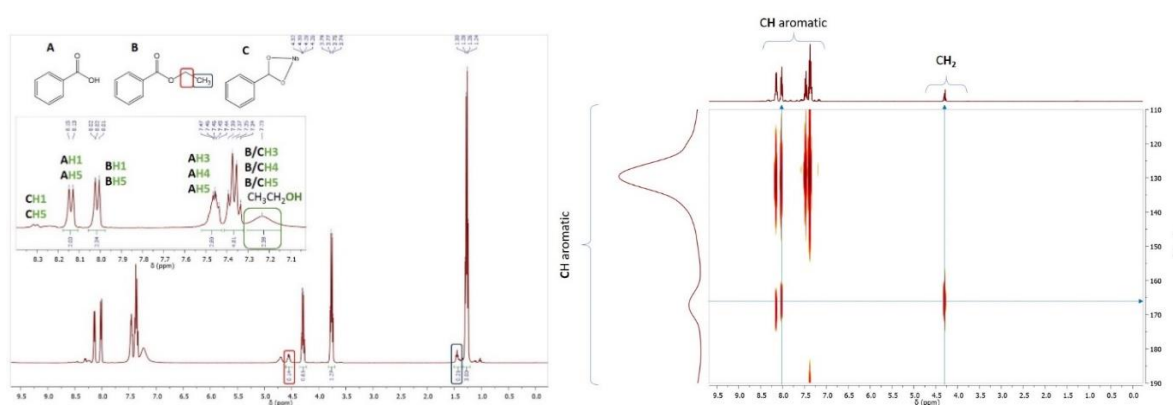


Figure III-19. ^1H NMR spectra focused in the aromatic region for the supernatant of complex **Nb(V)-1** before (top left) and after the crystallization (top right) with a focus in the aromatic region and ^{13}C -HMBC spectrum (bottom).

Before crystallization in system **Nb(V)- 4**, four signals centered at 8.71 ppm, 8.16 ppm, 8.05 ppm and 7.71 ppm are assigned to H1, H2 H3 and H4, respectively, and are related to the

aromatic region (Figure III-20, top left). They correspond to the acid form of the ligand (4'-methylbiphenyl-4-carboxylic acid). The $-\text{CH}_3$ group is also present in the aliphatic region at 2.87 ppm alongside with the niobium ethoxide precursor (signals at 4.96 ppm and 1.77 ppm). After crystallization, some modifications appear in the spectrum (Figure III-20, top right). In the aromatic region, four main doublets are visible at 8.59 ppm, 8.07 ppm, 7.94 ppm and 7.60 ppm for protons H1_A, H2_A, H3_A and H4_A, respectively. These protons belong to the acid form (A) of the ligand. Two small doublets are also visible on each side of the H1_A signal at 8.65 ppm and 8.46 ppm. The HMBC 2D measurement reveals that the doublet located at 8.46 ppm belongs to the ethyl ester form of the ligand (B) as it is correlated to the $-\text{CH}_2-$ group (small signal located at 5.05 ppm) of the ethyl ester (Figure III-20, bottom). Consequently, the second doublet at 8.65 ppm stands for the presence of a small amount of acid ligand complexed to the niobium centers (C) prior to crystallization.

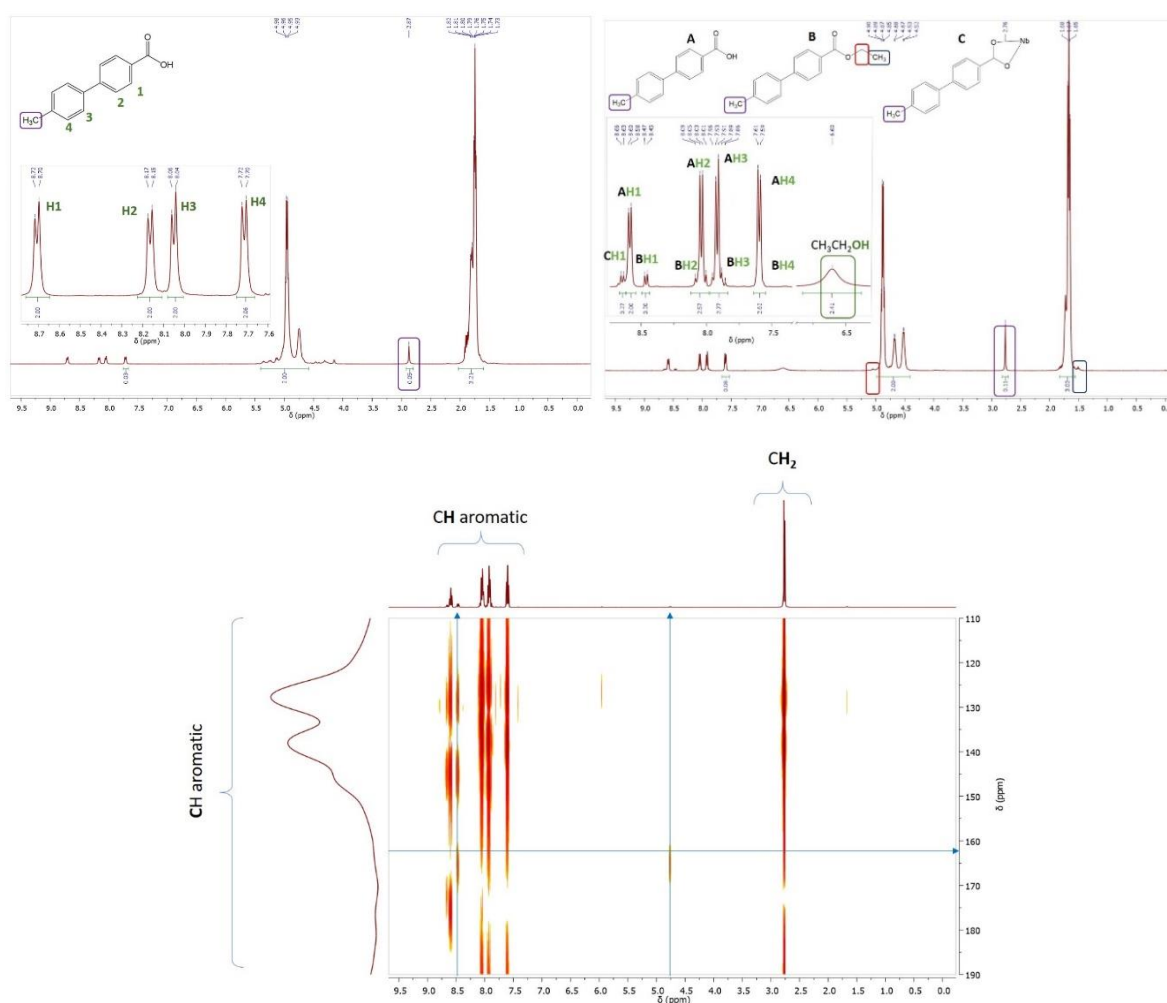


Figure III-20. ^1H NMR spectra focused in the aromatic region for the supernatant of complex Nb(V)-4 before (top left) and after the crystallization (top right) with a focus in the aromatic region and ^{13}C -HMBC spectrum (bottom).

III. 1.5 Discussion

The reaction of a carboxylic acid with the $\text{Nb}_2(\mu_2\text{-OEt})_2(\text{OEt})_8$ unit generates dinuclear units in which one or two central bridging $\mu_2\text{-OEt}$ groups are replaced by the carboxylate arms of the aromatic ligand (Figure III-21 [A]). Indeed, one observes the complexation by one carboxylate in compounds **Nb(V)-3** and **Nb(V)-5**, but still a bridging $\mu_2\text{-OEt}$ group is present (as well as a $\mu_2\text{-oxo}$ group) in $[\text{Nb}_2(\mu_2\text{-O})(\mu_2\text{-OEt})(L)(\text{OEt})_6]$ (L = bidentate aryl monocarboxylate). When two carboxylate bridges occurs in the dimer, only one central $\mu_2\text{-oxo}$ group is found in compounds **Nb(V)-2**, **Nb(V)-4** and **Nb(V)-6** of type $[\text{Nb}_2(\mu_2\text{-O})(L)_2(\text{OEt})_6]$. The substitution of the $\mu_2\text{-OEt}$ groups by one carboxylate arm, releases ethanol molecule (coming from H exchange between $\text{R-CO}_2\text{H}$ and $\text{Nb-OEt} \rightarrow \text{R-CO}_2\text{-Nb}$ and Et-OH) in the medium which is able to further react with free carboxylic acid through an esterification process with the in situ production of water, leading to the hydrolysis and Nb-O-Nb condensation^[16] (Figure III-21 [B]). This esterification reaction has been observed in the supernatant liquor by infrared spectroscopy for the crystallization of compound **Nb(V)-1** (Figure A10, paragraph A4, Appendix) and by ^1H NMR for compounds **Nb(V)-1**, **Nb(V)-2** and **Nb(V)-4** (Figures 12-20). This carboxylate complexation is relatively rapid since IR spectra clearly indicates the formation of such niobium carboxylate species in solution after 1-hour reaction. Therefore, the monocarboxylate niobium dimeric complexes **Nb(V)-3** and **Nb(V)-5** can be viewed as a first step of the carboxylate complexation, with one bridging $\mu_2\text{-ethoxy}$ leaving groups substituted by one bidentate carboxylate bridging group. The presence of the additional bridging $\mu_2\text{-oxo}$ group requires the withdrawal of two terminal ethoxy groups, which contributes to the release of extra ethanol molecules in the reaction medium (from H exchange between H_2O and $2 \times \text{Nb-OEt} \rightarrow \text{Nb-O-Nb}$ and $2 \times \text{Et-OH}$; (Figure III-21 [B])). The second step of the carboxylate complexation would then lead to the formation of a dinuclear species containing two carboxylate linkers, as observed in compounds **Nb(V)-2**, **Nb(V)-4** and **Nb(V)-6**, with the substitution of the second bridging $\mu_2\text{-OEt}$ group by an additional carboxylate ligand (Figure III-21 [C]).

Moreover, these two distinct configurations of Nb/Ligand ratio of 2/1 or 2/2 may differ from steric hindrance of the bulky aromatic molecule, as illustrated with the position of the bridging carboxylates in *ortho* or *meta* (or *para*), relative to the position of adjacent neighboring benzene ring. Thus, the *ortho* position of carboxylate group in 1-naphthoate

(Nb(V)-3) or anthracene-9-carboxylate (**Nb(V)-5**) ligands gives rise to the monocarboxylate niobium dimeric complexes, whereas the respective *meta* (2-naphthoate; **Nb(V)-2**) or *para* (4-methyl-biphenylmonocarboxylate; **Nb(V)-4**) position of the carboxylate group leads to the formation to the dicarboxylate niobium dimeric complexes. However, all these coordination complexes have been synthesized directly from the mixture of the liquid phase of niobium ethoxide with a monocarboxylic acid source, with quite low yields (< 20 %_{Nb}). One limiting step of such reaction could be the relatively low solubility of such aromatic monocarboxylic acids in the pure niobium ethoxide solution, which may result in Nb/Ligand ratio of 2/1 or 2/2 in dinuclear cores, independently of the steric hindrance or position of the carboxylate function, of the different monocarboxylate molecules. Indeed, in the different synthesis batches, we observed some difficulties to dissolve the monocarboxylic acid. Unreacted starting ligands were often visible as crystallizing as by-product together with the niobium coordination complexes. Depending on the solubility of the carboxylic acid in niobium ethoxide, undissolved starting ligand sometimes remains on the bottom of the vial without reacting, while the ligand placed on the top that comes first in contact with niobium ethoxide is dissolved and reacts to form crystals of the present products. By mild heating (since alkoxides are reported not to be stable in great temperatures, sublimed around 100 °C,^[22] we can observe the solubilization (clear solution) but not a crystallization.

In order to investigate the influence of the monocarboxylic acid concentration, we thus investigated a second series of syntheses involving the addition of alcohol solvent. When isopropanol (HOⁱPr) was used in molar ratio 0.8 Nb(OEt)₅ /13.1 HOⁱPr (volume ratio 0.2 Nb(OEt)₅ /1 HOⁱPr), a clear solution was systematically obtained after mixing the different source reactants (niobium ethoxide, monocarboxylic acid, isopropanol). However, when using anthracene-9-carboxylic acid, we were able to isolate in such isopropanol/niobium ethoxide mixture, a second dinuclear complex (**Nb(V)-6**) containing two carboxylate ligands instead of one in **Nb(V)-5** (synthesized in pure niobium ethoxide solution). The isopropanol solvent is assumed to promote the dissolution of the poly-benzene carboxylic acid in order to enhance the carboxylate complexation. Therefore, the formation of the monocarboxylate or dicarboxylate dimeric niobium-centered complexes is not directly correlated to the steric hindrance of the organic linker in this case.

Another aspect of the production niobium carboxylate from metal alkoxide source is the occurrence of multiple nuclearities for niobium, which have been isolated in a tetranuclear core with benzoate and 2-naphtoate bidentate bridging linkers, or octanuclear core with 2-naphtoate one. With benzoic acid (**Nb(V)-1**), only a tetrameric moiety is observed with four niobium centers, located at each node of square geometry, and linked to each other through μ_2 -oxo groups, resulting in a $[\text{Nb}_4(\mu_2\text{-O})_4(\text{L})_4(\text{OEt})_8]$ core. The benzene rings of the four bidentate carboxylate linkers are pointed along the square plane direction for two of them, and up and downward the square plane for the two others. It is interesting to observe that the in-situ generation of water from esterification process is particularly efficient with the benzoic acid, leading directly to a tetranuclear species, instead of the dinuclear one, as observed with other poly-benzene-based monocarboxylic acids (compounds **Nb(V)-(2-6)**). Indeed, the ethyl benzoate ester is visible just after one-hour reaction in the mother liquor (Figure A10, paragraph A4, Appendix) whereas it not observed for the other aryl acids, for which ester forms are seen when crystallized phase is produced (see ^1H NMR, for the systems **Nb(V)-2** and **Nb(V)-4**, for instance figures 13-16, 20). In fact, a previous study has reported the occurrence of such dinuclear species containing a central μ_2 -oxo group in a benzoate complex $[\text{Nb}_2\text{Cl}_6(\text{O}_2\text{C-C}_6\text{H}_5)_2\text{O}]^{[19]}$, when the niobium source was NbCl_5 , and mixed in chloroform or carbon tetrachloride, which was then heated at 60-110°C. For the latter, the origin of the bridging oxygen atom comes from the formation of acyl chloride ($3 \text{R-CO}_2\text{H} + 2\text{NbCl}_5 \rightarrow \text{R-COCl} + \text{Nb}_2\text{Cl}_6(\text{O}_2\text{C-C}_6\text{H}_5)_2\text{O}$), which releases one available oxo species for the Nb-O-Nb condensation. The yield of acyl chloride reaction seems to be less efficient for the generation of dinuclear unit $[\text{Nb}_2(\mu_2\text{-O})(\text{L})_2\text{Cl}_6]$ compared to that giving rise straightly to a higher condensed species as found in the $[\text{Nb}_4(\mu_2\text{-O})_4(\text{L})_4(\text{OEt})_8]$ core. As suggested by different authors^[15-17], the tetranuclear entity $[\text{Nb}_4(\mu_2\text{-O})_4(\text{L})_4(\text{OEt})_8]$ can be viewed as the assembly of two dinuclear $[\text{Nb}_2(\mu_2\text{-O})(\text{L})_2(\text{OEt})_6]$ bricks via two additional μ_2 -oxo groups, coming from the removal of four terminal ethoxy groups (Figure III-21 [D] and 22). This tetrameric entity can thus be considered as a second step of condensation with the formation of additional double Nb-O-Nb linkages.

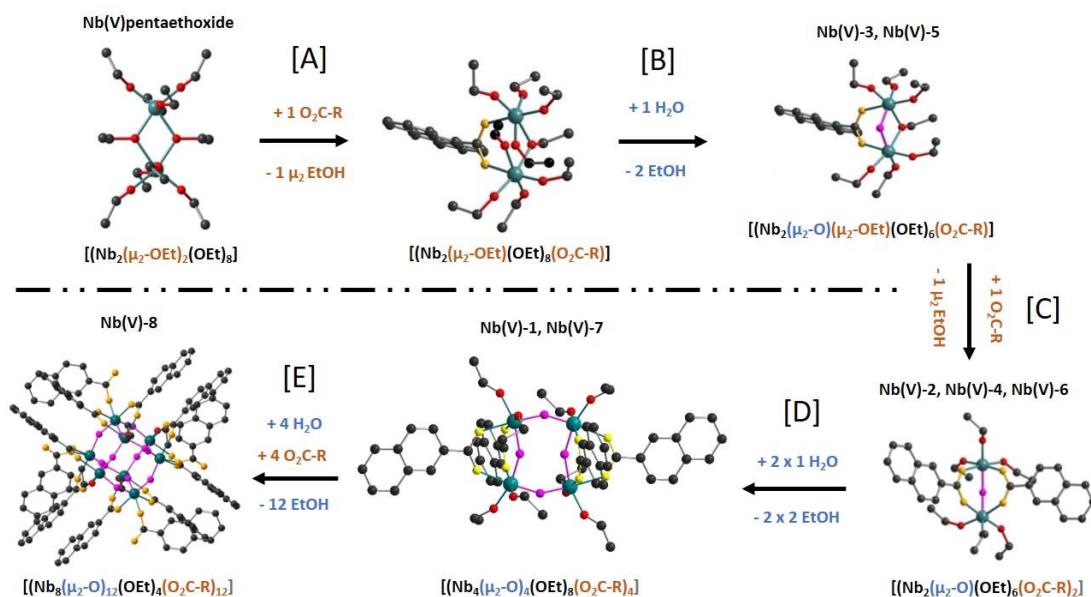


Figure III-21. Schematic proposed reactional pathways for the formation of dinuclear, tetranuclear and octanuclear cores of niobium(V) monocarboxylates coordination complexes **Nb(V)-(1-8)**. For compound **Nb(V)-8**, only bidentate 2-naphtoate linkers are shown; terminal monodentate 2-naphtoate ligand are not shown for clarity. Green: niobium; dark grey: carbon; red: oxygen from ethoxy group; purple: bridging oxygen between Nb centers; orange: oxygen from bidentate carboxylate groups.

With benzoic acid, it was only possible to isolate either a crystalline dinuclear or tetranuclear species by changing the niobium source (NbCl_5 or $\text{Nb}(\text{OEt})_5$). It seems that multiple nuclearity was not reported in literature for a given niobium precursor. Indeed, it was proposed that steric hindrance of the ligand might orientate the nuclearity of the complex as illustrated in the work of Boyle^[17], for which a dimer was obtained with a bulky molecule (pivalic acid), whereas a tetramer is obtained with a less bulky molecule (terbutylacetic acid), prepared in the same synthetic conditions. In fact, by using 2-napthoic acid, we show here that the nuclearity of the inorganic core is controlled by the hydrolysis rate. For a low water content (coming from esterification reaction at room temperature), the dinuclear core $[\text{Nb}_2(\mu_2\text{-O})(\text{L})_2(\text{OEt})_6]$ (**Nb(V)-2**) is observed, whereas the tetranuclear core $[\text{Nb}_4(\mu_2\text{-O})_4(\text{L})_4(\text{OEt})_8]$ (**Nb(V)-7**) has been identified in a closed reaction medium saturated with 55% water humidity. This suggests that an increasing water content promotes the Nb-O-Nb condensation process, which can favor the formation of higher nuclearity in niobium carboxylate complexes. The last coordination complex observed in our system involving 2-napthoic acid, is the isolation of poly-oxo cluster containing eight niobium centers located at each node of a cubic geometry (**Nb(V)-8**). Indeed, its crystal structure exhibits one octanuclear moiety which is stabilized under two slightly different forms, with a general formula of $[\text{Nb}_8(\mu_2\text{-O})_{12}(\text{L})_8(\text{OEt})_{4+x}(\eta^1\text{-L})_{4-x}]$ ($x = 0$ or 2), with varying numbers of terminal

ethoxy/naphthoic acid groups. Apart that, this octamer is new in chemistry of niobium carboxylates poly-oxo clusters, it is a good illustration of a third step for the condensation Nb-O-Nb process, by considering the association of two tetramers $[\text{Nb}_4(\mu_2\text{-O})_4(\text{L})_4(\text{OEt})_8]$ through the addition of quadruple μ_2 -oxo ligand between the niobium centers (Figure III-21 [E]; Figure III-22). For **Nb(V)-8**, the hydrolysis rate is enhanced by using a solvothermal synthetic route (here heating at 100°C for 4 days in acetonitrile), which allows for the production of higher water content through esterification increasing yield. Similar reaction conditions thus led to the synthesis of a 16-nuclearity poly-oxo cluster in $[\text{Nb}_{16}\text{O}_{28}(\text{OEt})_{12}(\text{piv})_{12}]^{[29]}$.

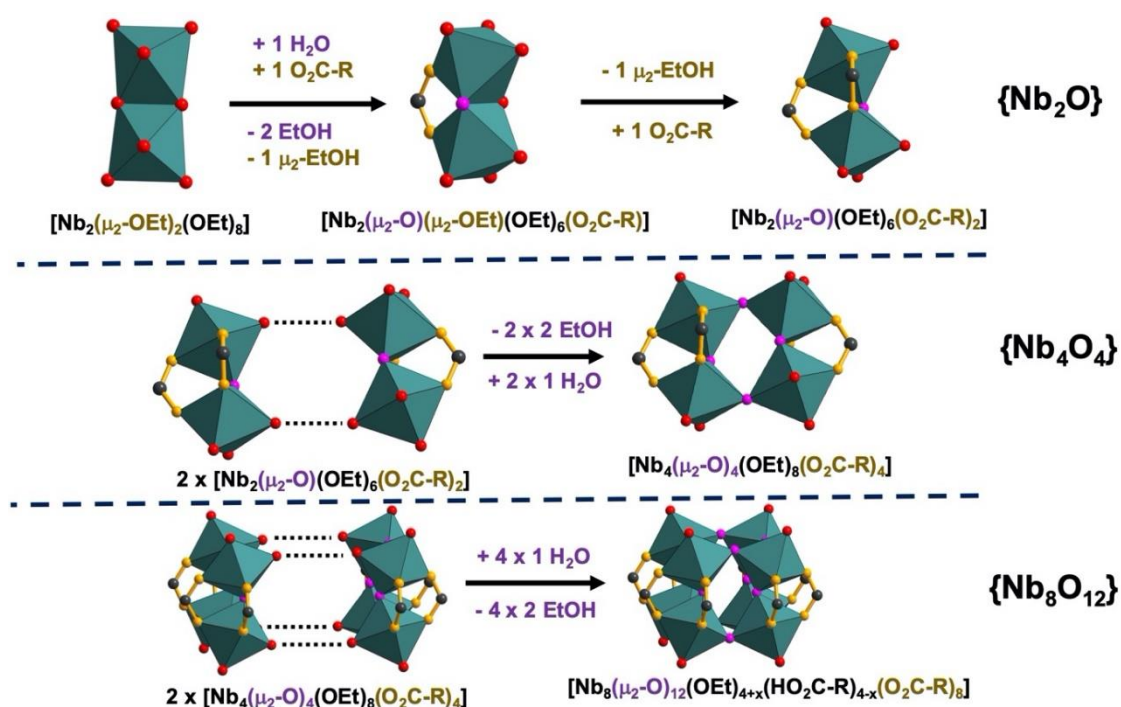


Figure III-22. Schematic proposed reactional pathways for the formation of dinuclear, tetranuclear and octanuclear cores of niobium(V) monocarboxylates coordination complexes **Nb(V)-(1-8)** with a polyhedral representation. For **Nb(V)-8**, only bidentate 2-naphtoate linkers are shown; terminal monodentate 2-naphtoate ligand are not shown for clarity. Green: niobium; dark grey: carbon; red: oxygen from ethoxy group; purple: bridging oxygen between Nb centers; orange: oxygen from bidentate carboxylate groups.

From this series, it was possible to play with the hydrolysis rate by isolating different steps of Nb-O-Nb condensation from non-oxo $\{\text{Nb}\}$ species to oxo species with $\{\text{NbO}_{0.5}\}$ (**Nb(V)-(2-6)**), $\{\text{NbO}_{1.0}\}$ (**Nb(V)-1** and **Nb(V)-7**), $\{\text{NbO}_{1.5}\}$ (**Nb(V)-8**) and $\{\text{NbO}_{1.75}\}^{[29]}$, knowing that the ultimate member would be the infinite dense niobium oxide network $\{\text{NbO}_{2.5}\}_\infty$ as found in Nb_2O_5 . It is noticeable to observe that the octanuclear $\{\text{Nb}_8\text{O}_{12}\}$ brick, as a corner-sharing octahedral arrangement of perovskite-related ReO_3 type structure, can be considered as a fragment of the Nb_2O_5 network. Although its crystal chemistry offers many complex

polymorphic stackings^[30], one may identify some blocks with such ReO_3 configurations, in some of them, related to different forms identified at various temperatures (Figure III-23).

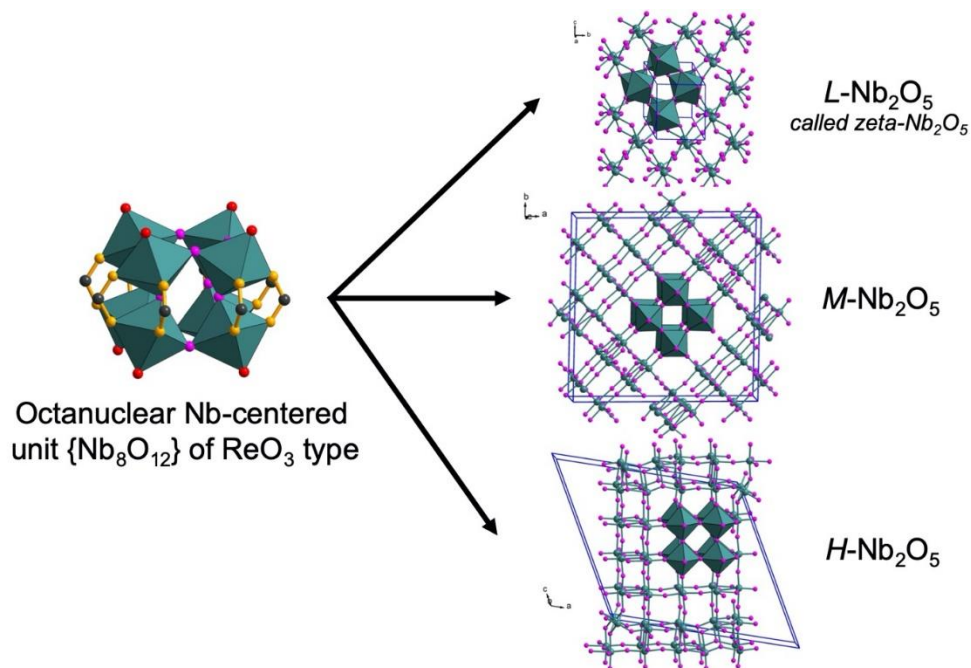


Figure III-23. Representation of the octanuclear brick $\{\text{Nb}_8\text{O}_{12}\}$ (**Nb(V)-8**) and its observation as perovskite-like ReO_3 fragment in different dense niobium oxides: L-(low T)- Nb_2O_5 ^[31], M-(medium T) Nb_2O_5 ^[32] and H-(medium T) Nb_2O_5 ^[33]

The different polynuclear niobium oxo-clusters **Nb(V)-(1-8)** are systematically constructed from octahedral NbO_6 polyhedra connected through a corner-sharing mode. This particular linkage fashion is surely promoted by the double bidentate carboxylate bridge, which acts as a pincer between two adjacent niobium atoms, and thus favors the oxo-corner fashion. This specific connection mode is nevertheless not observed in the chemistry of niobium-based polyoxometalates species, since the basic bricks are composed of the hexanuclear entity $[\text{Nb}_6\text{O}_{19}]^{8-}$ of Lindqvist type, or decaniobiate $[\text{Nb}_{10}\text{O}_{28}]^{6-}$, which both are characterized by edge-sharing NbO_6 octahedra.^[34] These anionic moieties are able to further react to generate a large number of highly condensed oxo clusters such as the giant $\{\text{Nb}_{288}\text{O}_{768}(\text{OH})_{48}(\text{CO}_3)_{12}\}$,^[35] for instance. The edge-sharing mode is also observed in purely niobium alkoxides such as the dimeric precursors^[21,22,36], hexanuclear $[\text{Nb}_6\text{O}_8(\text{O}^i\text{Pr})_{14}(\text{HO}^i\text{Pr})_2]$ species with isopropoxy groups^[37] or octanuclear species $[\text{Nb}_8\text{O}_{10}(\text{OEt})_{20}]$ with ethoxy groups.^[38] Another structural difference between the niobium-based polyoxometalates and the niobium alkoxides molecules is the distinct nature of the terminal oxo groups. The polyoxometalates are usually characterized by the occurrence of terminal niobyl-oxo groups,

which are not observed in the niobium mixed alkoxide-carboxylates, since the terminal oxo groups belong to alkoxo species decorating the external periphery of the polynuclear moiety.

Different molecular polynuclear compounds were synthesized with monocarboxylic acids and were deeply characterized. Nevertheless, generating a multidimensional network remains an important goal and thus monocarboxylic acids were replaced by dicarboxylic and tetracarboxylic acids. Their reactivity with Nb(V)ethoxide is studied in the second part of this chapter.^[39]

III. 2 Nb(V) polycarboxylate complexes

A part of the results has just been published in august issue of CrystEngComm (2022, 24, 5938-5948).^[39]

In the above part of this chapter, the reactivity of Nb(V) towards monocarboxylates was studied. It was possible to synthesize molecular Nb(V) poly-oxo clusters with different nuclearities. Using monocarboxylic acids as precursors it was expected that only molecular assemblies will be isolated. However, what was interesting to study afterwards, was the reactivity towards carboxylic ligands with multiple carboxylate branches, in order to increase the dimensionality of our Nb(V) compounds. As presented in Chapter I (paragraph I.3 “Towards niobium-containing multi-dimensional networks”), only one report has been published so far in this topic, by using terephthalate linker in Cp₂'-derived organo-metallic complex (Chapter I, Figure I-7).^[40]

III.2.1 Synthesis of Nb(V) polycarboxylate complexes

Compound Nb(V)-10 [(Nb₂(μ₂-O)(μ₂-OEt)(OEt)₆)₂(Nb(OEt)₄(HOEt))₂(C₁₀H₂O₈)]: A mixture of 0.75 mL (3 mmol) Nb(OCH₂CH₃)₅ and 76.2 mg (0.3 mmol) pyromellitic acid was placed in a 2 mL glass tube, sealed with a phenolic cap, and left at room temperature. Block-like transparent crystals appeared after 3 months. Compound **Nb(V)-10** was analyzed by optical and scanning electron microscope showing large block-shaped crystals up to 50 μm size. The resulting colorless crystals filtered off, washed with ethanol and dried at room temperature. Crystallization yield was 4.8 %_{Nb}. (Figure III-24, left).

Compound Nb(V)-11 [(Nb₂(μ₂-O)(μ₂-OEt)(OEt)₆)₂(C₁₄H₈N₂O₄)]: A mixture of 0.5 mL (2.7 mmol) Nb(OCH₂CH₃)₅ and 8 mg (0.027 mmol) 4,4'-azobenzene dicarboxylic acid was placed in a 2 mL

glass tube, sealed with a phenolic cap, and left at room temperature. Parallelepiped-shaped orange crystals appeared after 1 week. Compound **Nb(V)-11** was analyzed by optical microscope showing parallelepiped-shape crystals up to 70 μm size. The resulting orange crystals filtered off, washed with ethanol and dried at room temperature. Crystallization yield was 12.8 %_{Nb}. (Figure III-24, middle).

Compound Nb(V)-12 $[(\text{Nb}_2(\mu_2\text{-O})(\mu_2\text{-OEt})(\text{OEt})_6)_4(\text{C}_{16}\text{H}_8\text{N}_2\text{O}_8)]$: A mixture of 0.5 mL (2.7 mmol) $\text{Nb}(\text{OCH}_2\text{CH}_3)_5$ and 10 mg (0.027 mmol) 3,3',5,5'-azobenzene tetracarboxylic acid was placed in a 2 mL glass tube, sealed with a phenolic cap, and left at room temperature. Plate-like yellowish crystals appeared after 4 weeks with a size up to 20 μm size, as observed with optical microscope. The resulting yellowish crystals of **Nb(V)-12** were filtered off, washed with ethanol and dried at room temperature. Crystallization yield was 7.3 %_{Nb}. (Figure III-24, right).

Table III-5. Synthetical protocols for **Nb(V)-(10-12)**.

	Metal source	Ligand	Solvent	T	Time	Yield
Nb(V)-10	$\text{Nb}(\text{OEt})_5$ 0.75 mL 3 mmol	Pyromelitic acid 76.2 mg 0.3 mmol	-	RT	12 w	4.8 %
Nb(V)-11	$\text{Nb}(\text{OEt})_5$ 0.5 mL 2.7 mmol	4,4'-azobenzene dicarboxylic acid 8 mg 0.027 mmol	-	RT	1 w	12.8 %
Nb(V)-12	$\text{Nb}(\text{OEt})_5$ 0.5 mL 2.7 mmol	3,3',5,5'-azobenzene tetracarboxylic acid 10 mg 0.027 mmol	-	RT	4 w	7.3 %

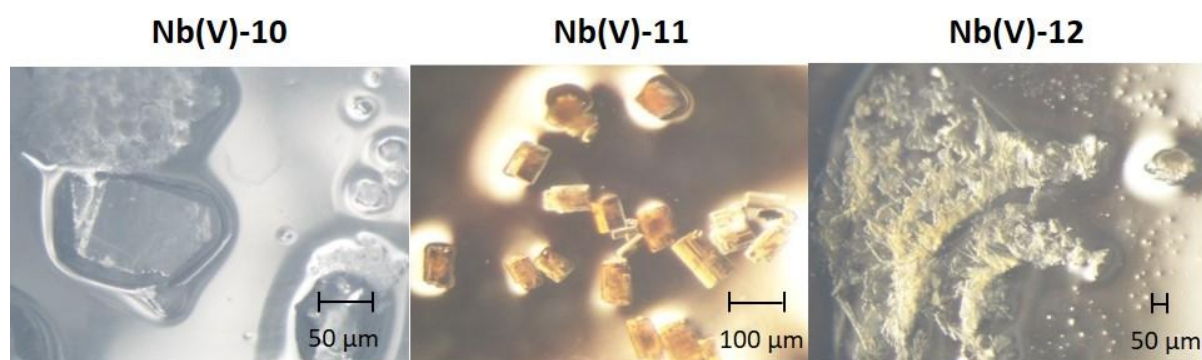


Figure III-24. Crystals of **Nb(V)-(10-12)** from left to right under optical microscope.

III. 2.2 Structural description

All the compounds **Nb(V)-10** → **Nb(V)-12** have been characterized by single-crystal X-ray diffraction analysis. Crystalline products have been also checked by powder X-ray diffraction for their purity (Figure A3, paragraph A3, Appendix).

The summary of the crystallographic data is summarized in the following Table III-6.

Table III-6. Crystal data and structure refinements for compounds **Nb(V)-(10 – 12)**.

	Nb(V)-10	Nb(V)-11	Nb(V)-12
Formula	C ₅₈ H ₁₂₂ Nb ₆ O ₃₄	C ₄₂ H ₇₈ N ₂ Nb ₄ O ₂₀	C ₇₂ H ₁₄₆ N ₂ Nb ₈ O ₄₀
Formula weight	1921.07	1302.7	2423.18
Temperature/K	107	100	100
Crystal type	colorless block	Orange block	Orange block
Crystal size/mm	0.85 x 0.52 x 0.45	0.24 x 0.24 x 0.12	0.132 x 0.098 x 0.083
Crystal system	monoclinic	monoclinic	triclinic
Space group	<i>C2/c</i>	<i>P2₁/n</i>	<i>P-1</i>
<i>a</i> /Å	24.0277(14)	15.3902(12)	8.0483(9)
<i>b</i> /Å	18.1923(11)	20.0542(14)	18.5558(19)
<i>c</i> /Å	19.0237(12)	17.5280(13)	18.624(2)
<i>α</i> /°	90	90	68.271(4)
<i>β</i> /°	97.308(3)	90.114(3)	81.253(5)
<i>γ</i> /°	90	90	84.084(5)
Volume/Å ³	8248.1(9)	5409.8(7)	2550.4(5)
<i>Z</i> , <i>ρ</i> _{calculated} /g.cm ⁻³	4, 1.547	4, 1.599	1, 1.578
<i>μ</i> /mm ⁻¹	0.884	0.898	0.945
<i>θ</i> range/°	1.71 - 26.42	1.32 - 26.41	1.339 - 26.428
Limiting indices	-30 ≤ <i>h</i> ≤ 30 -22 ≤ <i>k</i> ≤ 22 -22 ≤ <i>l</i> ≤ 23	-19 ≤ <i>h</i> ≤ 19 -25 ≤ <i>k</i> ≤ 23 -21 ≤ <i>l</i> ≤ 21	-10 ≤ <i>h</i> ≤ 10 -22 ≤ <i>k</i> ≤ 23 -15 ≤ <i>l</i> ≤ 31
Collected reflections	62529	78621	31082
Unique reflections	8239 [R(int) = 0.0350]	11078 [R(int) = 0.0479]	10333 [R(int) = 0.0999]
Parameters	612	660	655
Goodness-of-fit on F ²	1.050	1.022	1.010
Final R indices [I > 2σ(I)]	R1 = 0.0580 wR2 = 0.1379	R1 = 0.0306 wR2 = 0.0715	R1 = 0.0675 wR2 = 0.1173
R indices (all data)	R1 = 0.0750 wR2 = 0.1521	R1 = 0.0357 wR2 = 0.0741	R1 = 0.1615 wR2 = 0.1442
Largest diff. peak and hole/e.Å ⁻³	2.28 and -1.18	0.95 and -0.82	0.74 and -1.27

Compound **Nb(V)-10** [(Nb₂(μ₂-O)(μ₂-OEt)(OEt)₆)₂(Nb(OEt)₄(HOEt))₂(C₁₀H₂O₈)₂]

The crystal structure of compound **Nb(V)-10** displays an assembly of unusual centrosymmetric hexanuclear core centered around the pyromellitate ligand through niobium(V) connection with all its carboxylate arms (Figure III-25). Two of them, located in an opposite side in 1,4-position, act as a bidentate bridging linker to two adjacent niobium atoms Nb1 and Nb2 with a *syn-syn* configuration. These two niobium centers are six-fold coordinated in a distorted octahedral geometry, to one μ₂-oxo (O6) group (Nb1-O6 = 1.940(3) Å; Nb2-O6 = 1.925(4) Å), one bridging μ₂-ethoxy group (Nb1-O5_{Et} = 2.102(4) Å; Nb2-O5_{Et} = 2.147(4) Å) and three oxo groups from ethoxy molecules (Nb1-O_{Et} in the range 1.876(3)-1.893(4) Å; Nb2-O_{Et} in the range 1.865(4)-1.906(4) Å). The coordination sphere around the niobium atoms is

completed by one oxygen atom ($\text{Nb1-O1}_c = 2.205(3) \text{ \AA}$; $\text{Nb2-O7}_c = 2.206(3) \text{ \AA}$) from the bidentate carboxylate group of the pyromellitate ligand. The occurrence of the m_2 -oxo groups does well agree with the bond valence calculations (1.888 for O6).^[41] It results in a dinuclear motif in which the two niobium-centered octahedral polyhedra are sharing edge through both m_2 -oxo and m_2 -ethoxy groups. The bidentate carboxylate pincer related to the Nb1...Nb2 axis, adopts a rotation of 90° compared to the benzene ring plane. Within this dinuclear sub-unit, the Nb1...Nb2 bond length is $3.2467(7) \text{ \AA}$ with an Nb1-O6-Nb2 angle of $114.3(2)^\circ$. These metric values are closely related to those of the dinuclear niobium(V)-centered unit stabilized by only one carboxylate pincer, as it is observed in compound **Nb(V)-11** and **Nb(V)-12**, with the azobenzene dicarboxylate and tetracarboxylate ligands.

The two other carboxylate groups (in 2,5-position) exhibit a monodentate connecting mode with a third niobium center. However, the situation is a bit more complicated since this niobium atom is delocalized on two close positions (Nb3A and Nb3B), offering a statistical disorder for the octahedral environment. Indeed, this niobium is six-fold coordinated to one oxygen atom from the carboxylate group and five oxygen atoms from ethoxy groups in terminal position, reflecting a mobility freedom for this set of atoms. The Nb3A-O12A_c and Nb3B-O12B_c bond distances are $2.149(11)$ and $2.148(11) \text{ \AA}$, respectively. All the other Nb3-O_{Et} bond lengths are ranging between $1.873(10)$ and $1.901(11) \text{ \AA}$ for Nb3A, and between $1.852(12)$ and $1.898(19) \text{ \AA}$ for Nb3B, as expected for the niobium attached to ethoxy group. However, it is observed that one of the Nb3-OEt distances of one ethoxy group exhibits a much longer unusual distance of $2.254(11) \text{ \AA}$ for sub-unit with Nb3A and $2.209(10) \text{ \AA}$ for sub-unit with Nb3B. Indeed, this oxo group (O15A or O15B) also interacts through hydrogen bonding with the free remaining oxygen atom from the carboxylate arm of the pyromellitate ligand (see dotted line in the Figure III-25), as reflecting by the short O15A...O11A_c and O15B...O11B_c distances of $2.524(3) \text{ \AA}$ and $2.57(3) \text{ \AA}$, respectively. The presence of ethanol molecule (instead of EtO⁻) linked to the niobium Nb3 site is therefore considered for the fifth alkoxy ligand around Nb3. But due to disorder of the Nb3 site and the surrounding ethoxy/ethanol groups, it was not possible to clearly locate the hydrogen atoms of the EtOH species. The pyromellitate is fully deprotonated and acts as a hexadentate linker with six niobium atoms, four of them engaged in dinuclear moieties and two of them in mononuclear moieties. The resulting molecular species is neutral, due to the presence of one ethanol group attached to discrete

sub-unit of niobium (Nb3), ensuring hydrogen bonding with the free carboxyl oxygen of the pyromellitate ligand. It is found that the orientation of this carboxylate group is nearly along the benzene ring plane. The occurrence of these two types of niobium sub-units (dinuclear and mononuclear in a *trans* configuration) is surely controlled by the steric hindrance of these motifs since relatively short methyl-methyl distances of 4.27(1) Å are observed between those from the dinuclear units. Those prevent further niobium-oxo-niobium condensation in the mononuclear sub-unit. Anyway, it is an original condensation mode of the niobium ethoxy motifs through the polydentate ligand, 1,2,4,5-benzenetetracarboxylate, which has never been reported in literature up to now. Only reaction with monocarboxylate species has been used with the niobium(V) complexes.

Such a connection mode with bridging μ_2 -oxo, μ_2 -ethoxy and carboxylate groups with two adjacent niobium atoms was previously reported in one complex stabilized by the bis(hydroxymethyl)propionate molecule.^[22]

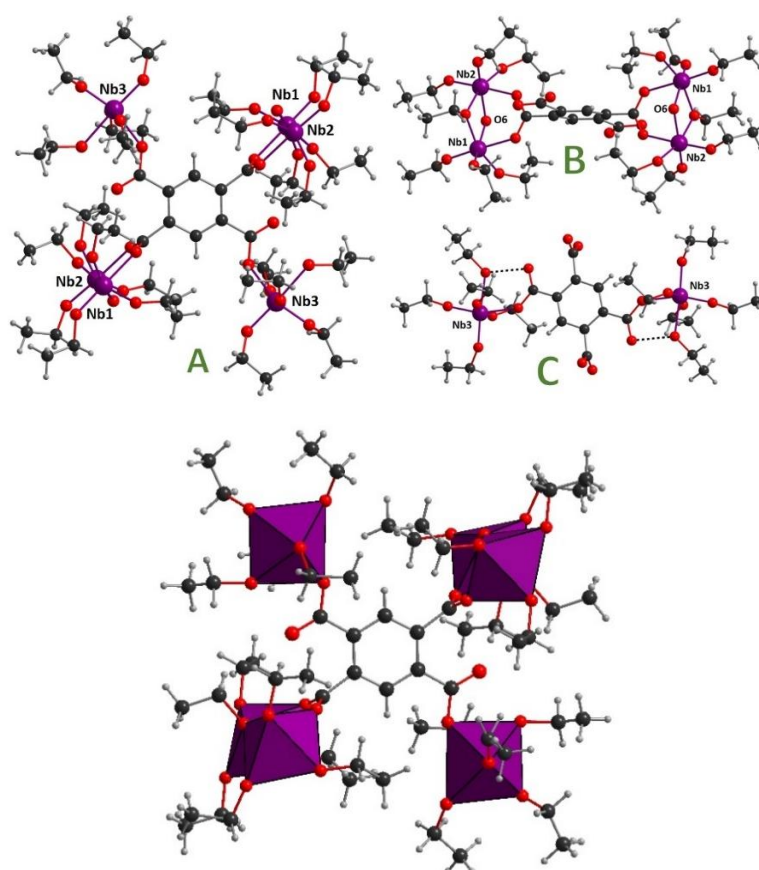


Figure III-25. Ball and stick (top) and polyhedral (bottom) representations of the molecular hexanuclear coordination **Nb(V)-10**. On left (top, A): view of the entire **Nb(V)-10**; on right (top): detailed views of the connection mode of the carboxylate arm in 1,4 position (B) and 2,5 position (C). One of the ethoxy groups linked to Nb1 site (through Nb1-O8 bonding) is disordered on two equivalent positions. Only one of these ethoxy groups is shown for clarity.

Compound Nb(V)-11 $[(\text{Nb}_2(\mu_2\text{-O})(\mu_2\text{-OEt})(\text{OEt})_6)_2(\text{C}_{12}\text{H}_6\text{O}_4)]$ with $\text{C}_{12}\text{H}_6\text{O}_4 = 4,4'$ -azobenzene dicarboxylate

Compound **Nb(V)-11** crystallizes in the monoclinic $P2_1/n$ space group. The crystal structure in compound **Nb(V)-11** displays a molecular system composed of one 4,4'-azobenzene dicarboxylate ligands linking two niobium(V) dimers (Nb1-Nb2 and Nb3-Nb4) through the two bidentate carboxylate functions, located on each side of the ligand (Figure III-26). In this system, the four niobium(V) cations are six-fold coordinated with a distorted octahedral geometry. The environment is exclusively composed of oxygen atoms coming from one μ_2 -bridging oxo (O6 for Nb1-Nb2 dimer and O15 for Nb3-Nb4 dimer) atom (Nb1-O6 = 1.930(2) Å; Nb2-O6 = 1.920(2) Å; Nb3-O15 = 1.926(2) Å and Nb4-O15 = 1.929(2) Å), one μ_2 -bridging ethoxy group (Nb1-O5_{Et} = 2.114(2) Å; Nb2-O5_{Et} = 2.115(2) Å; Nb3-O16_{Et} = 2.117(2) Å and Nb4-O16_{Et} = 2.123(3) Å) and three terminal ethoxy molecules (Nb1-O_{Et} in the range 1.865(2)-1.900(2) Å; Nb2-O_{Et} in the range 1.849(2)-1.893(3) Å; Nb3-O_{Et} in the range 1.866(2)-1.900(3) Å and Nb4-O_{Et} in the range 1.863(3)-1.884(3) Å). The coordination sphere of each niobium centers is completed by one oxygen atom coming from the bidentate carboxylate functions of the azobenzene dicarboxylate ligand (Nb1-O1_c = 2.188(2) Å; Nb2-O7_c = 2.227(2) Å; Nb3-O11_c = 2.191(2) Å and Nb4-O17_c = 2.212(2) Å). In both dimers, the presence of the μ_2 -oxo bridging atom is confirmed by BVS calculations (1.926 and 1.913 for O6 and O15 respectively)^[41]. Consequently, in the dimers, the two niobium centers share on edge through the binding of the bridging μ_2 -oxo and μ_2 -ethoxy groups. The bidentate carboxylate function related to the Nb1...Nb2 axis and Nb3...Nb4 axis, adopts a rotation of 20.868(83)° and 23.636(81)° respectively compared to the benzene ring plane. The two aromatic rings planes are slightly rotated with an angle of 3.106(98)°. In these two dinuclear sub-units, the Nb1...Nb2 and Nb3...Nb4 bond length is 3.2222(5) Å and 3.2412(5) Å with Nb1-O6-Nb2 and Nb3-O15-Nb4 angles of 113.64(12)° and 114.46(13)° respectively. The coordination modes of the niobium dimers in this compound is similar to the one described for the dimers in compound **Nb(V)-10**.

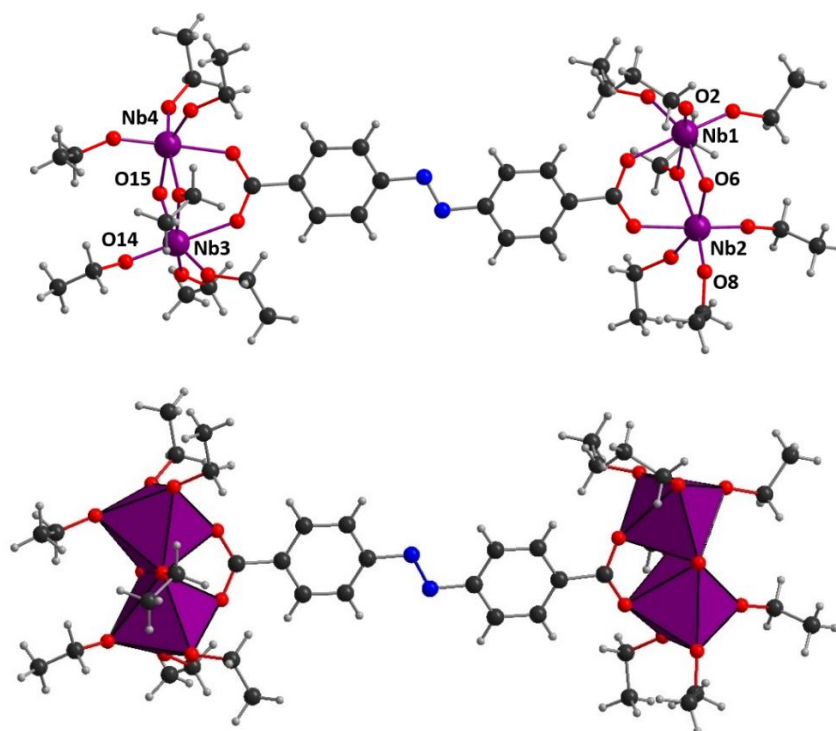


Figure III-26. Ball and stick (top) and polyhedral (bottom) representations of the molecular tetranuclear coordination complex **Nb(V)-11**. The ethoxy groups linked to Nb1 site (through Nb1-O2 bonding), Nb2 site (through Nb2-O8 bonding) and Nb3 site (through Nb3-O14 bonding) and Nb3 site (through Nb3-O14 bonding) are disordered on two equivalent positions. Only one of these ethoxy groups is shown for clarity.

Compound **Nb(V)-12** $[(\text{Nb}_2(\mu_2\text{-O})(\mu_2\text{-OEt})(\text{OEt})_6)_4(\text{C}_{16}\text{H}_8\text{N}_2\text{O}_8)]$: with $\text{C}_{16}\text{H}_8\text{N}_2\text{O}_8 = 3,3',5,5'$ -azobenzene tetracarboxylate

Compound **Nb(V)-12** crystallizes in the monoclinic $P-1$ space group. The asymmetric unit of the crystal structure displays one half of one 3,3',5,5'-azobenzenetetracarboxylate ligand linking two niobium(V) dimers (Nb1-Nb2 and Nb3-Nb4) through two bidentate carboxylate functions. The presence of an inversion center located between the two nitrogen atoms of the azo ligand generate the full molecular compound where the ligand binds four niobium dimers (Figure III-27). The composition of the dimers is similar to the one described for compounds **Nb(V)-10** and **Nb(V)-11**. All niobium(V) cations are six-fold coordinated with a distorted octahedral geometry and, their environment is exclusively composed of oxygen atoms coming from one m_2 -bridging oxo (O1 for Nb1-Nb2 dimer and O11 for Nb3-Nb4 dimer) atom (Nb1-O1 = 1.913(4) Å; Nb2-O1 = 1.944(4) Å; Nb3-O11 = 1.930(6) Å and Nb4-O11 = 1.933(5) Å), one μ^2 -bridging ethoxy group (Nb1-O7_{Et} = 2.111(4) Å; Nb2-O7_{Et} = 2.124(4) Å; Nb3-O17_{Et} = 2.124(6) Å and Nb4-O17_{Et} = 2.121(6) Å) and three terminal ethoxy molecules (Nb1-O_{Et} in the range 1.855(5)-1.907(4) Å; Nb2-O_{Et} in the range 1.858(5)-1.894(5) Å; Nb3-O_{Et} in the range 1.865(6)-1.883(5) Å and Nb4-O_{Et} in the range 1.846(5)-1.904(6) Å). The coordination sphere of each

niobium centers is completed by one oxygen atom coming from the bidentate carboxylate functions of the azobenzene dicarboxylate ligand ($\text{Nb1-O3}_c = 2.202(4) \text{ \AA}$; $\text{Nb2-O2}_c = 2.234(4) \text{ \AA}$; $\text{Nb3-O12}_c = 2.234(4) \text{ \AA}$ and $\text{Nb4-O13}_c = 2.188(4) \text{ \AA}$). In both crystallographically independent dimers, the presence of one μ_2 -oxo bridging atom is confirmed by BVS calculations (1.909 and 1.892 for O1 and O11 respectively)^[41]. Alike the other niobium dimers in compounds **Nb(V)-10** and **Nb(V)-11**, the two niobium centers share on edge through the binding of the bridging μ_2 -oxo and μ_2 -ethoxy groups. The bidentate carboxylate function related to the Nb1...Nb2 axis and Nb3...Nb4 axis, adopts a rotation of $9.797(152)^\circ$ and $7.398(193)^\circ$ respectively compared to the benzene ring plane. The two aromatic ring planes are perfectly coplanar and no deviation angle is measurable. In these two dinuclear sub-units, the Nb1...Nb2 and Nb3...Nb4 bond length is $3.2322(9) \text{ \AA}$ and $3.2184(12) \text{ \AA}$ with Nb1-O1-Nb2 and Nb3-O11-Nb4 angles of $113.9(2)^\circ$ and $112.8(3)^\circ$ respectively. The coordination modes of the niobium dimers in this compound, generating $\{\text{Nb}_2\text{O}\}$ sub-groups are identical to the one described for the dimers in compound **Nb(V)-10** and **Nb(V)-11**.

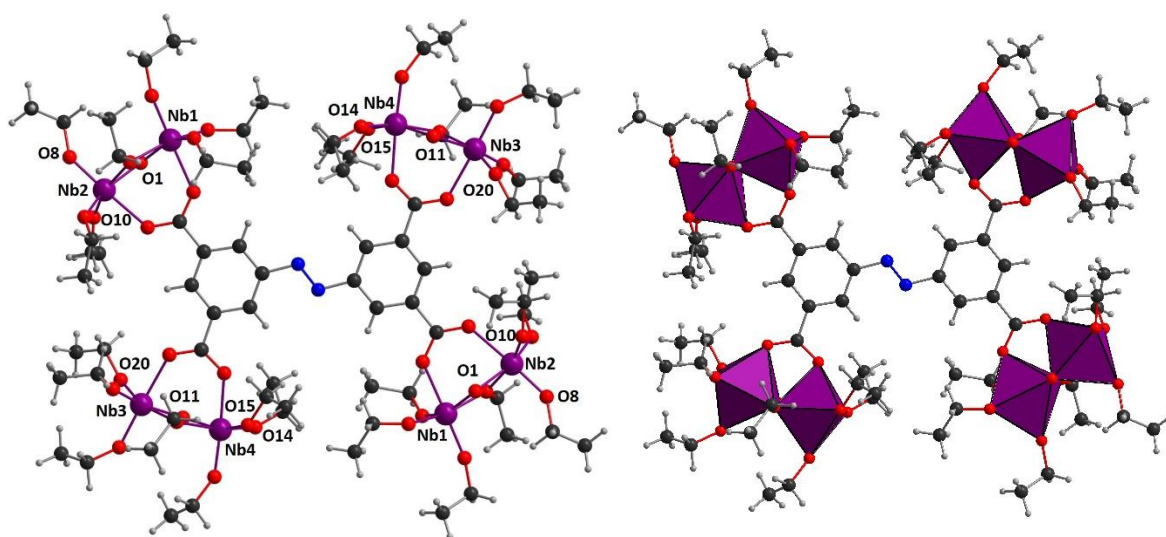


Figure III-27. Ball and stick (left) and polyhedral (right) representations of the molecular octanuclear coordination complex **Nb(V)-12**. The ethoxy groups linked to Nb1 site (through Nb1-O6 bonding), Nb2 site (through Nb2-O10 bonding), Nb3 site (through Nb3-O20 bonding) and Nb4 site (through Nb4-O14 and Nb4-O15 bondings) are disordered on two equivalent positions. Only one of these ethoxy groups is shown for clarity.

III. 2.2.2 Structural discussion

The reaction of the aromatic polycarboxylic ligands with the niobium(V) ethoxide precursor lead to the formation of three crystalline molecular coordination compounds containing a number of niobium centers going from four to eight which is comparable from this aspect to most of the compounds obtained with various monotopic ligands in literature

or very recently, in our group.^[42] The crystalline phase obtained in the three systems was confirmed to be pure by powder X-ray diffraction analysis (Figure A3, paragraph A3, Appendix). The main point of differentiation lies in the arrangement of the molecular systems. Indeed, in the case of monotopic ligand, the coordination complexes are systematically constructed around the polynuclear niobium clusters with the organic ligands surrounding it whereas, in compounds **Nb(V)-(10-12)**, the ligand plays the central role with the niobium moieties surrounding it. This observation is obviously logical, but could explain the difficulty to grow niobium clusters with high nuclearities when using polycarboxylate ligands. In this view, a similar arrangement was reported for a reduced niobium(IV) form complex, stabilized by ditopic (terephthalic or isophthalic acid) or tritopic (trimesic acid) aromatic linker, with the series of $[(Cp'_2Nb)_{2or3}(ligand)]$ where Cp' is a cyclopentadienyl species of type $\eta^5-C_5H_4SiMe_3$. In the latter, the central di- or tritopic carboxylate ligand connects two or three niobium(IV) center, via chelating connection modes each carboxylate arms.^[40]

The coordination modes of the carboxylate function differ within **Nb(V)-10** in comparison with **Nb(V)-11** and **Nb(V)-12**. In the latter, each arm of the carboxylate ligands appears well spaced and, are engaged, in a bidentate bridging mode, to two and four dimeric niobium $Nb_2(\mu_2-O)(\mu_2-OEt)$ moieties. No particular steric hindrance due to the ethoxy groups is observed around the niobium centers and, the binding functions form relatively flat coordination angles in both compounds, ranging from $7.398(193)^\circ$ to $23.636(81)^\circ$. On the opposite, in **Nb(V)-10**, the four carboxylate groups of the pyromellitate ligand are relatively close causing a drastic change in these coordination modes due to the steric hindrance generated by the ethoxy ligands. Consequently, the two carboxylate functions adapt their coordination and adopt a 90° rotation angle compared to the benzene ring. In addition, the two other carboxylate functions located in adjacent position on the benzene ring appears unable to bind a niobium dimer and only one niobium centre is complexed in a monodentate way.

III.2.3 Infrared spectroscopy in Nb(V) polycarboxylate complexes

The three different niobium(V) ethoxide – polycarboxylic acid systems in **Nb(V)-(10-12)**, described above, were investigated by using infrared spectroscopy, in order to study their crystallization process. For each batch, the supernatant solutions have been studied just after the starting reactants mixing at $t = 1h$ at room temperature, and then after the crystallization

of the compounds (1-month duration for the three samples). On the spectrum, several zones are of interest and can be attributed to the ethoxide ligands.^[27] Indeed, the 3050-2750 cm^{-1} range is related to the $\nu(\text{C-H})$ stretching vibrations of the ethyl groups (with typical bands at approximately 2970_(asym) and 2860_(sym) cm^{-1}) and, the 1480-1370 cm^{-1} zone is related to the $\nu(\text{C-H})$ bending vibrations of the methyl groups (with typical bands in the range 1470-1404 and around 1375 cm^{-1}). The bands about 1200-1000 cm^{-1} are assigned to the $\nu(\text{C-O})$ vibrations coming from the ethoxide group linked to niobium center through Nb-O-C_{Et} linkage. Typical peaks are found at 1100-1090 cm^{-1} and 1060-1040 cm^{-1} . The broad peaks centered at 529-522 cm^{-1} are related to $\nu(\text{Nb-O})$ stretching modes.^[28] These different signatures are observed either in the niobium precursor, in the supernatant solutions and in crystallized niobium complexes, as expected.

For our interest in the formation of niobium carboxylate complexes, we focused our attention on the 1750-1550 cm^{-1} region, where free carboxylic acid $\nu(\text{C=O})$, and bonded carboxylate $\nu_{\text{asym}}(\text{COO})$ and $\nu_{\text{sym}}(\text{COO})$ stretching vibrations are typically found. For complexes **Nb(V)-(10-12)**, we observed the same trends (Figures A19-A21, paragraph A4, Appendix), since unprotonated carboxylate ligands are always visible in the supernatant solutions after mixing the chemical reactants (Table III-7). Indeed, for compound **Nb(V)-10** system, the band at 1698 cm^{-1} , is related to the $\nu(\text{C=O})$ stretching from pyromellitic acid, but disappears when it is mixed with the niobium ethoxide solution. The corresponding vibration stretching is shifted to 1598 cm^{-1} and 1541 cm^{-1} and is related to the $\nu_{\text{asym}}(\text{COO})$ and $\nu_{\text{sym}}(\text{COO})$, respectively. It reveals the bonding between carboxylate group of the ligand and niobium centers^[16] in supernatant solution, just after 1h mixing. This observation indicates the relatively rapid complexation of the starting niobium ethoxide by the carboxylate group occurring at room temperature in less than an hour, and therefore the presence of niobium-ethoxide-carboxylate in solution. Interestingly, a new vibration band appears at 1729 cm^{-1} in both the supernatant after one month and the crystalline phase. It is assigned to the $\nu(\text{C=O})$ coming from the formation of an ethyl-pyromellitate ester. Such formation was previously reported on the synthesis of a tetranuclear niobium acetate compound^[16] and is expected to come from the reaction of the acid with the ethoxide groups (forming ethyl-ester and water) coming from the niobium precursor. As a result, it indicates the complexation of the carboxylic ligand to the niobium centers releasing some of the ethoxy molecules allowing the

esterification reaction. On the other side a dehydration reaction is also a possible way, but not in this case, as the $\nu(\text{C}=\text{O})$ coming from the formation of an anhydride would have existed in higher wavenumbers ($>1770 \text{ cm}^{-1}$).^[43]

The reactivity of the carboxylic acid toward the niobium ethoxide described above is also observed for the different crystallization processes of compounds **Nb(V)-11** and **Nb(V)-12**. The $\nu(\text{C}=\text{O})$ stretching from 4,4'-azobenzenedicarboxylic acid and 3,3',5,5'-azobenzene tetracarboxylic acid is observed at 1681 cm^{-1} and 1685 cm^{-1} , respectively. They both disappear when the ligand is mixed with the niobium ethoxide solution to give the corresponding vibration at 1591 cm^{-1} , 1543 cm^{-1} , 1605 cm^{-1} and 1559 cm^{-1} , related to the $\nu_{\text{asym}}(\text{COO})$ and $\nu_{\text{sym}}(\text{COO})$, for crystals of compound **Nb(V)-11** and **Nb(V)-12**, respectively. However, the infrared signatures differ from what could be expected for both supernatant solutions before and after crystallization. The $\nu(\text{COO})$ vibration bands are present but appears extremely weak, indicating that the niobium carboxylate compounds are present in solution at a very low concentration. That can be explained due to two reasons, as the ligands solubilize slowly by the time and that "soluble" niobium-ethoxide-carboxylate complex is probably quickly transformed into the solid crystalline form. ^1H NMR spectra of the supernatant after 1 hour confirm this suggestion as the signals corresponding to the ligand are extremely weak.

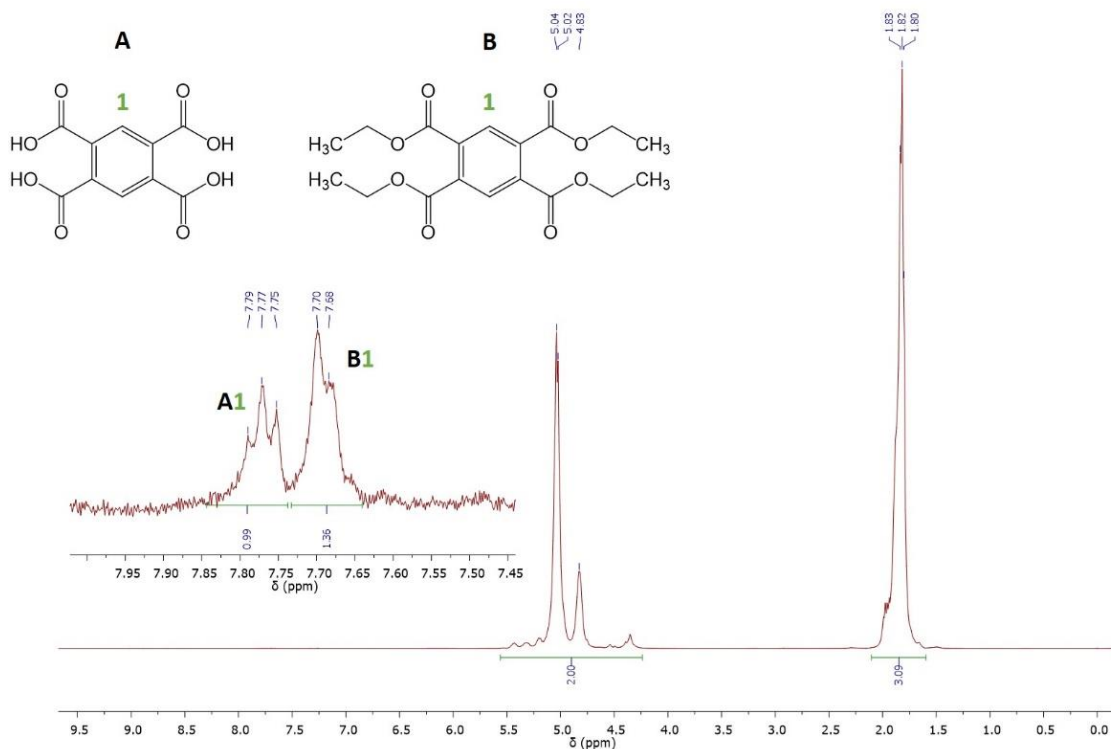
Table III-7. Comparison of the $\nu(\text{C}=\text{O})$ vibrations (from carboxylic acid function) and $\nu(\text{COO})$ vibrations (from carboxylate function) for the complexes **Nb(V)-(10-12)** (in cm^{-1}).

		$\nu(\text{C}=\text{O})_{\text{acid}}$	$\nu_{\text{asym}}(\text{COO})$	$\nu_{\text{sym}}(\text{COO})$
Nb(V)-10	pyromellitic acid	1698	/	/
	supernatant (1 hour)	/	1598	1541
	supernatant (1 month)	/	n.o. ^[a]	1570
	crystalline product	/	n.o. ^[a]	1566
Nb(V)-11	4,4'-azobenzene dicarboxylic acid	1681	/	/
	supernatant (1 hour)	/	1597	1541
	supernatant (1 month)	/	1597	1551
	crystalline product	/	1591	1543
Nb(V)-12	3,3',5,5'-azobenzene tetracarboxylic acid	1685	/	/
	supernatant (1 hour)	/	1598	1538
	supernatant (1 month)	/	n.o. ^[a]	n.o. ^[a]
	crystalline product	/	1605	1559

^[a]n.o. : not observed.

III.2.4 Nuclear Magnetic Resonance study (liquid state)

The crystallization process of the three systems was also investigated using solution ^1H NMR and ^{13}C - ^1H HMBC correlations. We have analyzed the supernatant solutions before and after crystallization occurs. For system **Nb(V)-11** and **Nb(V)-12**, no information regarding the state of the ligands (acid form, ester form or complexed form) were obtained despite our efforts. In contrast, the measurements performed on system **Nb(V)-10** (with the pyromellitic ligand) give some insight on the crystallization process, based on the signals present in the aromatic region of the spectra. In system **Nb(V)-10**, the aromatic region of the spectrum in the supernatant after one hour already shows the presence of several extremely weak peaks distributed over two main signals centered at 7.77 ppm and 7.70 ppm (Figure III-28, top). It suggests that the ligand already react with some ethanol molecules coming from the niobium precursor to form ethyl esters derivatives as the acid form of the ligand should only give one signal. After one month, the ^1H supernatant spectrum shows the presence of numerous peaks, two of them being related to an ester form of the ligand as shown by the ^1H - ^{13}C HMBC correlation (Figure III-28 middle and bottom). The other signals may be related to complex form of the ligand or to ligands with partial esterification of the four carboxylic functions.



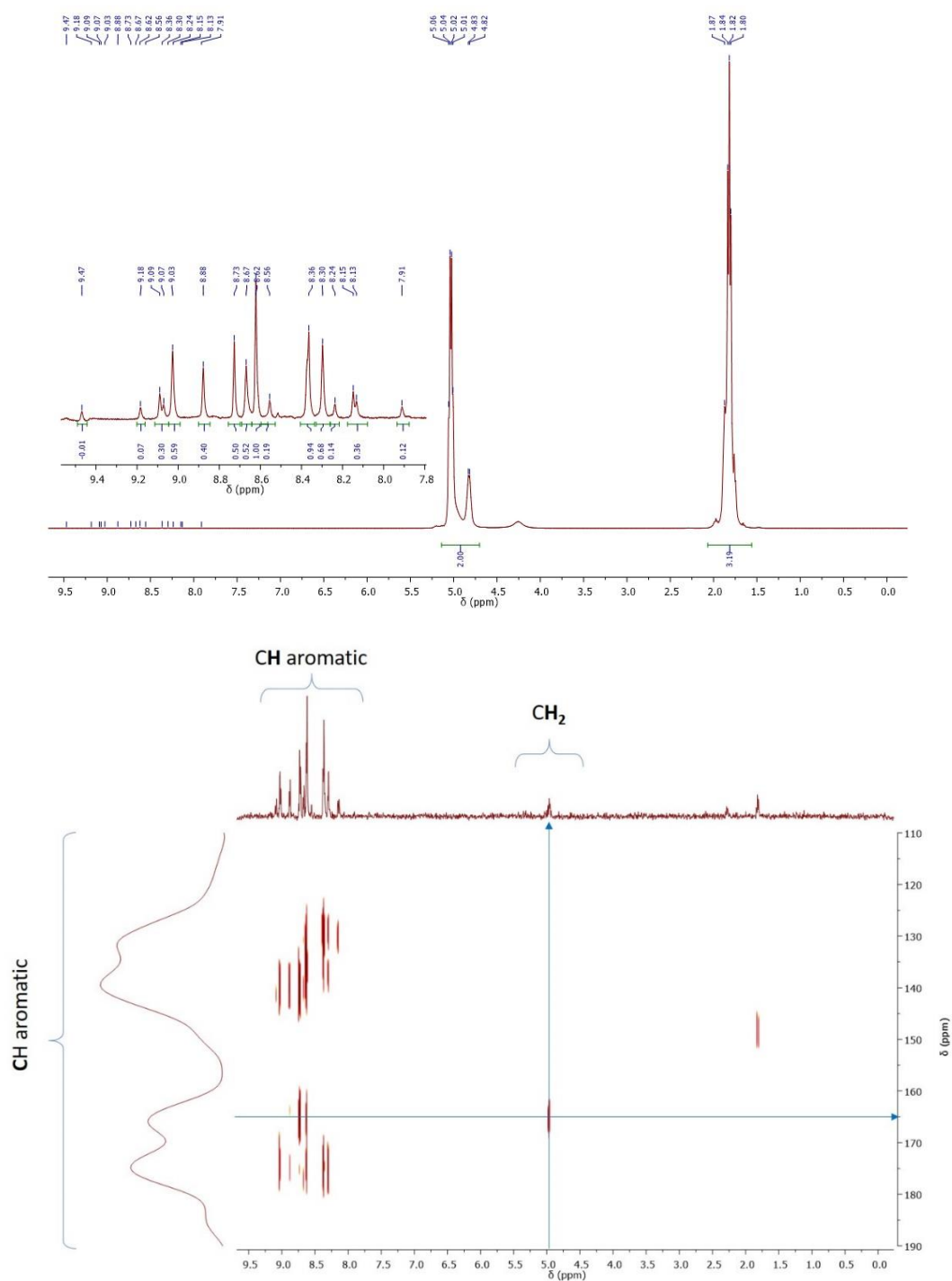


Figure III-28. ^1H NMR spectra for the supernatant in the synthesis of **Nb(V)-10** before (top) and after the crystallization (middle) with a focus in the aromatic region. ^{13}C -HMBC spectrum for the supernatant solution of **Nb(V)-10** after crystallization (bottom).

III. 3 ^{93}Nb solid state NMR of the coordination niobium(V) complexes

The niobium(V) carboxylate molecular coordination complexes with various well-defined nuclearities, are good candidates for their characterization by analyzing their ^{93}Nb solid-state NMR signatures from powdered crystalline samples. ^{93}Nb is a 100% natural

abundant isotope and possesses a relatively large gyromagnetic ratio ($\gamma = 6.567 \cdot 10^7 \text{ rad} \cdot \text{s}^{-1} \cdot \text{T}^{-1}$; close to that of ^{27}Al or ^{13}C , for instance). However, it is a $I = 9/2$ nuclear spin, with a large quadrupole moment ($Q = -32 \cdot 10^{-30} \text{ m}^2$), inducing a dominant second-order quadrupolar broadening of the central transition ($-\frac{1}{2} \rightarrow +\frac{1}{2}$), which is found to be ca. 30% stronger than found for ^{27}Al for a given distortion^[44,45]. Moreover, the ^{93}Nb solid state NMR signature is also usually characterized by large chemical shift range (up to -4000 ppm), which depends greatly on the coordination number and the geometry around niobium coordination sphere.^[44] All these features make difficult to collect and fully interpret ^{93}Nb NMR spectra, for which this element is thus less studied in literature. In this study, we want to take the advantage of the isolation of different niobium-centered cores, for which the metallic cation is octahedrally coordinated to a variable number of oxo, ethoxy and carboxylate groups $\{\text{Nb}(\mu_2\text{-O})_{1-2}(\text{OEt})_{2-4}(\text{O}_{\text{carboxy}})_{1-2}\}$, found in different nuclearities of $\{\text{Nb}_2\text{O}\}$ and $\{\text{Nb}_4\text{O}_4\}$ clusters. The dodecameric cluster, $\{\text{Nb}_{12}\text{O}_{23}\}$, obtaining two different coordination spheres (octahedron – VI and square bipyramid – V) has been also investigated, as these two arrangements can be distinguished by ^{93}Nb NMR spectra. The present study investigates the ^{93}Nb spectra of the compounds **Nb(V)-1, 2, 4, 5, 7, 9** and **11**, by using static and MAS techniques in an 800 MHz NMR spectrometer.

For **Nb(V)-1** (tetranuclear core stabilized by benzoate ligands), the signal of ^{93}Nb (Figure III-29, top) corresponds to the spectra measured in static (blue line) and the green line the one in rotation (62.5 kHz). Both signals are extremely large (-500 to -2500 ppm), despite a very high rotation speed, and are not well adapted to a clear interpretation. Thus, starting from the structural file (.cif data), VASP ^{93}Nb calculations were made to generate the theoretical spectrum for **Nb(V)-1**. This strategy was inspired by the calculations made by O. B. Lapina *et al.*^[46] for several compounds like AlNbO_4 , $\text{VNb}_9\text{O}_{25}$, $\text{K}_8\text{Nb}_6\text{O}_{19}$ and Cs_3NbO_8 . The simulated (black line) and the experimental (green line) spectra are fitting well (Figure III-29). Furthermore, the simulated spectrum exhibits an occurrence of two niobium sites (represented as two grey lines) in agreement with the expected number of crystallographically unique metal sites revealed by single-crystal X-ray diffraction. The same approach was applied for the spectrum in static condition (Figure III-29 down right). Consequently, the two crystallographically unique sites of **Nb(V)-1** are verified by the experimental ^{93}Nb NMR spectrum.

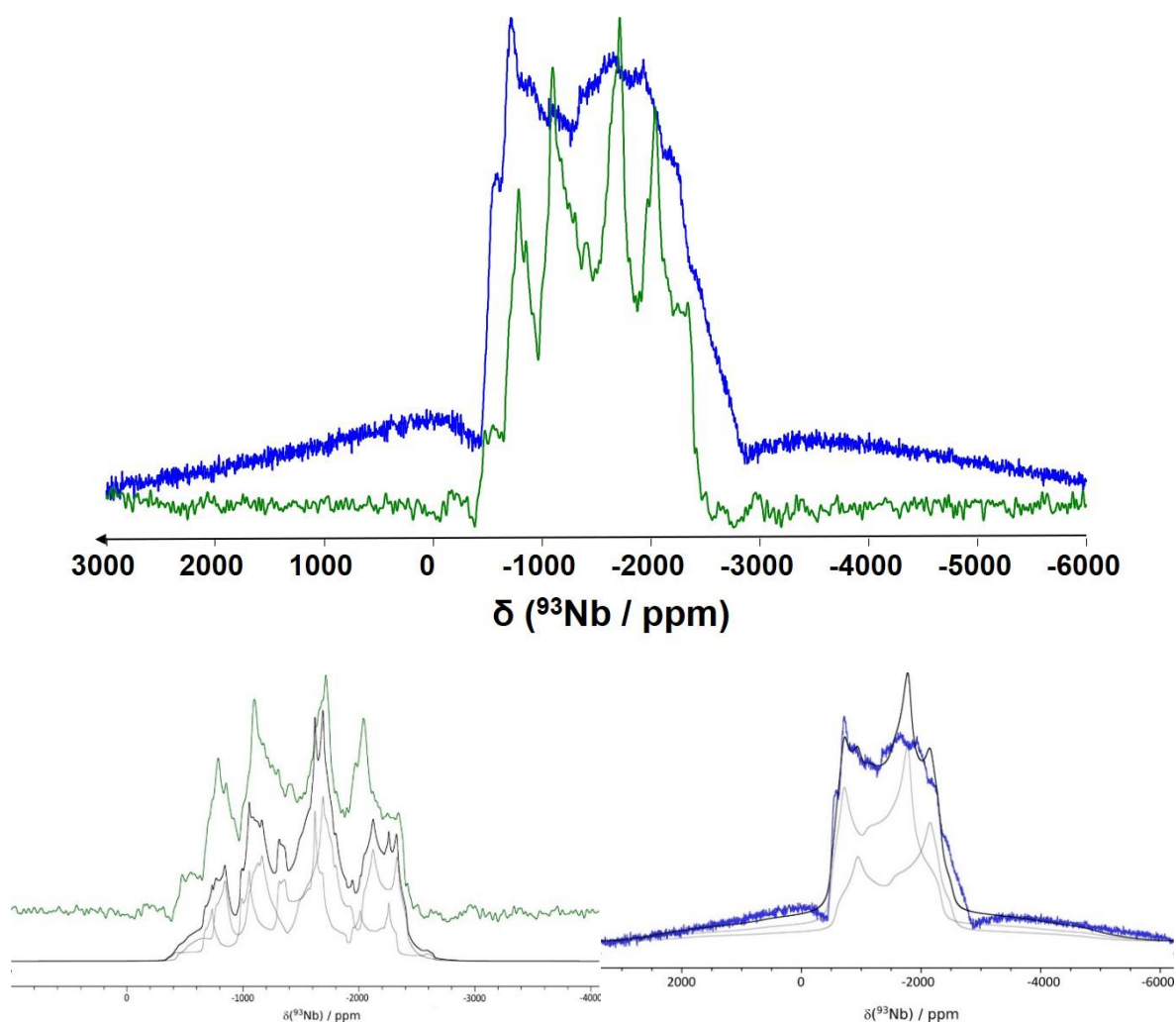


Figure III-29. (top) Solid state NMR ^{93}Nb spectra of complex **Nb(V)-1**: static condition (blue) and MAS rotation (green), (bottom left) solid state NMR ^{93}Nb spectra of complex **Nb(V)-1** in rotation (green), the calculated spectra for the two sites (grey) and their sum (black), (bottom right) solid state NMR ^{93}Nb spectra of **Nb(V)-1** in static (blue) and the calculated spectra for the two sites (grey) and their sum (black).

According to the VASP ^{93}Nb calculations, the parameters C_Q , η_Q , δ_{iso} and CSA were calculated and presented in Table III-8 for both of niobium sites. Nuclear quadrupole coupling constant (C_Q) is measured in kHz or MHz and shows the magnitude of the quadrupolar interaction. So far, the values of C_Q for different niobium oxide systems vary between 11 and 87 MHz (for Na_5NbO_5 and PrNbO_4 respectively). The values of C_q for **Nb(V)-1** seem to be in the range of the reported values. The asymmetry parameter (η_Q) takes values in the range 0-1. It depends on the local symmetry and the η_Q values for the two niobium sites Nb1 and Nb2 in **Nb(V)-1** are 0.250 and 0.212, respectively. Another calculated parameter is the isotropic chemical shift (δ_{iso}) that gives the extracted values of -1334 and -1233 ppm, respectively. For six-coordinate niobium centers the δ_{iso} value can differ from -900 to -1400 ppm, so once again the values found for **Nb(V)-1** are coherent. The signal of ^{93}Nb spectra can be affected not only

by quadrupolar interactions but also by chemical shift anisotropy (CSA) along with the quadrupole coupling constant, making the signal difficult to interpret. The CSA is quite high for **Nb(V)-1** (300-360ppm), thus NMR experiments at 400 MHz were performed in order to minimize the CSA, but the signal intensity was too low.

Table III-8. Calculations VASP ^{93}Nb for **Nb(V)-1**.

C_Q (MHz)	η_Q	δ_{iso} (ppm)	CSA (ppm)
86.9	0.250	-1334	298
85.6	0.212	-1233	359

Same experiments in static and in rotation were performed for compounds **Nb(V)-2,4,5,7,9,11** (Figure III-30). In **Nb(V)-2,4,5,7** there are two, one, four and two crystallographically unique niobium sites, respectively. Like before, spectra collected in static condition are shown in blue and those measured under spinning in green. For the case of **Nb(V)-7**, some VASP calculations attempts were made to generate a calculated spectrum (red line). However, the result in this case is much more difficult to fit and interpret the experimental signatures. The difficulties observed during the VASP calculations could be explained by the presence of larger organic molecules that may result into a less local symmetrical structure. Even if **Nb(V)-9** can be considered as a high nuclearity niobium cluster $\{\text{Nb}_{12}\}$ and not as symmetrical as the others, the fact that it contains two different coordination sites makes **Nb(V)-9** an interesting compound for recording its ^{93}Nb NMR spectrum. Indeed, a second component at ≈ 400 ppm is visible in the shoulder of the large resonance band, in the 800 MHz spectra (spinning at 62,5 kHz; Figure III-30), and might be assigned to the signature of five-coordinated niobium. It would agree the lower range (-900 to -980 ppm for five-coordinated and -900 to -1360 ppm for six-coordinated Nb sites) reported in literature^[44] for such environment.

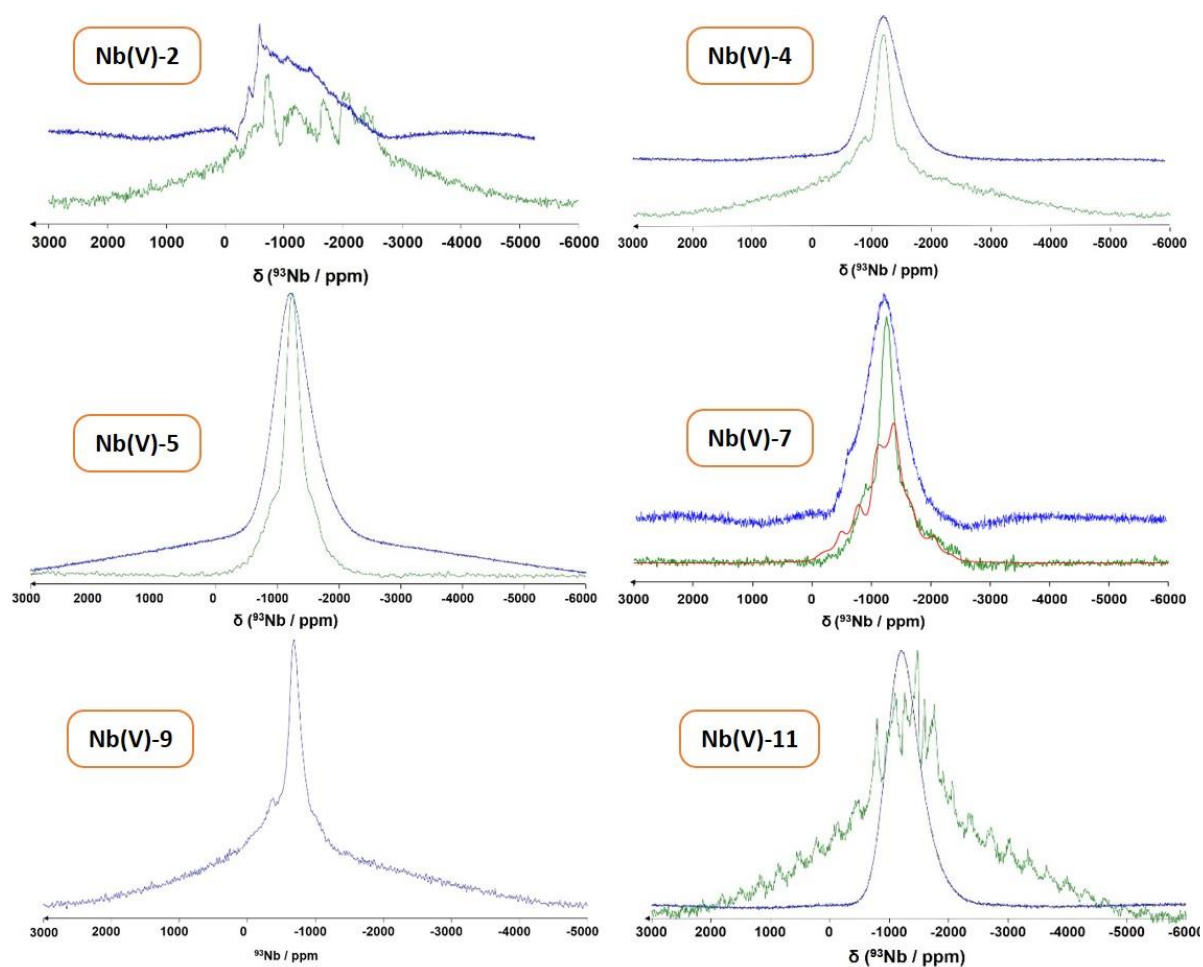


Figure III-30. Solid state NMR ^{93}Nb spectra of complexes **Nb(V)-2,4,5,7,9,11** in static condition (blue), MAS rotation (green) and calculated for the **Nb(V)-7** (red).

III. 4 Conclusions

To summarize the work of this chapter, multiple molecular niobium(V) cores have been isolated after complexation with a series of mono and poly carboxylic acids. Niobium(V)pentaethoxide was selected as precursor, as the ethoxide groups it contains could easily be replaced by carboxylates. Indeed, twelve different discrete molecules of niobium carboxylates poly-oxo clusters have been obtained with nuclearities varying from $\{\text{Nb}_2\}$, $\{\text{Nb}_4\}$, $\{\text{Nb}_8\}$, up to $\{\text{Nb}_{12}\}$ with various fashions of oxo bridges connecting the Nb centers. The source of water that generate this oxo groups is associated to an esterification process between the carboxylic acid and ethanol groups (coming from the leaving ethoxy groups). This process allows not only the generation of water, but also its slow release into the solution, something that helps condensation. Sometimes, special synthetic conditions, as the moisture atmosphere or/and elevated temperature were used in order to act synergetic to esterification. These additional methods resulted into the isolation of higher nuclearity

niobium-based poly-oxo clusters (notably $\{\text{Nb}_4\}$, $\{\text{Nb}_8\}$ or $\{\text{Nb}_{12}\}$). The reactional pathways demonstrate that as a first step, the addition of a monocarboxylic acid to the niobium ethoxide ($\text{Nb}_2(\text{OEt})_{10}$) led to the formation of dinuclear unit ($\text{Nb}_2\text{O}(\text{carboxylate})_{1 \text{ or } 2}$), where the two bridging ethoxy groups are replaced by a carboxylate and an oxo group. If a second carboxylate is involved, then two ethoxy groups leave in the form of ethanol. Two dinuclear clusters can be assembled to give a tetranuclear unit ($\text{Nb}_4\text{O}_4(\text{carboxylate})_4$), in which eight ethoxy groups are remaining. The latter can be further condensed twice again, to produce an octanuclear brick ($(\text{Nb}_8\text{O}_{12}(\text{carboxylate})_8)$), in which four ethoxy groups are remaining. By altering the precursor to $\text{NbCl}_4(\text{THF})_2$ in order to have a chloride that is well dissolved, we managed to obtain the large oxocluster of $\{\text{Nb}_{12}\text{O}_{23}\}$ that contains two different coordinations. Eleven niobium atoms adopt a 6-fold coordination, whereas, the twelfth adopts a 5-fold coordination. These different well-defined niobium(V)-centered cores can be considered as potential inorganic building units for the generation of extended networks by using polydentate carboxylic acid ligands.

Current works are now exploring the structural flexibility of utilizing such polynuclear units for the formation of MOF-like architectures. We may even be able to predict if some of these clusters can be conducive to form such multidimensional frameworks. For example, the tetranuclear unit (**Nb(V)-1**, **Nb(V)-7**) contains all the benzoates on the same plane. This means that if terephthalates replace benzoates, the resulting framework will be a 2D layered compound (Figure III-31). Therefore, to get a 3D framework, it will be wise the use of polycarboxylate ligands like trimesic or pyromellitic acid. Regarding the octanuclear unit (**Nb(V)-8**), the same case occurs, as all naphthoates belong to a single plane and thus, with the use of a dicarboxylic acid, the maximum that can be obtained is a 2D layered compound. However, again, the solution could be a polycarboxylic acid as organic precursor. In the recent study, we successfully reacted Nb(V) centers with polycarboxylic acids (pyromellitic acid, 3,3',5,5'-azobenzene tetracarboxylic acid), but even the use of polycarboxylic acids led to a molecular organization, so we assume that this suggestion stays quite speculative and hypothetical. However, longer polycarboxylic acids, or a combination of them, could also be tested, in order to overcome some possible stereochemical restrictions, as tetranuclear and octanuclear niobium(IV) cores are quite voluminous.

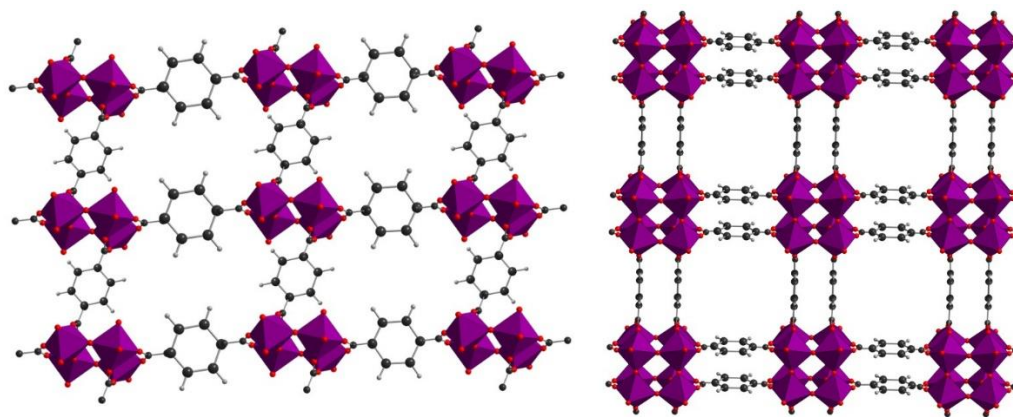


Figure III-31. Possible configurations of niobium(V) multidimensional networks with the use of **Nb(V)-1** and **Nb(V)-8** as an inorganic building block (with red points, the places where a polytopic ligand can substitute the monotopic one).

As it concerns the dodecameric cluster of **Nb(V)-9**, it is quite complexing and the two different types of coordination involved (5-fold and 6-fold) makes the poly-oxo cluster even less symmetrical. Thus, a prediction of a multidimensional network incorporating **Nb(V)-9** is quite difficult to design. However, the spots where carboxylate groups are complexed, point out to different directions and so even with the use of a dicarboxylic acid, a 3D network might be obtained.

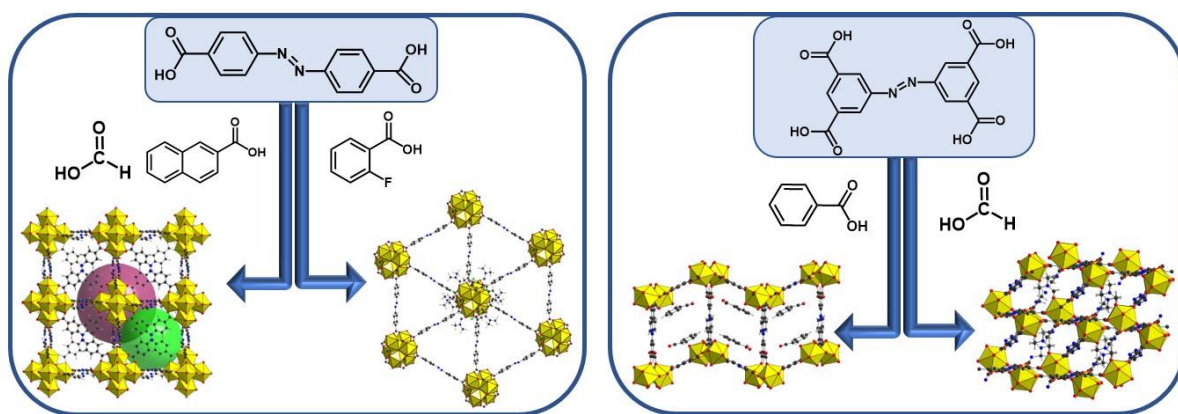
III. 5 References

- [1] M. A. Syzgantseva, C. P. Ireland, F. M. Ebrahim, B. Smit, O. A. Syzgantseva, *J. Am. Chem. Soc.* **2019**, *141*, 6271–6278.
- [2] S. Ahn, N. E. Thornburg, Z. Li, T. C. Wang, L. C. Gallington, K. W. Chapman, J. M. Notestein, J. T. Hupp, O. K. Farha, *Inorg. Chem.* **2016**, *55*, 11954–11961.
- [3] M. Rivera-Torrente, C. Hernández Mejía, T. Hartman, K. P. de Jong, B. M. Weckhuysen, *Catal. Letters* **2019**, *149*, 3279–3286.
- [4] A. Cadiau, K. Adil, P. M. Bhatt, Y. Belmabkhout, M. Eddaoudi, *Science (80-.)* **2016**, *353*, 137–140.
- [5] M. E. Ziebel, J. C. Ondry, J. R. Long, *Chem. Sci.* **2020**, *11*, 6690.
- [6] N. Galešić, N. Brničević, B. Matković, M. Herceg, B. Zelenko, M. Šljukić, B. Prelesnik, R. Herak, *J. Less-Common Met.* **1977**, *51*, 259–270.
- [7] L. Eriksson, G. Svensson, V. Tabachenko, J. Sjöblom, T. K. Thorsen, P. Coppens, O. Buchardt, *Acta Chem. Scand.* **1993**, *47*, 1038–1040.
- [8] B. Kojić-Prodić, R. Liminga, S. Ščavaničar, *Acta Crystallogr. Sect. B* **1973**, *29*, 864–869.
- [9] G. Mathern, R. Weiss, *Acta Crystallogr. Sect. B* **1971**, *27*, 1610–1618.
- [10] M. Šestan, B. Perić, G. Giester, P. Planinić, N. Brničević, *Struct. Chem. 2005 164* **2005**, *16*, 409–414.
- [11] D. C. Bradley, C. E. Holloway, *J. Chem. Soc. A Inorganic, Phys. Theor.* **1968**, 219–223.
- [12] K. Haåkansson, U. Welander, B. Mattiasson, *Water Res.* **2005**, *39*, 648–654.
- [13] D. Andriotou, S. Duval, C. Volkringer, X. Trivelli, W. E. Shepard, T. Loiseau, *Chem. – A Eur. J.* **2022**, e202201464.
- [14] N. E. Brese, M. O’Keeffe, IUCr, *Acta Crystallogr. Sect. B* **1991**, *47*, 192–197.
- [15] L. G. Hubert-Pfalzgraf, V. Abada, S. Halut, J. Roziere, *Polyhedron* **1997**, *16*, 581–585.
- [16] N. Steunou, C. Bonhomme, C. Sanchez, J. Vaissermann, L. G. Hubert-Pfalzgraf, *Inorg. Chem.* **1998**, *37*, 901–910.
- [17] T. J. Boyle, N. L. Andrews, T. M. Alam, M. A. Rodriguez, J. M. Santana, B. L. Scott, *Polyhedron* **2002**, *21*, 2333–2345.
- [18] J. H. Thurston, K. H. Whitmire, *Inorg. Chem.* **2003**, *42*, 2014–2023.
- [19] D. A. Brown, M. G. H. Wallbridge, N. W. Alcock, *J. Chem. Soc. Dalt. Trans.* **1993**, 2037–2039.
- [20] A. A. Pinkerton, D. Schwarzenbach, L. G. Hubert-Pfalzgraf, J. G. Riess, *Inorg. Chem.* **2002**, *15*, 1196–1199.
- [21] G. G. Nunes, G. A. Seisenbaeva, V. G. Kessler, *J. Sol-Gel Sci. Technol. 2007 431* **2007**, *43*, 105–109.
- [22] T. J. Boyle, T. M. Alam, D. Dimos, G. J. Moore, C. D. Buchheit, H. N. Al-shareef, E. R. Mechenbier, B. R. Bear, J. W. Ziller, **1997**, *2*, 3187–3198.
- [23] F. Laves, W. Petter, H. Wulf, F. Laves, W. Petter, H. Wulf, *NW* **1964**, *51*, 633–634.
- [24] P. B. Arimondo, F. Calderazzo, R. Hiemeyer, C. Maichle-Mössmer, F. Marchetti, G. Pampaloni, J. Strähle, *Inorg. Chem.* **1998**, *37*, 5507–5511.
- [25] M. Reinhard, A. Lagutschenkov, P. Maitre, P. Boissel, G. Niedner-Schatteburg, **2004**, DOI 10.1021/jp037337i.
- [26] M. T. Dunstan, F. Blanc, M. Avdeev, G. J. McIntyre, C. P. Grey, C. D. Ling, *Chem. Mater.* **2013**, *25*, 3154–

- 3161.
- [27] Y. Cai, S. Yang, S. Jin, H. Yang, G. Hou, J. Xia, *J. Cent. South Univ. Technol.* **2011**, *18*, 73–77.
- [28] C. Djordjević, V. Katović, *J. Inorg. Nucl. Chem.* **1963**, *25*, 1099–1109.
- [29] M. D. Korzyński, L. S. Xie, M. Dincă, *Helv. Chim. Acta* **2020**, *103*, e2000186.
- [30] L. A. Reznichenko, V. V. Akhnazarova, L. A. Shilkina, O. N. Razumovskaya, S. I. Dudkina, *Crystallogr. Reports* **2009**, *54*, 483–491.
- [31] T. S. Ercit, *Miner. Pet.* **1991**, *43*, 217–233.
- [32] W. Mertin, S. Andersson, R. Gruehn, *J. Solid State Chem.* **1970**, *1*, 419–424.
- [33] K. Kato, *Acta Crystallogr. Sect. B Struct. Crystallogr. Cryst. Chem.* **1976**, *32*, 764–767.
- [34] J. Dopta, L. K. Mahnke, W. Bensch, *CrystEngComm* **2020**, *22*, 3254–3268.
- [35] Y. L. Wu, X. X. Li, Y. J. Qi, H. Yu, L. Jin, S. T. Zheng, *Angew. Chemie - Int. Ed.* **2018**, *57*, 8572–8576.
- [36] E. P. Turevskaya, N. Y. Turova, A. V. Korolev, A. I. Yanovsky, Y. T. Struchkov, *Polyhedron* **1995**, *14*, 1531–1542.
- [37] G. A. Seisenbaeva, A. I. Baranov, P. A. Shcheglov, V. G. Kessler, *Inorganica Chim. Acta* **2004**, *357*, 468–474.
- [38] D. C. Bradley, M. B. Hursthouse, P. F. Rodesiler, *Chem. Commun.* **1968**, 1112–1113.
- [39] D. Andriotou, S. Duval, X. Trivelli, C. Volkringer, T. Loiseau, *CrystEngComm* **2022**, *24*, 5938–5948.
- [40] A. Antiñolo, S. García-Yuste, I. López-Solera, A. Otero, J. C. Pérez-Flores, I. Del Hierro, L. Salvi, H. Cattey, Y. Mugnier, *J. Organomet. Chem.* **2005**, *690*, 3134–3141.
- [41] N. E. Brese, M. O’Keeffe, *Acta Crystallogr. Sect. B* **1991**, *47*, 192–197.
- [42] D. Andriotou, S. Duval, C. Volkringer, X. Trivelli, W. E. Shepard, T. J. Loiseau, *Chem. – A Eur. J.* **2022**, DOI 10.1002/CHEM.202201464.
- [43] W. G. Dauben, W. W. Epstein, *J. Org. Chem.* **1959**, *24*, 1595–1596.
- [44] O. B. Lapina, D. F. Khabibulin, K. V. Romanenko, Z. Gan, M. G. Zuev, V. N. Krasil’nikov, V. E. Fedorov, *Solid State Nucl. Magn. Reson.* **2005**, *28*, 204–224.
- [45] J. V. Hanna, K. J. Pike, T. Charpentier, T. F. Kemp, M. E. Smith, B. E. G. Lucier, R. W. Schurko, L. S. Cahill, *Chem. – A Eur. J.* **2010**, *16*, 3222–3239.
- [46] E. Papulovskiy, A. A. Shubin, V. V. Terskikh, C. J. Pickard, O. B. Lapina, *Phys. Chem. Chem. Phys.* **2013**, *15*, 5115–5131.

Chapter IV

Coordination polymers of thorium(IV) with azobenzene-polycarboxylate based ligands



This chapter studies the formation of different thorium(IV) coordination polymers with 4,4'-azobenedicarboxylic acid (H_2abdc) and 3,3',5,5'-azobenzene-tetracarboxylic acid (H_4abtc). As the chemistry of thorium is relatively rich, by changing the ligand or/and the synthetic conditions, different coordination polymers have been isolated. More specifically, two phases were obtained with $abdc$ (**Th-abdc-1**, **Th-abdc-2**) and other two with $abtc$ (**Th-abtc-1**, **Th-abtc-2**). The **Th-abdc-1** phase belongs to the well-known family of the UiO-n-type metal-organic frameworks. All phases were tested for gas sorption of N_2 , Kr, Xe, CH_4 and CO_2 .

CHAPTER IV - Coordination polymers of tetravalent thorium with azobenzene ligands

In this chapter, the goal is to explore thorium-based systems incorporating azobenzene ligand derivatives (Figure IV-1, A). Azobenzene ligands are quite interesting for generating porous coordination polymers due to their long chain. They have been reported as organic building units in some metal-organic frameworks (MOFs) with different metals like Cu(II),^[1,2] Al(III),^[3] Zr(IV),^[3,4] Ln(III) (Ln=Eu, Gd, Tb),^[5] Zn(II)^[6,7] and Cd(II)^[6,7], Co(II),^[7] Mn(II)^[7] and Y(III).^[4]

On the other side, a lot of oxo/polyoxo actinide clusters have been isolated as inorganic secondary building units (SBUs) giving rise to porous three-dimensional Metal-Organic Frameworks (MOFs). The size of the pores depends highly on the size of the organic chain length and thus its of high importance to generate frameworks with long ligands. Among the infinite library of large organic ligands, azobenzendicarboxylates (Figure IV-1, A) are well adapted for the production of highly porous and very stable MOFs, especially with tetravalent metals (e.g. Zr⁴⁺).^[8] To the best of our knowledge, this type of ligand that has never been reported to link Th(IV) species. These ligands (Figure IV-1, A) contain an azo bond between two phenyl rings, multiple carboxylic acid branches usually connected to the 4,4' and 3,3'-5,5' positions. These azobenzene-derivative ligands are not commercially available but are based on a relatively simple organic synthesis procedure^[9], that will be presented later in this chapter (Paragraph 1.1). This chapter is organized in two parts, where four thorium(IV) coordination polymers will be introduced. The first part includes the **two phases obtained with 4,4'-azobenzenedicarboxylic acid** and the second one the other **two phases obtained with 3,3',5,5'-azobenzenetetracarboxylic acid**.

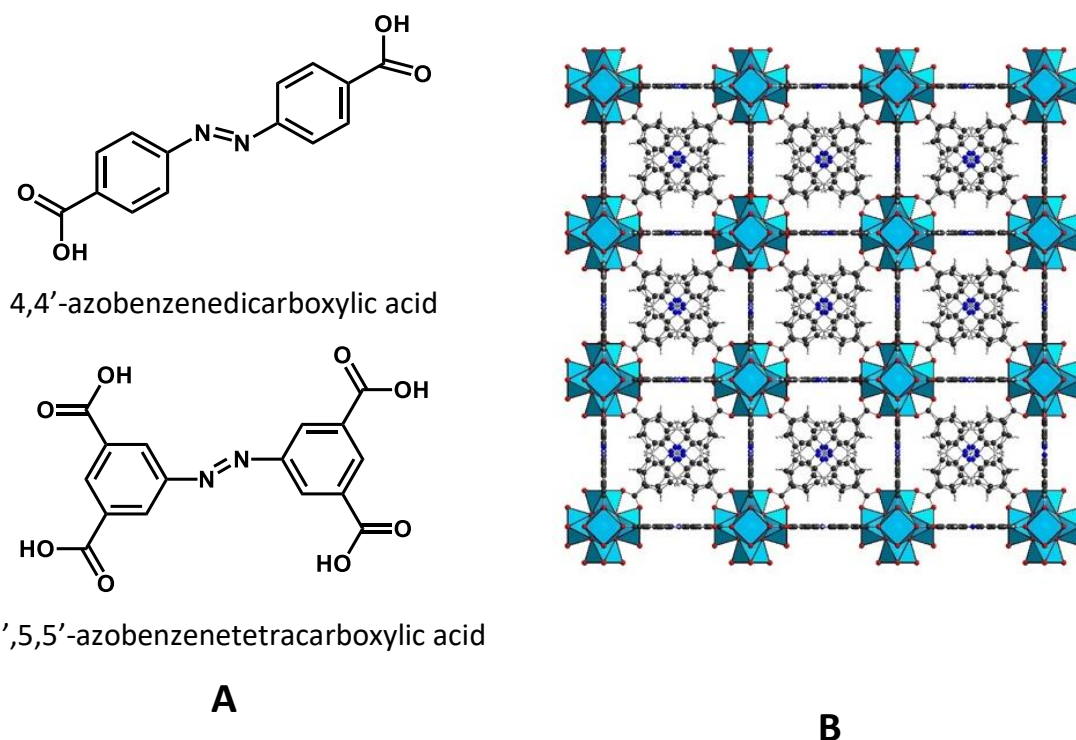


Figure IV-1. Designs of the ligands 4,4'-azobenedicarboxylic acid (A, top) and 3,3',5,5'-azobenzenetetracarboxylic acid (A, bottom). Framework of $Zr_6O_4(OH)_4(abdc)_6$ (B).^[8]

IV.1 Thorium(IV) coordination polymers with 4,4'-azobenedicarboxylic acids

The following part studies the reactivity of tetravalent thorium with 4,4'-azobenedicarboxylic acids in *N,N*-dimethylformamide. The influence of chemical parameters (acid/thorium ratio, H_2O /thorium ratio, dilution, nature and quantity of modulator) will be investigated. The two phases obtained by this system, named **Th-abdc-1** and **Th-abdc-2**, will be described and characterized by X-ray diffraction, infrared spectroscopy and thermogravimetric analysis. The amount of structural defects inherent to the topology of certain MOF-like structures will be also calculated by NMR experiment. Finally, gas sorption measurement will be tested for the porous systems.

IV. 1.1 Synthesis of precursors

The precursor of thorium(IV) used in the following study is thorium tetrachloride tetrahydrate ($ThCl_4 \cdot 4H_2O$).

Thorium tetrachloride tetrahydrate ($ThCl_4 \cdot 4H_2O$) was prepared by a solution of 5 g (10.4 mmol) thorium nitrate tetrahydrate ($Th(NO_3)_4 \cdot 4H_2O$, Fluka, 99 %) into 25 mL (81.7 mol) 37 % hydrochloric acid (HCl). The solution was refluxed, leading the production of NO_x vapors. The

reflux is maintained until the end of NO_x vapors production (≈ 6 hours). After the solution is cooled down at room temperature, it is concentrated by evaporation and left at room temperature to crystallize into ThCl₄·4H₂O (white powder).

The organic linker (4,4'-azobenzenedicarboxylic acid, H₂abdc) was also synthesized to a protocol inspired from the literature.^[9]

4-Nitrobenzoic acid (6.5 g, 36.0 mmol) and sodium hydroxide (25 g, 0.6 mol) were added in 120 mL H₂O and heated at 60 °C until dissolution. An aqueous solution of glucose (40 g in 75 mL water) was heated up to 60 °C as well and then was added drop-wise to the previous solution. When the two solutions are mixed, the final solution is left to cool down for 30 minutes and then stirred for 16 hours under air flow. The solution is then transferred to an ice bath and then filtered. The precipitate is dissolved in 125 mL of water and acidified with the addition of drops of 37% hydrochloric acid, until the precipitation of an orange powder. The precipitate was filtered, washed and dried at room temperature.

IV. 1.2 Composition diagram of the system ThCl₄/H₂abdc/modulator/DMF/H₂O

Even though Th(IV) is a stable oxidation state, all handlings before the thermal treatment, have been done in an inert atmosphere (Argon) in a glove box in order to avoid contamination during manipulation of thorium(IV) powder.

The precursors ThCl₄·4H₂O, 4,4'-azobenzenedicarboxylic acid (H₂abdc) and formic acid as modulator were dissolved in *N,N*-dimethylformamide (DMF) with or without the addition of water, heated for 36 hours in variable temperatures (100-150 °C). In addition to temperature, three other parameters studied in the current system: the ratio of H₂abdc /Th from 1 to 3 (or from 7.2 to 21.7 mg), the ratio of H₂O/Th from 0 to 120 (or from 0 to 100 μL) and the ratio of DMF/Th from 250 to 500 (or 0.5 and 1 mL). While different conditions were tested, all the others were kept fixed as seen in the top of the Figure IV-2, a diagram that shows the distribution of the solids obtained after each synthesis and characterization by powder X-ray diffraction. The molar ratio Th/modulator was fixed at 1:40, inspired by previous work^[10], where they tested different modulators for the synthesis of UiO-66 and they reported that between 10 and 50 molar equivalent is the optimum amount of modulator.

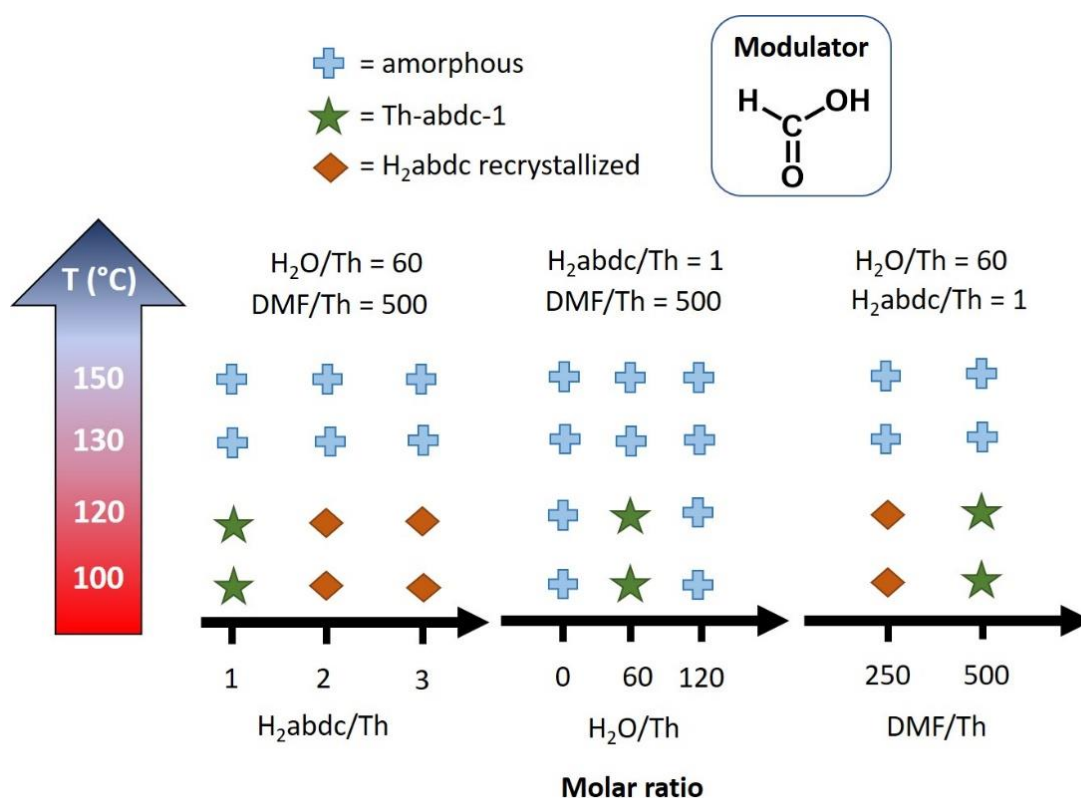


Figure IV-2. Schematic diagram of the parameters changed in the system ThCl₄/H₂abdc/modulator/DMF/H₂O depending on the temperature.

For all syntheses there was a precipitate after thermal treatment. However, most of the times the solid was not crystalline (blue cross in Figure IV-2). In all of the cases this amorphous solid is orange in color, so we exclude to have the formation of an oxide (thorium oxide is white). For the amorphous phases a band at 1650 cm⁻¹ is observed by infrared spectroscopy (Figure A22, paragraph A4, Appendix) that indicates the presence of C=O bonds either by the azobenedicarboxylate or by DMF molecules. This further supports the absence of amorphous thorium oxide. At a first glance, increasing the temperature does not favor crystallization in this system, and thus the optimal temperature is found in the range 100-120 °C. When the ratio H₂abdc/Th is 1, an orange solid related to **Th-abdc-1** is crystallized (green star in Figure IV-2) with the other parameters fixed (H₂O/Th at 60 and DMF/Th at 500). By increasing the organic dicarboxylic acid content, the observation of a final crystalline orange product corresponds to the recrystallized ligand (orange rhomb in Figure IV-2). The presence of water seems necessary to obtain the **Th-abdc-1** phase, but only when the ratio H₂O/Th is 60 and not more. Another parameter tested was the concentration of the mixture, by varying the DMF/Th ratio. By decreasing the ratio DMF/Th, the concentration is increased in the solution and that results in recrystallization of the ligand.

IV. 1.3 The thorium azobenzenedicarboxylate (**Th-abdc-1**) phase

IV. 1.3.1 Synthesis of **Th-abdc-1**

As seen from the phase diagram above, a phase of **Th-abdc-1** is formed for specific synthetical conditions with a controlled amount of water and the addition of a modulator (formic acid). In the absence of modulator, the product obtained is a powder and the crystallinity is very low (further discussed later in this chapter in paragraph 1.5, where a study about the optimal amount of modulator is presented). The synthetical protocol is summarized in Table IV-1.

Table IV-1. Synthesis protocols of *Th-abtc-1-(form)*.

Metal source	Ligand	Modulator	Solvent		T	Time	Yield
ThCl ₄ ·4H ₂ O	H ₂ -abdc	Formic acid	DMF	H ₂ O	100 °C	36 h	45%
10 mg	6.2 mg	33 μL	1 mL	30 μL			
0.023 mmol	0.023 mmol	0.82 mmol	13 mmol	0.82 mmol			

After thermal treatment at 100°C of the above reactant's mixture in a 2 mL glass vial with formic acid as a modulator, orange octahedral crystals of less than 10 μm appeared on the bottom of the vial as shown in the SEM image (Figure IV-3). This phase is stable under air for some weeks. However, the size of the crystals was too small and thus, not suitable to obtain the structure from single-crystal X-ray diffraction.

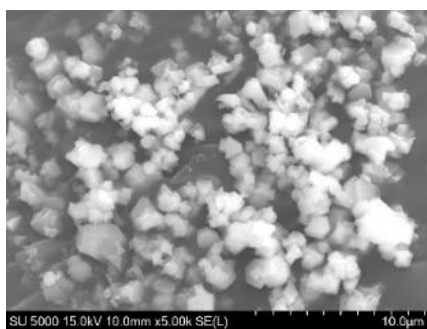


Figure IV-3. SEM image of the *Th-abdc-1* phase with formic acid as modulator.

In order to overcome this difficulty and increase the size of the crystals, other types of modulators were tried. A modulator in materials synthesis is a second acid, usually a monocarboxylic one, that is in competition with the main ligand, slows down the ligand exchange and promotes the crystal growth. In the present system, other modulators that were tested was the benzoic acid, 2-fluorobenzoic acid, pentafluorobenzoic acid, 4-biphenylcarboxylic acid and anthracene-9-carboxylic acid (Table IV-2). In general, there are

some studies that showed the importance of modulators nature and their concentrations in a synthesis to help the crystallization process and the final properties (as a higher BET specific surface area),^[11,12] but it is not yet clear what makes efficient a modulator and in which amount for a given final MOF. That is why many different monocarboxylic acids were tested as modulators in the following synthesis. The ratio Th/modulator is fixed in all syntheses as 1:40 (Table IV-2).

Table IV-2. Synthesis protocols of *Th-abdc-1* using different modulators.

Metal source	Ligand	Modulator	Solvent		T	Time	Yield (% _{Th})
			DMF	H ₂ O			
ThCl ₄ ·4H ₂ O 10 mg 0.023 mmol	H ₂ .abdc 6.2 mg 0.023 mmol	benzoic acid 112 mg 0.92 mmol	1 mL 13 mmol	30 µL 0.16 mmol	100 °C	36 h	50%
ThCl ₄ ·4H ₂ O 10 mg 0.023 mmol	H ₂ .abdc 6.2 mg 0.023 mmol	2-fluorobenzoic acid 129 mg 0.92 mmol	1 mL 13 mmol	30 µL 0.16 mmol	100 °C	36 h	37%
ThCl ₄ ·4H ₂ O 10 mg 0.023 mmol	H ₂ .abdc 6.2 mg 0.023 mmol	Pentafluorobenzoic acid 195 mg 0.92 mmol	1 mL 13 mmol	30 µL 0.16 mmol	100 °C	36 h	52%
ThCl ₄ ·4H ₂ O 10 mg 0.023 mmol	H ₂ .abdc 6.2 mg 0.023 mmol	2-naphthoic acid 158 mg 0.92 mmol	1 mL 13 mmol	30 µL 0.16 mmol	100 °C	36 h	45%
ThCl ₄ ·4H ₂ O 10 mg 0.023 mmol	H ₂ .abdc 6.2 mg 0.023 mmol	Biphenyl-4-carboxylic acid 182 mg 0.92 mmol	1 mL 13 mmol	30 µL 0.16 mmol	100 °C	36 h	50%
ThCl ₄ ·4H ₂ O 10 mg 0.023 mmol	H ₂ .abdc 6.2 mg 0.023 mmol	Anthracene-9-carboxylic acid 204 mg 0.92 mmol	1 mL 13 mmol	30 µL 0.16 mmol	100 °C	36 h	40%

The final products of these syntheses after thermal treatment, were observed under scanning electron microscope to investigate their size and shape according to the nature of the modulator used in the synthesis (Figure IV-4). When benzoic acid, 2-fluorobenzoic acid and pentafluorobenzoic acid are used, the resulting crystals are octahedral-shaped around ≈10-30 µm. The crystals made with pentafluorobenzoic acid and 4-biphenylcarboxylic acid seem also like octahedrals, but less well-crystallized and smaller in size (≈ 1-10 µm). So far, with almost all the modulators, octahedral-shaped crystals were isolated. However, this was not the case with anthracene-9-carboxylic acid, where big plate-crystals were observed by

SEM ($\approx 120 \mu\text{m}$). These crystals, corresponding to a thorium(IV) hexamer stabilized by anthracenoates, were further studied in Chapter V.

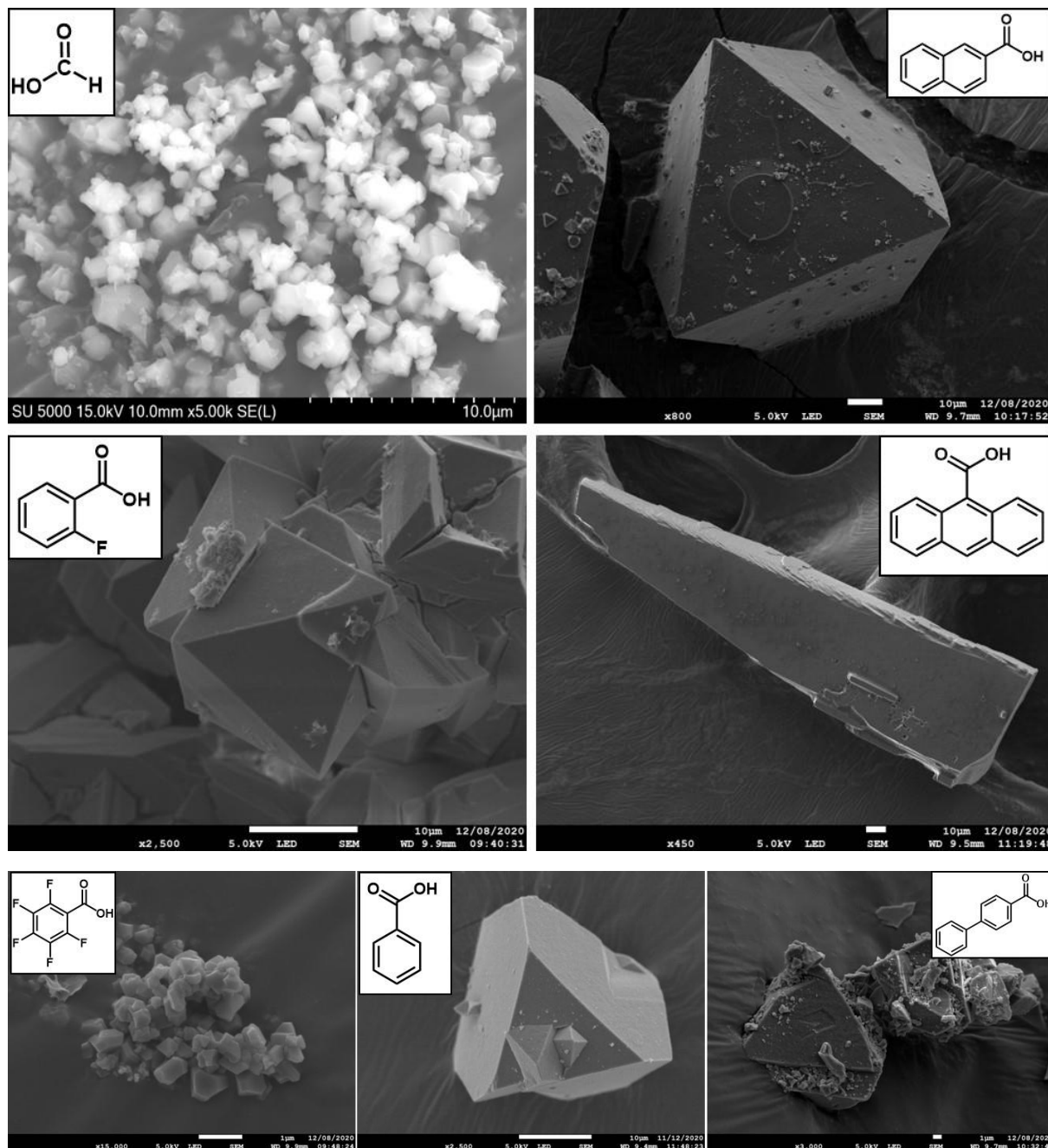


Figure IV-4. SEM images of crystals synthesized by the use of different modulators (white cage) with a Th/modulator molar ratio fixed at 1:40.

However, powder X-ray diffraction patterns show that not all the octahedrally-shaped crystallites are related to the **Th-abdc-1** phase (Figure IV-5). In fact, only the use of formic acid and 2-naphthoic acid led to isolate the **Th-abdc-1** compound as a single-phase. When 2-fluorobenzoic acid is used as modulator, the formation of a second phase (noted **Th-abdc-2**)

is observed. Whereas in **Th-abdc-1** the modulator is not observed by single-crystal X-ray diffraction as it is an average measurement, in **Th-abdc-2** the modulator is coordinated to Th(IV) and partially replacing the main azobenzene dicarboxylate ligand as studied later in this chapter (paragraph 1.6). The rest of the modulators that were tested (pentafluorobenzoic acid, 4-biphenylcarboxylic acid and benzoic acid) result to a third, not well crystalline phase and their powder X-ray diffraction patterns consist of Bragg peaks of both phases in low angles (Figure IV-5, blue cage).

Therefore, they are considered impure and the interest of this thesis will be turned into the identification, characterization and analysis of the two compounds obtained, **Th-abdc-1** (formic acid – other XRD pattern, naphthoic acid – blue XRD pattern) and **Th-abdc-2** (2-fluorobenzoic acid – red XRD pattern), which have been obtained as single-phase.

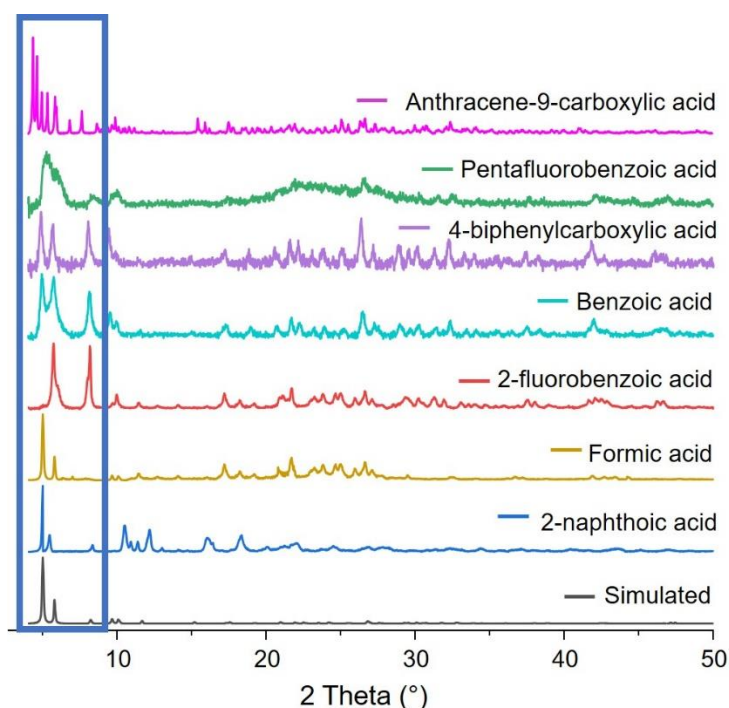


Figure IV-5. Powder X-ray diffraction patterns of all the isolated powders with different modulators with a focus on the low angles in order to distinguish the different phases (blue cage). X-ray source; Copper $K\alpha$ radiation; ($\lambda_{CuK\alpha}=1.5406 \text{ \AA}$).

It seems also that except of formic acid, 2-naphthoic acid found also to be an efficient modulator for the isolation of the **Th-abdc-1** phase and most importantly, the crystals formed as sufficiently big for single-crystal X-ray-diffraction (Figure IV-6).

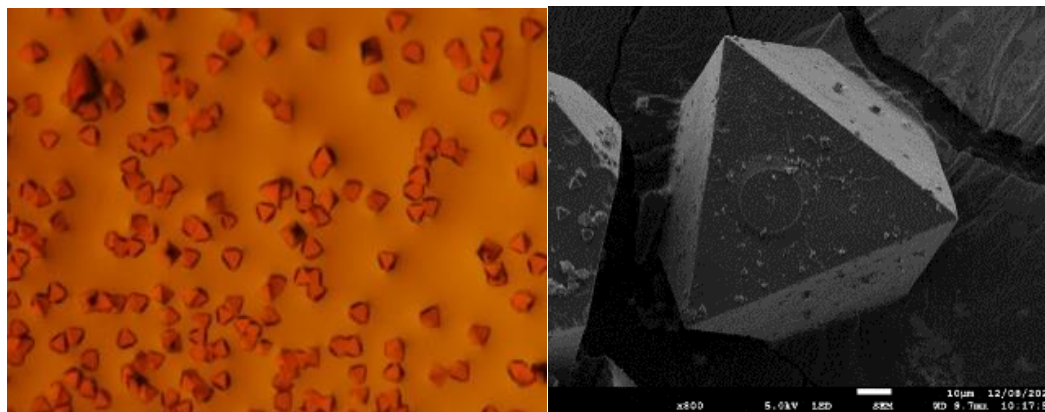


Figure IV-6. Optical microscope image (left) and SEM image of the **Th-abdc-1** with 2-naphthoic acid as modulator.

IV. 1.3.2 Structural description of **Th-abdc-1**

The X-ray data collection of **Th-abdc-1** was made with a Bruker APEX DUO diffractometer of the lab from crystals made with 2-naphthoic acid. The location of the different parts of the abdc ditopic ligand was not possible from the single-crystal XRD analyzes due to large statistical disorder. Indeed, only seven major electronic density peaks describing a distorted heptagonal plane, were observed from the Fourier maps in the surrounding around the phenyl groups. This configuration was not compatible with the carbon atoms positions of the expected hexagonal benzene ring, even if some partial occupancies are considered. The same issue is observed for the expected trans N=N bonding, with the localization of two closely electronic densities peaks (at 0.61 Å to each other), but positioned perpendicular to the ligand axis. This situation differs from the previous analyzes of the UiO-type compounds synthesized with zirconium, since a model based on three positions for the phenyl groups and four positions for nitrogen atoms of the diazo groups, was found with partial occupancies.^[13] Attempts have been made in solving the structure in a lower symmetry $I4/m$ space group in order to locate the abdc connecting ligand atoms with less disorder, as mentioned by the authors Schaate et al..^[14] They were able to find the positions of carbon and nitrogen atoms of the abdc ligands in the Zr-based UiO-like framework,^[15] without requiring disordering model. In our present study, refinement results in $I4/m$ did not converge to an acceptable model since atomic disordering did still remain as we observed in $Fm-3m$ space group.

In order to get a complete view of the structure, we carry out modelling calculations, in collaboration with Caroline Mellot-Draznieks from Collège de France (Paris), for a proper localization of the connecting ditopic diazo-based ligand. The crystallographical model was

considered in the centrosymmetric primitive triclinic (*P*-1) cell and the crystallographic table for both experimental and calculated data is given in Table IV-3.

Table IV-3. Crystal data and structure refinements for *Th-abdc-1*.

	Th-abdc-1	
	Experimental	Calculated
Formula	C _{30.42} N _{1.98} O _{38.69} Th _{5.95} H _{0.25}	C ₄₂ H ₃₂ Ne ₆ O ₁₉ Th ₃
Formula weight	2393.43	1620.85
Temperature/K	100	-
Crystal type	octahedral	-
Crystal size/mm³	0.141 × 0.107 × 0.104	-
Crystal system	cubic	triclinic
Space group	<i>Fm-3m</i>	<i>P</i> -1
a/Å	30.4623(12)	21.85243
b/Å	30.4623(12)	21.72703
c/Å	30.4623(12)	21.87988
α/°	90	59.86
β/°	90	59.91
γ/°	90	59.57
Volume/Å³	28268(3)	7308.805891
Z, ρ_{calculated}/g.cm⁻³	4.032/0.567	2
μ/mm⁻¹	3.165	-
Θ range/°	2.674-52.708	-
Limiting indices	-21 ≤ h ≤ 37 -38 ≤ k ≤ 33 -35 ≤ l ≤ 23	-
Collected reflections	20638	-
Unique reflections	1487 [R _{int} = 0.0454]	-
Parameters	47	-
Goodness-of-fit on F²	1.219	-
Final R indices [I > 2σ(I)]	R ₁ = 0.0646 wR ₂ = 0.1897	-
R indices (all data)	R ₁ = 0.0787 wR ₂ = 0.2040	-
Largest diff. peak and hole/e.Å⁻³	1.24 and -1.88	-

In this structure, the thorium(IV) center is 9-fold coordinated with nine oxygen atoms adopting a monocapped square antiprismatic geometry, from which four carboxylate oxygens deriving from azobenzene ligands with a Th-O bond distance of 2.414-2.607 Å. The other four oxygens adopt a bridging of μ₃-oxo and μ₃-hydroxo mode between thorium atoms with Th-O bond distances of 2.286-2.307 Å and 2.487-2.537 Å, respectively. The last oxygen comes from a terminal water molecule with Th-O bond distance of 2.756-2.828 Å. (Figure IV-7). The values of Th-O distances seem to be in agreement with the similar structural configuration of Th-UiO-66 (terephthalate) found in literature.^[16]

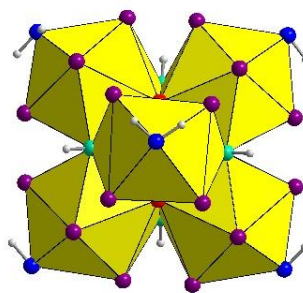
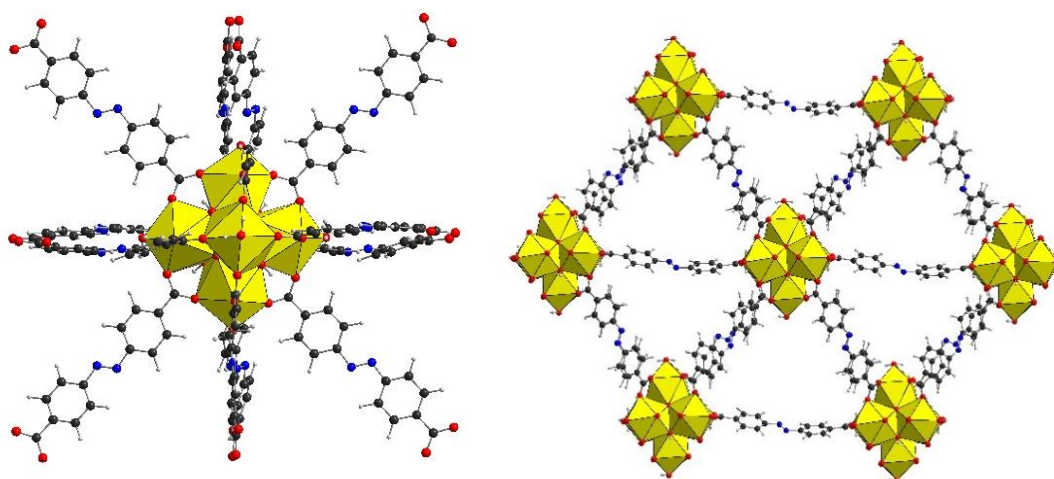


Figure IV-7. Thorium hexameric cluster (according to the calculated model), where the different types of oxygens are presented in different colors. O_{H_2O} ; blue, $O_{hydroxo}$; turquoise, O_{oxo} ; red, O_{carb} ; purple.

This cluster is surrounded by twelve azobenzenedicarboxylate ligands with the formula $[Th_6O_4(OH)_4(abdc)_{12}(H_2O)_6]$ (Figure IV-8, top left). In fact, each ditopic ligand belongs to two adjacent clusters so the ideal formula is $[Th_6O_4(OH)_4(H_2O)_6]_n$ (Figure IV-8, right). This extension of the framework leads to a three-dimensional structure as shown on the bottom of Figure IV-8, with the typical topology of the UiO- n archetype.^[15] The latter is characterized by the occurrence of two types of cavities, one tetragonal (green) and one octahedral (violet) with related diameters of 14 and 18 Å in the present use of azobenzenedicarboxylate linker. For instance, the Th-UiO-66 (terephthalate) the size of the pores are 3 and 10 Å respectively.^[16] This is quite normal, as azobenzene carboxylates are longer organic chains than terephthalates. The **Th-abdc-1** framework can be also named (Th)-UiO-abdc.



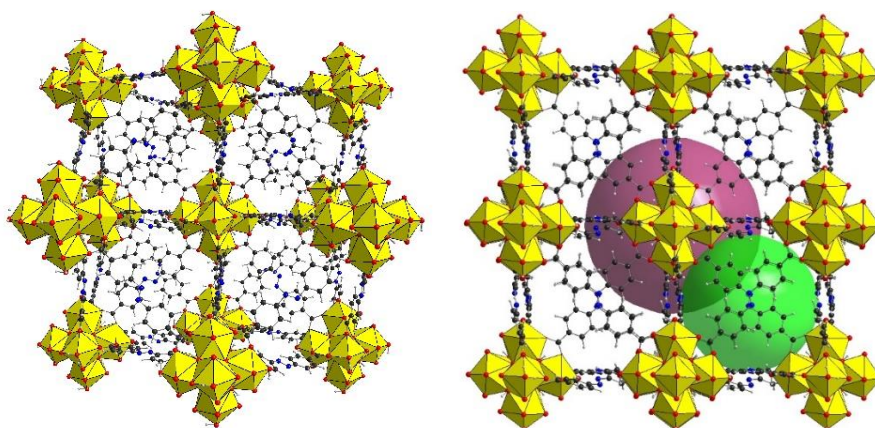


Figure IV-8. Crystal structure along a axis of the **Th-abdc-1** phase as $[Th_6O_4(OH)_4(abdc)_{12}(H_2O)_6]$ (top left), $[Th_6O_4(OH)_4(abdc)_6(H_2O)_6]_n$ (top right), and in the (a,b) plane the 3-D framework in central projection (bottom left) and the 3-framework (bottom right) with the octahedral (violet) and tetragonal (green) type of cavities.

The addition of modulator in the synthesis may induce creates some structural defects, involving the replacement of a dicarboxylate ligand by two monocarboxylate ligands (Figure IV-9). In the case of using formic acid, the correct way of writing the formula is $[Th_6O_4(OH)_4(abdc)_{6-x}(\text{formate})_{2x}(H_2O)_6]$. Formate molecules count as $2x$ in the formula as formic acid is a monocarboxylic acid and in order the charge to be balanced, one azobenedicarboxylate ligand is considered to be replaced by two formates (or naphthoates when the modulator is naphthoic acid).

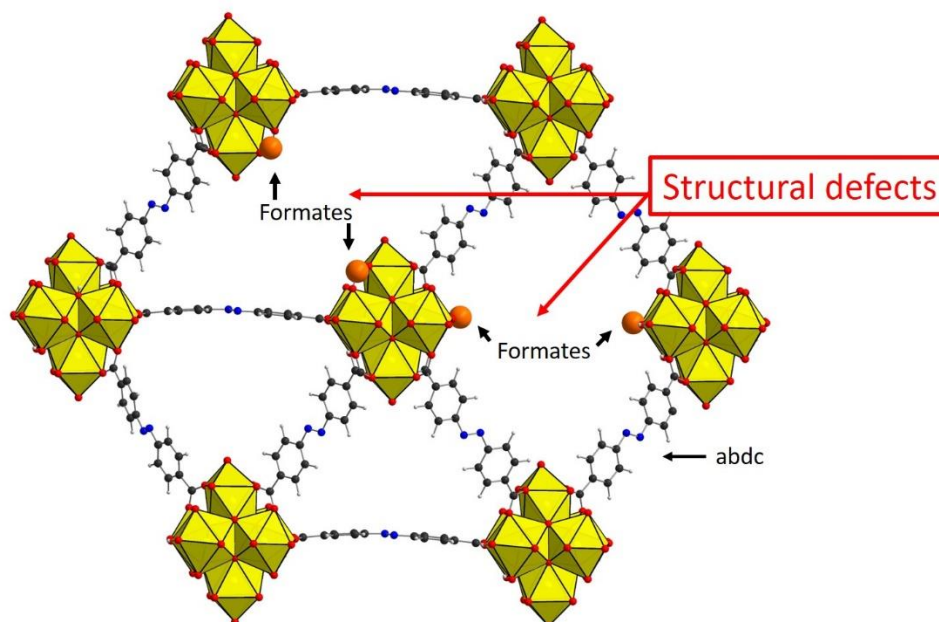


Figure IV-9. Illustrations of the defect formed with the addition of a monocarboxylic acid as a modulator during the synthesis of **Th-abdc-1**.

The exact composition within the structure is deduced from a liquid Nuclear Magnetic Resonance experiment (^1H , 400 MHz). In a 2 mL vial, **Th-abdc-1** (20 mg) were digested in a standard deuterated solution of NaOD in D_2O (1 mL, 4M). The solution was left in an ultrasound bath for 30 min in room temperature. White powder of $\text{Th}(\text{OH})_4$ appeared on the bottom of the vial, which was filtered to be removed. The supernatant was analyzed by liquid ^1H NMR (Figure IV-10) for both samples **Th-abdc-1-(form)** and **Th-abdc-1-(naph)**. **Th-abdc-1-(naph)** will be presented first, as the interpretation is more simple.

In the ^1H NMR spectrum of digested MOF using naphthoic acid as modulator (Figure IV-9), the two doublets centered at 7.86-7.88 and 7.74-7.76 ppm correspond to the eight protons in the azobenzene molecule (red and blue cages). The rest of the intense peaks correspond to the protons of naphthoate (green and pink cage). Since the formula is $[\text{Th}_6\text{O}_4(\text{OH})_4(\text{abdc})_6-x(\text{naphthoate})_{2x}(\text{H}_2\text{O})_6]$, from the integration of the spectrum we find that $x=0.57$, so the final formula including the defect is $[\text{Th}_6\text{O}_4(\text{OH})_4(\text{abdc})_{5.43}(\text{naphthoate})_{1.14}(\text{H}_2\text{O})_6]$.

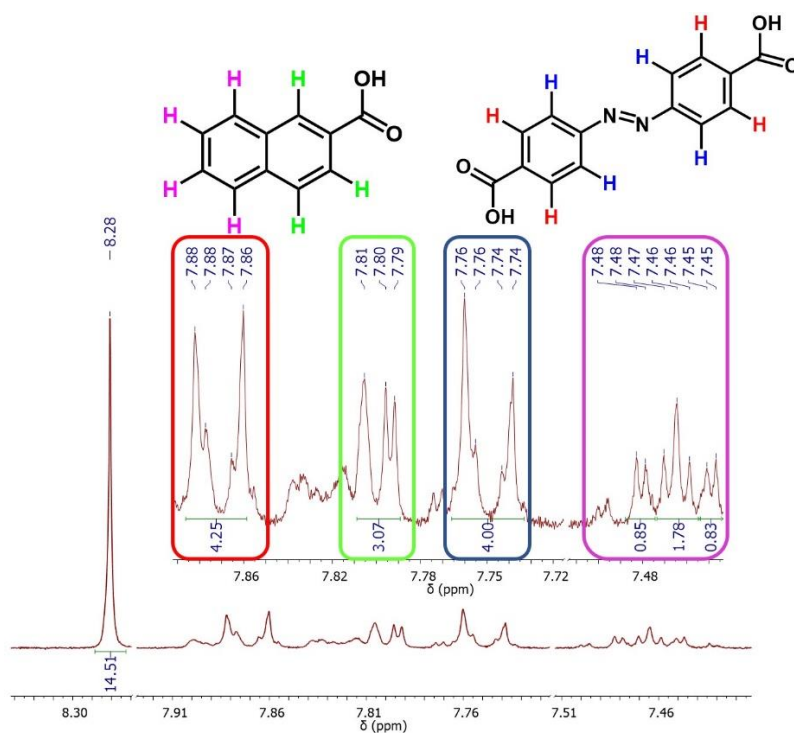


Figure IV-10. ^1H NMR spectrum of the supernatant of **Th-abdc-1-(naph)** digested into a 4M solution of NaOD (zoom in the region from 7.4-7.9 ppm).

Except of the signal of naphthoic acid and azobenzene ligand, signal of formic acid is detected by NMR spectrometry in higher chemical shifts at 8.28 ppm (Figure IV-11). This is

explained, as formic acid would be a product of the decomposition of encapsulated DMF (synthesis solvent) during the reaction of NaOD in D₂O for the digestion step. Thus, when formic acid is used as a modulator, the signal of formic acid is significantly big as it comes from the sum of these two sources (Figure IV-11). This affects the quantification of the structural defect when the modulator used is formic acid. In order to overcome this barrier and try to evaluate the correct formula, we integrated the amount of formic acid produced by NaOD decomposition of DMF in the sample of **Th-abdc-1-(naph)**. Then we subtracted this integration from the signature of formic acid for the ¹H NMR spectrum of **Th-abdc-1-(form)**. For example, in Figure IV-10, the signal of formic acid resonates at 8.23 ppm with an integration of 14.51. From this integration with the value 14.51 is considered as a background and it was subtracted from 16.21 (Figure IV-11). Finally, an estimation of the formula can be [Th₆O₄(OH)₄(abdc)_{5.19}(formate)_{1.62}(H₂O)₆] for **Th-abdc-1-(form)**.

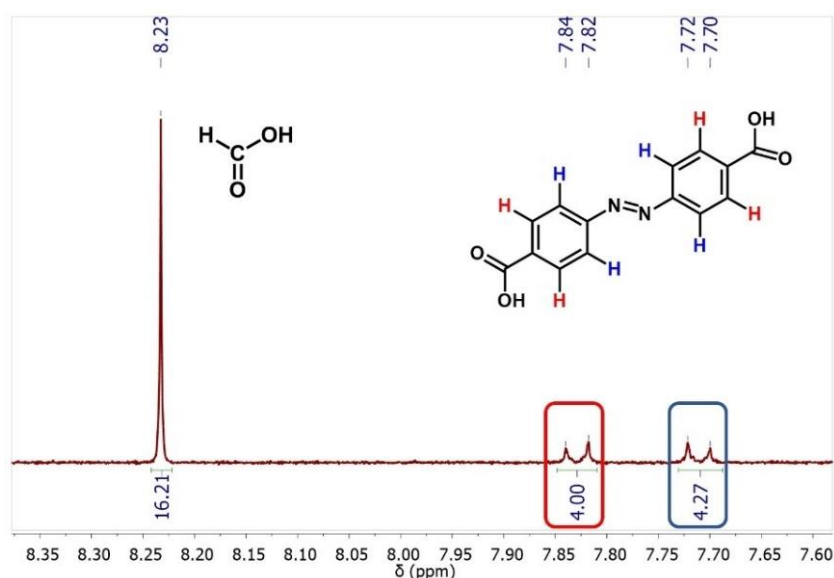


Figure IV-11. ¹H NMR spectrum of the supernatant of **Th-abdc-1-(form)** digested into a 4M solution of NaOD.

IV. 1.3.3 Characterization of **Th-abdc-1** by infrared spectroscopy and thermogravimetric analysis

The **Th-abdc-1** (both **Th-abdc-1-(form)** and **Th-abdc-1-(naph)**) phases were characterized by infrared spectroscopy and thermogravimetric analysis, in order to detect if there are any differences between the structures.

The infrared spectroscopy (Figure IV-12) shows a band at $\approx 1654\text{--}1658\text{ cm}^{-1}$ and another one at $\approx 1096\text{ cm}^{-1}$ that correspond to a $\nu(\text{C}=\text{O})$ and a $\nu(\text{C}-\text{N})$ vibration respectively. These bands confirm the presence of free DMF in the pores of **Th-abdc-1**, as they are characteristic for DMF molecules.^[17] The bands at $\approx 1598\text{ cm}^{-1}$ and at $\approx 1395\text{--}1401\text{ cm}^{-1}$ correspond to the

asymmetric and symmetric vibration $\nu(\text{COO})$ of the coordinated carboxylic acids. The ones at $1547\text{--}1550\text{ cm}^{-1}$ correspond to $\text{C}=\text{C}$ aromatic bonds, the vibration between aromatic carbons $\nu(\text{C}=\text{C})$ can be found $\approx 1395\text{--}1401\text{ cm}^{-1}$ and the torsion of OH and CH at $\approx 789\text{--}793\text{ cm}^{-1}$. Finally, no sign of modulators is observed via infrared spectroscopy, as no differences between the two compounds are detected. This can be, because their amount may be too low to be detected. This hypothesis can be further validated by thermogravimetric analysis.

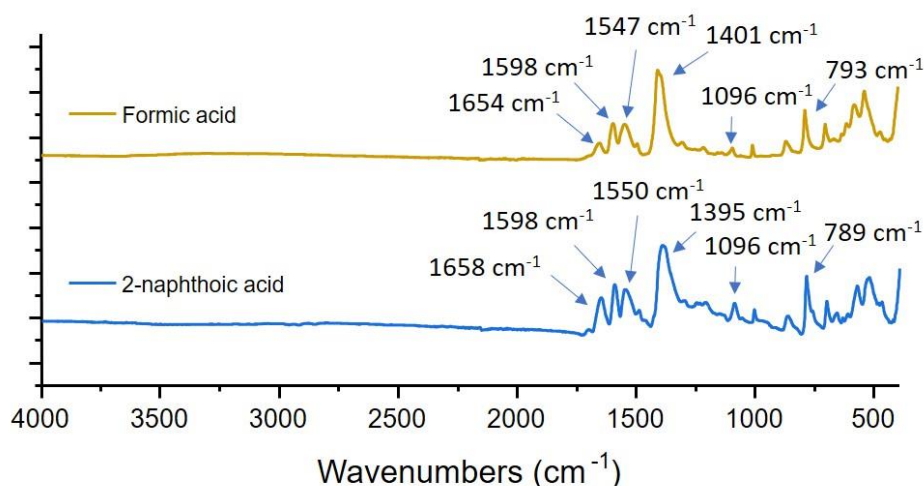


Figure IV-12. Infrared spectra of **Th-abdc-1** phases.

The thermogravimetric analysis (TGA) of the **Th-abdc-1-(naph)** phase, with a formula $[\text{Th}_6\text{O}_4(\text{OH})_4(\text{abdc})_{5.43}(\text{naphthoate})_{1.14}(\text{H}_2\text{O})_6]$, has a main weight loss at $\approx 480\text{ }^\circ\text{C}$, which corresponds to the azobenzene ligand and the collapse of the framework to form ThO_2 (Figure IV-13, top). If we assume that this residue of 46.3 % corresponds to $6x(\text{ThO}_2)$, then the experimental loss of 46.7 % (calc.: 48.2 % in total; 42.5 % from 5.42 azobenzenecarboxylates and 5.7 % from 1.15 2-naphthoates) corresponds well to the loss of 5.26 azobenzenecarboxylates and 1.10 2-naphthoates and is in accordance with the formula of the structure of the **Th-abdc-1** phase, $[\text{Th}_6\text{O}_4(\text{OH})_4(\text{abdc})_{5.43}(\text{naphthoate})_{1.14}(\text{H}_2\text{O})_6]$. There also an initiate 7.4 % loss at $\approx 200\text{ }^\circ\text{C}$ that corresponds to the loss of molecules trapped in the pores, like formic acid and DMF.

In the bottom of Figure IV-13 the thermodiffractogram for **Th-abdc-1-(form)** is shown. The two main Bragg peaks between $5\text{--}6^\circ$ (2θ) are hidden behind the background noise, however the other two low intensities peaks around 10° (2θ) can be visualized (zoom in the green circle). After $380\text{ }^\circ\text{C}$ the characteristic peaks for the UiO-phase (black patterns) disappear and by $440\text{ }^\circ\text{C}$ the formation of ThO_2 is observed (red patterns, with the

characteristic Bragg peak at 9.65° and 10.04° (2θ)), something that is in accordance with the TGA.

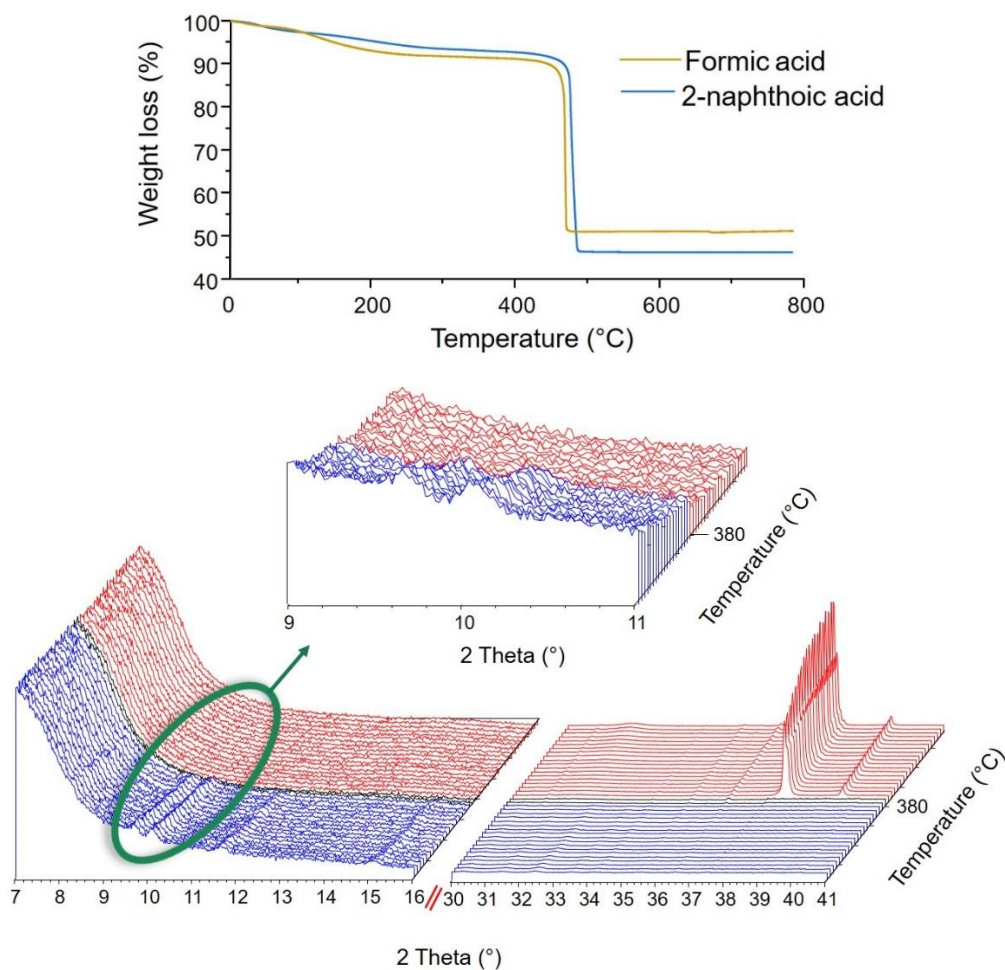


Figure IV-13. Thermogravimetric curve of **Th-abdc-1** phases (top) and X-ray thermodiffactograms for **Th-abdc-1-(form)** under air with a heating rate of $0.08\text{ }^\circ\text{C}\cdot\text{s}^{-1}$. X-ray source; Copper K α radiation; ($\lambda_{\text{CuK}\alpha}=1.5406\text{ \AA}$).

IV. 1.3.4 Modulator content (formic acid)

The modulator content in a synthesis plays an important role which is studied in this paragraph. The most efficient modulator for the synthesis of well crystallized and suitable size single crystals of **Th-abdc-1** solid, is the 2-naphthoic acid. However, the highest BET surface area is obtained with formic acid and that is why the last was used in the study of the modulator content.

Different molar equivalents of modulators from 0 to 100 (with respect to thorium) were tested, to optimize the BET surface area of the **Th-abdc-1** phase.

After thermal treatment ($100\text{ }^\circ\text{C}$), of the starting reactants mixtures containing 0 to 60 molar equivalents of formic acid, an orange crystalline precipitate is isolated, whereas for the

sample with 100 molar equivalents, transparent colorless crystals are obtained. All samples were further studied by scanning electron microscopy (Figure IV-14), powder X-ray diffraction (Figure IV-15) and BET specific area experiments (Figure IV-16). At 0 equivalent (without modulator), the SEM image reveals shapeless crystallites of 2 μm size. The powder X-ray diffraction pattern indicates low intense and very broad Bragg peaks located at 5.00° and 5.47° (2θ), reflecting a low crystallinity for the resulting powder.

With the addition of formic acid at 10 and 20 molar equivalents, the SEM images show a precipitate that starts to have a more specific octahedral-shape, with size of crystallites around 5 μm . From the powder X-ray diffraction pattern (Figure IV-15), we can see that with the addition of 10 and 20 molar equivalents of modulator, the pattern gets more intense and the peaks narrower.

At 40 and 60 equivalents the SEM images show clearly the growth of octahedral-shaped crystals of $\approx 10 \mu\text{m}$. When higher content of formic acid is added (100 eq), the isolated crystals are colorless tablet-like agglomerates and they are quite bigger and crystallize as agglomerates of $\approx 200 \mu\text{m}$.

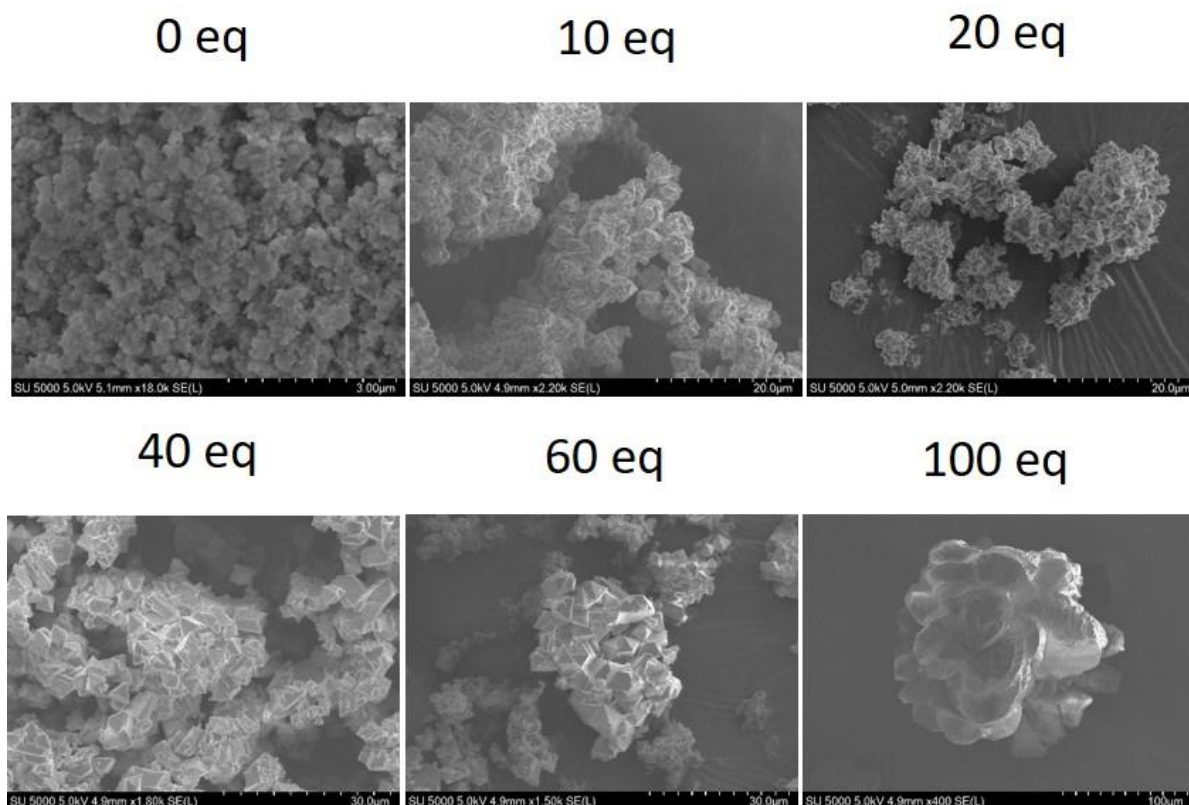


Figure IV-14. SEM images for different quantities of modulator for *Th-abdc-1-(form)*.

The evolution of the crystallinity seen by the SEM images, is observed from the powder X-Ray diffraction images as well (Figure IV-15). The sample with the higher crystallinity is the one prepared with 40 equivalents of formic acid, with the decreasing Bragg peaks widths, related to the UiO-n type signature (in our case, to the **Th-abdc-1** phase). The loss of crystallinity at 60 eq can be explained by the structural defect of the framework due to the partial substitution of azobenzenedicarboxylate linker by formate groups, although SEM images showing well-shaped octahedral crystals of relatively large size (30 μm). In general, there is an optimal amount of modulator, because when too much modulator is added, there is too much defect and that affects the long-range order and crystallinity of the framework.

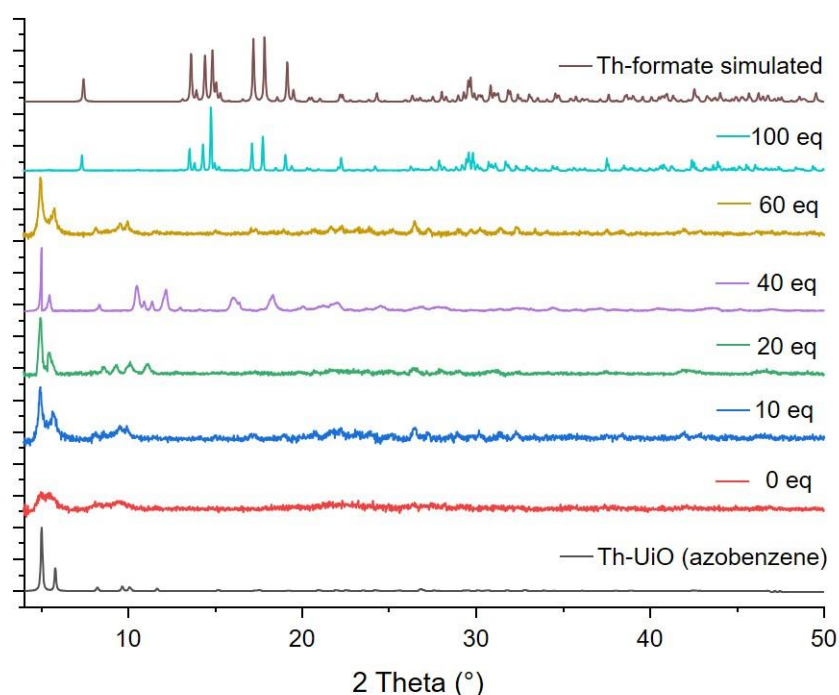


Figure IV-15. Powder X-ray diffraction patterns of different equivalents of formic acid as modulator in **Th-abdc-1-(form)**. X-ray source; Copper K α radiation; ($\lambda_{\text{CuK}\alpha}$ =1.5406 Å).

In the present study at 60 eq there might be too many defaults affecting the powder XRD pattern signature, with broad Bragg peaks (but still located 4.98 and 5.66°, belonging to the **Th-abdc-1** phase). At 100 molar eq of formic acid, a distinct phase, the formation of a thorium formate identified as $[\text{Th}_2(\text{HCOO})_8(\text{H}_2\text{O})(\text{DMF})] \cdot (\text{H}_2\text{O})_3$ (noted Th-SINAP-6) is observed, and has already been reported in 2009 by J. Q. Wang et al (Figure IV-16).^[18] The isolation of this compound is a result of the huge amount of formic acid introduced in the synthesis. The concentration of formic acid is extremely superior than the one of abdc that only formate reacts with Th(IV) and this reaction leads to the formation of the following

crystalline compound of thorium(IV) formate. In this structure, the Th(IV) center is 9-fold coordinated and stabilized by seven formates as monodentate ligands, one formate that adopts a bridging mode to connect two thorium atoms. This 9-fold coordination environment is completed with one carbonyl oxygen coming from a terminal DMF molecule (for Th1) and an oxygen from a terminal water molecule (for Th2). The remaining carboxyl oxygens are free and not involved in bonding with other thorium atoms, building up infinite zig-zag chains.

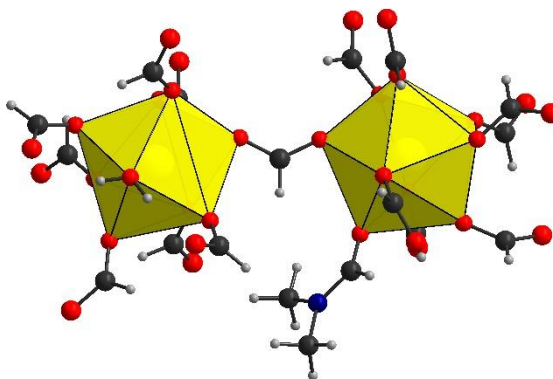


Figure IV-16. Crystal structure of the monomeric Th(IV) nodes in $(Th_2(HCOO)_8(H_2O)(DMF))$.^[18]

The specific surface values of the **Th-abdc-1** phase with different equivalents of modulator (formic acid) were estimated according to the BET model with previous activation process under secondary pump at 80 °C. More details about the conditions are given in paragraph A2 in Appendix. In accordance with the previous results of the study around the optimal quantity of modulator, the BET surface area experiments shown (Table IV-4) that the sample containing 40 eq of modulator possesses the highest BET (1196 m²/g). In general, the BET is higher with formic acid and not with naphthoic acid (843 m²/g). That is logic, since from ¹H NMR the defect calculated was higher in the case of formic acid, so the more modulator is replacing the azobenzenecarboxylate, more free space is creating in the framework, and BET is higher. Moreover, with naphthoate, there is a higher steric hindrance, which should lead to a smaller BET value.

Table IV-4. Values of BET specific surface area and pore volumes depending on the quantity of formic acid (modulator).

Quantity of formic acid (molar eq)	BET specific surface area	Pore volume
0	60(4) m ² /g	0.07(1) cm ³ /g
10	100(5) m ² /g	0.10(3) cm ³ /g
20	360(11) m ² /g	0.20(5) cm ³ /g
40	1196(29) m ² /g	0.54(4) cm ³ /g
60	425(13) m ² /g	0.22(2) cm ³ /g

IV. 1.3.5 Gas sorption experiments and enthalpies of adsorption of the **Th-abdc-1**

In this paragraph, the capture of four different gases within the pores of **Th-abdc-1** (**form**) will be tested with krypton, xenon, methane and carbon dioxide. Their enthalpies of adsorption will be calculated according to the method described below. Following the specific surface experiments on different equivalents of formic acid, the optimal amount found to be 40 equivalents with a BET surface area of $\approx 1200 \text{ m}^2/\text{g}$, after activation at $120 \text{ }^\circ\text{C}$ (details in table A1, paragraph A2, Appendix). This sample was selected for further gas sorption experiments.

Xenon and krypton are gases that show a great interest in the nuclear scientific community, as they are products of uranium fission reactions occurring in nuclear power plants. Their capture in porous structures is quite important as well, as their separation. So far, different MOFs were used for krypton and xenon sorption, like UiO-66(Zr)^[19], UiO-66-NH₂(Zr)^[20], MIL-100(Fe)^[19] and MIL-101(Cr)^[19] along with the relative Xe/Kr selectivity that was predicted from the ration of Henry's constants.^[21]

The physical adsorption of a gas in a surface is an exothermic phenomenon and its evolution is expressed by a value called enthalpy of adsorption. This value is possible to be calculated, when measurements at three temperatures, relatively close to each other are done. For a reversible physisorption of gases into porous materials, the enthalpy of adsorption needs to be between -17 kJ mol^{-1} and -45 kJ mol^{-1} .^[22]

Isotherms of adsorption for all above gazes were obtained at three different temperatures (273, 283 and 293 K), for which the temperature of the bath was controlled by a Pilot ONE controller (huber). The isosteric enthalpies of adsorption (ΔH°_{ads}) for each gas were calculated with the help of Chausius-Clapeyron equation:

$$\Delta H^\circ(\theta)_{ads} = R \frac{\partial \ln P}{\partial (1/T)}$$

where R is the ideal gas constant, P the pression at a temperature T given for a covering θ of the surface. For a standard volume adsorbed, defined by three different isotherms, there will be three different pressures of adsorption (Figure IV-17). Krypton adsorption tested in three temperatures (273, 283 and 293 K) and the quantity adsorbed found was 9.3, 8.1 and 7.1 cm^3/g respectively at 900 mmHg. Sometimes these values are reported in literature as

mmol/g, so in order to compare them, we converted $\text{cm}^3\cdot\text{g}^{-1}$ to $\text{mmol}\cdot\text{g}^{-1}$ dividing by $22.4 \text{ L}\cdot\text{mol}^{-1}$.

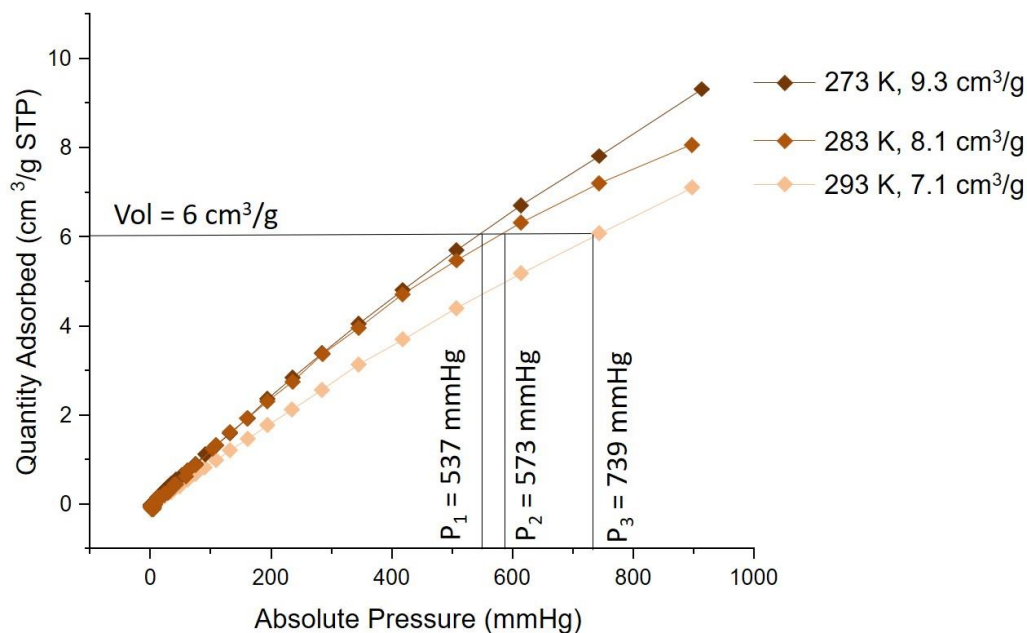


Figure IV-17. Isotherms of krypton adsorption for *Th-abdc-1(form)* at three different temperatures and schema behind the calculations for the enthalpy values.

According to the above equation, when $\ln P$ is traced by $1/T$, it gives a linear relation with the slope equal to $\Delta H^\circ_{ads}/R$ (Figure IV-18). Thus, with a linear fit of these graphs, the isosteric enthalpies of adsorption (ΔH°_{ads}) for each gas were calculated.

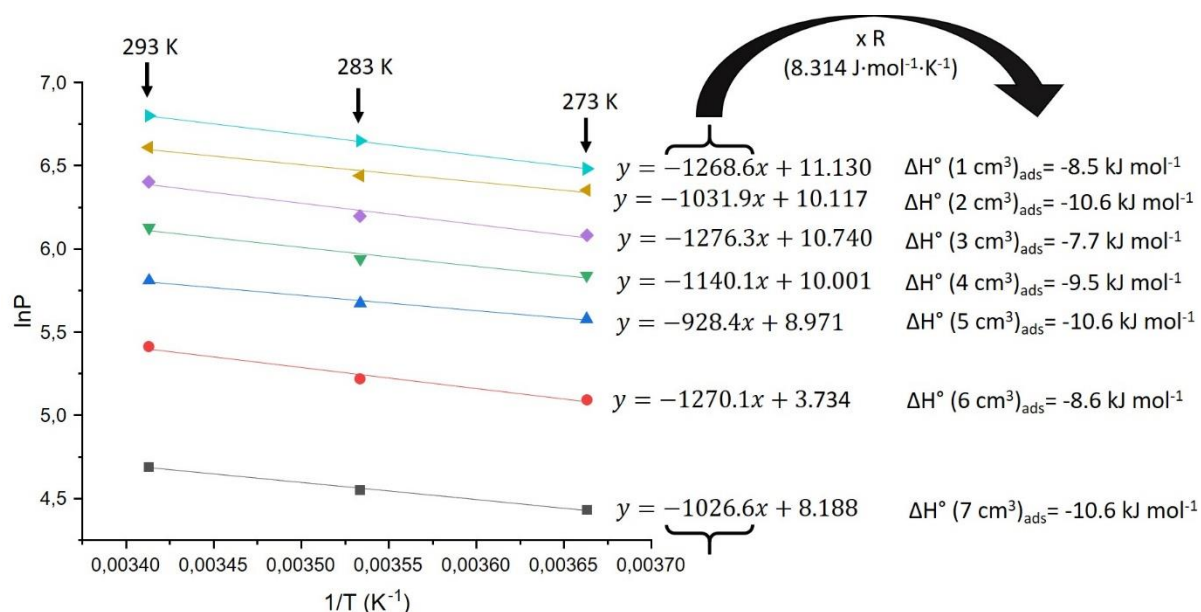


Figure IV-18. Example of the calculation of enthalpies of adsorption for *Th-abdc-1(form)* for seven volumes adsorbed and three temperatures.

The higher the absolute value of the enthalpy, the more possible for the gas to form strong interactions with the surface of the pores. In the case of noble gases, as krypton and xenon, enthalpies of adsorption are expected to have a lower value due to their lower reactivity with the surrounding environment. The enthalpy of adsorption for krypton found to be between -8 and -11 $\text{kJ}\cdot\text{mol}^{-1}$ (Figure IV-19).

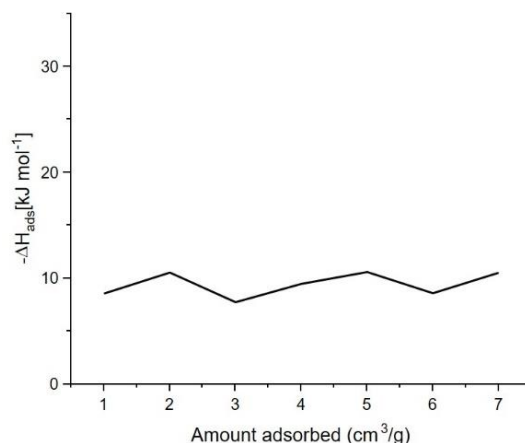


Figure IV-19. Diagram of enthalpies depending the volume of krypton adsorbed. (7 points of measurement)

The uptake of xenon in **Th-abdc-1** is higher than krypton with values of 35.9, 26.5 and 23.7 $\text{cm}^3\cdot\text{g}^{-1}$ for 273, 283 and 293 K respectively at 900 mmHg (Figure IV-20, left). According to literature, all MOFs in Table IV-5 demonstrate a higher xenon uptake than krypton. That is because, xenon is also a noble gas but bigger and has higher polarizability, so it is able to interact more with the surface of the pores. This affects the enthalpy of adsorption that was found to be between -16 and -22 $\text{kJ}\cdot\text{mol}^{-1}$, values slightly higher than the ones for krypton (Figure IV-20, right).

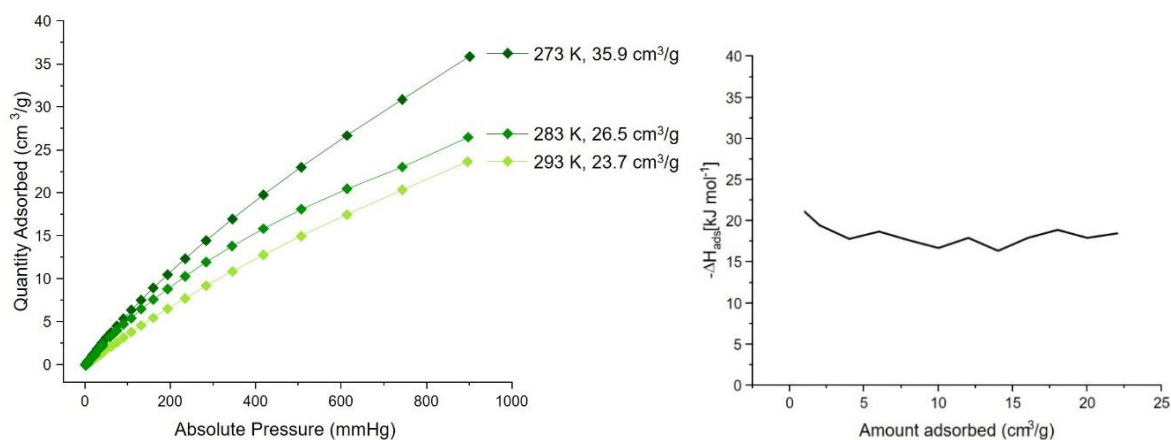


Figure IV-20. Isotherms of xenon adsorption for **Th-abdc-1(form)** at three different temperatures (left) and values of enthalpies (11 points of measurement) depending on the volume of xenon adsorbed (right).

The values of xenon and krypton sorption in **Th-abdc-1** seem to be in the range of the values obtained for similar MOF structures (Table IV-5). However, the values remain lower than UiO-66 for example and this can be due to the difference of the size of the pores. In UiO-66 the pores are 3 and 10 Å, whereas in **Th-abdc-1** the pores are 14 and 18 Å. The bigger pores, can thus create less interactions with the adsorbent and let it pass through without capture. That is why, size of pores is important in order to target a selective adsorption. Accordingly, the Xe/Kr selectivity seems to be relatively higher (5.9) for **Th-abdc-1** compared to other MOFs, which confirms that the bigger xenon is easier adsorbed than krypton.

Table IV-5. Xenon and Krypton uptake capacity at 1 bar and 293 K of **Th-abdc-1(form)** compared with other reported MOFs, and the relative Xe/Kr selectivity predicted from the ratio of Henry's constants.

MOF	S_{BET} ($\text{m}^2 \cdot \text{g}^{-1}$)	$\text{Xe}_{(\text{ads})}$ ($\text{mmol} \cdot \text{g}^{-1}$)	Q_{st} (kJ mol^{-1})	$\text{Kr}_{(\text{ads})}$ ($\text{mmol} \cdot \text{g}^{-1}$)	Q_{st} ($-\text{kJ} \cdot \text{mol}^{-1}$)	Xe/Kr selectivity
Th-abdc-1(form)	1196	1.06	19	0.32	10	5.9
Th-SCU-11 ^[23]	1272	2.25	-	0.55	-	5.7
UiO-66(Zr) ^[19]	1199	2.10	25	0.60	-	6.7
UiO-66_NH ₂ (Zr) ^[20]	925	1.35	-	0.35	-	7.7
MIL-100(Fe) ^[19]	1947	1.50	20.9	0.35	-	5.1
MIL-101(Cr) ^[19]	3445	1.80	21.4	0.60	-	4.2

In the case of methane (CH_4), the quantity adsorbed is 13.4, 6.6 and 6.1 $\text{cm}^3 \cdot \text{g}^{-1}$ at 900 mmHg for 273, 283 and 293 K respectively (Figure IV-21, left) and the values of enthalpies calculated are between -30 and -32 kJ mol^{-1} (Figure IV-21), values that seem normal for a reversible adsorption-desorption of a gas into porous materials.^[22]

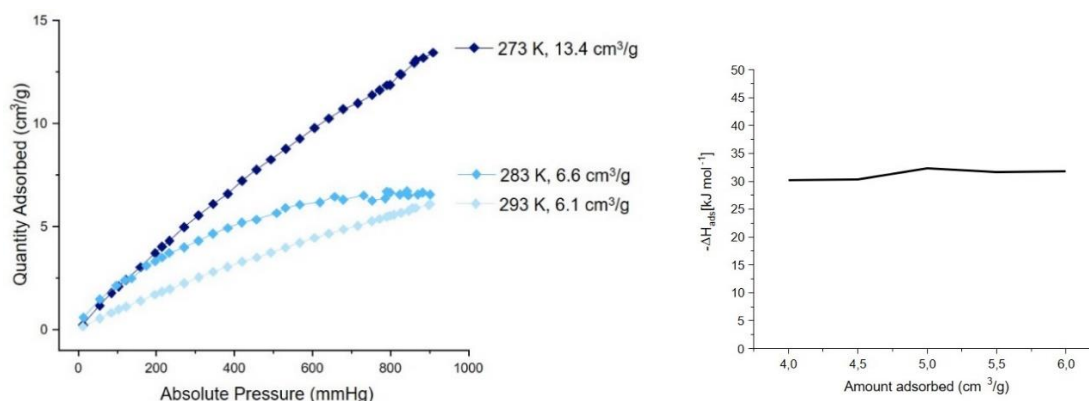


Figure IV-21. Isotherms of methane adsorption for **Th-abdc-1(form)** at three different temperatures (left) and values of enthalpy depending on the volume of methane adsorbed (right).

In Table IV-6, a comparison is made between the phase of **Th-abdc-1**, described in this work, with other reported MOFs that show efficiency in methane uptake. **Th-abdc-1**

demonstrates a slightly higher methane uptake than UiO-66, along with a higher heat of adsorption ($-31 \text{ kJ}\cdot\text{mol}^{-1}$) that indicates a reversible physio-sorption process.

Table IV-6. Comparison of BET surface area and methane uptake for **Th-abdc-1** with other reported MOFs at 273 K at 1 bar.

	$S_{\text{BET}} (\text{m}^2\cdot\text{g}^{-1})$	$\text{CH}_{4(\text{ads})} 273\text{K} (\text{mmol}\cdot\text{g}^{-1})$	$Q_{\text{st}} (-\text{kJ}\cdot\text{mol}^{-1})$
Th-abdc-1-(form)	1195	0.6	31
UiO-66 ^[24]	568	0.51 (269 K)	20.3
U4-BDC-6 ^[25]	497	1.5	24.8

In the case of carbon dioxide (CO_2), the quantity adsorbed is 40.3, 37.5 and 11.7 $\text{cm}^3\cdot\text{g}^{-1}$ for 273, 283 and 293 K respectively at 760 mmHg (Figure IV-22, left). The enthalpies of adsorption calculated between -43 and $-54 \text{ kJ}\cdot\text{mol}^{-1}$ (Figure IV-22, right), values that seem slightly higher than the ones expected in a reversible physio-sorption ($17\text{--}40 \text{ kJ}\cdot\text{mol}^{-1}$) and that indicates covalent interactions of CO_2 and the pores of **Th-abdc-1**, since carbon dioxide is a quite polar molecule.

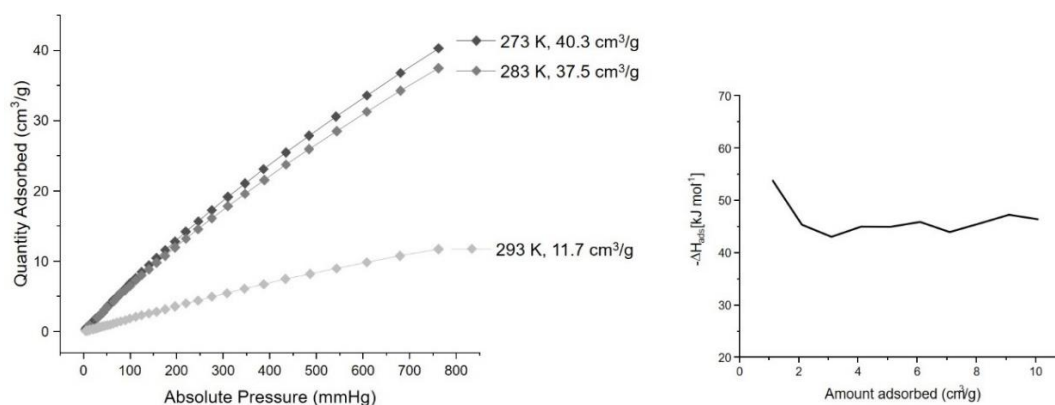


Figure IV-22. Isotherms of carbon dioxide adsorption for **Th-abdc-1-(form)** at three different temperatures (left) and values of enthalpy depending on the volume of carbon dioxide adsorbed (right).

In Table IV-7, a comparison is made between the phase of **Th-abdc-1**, described in this work, with other reported MOFs containing either a thorium hexamer SBU, or the same azobenzene ligand, or an analogue organic chain (biphenyl carboxylic acids). From the values, it is observed that **Th-abdc-1** demonstrates a performance in CO_2 uptake, close to the highest values reported in literature for structurally similar MOFs ($\approx 2 \text{ mmol}\cdot\text{g}^{-1}$). It is interesting to compare **Th-abdc-1** with the very similar Zr-UiO-abdc, as even if the later has a double BET specific surface area value, the quantity of CO_2 adsorbed is the same (1.8 and 2.0 $\text{mmol}\cdot\text{g}^{-1}$ for Tb-abdc-1 and Zr-UiO-abdc respectively). To explain this behavior, heat of adsorption values are useful, as our **Th-abdc-1** presents a much higher heat of adsorption ($48 \text{ kJ}\cdot\text{mol}^{-1}$) that the

zirconium analogue ($18.8 \text{ kJ}\cdot\text{mol}^{-1}$). Consequently, **Th-abdc-1** seems to interact more with CO_2 and thus exhibit higher uptake values.

Table IV-7. Comparison of BET surface area and CO_2 sorption with other similar reported MOFs.

	$S_{\text{BET}} (\text{m}^2\cdot\text{g}^{-1})$	$\text{CO}_{2(\text{ads})} (\text{mmol}\cdot\text{g}^{-1})$	$Q_{\text{st}} (\text{kJ}\cdot\text{mol}^{-1})$
Th-abdc-1	1195	1.8 (273 K) / 0.52 (293 K)	48
Zr-UiO-abdc ^[8]	2122	2.0 (273 K)	18.8
Pu-UiO-66 ^[26,27]	709	0.23 (298 K)	-
UiO-66 ^[24]	568	1.97 (273 K)	30

*the measurement was performed with the thorium analogue.

IV. 1.4 The thorium azobenzenedicarboxylate (**Th-abdc-2**) phase

This part is dedicated to the synthesis and characterization of the second compound, identified in the chemical system involving thorium(IV) and 4,4'-azobenzendicarboxylic acid.

IV. 1.4.1. Synthesis of **Th-abdc-2**

As seen from the diffractograms above (Figure IV-5), the phase of **Th-abdc-2** is formed for specific synthetical conditions with a controlled amount of water ($\text{Th}/\text{H}_2\text{O} = 1/7$) and the addition of 2-fluorobenzoic acid as modulator. The synthesis protocol of **Th-abdc-2** is given detailed in Table IV-8.

Table IV-8. Synthesis protocols of **Th-abdc-2**.

Metal source	Ligand	Modulator	Solvent		T	Time	Yield
$\text{ThCl}_4\cdot 4\text{H}_2\text{O}$	$\text{H}_2\cdot\text{abdc}$	2-fluorobenzoic acid	DMF	H_2O	100 °C	36 h	34%
10 mg	6.2 mg	115 mg	1 mL	30 μL			
0.023 mmol	0.023 mmol	0.82 mmol	13 mmol	0.16 mmol			

After thermal treatment, orange octahedral crystals of $\approx 10 \mu\text{m}$ appeared on the bottom of the vial as shown in the optimal microscope image (Figure IV-23 left). SEM images verify the form and the size of **Th-abdc-2** crystals (Figure IV-23 right). The crystals were washed with DMF (1x2 mL) and dichloromethane (5x2 mL) and dried under primary pump in glove box. This phase is stable under air for some weeks.

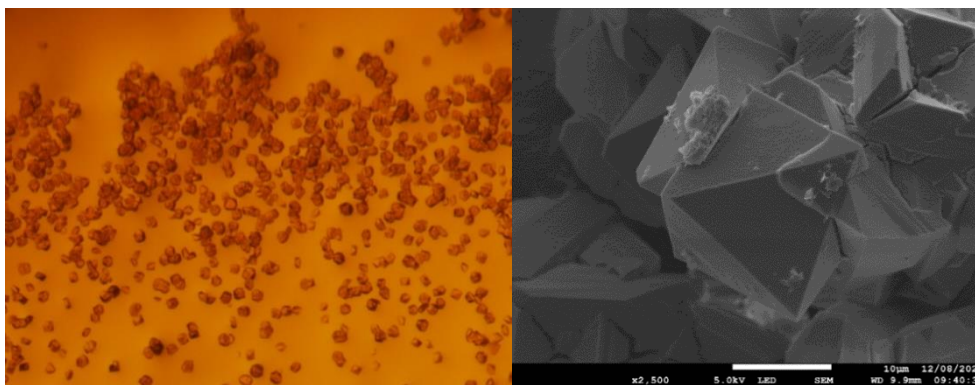


Figure IV-23. Optical microscope image (left) and SEM image of the *Th-abdc-2* phase.

The small size of the crystals ($< 10 \mu\text{m}$) does not allow the performance of single-crystal X-ray diffraction. Therefore, a high-resolution powder X-ray diffractogram was obtained (Figure IV-24, blue line) by means, on a Bruker D8 Advance diffractometer (LynxEye detector) in a Bragg–Brentano θ – θ mode using Cu-K α radiation (1.5406 \AA) in Lille. This powder pattern was recorded within an angular range of 3 – 110° in 2θ , with steps of 0.02° and counting time of 5 s per step. The accumulation time was set at 5 s , so that intensity of the diffraction is high enough to be analyzed. We then perform calculations in collaboration with our colleague Dr. Adel Mesbah at IRCELYON for the structure resolution.

The collected PXRD pattern was indexed using the X-cell algorithm implemented in the Reflex program from Materials studio.^[28] Despite the poor data, the best unit cell was found in the trigonal system in the $R\text{-}3c$ space group with $a = 21.6264 \text{ \AA}$, $c = 54.1242 \text{ \AA}$. After the Pawley refinement^[29], the thorium and the oxygen atoms were detected by expo2014.^[30] The localization of the organic molecules was performed using the FOX program^[31] showing an inversion symmetry center on the 4,4'-azobenzenedicarboxylic molecule, thus in order to find the model half of the molecule was introduced and the rest was generated by symmetry (including the azo $\text{N}=\text{N}$ bond). Because of the quality of the PXRD data and the large value of the unit cell volume of $21945(6) \text{ \AA}^3$, the realization of a complete Rietveld refinement was not possible, however few cycles with fixed atomic positions led a consistent refinement which we assume to be very close to the accurate solution with $a = 21.623(4) \text{ \AA}$ and $c = 54.537(55) \text{ \AA}$. Figure IV-24 views on the left side the collected data and simulated pattern of the obtained structure.

After calculations, a cif file was obtained and the simulated powder X-ray diffraction pattern (black line) shows that the **Th-abdc-2** phase corresponds well to the model of the

structure presented in the cif file (Figure IV-24, right). The experimental powder X-ray diffractogram of **Th-abdc-2** is presented with two different accumulation times (0.5 and 5 s).

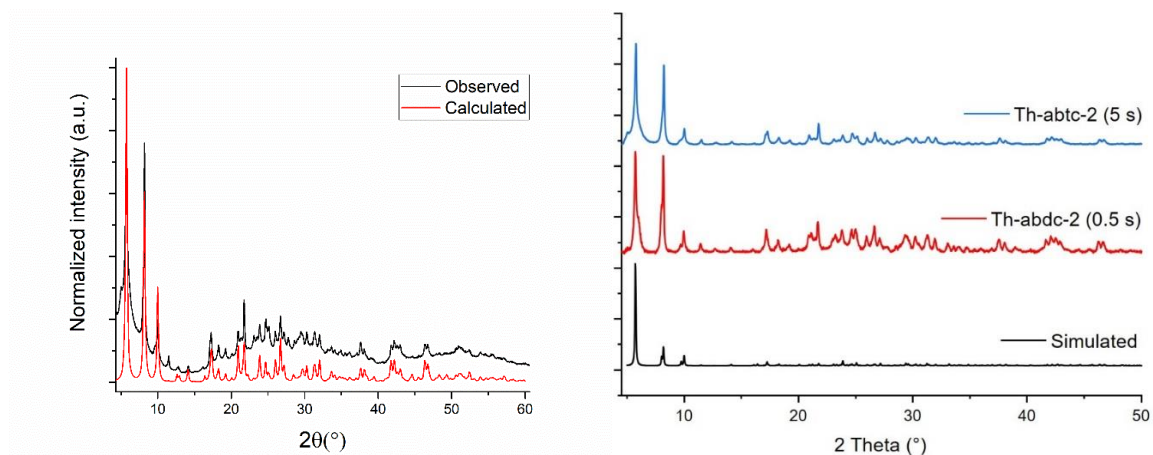


Figure IV-24. (left) comparison of the observed and the calculated powder X-ray diffraction patterns, (right) Powder X-ray diffraction patterns of **Th-abdc-2** with 0.5 and 5 s of exposure time and its simulated pattern. X-ray source; Copper $K\alpha$ radiation; ($\lambda_{CuK\alpha}=1.5406 \text{ \AA}$).

IV. 1.4.2 Structural description of **Th-abdc-2**

Powder X-ray diffraction analysis revealed a structure with the formula $[\text{Th}_6\text{O}_4(\text{OH})_4(\text{abdc})_3(\text{fluorobenzoate})_6(\text{DMF})_6]$ crystallizing in the trigonal symmetrical system ($R\text{-}3c$ ($n^\circ 167$)). The crystallographic data of **Th-abdc-2** are presented in Table IV-9.

Table IV-9. Crystal data and structure refinements for **Th-abdc-2**.

Th-abdc-2	
Formula	$\text{C}_{17}\text{H}_{14}\text{FN}_2\text{O}_{6.3}\text{Th}$
Formula weight	1057.42
Temperature/K	-
Crystal type	-
Crystal size/ mm^3	-
Crystal system	rhombohedral
Space group	$R\text{-}3c$
$a/\text{\AA}$	21.623(4)
$b/\text{\AA}$	21.623(4)
$c/\text{\AA}$	54.537(55)
$\alpha/^\circ$	90
$\beta/^\circ$	90
$\gamma/^\circ$	120
Volume/ \AA^3	21945(6)
Z , $\rho_{\text{calculated}}/\text{g.cm}^{-3}$	0
μ/mm^{-1}	-
θ range/ $^\circ$	-
Limiting indices	-
Collected reflections	-
Unique reflections	-
Parameters	-
Goodness-of-fit on F^2	-
Final R indices [$>2\sigma(I)$]	-
R indices (all data)	-
Largest diff. peak and hole/ e.\AA^{-3}	-

The powder XRD analysis indicated a chemical formulation related to $[\text{Th}_6\text{O}_4(\text{OH})_4(\text{abdc})_3(\text{fluorobenzoate})_6(\text{DMF})_6]$ for **Th-abdc-2**, a two-dimensional network, composed of a thorium hexamer as an inorganic SBU and abdc ligands as linkers between them, forming a layered compound (Figure IV-25, top). The stacking of these layers is revealed to be an a, b, c stacking (Figure IV-25, bottom, layer a: yellow; layer b: green; layer c: red).

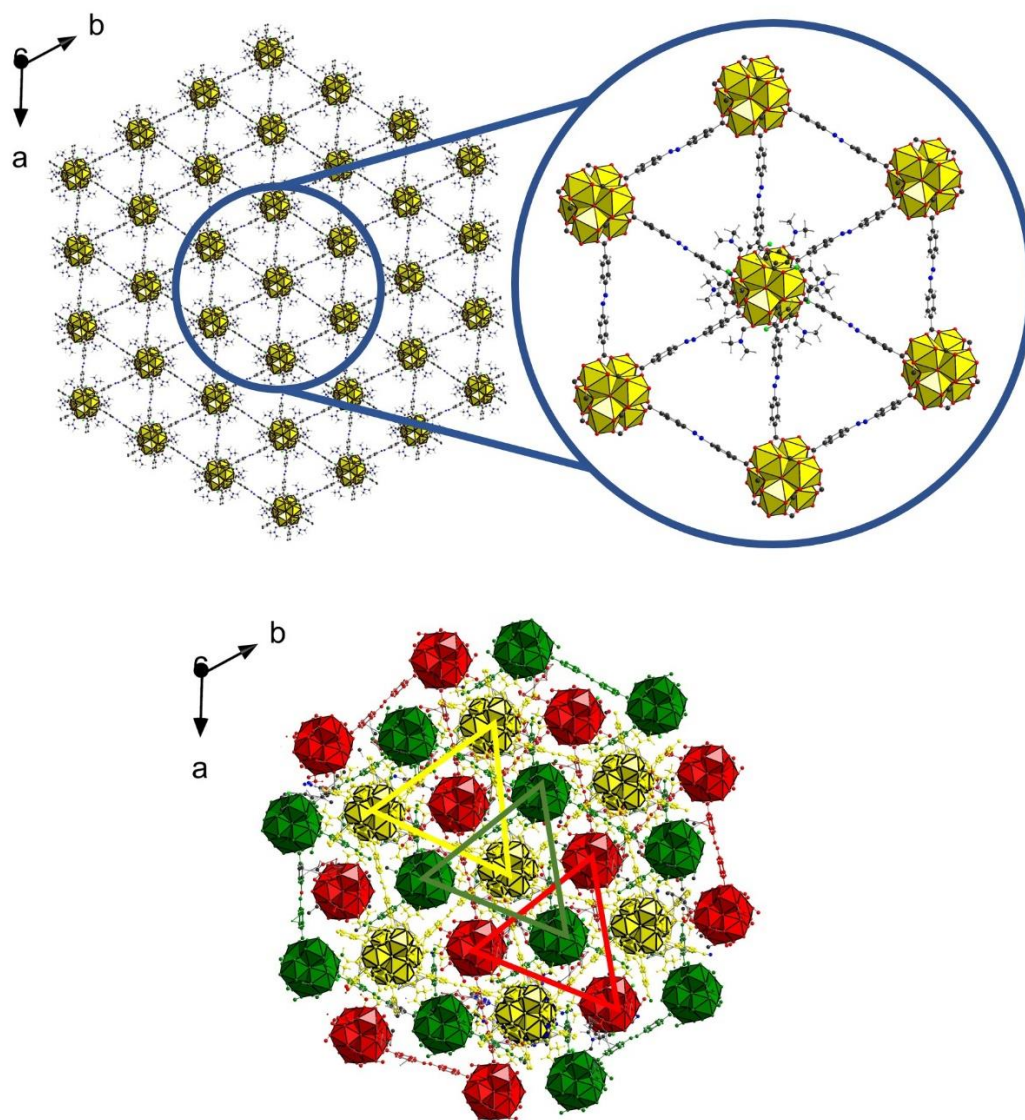


Figure IV-25. A single layered network of **Th-abdc-2** along the a axis with a focus on the coordination environment around thorium hexamer and the connectivity between them (top) (color code: thorium: yellow; oxygen: red; nitrogen: blue; carbon: black; hydrogens: grey). Three distinct layers of the a, b, c stacking (bottom) (color code: layer a: yellow; layer b: green; layer c: red)

The structure of compound $[\text{Th}_6\text{O}_4(\text{OH})_4(\text{abdc})_3(\text{fluorobenzoate})_6(\text{DMF})_6]$ contains an hexameric thorium(IV) cluster with a nine-fold coordination environment and a monocapped square antiprismatic geometry for the thorium center. The latter is crystallographically unique

and connected with nine oxygen atoms, two oxo and two hydroxo oxygens (in order to have a neutral charge final structure) as well as an oxygen atom coming from a terminal DMF molecule (Figure IV-26, left). The coordination sphere is completed with four carboxylate oxygens, this time only two of them deriving from the abdc ligand's carboxylate functions and the other two from 2-fluorobenzoate molecules of the modulator. We can differentiate various Th-O bond distances, where Th-O_{carb} bonds are 2.337-2.363 Å and 2.466-2.458 Å deriving from dicarboxylate and monocarboxylate ligands, respectively. Terminal DMF molecules are bonded with Th-O_{DMF} bonds of 2.605 Å. As for the rest of Th-μ₃-O, we can differentiate two groups of bonds, one with distances of 2.341-2.422-2.430 Å and another one with slightly longer distances of 2.458-2.458-2.577 Å. The longer distances could be attributed to μ₃-hydroxo groups, whereas the shorter to μ₃-oxo.

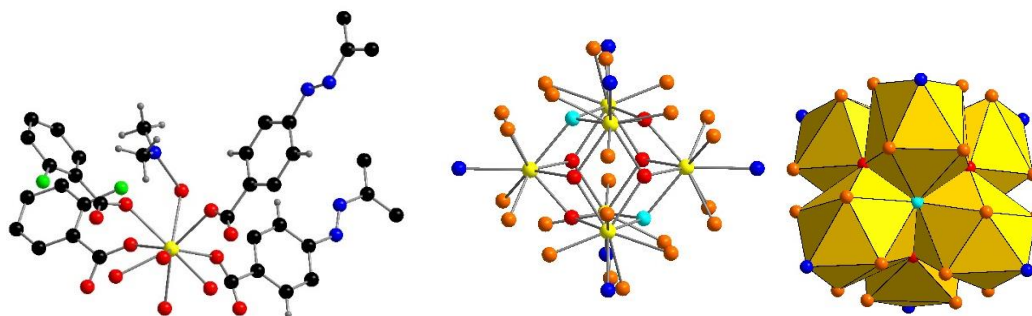


Figure IV-26. Coordination around thorium(IV) species (left), hexameric cluster presents in ball and stick (middle) and in polyhedra (right). Color code: O_{DMF}: blue; O_{carb}: orange; O_{oxo}: red; O_{hydroxo}: turquoise.

The positioning of the 2-fluorobenzoate molecules (Figure IV-27) is crucial because the partial replacement of the dicarboxylates by the monocarboxylates, blocks the extension of the framework in the third dimension, resulting to a final two-dimensional framework.

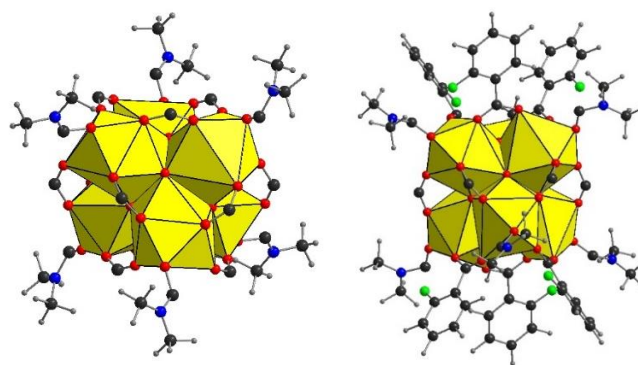


Figure IV-27. Crystal structure of the inorganic SBU of Th-abdc-2 surrounding by terminal DMF molecules (left) and 2-fluorobenzoate molecules and DMF (right).

Each layer is connected with each other with σ - π (sigma-pi) or “edge-to-face” interactions between the aromatic protons and the aromatic rings of the fluorobenzoates, type of interaction that has previously reported.^[32] The fluorobenzoate and the azobenzene dicarboxylate adopt a 116.8° and 71.9° tilted arrangement with an H-to-carbon distance of 1.6969 and 2.6843 Å (Figure IV-28). Moreover, the existence of DMF instead of water as a terminal molecule compared to **Th-abdc-1**, occupies more space of the potential pores. When we look perpendicularly to a layer, it seems that there are some triangular windows. When removing the radii DMF, that window’s diameter is 11 Å. Porosity experiments are presented and discussed below in paragraph 1.7.4. DMF molecules are pointing toward the a,b plane, inside the trigonal window and on the other side, fluorobenzoates are pointing through the c axis.

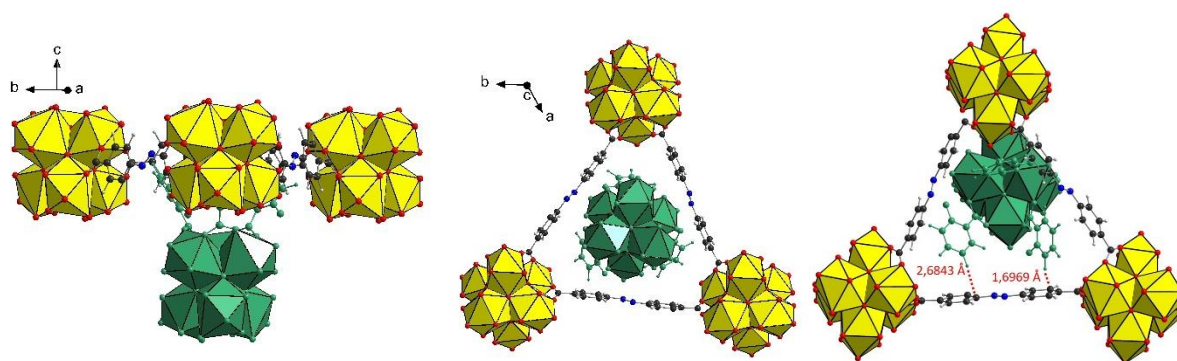


Figure IV-28. Two distinct layers represented in yellow and green along the (a,b) plane (left), the trigonal windows along c axis (middle) and representation of the “edge-to-face” interactions between the layers (right).

As observed with **Th-abdc-1**, the further substitution of one dicarboxylate ligand by two monocarboxylate ligands cannot be ruled out. Thus, the correct way of writing the formula could be $[\text{Th}_6\text{O}_4(\text{OH})_4(\text{abdc})_{3-x}(\text{fluorobenzoate})_{(6+2x)}(\text{DMF})_6]$ if the abdc content is lower than abdc/fluorobenzoate ratio of 3, as revealed from the powder XRD analysis.

The exact composition within the structure is calculated by liquid NMR experiment (^1H , 400 MHz). In a 2 mL vial, **Th-abdc-2** (20 mg) were digested in a standard deuterated solution of NaOD in D_2O (1 mL, 4M). The solution was left in an ultrasound bath for 30 min in room temperature. White powder of $\text{Th}(\text{OH})_4$ appeared on the bottom of the vial, which was filtered to be removed. In the ^1H NMR spectrum (Figure IV-29) of the supernatant, the two doublets centered at 7.89-7.91 and 7.77-7.79 ppm correspond to the eight protons in the azobenzene molecule (red and blue cages). The rest of the intense peaks correspond to the protons of

fluorobenzoate (green, light blue and pink cages). Since the formula is $[\text{Th}_6\text{O}_4(\text{OH})_4(\text{abdc})_{3-x}(2\text{-fluorobenzoate})_{(6+2x)}(\text{DMF})_6]$, from the integration of the spectrum we find that $x=0.87$, so the final formula including the defect is $\text{Th}_6\text{O}_4(\text{OH})_4(\text{abdc})_{2.48}(\text{fluorobenzoate})_{7.04}(\text{DMF})_6$.

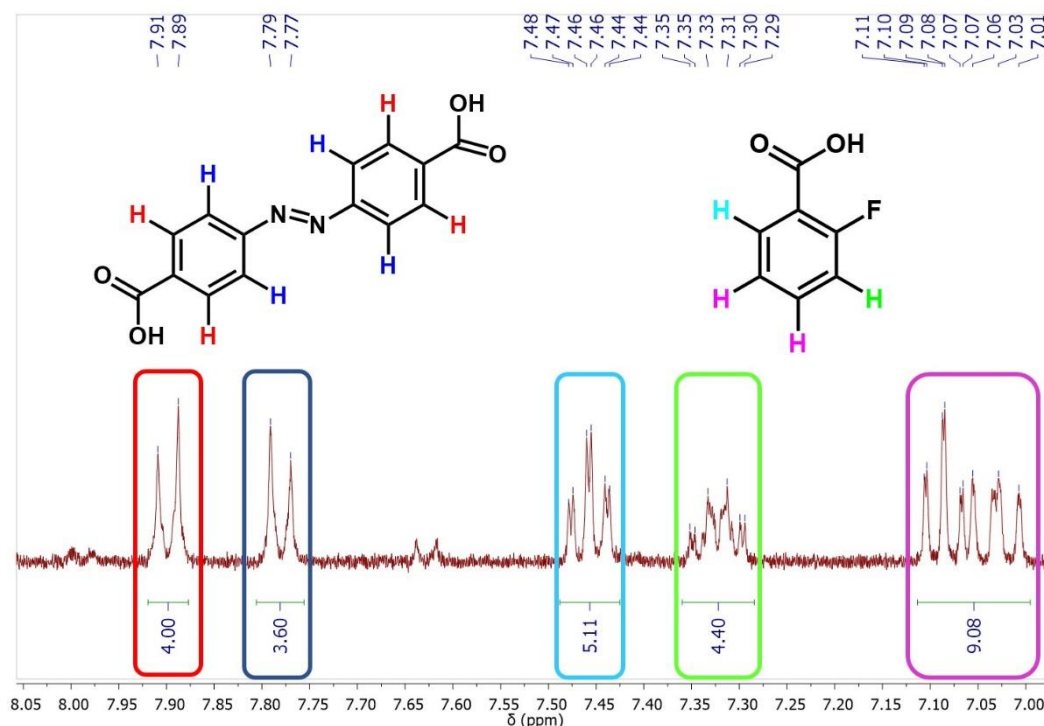


Figure IV-29. ^1H NMR spectrum of the supernatant **Th-abdc-2** digested into a 4M solution of NaOD.

IV. 1.4.3 Characterization of **Th-abdc-2** by infrared spectroscopy and thermogravimetric analysis

The **Th-abdc-2** phase was characterized by infrared spectroscopy and thermogravimetric analysis.

The infrared spectroscopy (Figure IV-30) shows two bands at $\approx 2931\text{-}2863\text{ cm}^{-1}$, characteristic for the aromatic $\nu(\text{C-H})$ vibrations. A broad band is also present at $\approx 3457\text{ cm}^{-1}$, which should derive from a hydrogen bond. Passing on to the carbonyl zone, the spectrum shows a band at $\approx 1656\text{ cm}^{-1}$ and another one at $\approx 1089\text{ cm}^{-1}$ that correspond to a $\nu(\text{C=O})$ and a $\nu(\text{C-N})$ vibration respectively. These bands confirm the presence of DMF in **Th-abdc-2**, as they are characteristic for DMF molecules.^[17] The bands at $\approx 1602\text{ cm}^{-1}$ and at $\approx 1565\text{ cm}^{-1}$ correspond to the asymmetric and symmetric vibration $\nu(\text{COO})$ of the coordinated carboxylate ligand. The vibration between aromatic carbons $\nu(\text{C=C})$ can be found $\approx 1389\text{ cm}^{-1}$ and the torsion of OH and CH at $\approx 789\text{ cm}^{-1}$.

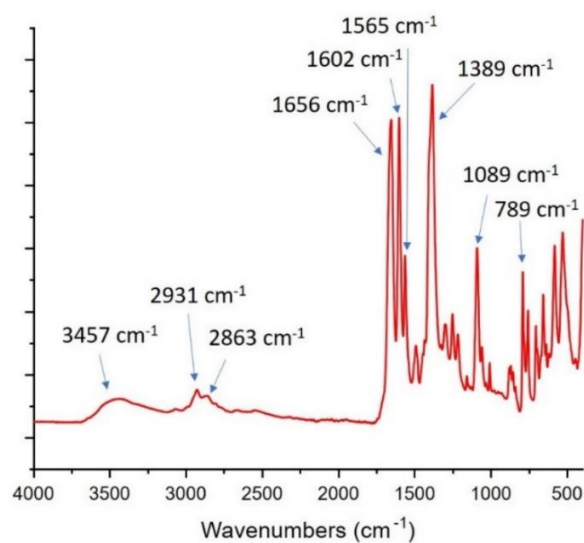


Figure IV-30. Infrared spectra of *Th-abdc-2*.

The thermogravimetric analysis (TGA) of the **Th-abdc-2** phase has a main weight loss at ≈ 475 °C, which corresponds to the carboxylate ligands (azobenzene and 2-fluorobenzoate). If we assume that the experimental residue of 38.7 % corresponds to $6x(\text{ThO}_2)$, then the experimental loss of 39.3 % (calc.: 40.3 %) corresponds to the loss of 2.48 azobenzene ligands and 7.04 fluorobenzoates and is in accordance with the structure of the **Th-abdc-2** if we consider the defect coming from the presence of modulator.

A second weight loss at ≈ 350 °C, corresponds to the six coordinated DMF molecules. This loss of 10.4 % (calc.: 10.7 %) is assigned to the loss of six molecules of DMF. There also ≈ 14 % of loss from 50 to 200 °C that corresponds to the loss of free DMF trapped in the pores of the MOF (Figure IV-31).

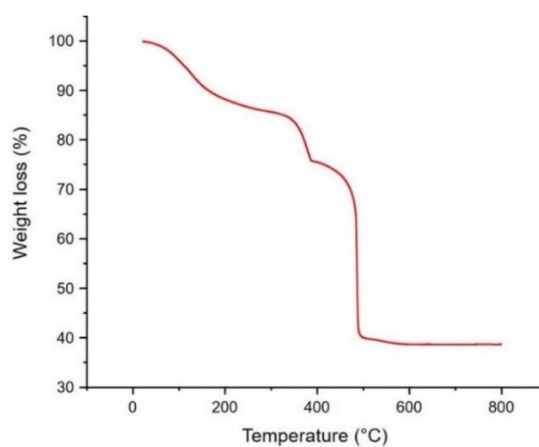


Figure IV-31. Thermogravimetric curve of *Th-abdc-2*.

The X-ray thermodiffraction was not performed as the thermodiffractometer has a lower sensitivity detector and the compound diffracts weakly. For example, the powder X-ray diffraction pattern that was made for the calculation of the structure was measured with an expose time of 5 s per angle and was still not diffracting and so data were not collected.

IV. 1.4.4 Gas sorption experiments in **Th-abdc-2**

BET experiments were performed, with an activation at 80 °C (details in table A1 in Appendix), but no nitrogen sorption was possible at 77K. This can happen due to the coordinated DMF molecules that block that takes up some space of the pores. Consequently, BET surface cannot be calculated. However, another smaller gas, carbon dioxide was tested successfully, with uptakes of 8, 8.3 and 10.4 cm³/g at 760 mmHg (at 273, 283 and 293 K respectively). Carbon dioxide uptakes were tested in three temperatures (at 273, 283 and 293 K) in order to evaluate the enthalpy values for CO₂ sorption. This shows that carbon dioxide has a small enough kinetic diameter (Table IV-10) to diffuse in **Th-abdc-2**.^[33]

Table IV-10. Kinetic diameter of different gases.^[33]

Gas	Formula	Kinetic diameter (Å)
Nitrogen	N ₂	3.64
Carbon dioxide	CO ₂	3.30

Measurements of CO₂ adsorption for three temperatures were made in order to calculate the enthalpy of adsorption and have a better view about the type of interactions formed between carbon dioxide and the surface of the pores (Figure IV-32). The enthalpies of adsorption in this case (-10 kJ.mol⁻¹), are lower than what we observed for the **Th-abdc-1** (-45 kJ.mol⁻¹). This means that in CO₂ interacts less with **Th-abdc-2** and more with **Th-abdc-1**. In the literature, enthalpies of adsorption for UiO-66 are between 25 and 35 kJ.mol⁻¹.^[34]

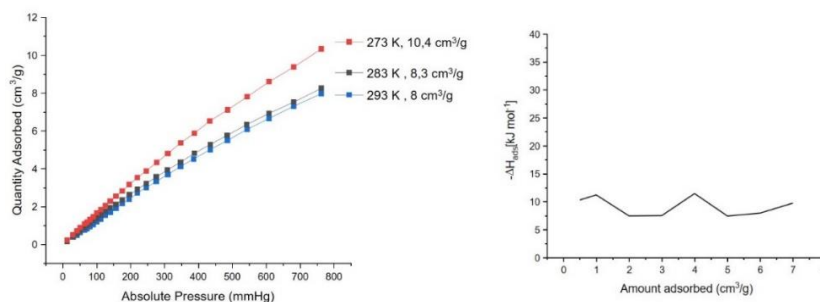


Figure IV-32. Isotherms of carbon dioxide adsorption for **Th-abdc-2** at three different temperatures (left) and values of enthalpies depending on the volume of carbon dioxide adsorbed (right).

IV.2 Thorium(IV) coordination polymers with 3,3',5,5'-azobenzene tetracarboxylic acid

The following part reports studies the reactivity of tetravalent thorium with 3,3',5,5'-azobenzene dicarboxylic acid (H_4abtc) in *N,N*-dimethylformamide solvent giving rise to the production of two distinct phases, named **Th-abtc-1** and **Th-abtc-2**. In order to isolate them, the influence of chemical parameters (H_2O /thorium ratio, temperature, type of modulator) will be studied. These phases will be described and characterized by X-ray diffraction, infrared spectroscopy and thermogravimetric analyses. The amount of structural defects will be also calculated by NMR experiment.

IV. 2.1 Composition diagram of the system $ThCl_4/H_4abdc/modulator/DMF/H_2O$

The study of the synthesis medium composed of thorium(IV), the ligand azobenzene tetracarboxylate and a modulator was done in solvothermal conditions for a time fixed at 36 hours and for temperatures varying from 100 to 150 °C. As for previous **Th-abdc-1** and **Th-abdc-2** compounds, all handlings before the thermal treatment, have been done in an inert atmosphere (Argon) before the thermal treatment. The precursor of tetravalent thorium used in the following study is thorium tetrachloride tetrahydrated ($ThCl_4 \cdot 4H_2O$), as described in paragraph 1.1.

The organic linker (3,3,5,5'-azobenzene dicarboxylic acid, H_4abdc) was also synthesized to a protocol adapted from the literature.^[9]

5-Nitroisophthalic acid (9.5 g, 44.9 mmol) and sodium hydroxide (25 g, 0.6 mol) were added in 120 mL H_2O and heated at 60 °C until dissolution. An aqueous solution of glycose (25 g in 50 mL water) was heated up to 60 °C as well and then was added drop-wise to the previous solution. When the two solutions are mixed, the final solution is left to cool down for 30 minutes and then stirred for 16 hours under air flow. The solution is then transferred to an ice bath and then filtered. The precipitate is dissolved in 125 mL of water and is acidified with the addition of drops of 37% hydrochloric acid so that an orange powder precipitates. The precipitate was filtered, washed and dried.

The precursors $ThCl_4 \cdot 4H_2O$ and 3,3',5,5'-azobenzene dicarboxylic acid (H_4abdc) were dissolved in *N,N*-dimethylformamide (DMF) with or without the addition of controlled amount

of water, heated for 36 hours in variable temperatures (100-150 °C). Two other parameters were studied in the current system: the ratio of H₂O/Th from 0 to 60 (or from 0 to 30 μL) and the nature of modulator (benzoic acid, 2-fluorobenzoic acid and formic acid). A diagram (Figure IV-33) summarizes the composition of every solids obtained after each synthesis and characterization by powder X-ray diffraction.

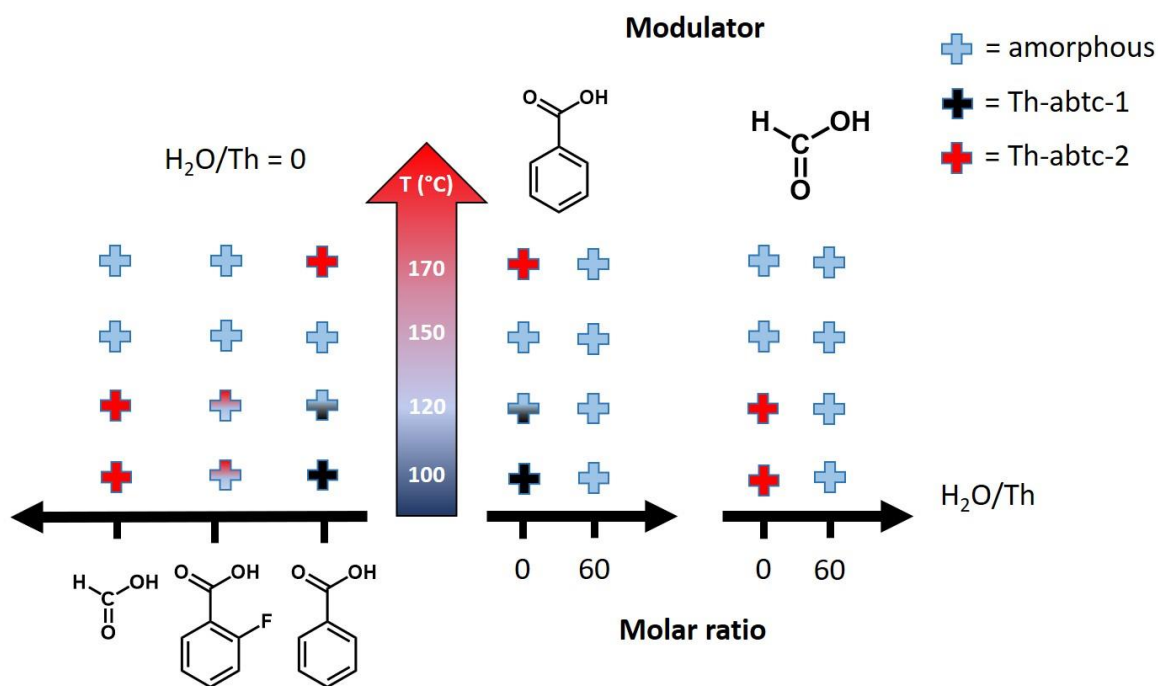


Figure IV-33. Schematic diagram of the parameters changed in the system ThCl₄/H₄abdc/modulator/DMF/H₂O depending on the temperature.

All the syntheses have led to a precipitate after the thermal treatment. However, most of the times the solid was an amorphous orange powder (light blue cross in Figure IV-33). As previously in this chapter, the amorphous phases are orange and thus, this is a first indication that this powder is not an amorphous thorium oxide. By infrared spectroscopy, a band at 1654 cm⁻¹ is observed that derives from a stretch of C=O bond from either the azobenzenetetracarboxylate or DMF molecules. At a first glance, it is observed that when modulator is changed, different phases are isolated (Figure IV-33, left part). With benzoic acid as modulator at 100 °C the phase **Th-abtc-1** is isolated (orange crystals). As temperature is increased an amorphous orange phase is generated from ≈ 120 °C to 150 °C and finally at 170 °C another phase, the **Th-abtc-2** is isolated (yellow powder). The latter is always obtained in absence of additional water. An explanation for this behavior is that by increasing the temperature we force the decomposition of DMF and more formic acid is produced. As the amount of formic acid increases, it is more likely that it will play the role of modulator in the

synthesis instead of benzoic acid, to finally isolate a different phase (**Th-abtc-2**). In order to validate our theory, we tried adding formic acid in the starting reaction medium as a modulator. Indeed, the **Th-abtc-2** phase is also isolated when formic acid is used instead of benzoic acid. Another modulator was tested as well (2-fluorobenzoic acid), but only a mixed phase of the above two is obtained. Finally, adding water does not help the crystallization in this system and provokes the precipitation of an amorphous light orange powder (Figure IV-32, right part).

IV. 2.2 The thorium azobenzenetetracarboxylate (**Th-abtc-1**) phase

IV. 2.2.1. Synthesis of **Th-abtc-1** phase

As seen from the phase diagram above, the **Th-abtc-1** phase is formed for specific synthetical conditions with benzoic acid as modulator and without the addition of water, at relatively low temperature (100°C) (Table IV-11).

Table IV-11. Synthesis protocols of **Th-abtc-1**.

Metal source	Ligand	Modulator	Solvent	T	Time	Yield
ThCl ₄ ·4H ₂ O	H ₄ -abdc	benzoic acid	DMF	100 °C	36 h	32%
10 mg	8.2 mg	600 mg	1 mL			
0.023 mmol	0.023 mmol	4.92 mmol	13 mmol			

After thermal treatment of the above mixture, orange parallelepipedic crystals of $\approx 10 \mu\text{m}$ appeared on the bottom of the vial as shown in SEM images (Figure IV-34). Despite the very small size of these crystals, an appropriate one was found, allowing the structural determination of this phase (see hereafter, paragraph 2.2.2).

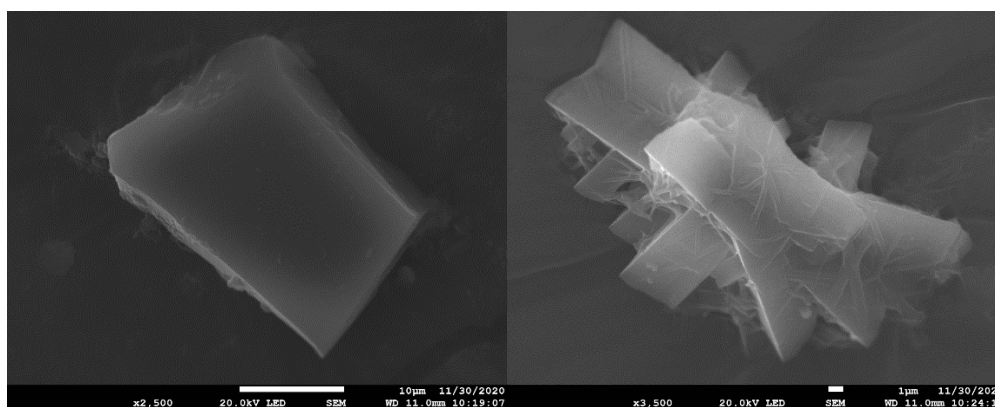


Figure IV-34. SEM image of the **Th-abtc-1** phase.

Powder X-ray diffraction patterns show that **Th-abtc-1** is a homogenous phase matching with the one of the structures resulted by single-crystal X-ray diffraction, for which the simulated one was generated (Figure IV-35). This phase is stable under air for some days.

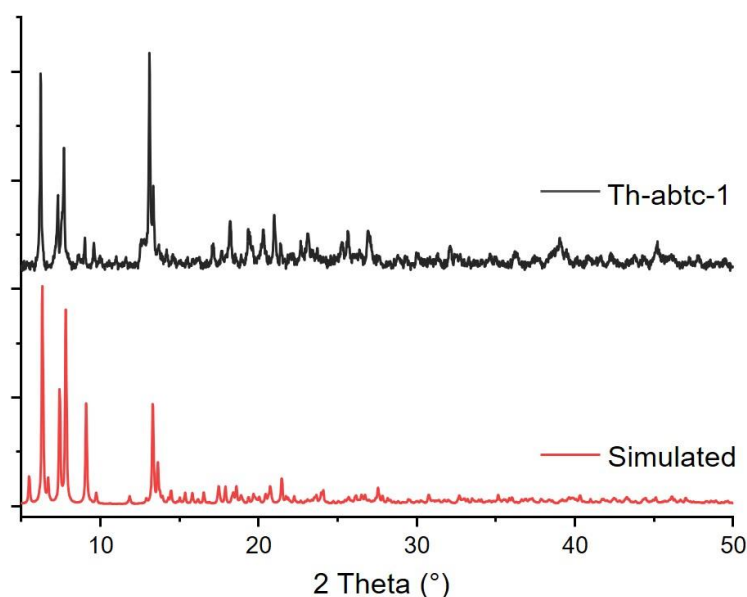


Figure IV-35. Powder X-Ray Diffraction patterns of **Th-abtc-1**. X-ray source; Copper $K\alpha$ radiation; ($\lambda_{CuK\alpha}=1.5406 \text{ \AA}$).

IV. 2.2.2. Structural description of **Th-abtc-1**

The structure was determined in the laboratory by single-crystal X-ray diffraction in a Bruker APEX at 99.9 K and under Mo radiation ($\lambda_{MoK\alpha}=0.71 \text{ \AA}$). The compound $[\text{Th}_2(\text{abtc})(\eta^1\text{-Habt})\text{(bz)}(\text{H}_2\text{O})_2]\cdot(\text{Hbz})_2$ crystallizes in the monoclinic symmetrical system ($P2_1/c$, $n^\circ 14$) and the crystallographic data can be found in Table IV-12.

Table IV-12. Crystal data and structure refinements for **Th-abtc-1**.

Th-abtc-1	
Formula	$\text{C}_{22.13}\text{H}_{10.38}\text{N}_2\text{O}_{10.75}\text{Th}$
Formula weight	694.36
Temperature/K	99.9
Crystal type	parallelepiped
Crystal size/ mm^3	$0.135 \times 0.074 \times 0.116$
Crystal system	monoclinic
Space group	$P2_1/c$
a/ \AA	13.8692(18)
b/ \AA	27.964(4)
c/ \AA	20.527(3)
$\alpha/^\circ$	90
$\beta/^\circ$	107.339(3)
$\gamma/^\circ$	90
Volume/ \AA^3	7599.5(17)
Z, $\rho_{\text{calculated}}/\text{g}\cdot\text{cm}^{-3}$	8/1.237
μ/mm^{-1}	3.963
θ range/ $^\circ$	2.538-37.78
Limiting indices	$-12 \leq h \leq 12$ $-25 \leq k \leq 25$ $-18 \leq l \leq 18$
Collected reflections	48383
Unique reflections	5989 [$R_{\text{int}} = 0.1945$]

Parameters	407
Goodness-of-fit on F^2	1.055
Final R indices [$I > 2\sigma(I)$]	$R_1 = 0.0813$, $wR_2 = 0.2269$
R indices (all data)	$R_1 = 0.1526$ $wR_2 = 0.2699$
Largest diff. peak and hole/ $e.\text{\AA}^{-3}$	3.15/-1.09

Single crystal X-ray diffraction revealed a three-dimensional framework, composed of a thorium centers connected to abtc ligands. This framework contains channels running along the a axis, that are filled with benzoic acid (Figure IV-36, left).

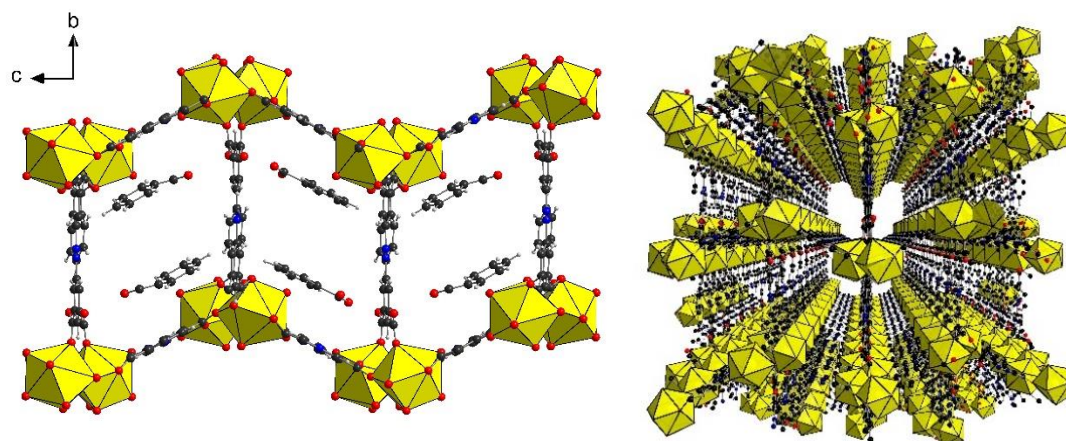


Figure IV-36. Framework of **Th-abtc-1** along a axis with a focus on the benzoic acid trapped in the pores (left), general image of the **Th-abtc-1** framework along a axis in a central projection mode. (color code: thorium: yellow; oxygen: red; nitrogen: blue; carbon: black; hydrogens: grey).

The compound $[\text{Th}_2(\text{abtc})(\eta^1\text{-Habtc})(\text{bz})(\text{H}_2\text{O})_2](\text{Hbz})_2$ contains two crystallographically unique thorium sites with a nine-fold coordination environment each. Each thorium is connected with nine oxygens, from which seven carboxyl oxygens of the abtc ligand, one oxygen from a bridging benzoate and an oxygen coming from a terminal water molecule located in oxygens O9 and O18 (Figure IV-37). These oxygen atoms are arranged in a highly distorted monocapped square antiprismatic geometry around the thorium atom. In **Th-abtc-1** there are two crystallographically unique azobenzenetetracarboxylates, one chelated where all carboxylates are bidentates abtc^{4-} (marked as L_A , figure IV-38, left) and another one, where two out of four carboxylates are monodentate $\eta^1\text{-Habtc}$ (marked as L_B , figure IV-38, middle). In the last one, there are two free C-O groups: one is protonated (carboxylic acid) and one deprotonated (carboxylate).

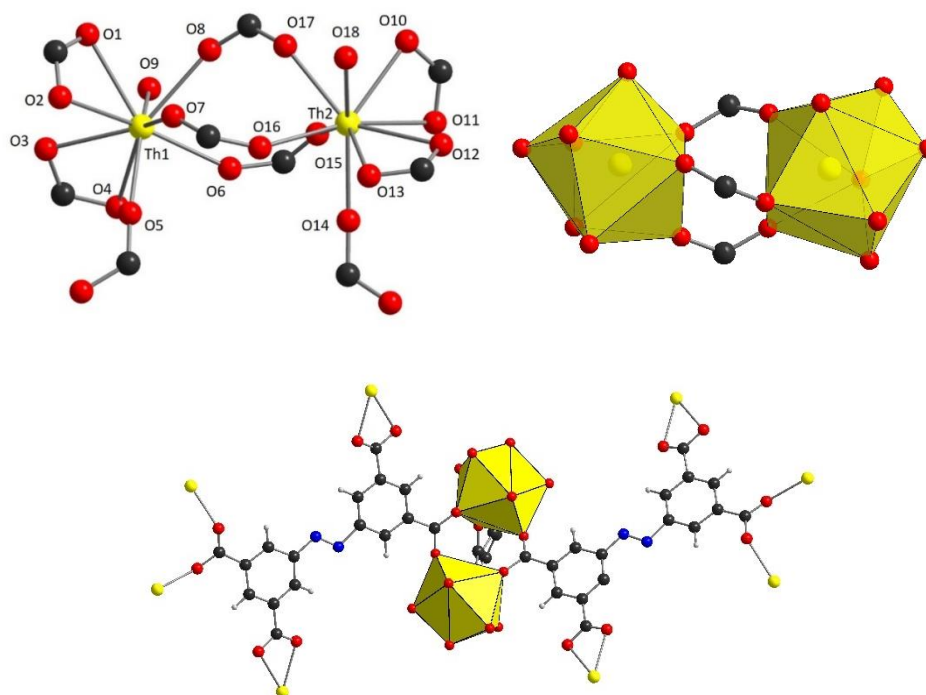


Figure IV-37. Coordination environment around thorium in the *Th-abtc-1* (top). Terminal water molecule is connected through O9 and O18. Bridging environment around a pair of thorium atoms for which only the ligand *abtc*⁴⁻ *L_A* is shown (bottom) (color code: thorium: yellow; oxygen: red; carbon: black; hydrogens: grey).

The two thorium atoms are bridged in a pair by three carboxylates, a distinct bidentate benzoate (O8-C-O17) and two *L_A* type (*abtc*) of ligands (O7-C-O16 and O6-C-O15). For each thorium atom, there are two chelating carboxylates (O1-C-O2, O3-C-O4 for Th1 and O10-C-O11, O12-C-O13 for Th2) from *L_A* (*abtc*) and one monodentate carboxylate (O5 and O14) from *L_B* (η^1 -*Habtc*). The distances between thorium-oxygen bonds for the different coordination modes are shown in Table IV-13. The uncertainties are quite high for this structure as the values are taken from a structure in isotropic thermal parameters, due to relatively poor XRD data (see Table IV-12, with relatively high R values).

Table IV-13. Thorium-oxygen bond distances in *Th-abtc-1*.

Bond	Length (Å)	Bond	Length (Å)
Th1-O1	2.46(2)	Th2-O10	2.49(2)
Th1-O2	2.58(2)	Th2-O11	2.45(1)
Th1-O3	2.48(2)	Th2-O12	2.46(2)
Th1-O4	2.57(2)	Th2-O13	2.63(2)
Th1-O5	2.31(2)	Th2-O14	2.31(2)
Th1-O6	2.30(2)	Th2-O15	2.41(2)
Th1-O7	2.40(2)	Th2-O16	2.35(2)
Th1-O8	2.37(2)	Th2-O17	2.39(2)
Th1-O9	2.46(2)	Th2-O18	2.46(2)

By taking into account the above bond lengths and according to bond valence calculations^[35], the values of 4.50 and 4.51 are found for the atom of Th1 and Th2 accordingly, which is in accordance with its charge of 4+. As for the terminal water molecules, the bond distances Th1-O9 and Th2-O18 are 2.46(2) and 2.46(2) (Å) respectively. According to bond valence calculations, these distances lead to a value V of 0.79.

The L_A type ($abtc^{4-}$) of ligand chelates completely with four pairs of thorium (Figure IV-38, left). The second crystallographically unique $Habtc^{3-}$ ligand (L_B) is coordinated with three pairs of thorium. In one side of the organic linker each one of the two adjacent carboxylic functions is chelating to one thorium center and on the other side the other two monodentate carboxylic functions are bridging the third dimer (Figure IV-38, middle). The monodentate carboxylic acids, have branched C-O distances of 1.26(5) and 1.21(5) Å, whereas the unbranched C-O distances are 1.19(5) and 1.28(7) (Å). The distances of the free C-O bonds show that one is deprotonated and the other one protonated respectively. These two types of azobenzene-derivative linker and the bridging benzoate surround each pair in a fashion shown on the right in Figure IV-38.

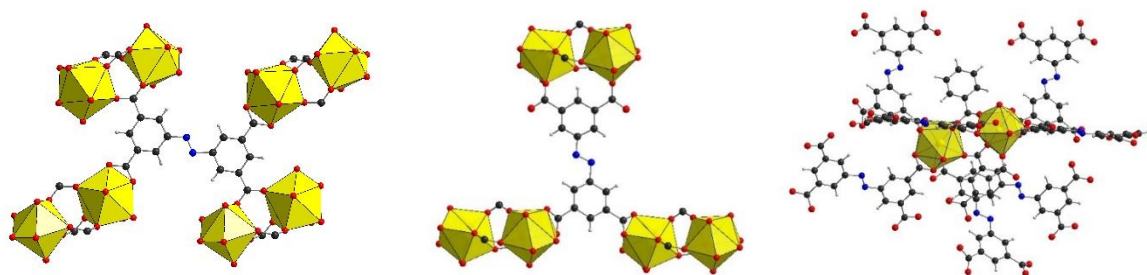


Figure IV-38. Coordination environment around L_A $abtc^{4-}$ ligand (left), L_B η^1 - $Habtc^{3-}$ ligand (middle), and around a Th-dimer (right) (color code: thorium: yellow; oxygen: red; nitrogen: blue; carbon: black; hydrogens: grey).

In this case, no 1H NMR experiment was done to calculate the defect due to the benzoic acid trapped into the parallelepiped-shaped 1D channels of **Th-abtc-1**. This amount will add up to the one coming from the defect and it will not be possible to distinguish the quantity of benzoates that replace azobenzene. There are two benzoic acids par channel (along a axis) and they interact with two different ways with the framework. Firstly, they form hydrogen bonding between the carboxylic protons and the free carbonyl groups with a distance of 3.09(1) Å and there is a π - π stacking with one of the two benzene rings of azobenedicarboxylate with a distance of 3.532 Å. In the absence of benzoic acids in the channels, we could estimate a void of 7.4 Å. We could remove the free benzoic acid from the

pores, but as it is shown from the thermostability studies (paragraph 2.2.3), once benzoic acid from the pores is removed, the framework is no more stable. The presence of benzoic acid is confirmed by infrared spectroscopy and thermogravimetric analysis in the next paragraph (Paragraph 2.2.3). Finally, the porosity of this framework studied under various conditions of activation, degassing and activation, but no porosity was found, due to the instability of the crystalline structure, which was also confirmed by X-ray thermodiffraction (Paragraph 2.2.3). The reason for this early collapse of the framework can be due to the presence of monodentate carboxylic functions that affect the thermal stability, since the second carboxylate oxygen remains free (Figure IV-38, left).

IV. 2.2.3. Characterization of **Th-abtc-1** by infrared and thermogravimetric analysis

Th-abtc-1 was characterized by infrared spectroscopy, thermogravimetric analysis and thermodiffraction.

The infrared spectroscopy (Figure IV-39) shows a broad band at $\approx 3057\text{ cm}^{-1}$ that corresponds to $\nu(\text{C-H})$ vibrations. As verified by the structure there is benzoic acid in the pores that can be seen in the infrared spectrum, where the band at $\approx 1705\text{ cm}^{-1}$ is assigned to the free carboxylic acid inside the pores. The bands at $\approx 1606\text{ cm}^{-1}$ and at $\approx 1583\text{ cm}^{-1}$ correspond to the asymmetric vibration $\nu_{as}(\text{COO})$ of the coordinated carboxylates (abtc and benzoates accordingly), where their symmetric vibration $\nu_{sym}(\text{COO})$ is at $\approx 1407\text{ cm}^{-1}$. The vibration between aromatic carbons $\nu(\text{C=C})$ can be found $\approx 1516\text{ cm}^{-1}$.

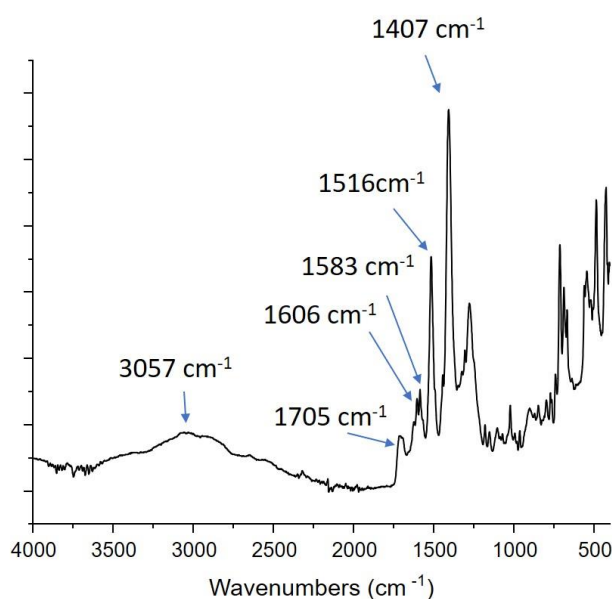


Figure IV-39. Infrared spectra of **Th-abtc-1**.

The thermogravimetric analysis (TGA) of **Th-abtc-1** has a main weight loss at ≈ 375 °C, which corresponds to the azobenzene ligand and the collapse of the framework to form ThO_2 . If we assume that the residue of 31.7 % corresponds to ThO_2 , then the experimental loss of 43.0 % (calc.: 43.0 %) at around 450 °C corresponds to the loss of 2 abtc ligands / 2 ThO_2 and is in accordance with the structure of $[\text{Th}_2(\text{abtc})(\eta^1\text{-Habtc})(\text{bz})(\text{H}_2\text{O})_2](\text{Hbz})_2$. The rest 25.5 % (calc.: 27.5 %) corresponds to the loss of the two benzoic acids trapped into the pores (Figure IV-40, top).

By comparing with the X-ray thermodiffractogram (Figure IV-40, bottom), the framework is structurally stable up to 60 °C, then until 420 °C an amorphous phase is formed and after we identify the formation of thorium oxide ThO_2 (PDF:00-004-0556). As a result, BET experiments shown no porosity as the framework loses its crystallinity after 60 °C.

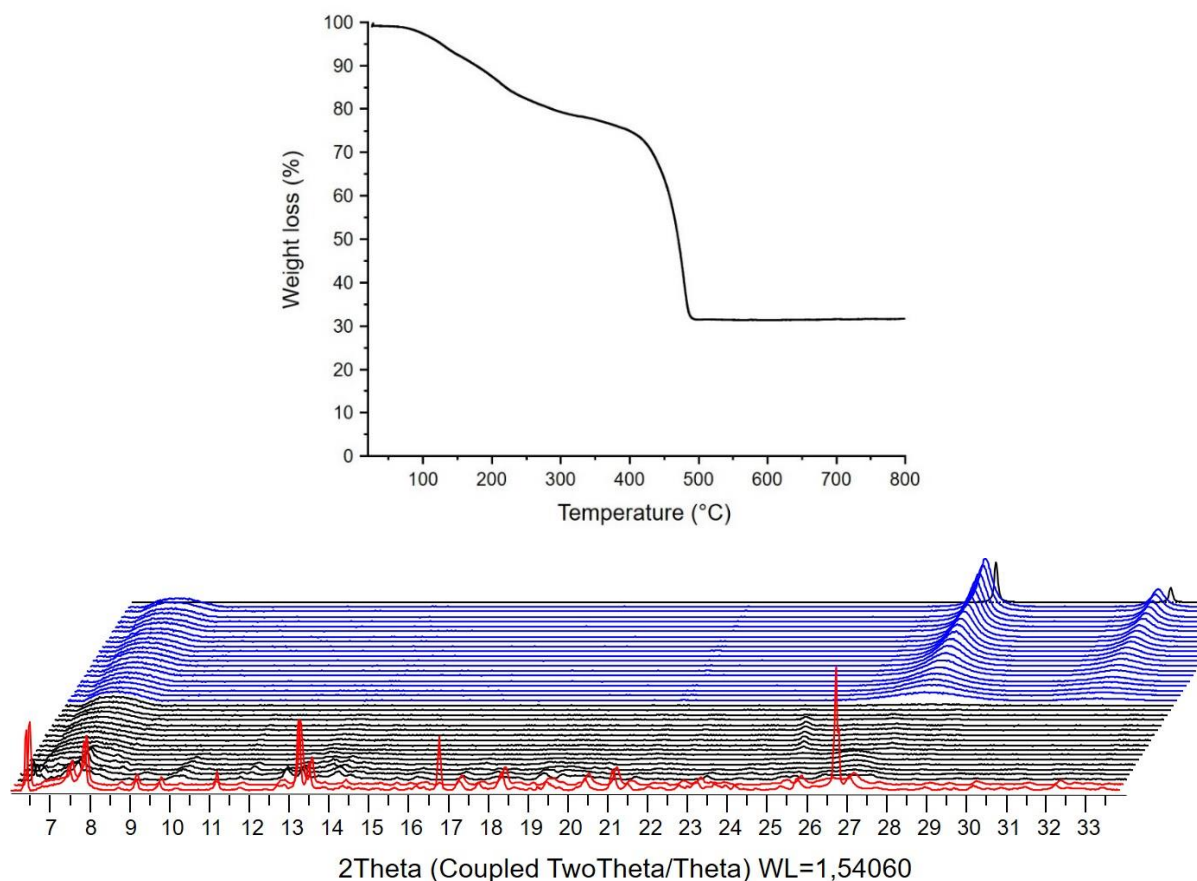


Figure IV-40. Thermogravimetric curve (top) and X-ray thermodiffractogram under air (bottom) for **Th-abtc-1**. X-ray source; Copper K α radiation; ($\lambda_{\text{CuK}\alpha}$ =1.5406 Å).

IV. 2.3 The thorium azobenzenetetracarboxylate (**Th-abtc-2**) phaseIV. 2.3.1. Synthesis of **Th-abtc-2** phase

As seen from the phase diagram above (Figure IV-33), the **Th-abtc-2** phase can be formed by two different synthetical routes. When modulator is benzoic acid, **Th-abtc-2-(bz)** is formed at 170 °C, whereas with formic acid as modulator (**Th-abtc-2-(form)**) the temperature can be down to 100 °C. The synthesis protocols of **Th-abtc-2** phase are detailed in Table IV-14.

Table IV-14. Synthesis protocols of **Th-abtc-2**.

Metal source	Ligand	Modulator	Solvent	T	Time	Yield
ThCl ₄ ·4H ₂ O 28.7 mg 0.065 mmol	H ₄ -abdc 23.3 mg 0.065 mmol	benzoic acid 300 mg 2.46 mmol	DMF 3 mL 39 mmol	170 °C	36 h	58%
ThCl ₄ ·4H ₂ O 10 mg 0.023 mmol	H ₄ -abdc 8.2 mg 0.023 mmol	Formic acid 188 µL 0.498 mmol	DMF 1 mL 13 mmol	100 °C	36 h	67%

From the first protocol (**Th-abtc-2-(bz)**), yellow powder appeared on the bottom of the vial, consisted of agglomerated crystals of $\approx 5 \mu\text{m}$, not suitable for single-crystal X-ray diffraction (Figure IV-41, top). After thermal treatment of the second protocol (**Th-abtc-2-(form)**), yellow crystals of about $\approx 20 \mu\text{m}$ were isolated (Figure IV-41, bottom). This phase seems to be more stable than the previous one and can retain its crystallinity for several weeks under air.

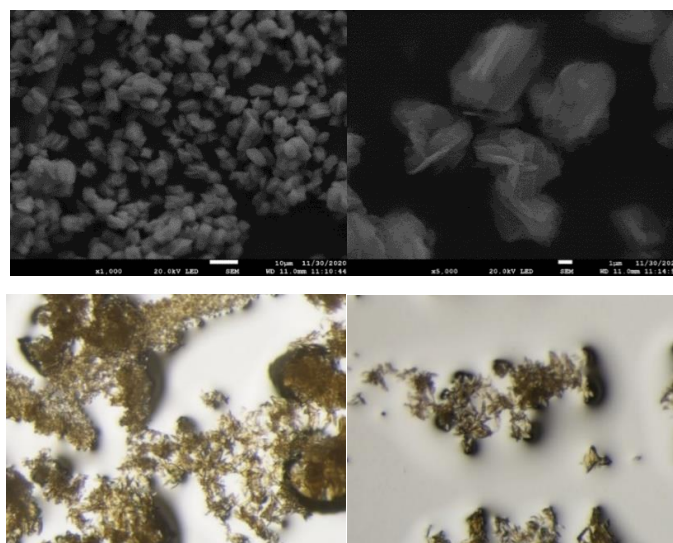


Figure IV-41. SEM image of the **Th-abtc-2-(bz)** phase (top) and optical microscope images of the **Th-abtc-2-(form)** phase (bottom).

Powder X-ray diffraction patterns show that **Th-abtc-2** is a homogenous phase matching with the one of the structures resulted by single-crystal X-ray diffraction, for which the simulated one was generated from the .cif file of **Th-abtc-2-(form)** (Figure IV-42).

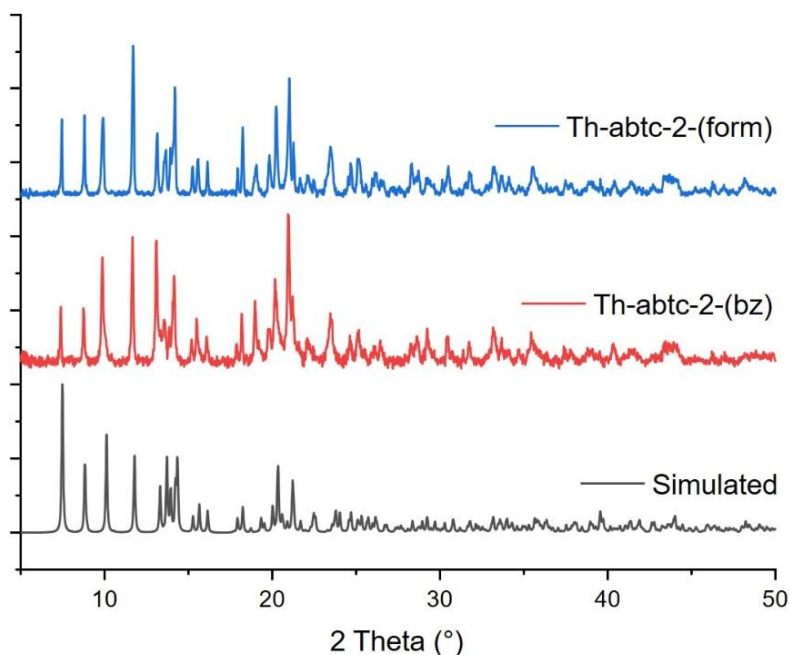


Figure IV-42. Powder X-ray diffraction patterns of **Th-abtc-2**. X-ray source; Copper K α radiation; ($\lambda_{\text{CuK}\alpha}$ =1.5406 Å).

IV. 2.3.2. Structural description of **Th-abtc-2**

Single crystal X-ray diffraction was performed with a crystal of **Th-abtc-2-(form)**, since their size of 20 μm found to be suitable. **Th-abtc-2** crystallizes in the triclinic symmetrical system ($P-1$ space group ($n^{\circ}2$)) and the structure was determined in the laboratory by single-crystal X-ray diffraction in a Bruker APEX DUO diffractometer (Table IV-15).

Table IV-15. Crystal data and structure refinements for **Th-abtc-2**.

Th-abtc-2	
Formula	C ₂₂ H ₂₀ N ₄ O ₁₀ Th
Formula weight	732.46
Temperature/K	100.13
Crystal type	
Crystal size/mm ³	
Crystal system	triclinic
Space group	$P-1$
a/Å	9.2540(4)
b/Å	11.0465(4)
c/Å	13.3253(5)
α /°	111.351(2)
β /°	103.995(2)
γ /°	96.997(2)
Volume/Å ³	1197.37(8)
Z, $\rho_{\text{calculated}}$ /g.cm ⁻³	12/4.578
μ /mm ⁻¹	37.146
θ range/°	3.452-50.72
Limiting indices	-11 \leq h \leq 11 -13 \leq k \leq 13 -16 \leq l \leq 16

Collected reflections	32090
Unique reflections	4396 [$R_{int} = 0.1146$]
Parameters	431
Goodness-of-fit on F^2	1.104
Final R indices [$I > 2\sigma(I)$]	$R_1 = 0.0376$ $wR_2 = 0.0793$
R indices (all data)	$R_1 = 0.0479$ $wR_2 = 0.0815$
Largest diff. peak and hole/ $e.\text{\AA}^{-3}$	0.97/-1.45

The crystal structure revealed a three-dimensional framework, composed of thorium monomers as an inorganic building unit and two types of abtc ligands as linkers between them. This framework contains voids that are filled with coordinated DMF (solvent), so the pores stay blocked (Figure IV-43, top). Coordinated DMF is also present in the structure (Figure IV-43, bottom left) and it is difficult to remove without destroy the framework (Figure IV-43, bottom right). If DMF molecules are removed, the expected channels are 3.8 Å diameter.

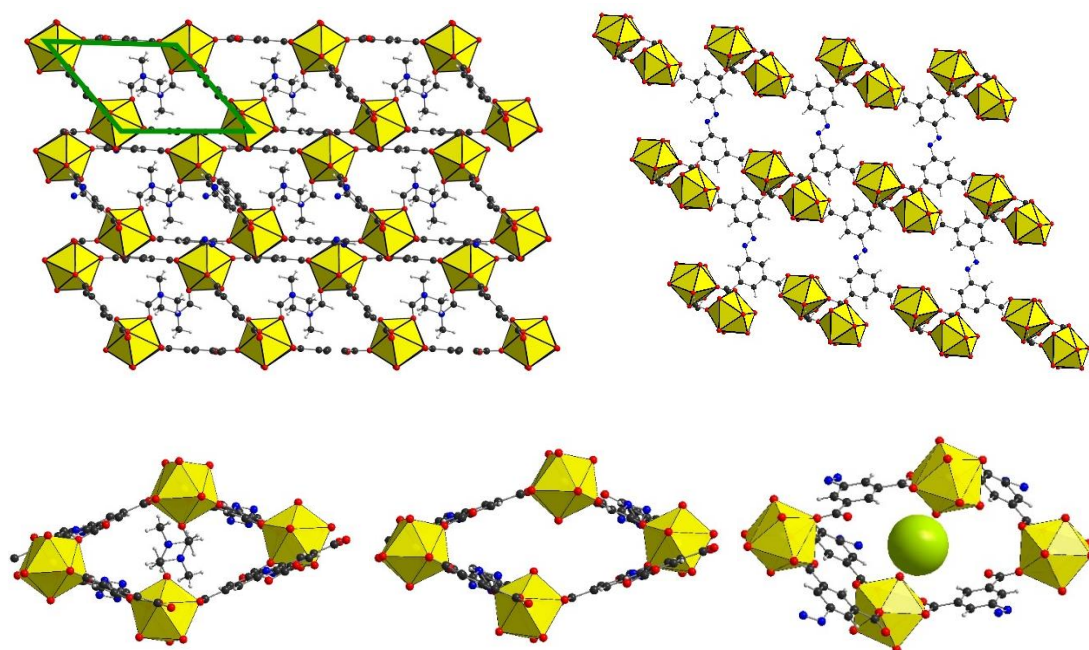


Figure IV-43. Framework of **Th-abtc-2** along (a,b) plane with a green cage to mark the cavities (top left), **Th-abtc-2** along c axis (top right), insight in the pores with (bottom left) and without (bottom middle) coordinated DMF molecules, representation of the cavities (bottom right) (color code: thorium: yellow; oxygen: red; nitrogen: blue; carbon: black; hydrogens: grey).

The compound $[\text{Th}_2(\text{abtc})(\eta^1\eta^1\text{-abtc})(\text{DMF})_4]$ contains one crystallographically unique thorium site with a nine-fold coordination environment, corresponding to a slightly distorted monocapped square antiprismatic geometry. Each thorium is connected with seven carboxylate oxygens of the abtc ligand and two oxygens coming from two different DMF molecules, one of which is disordered (Figure IV-44).

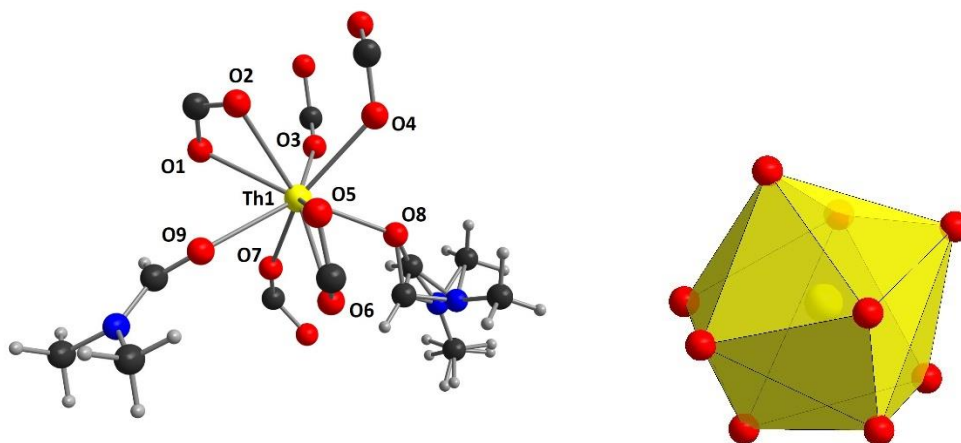


Figure IV-44. Coordination environment around thorium in the **Th-abtc-2**. One of the two DMF molecules is disordered. (color code: thorium: yellow; oxygen: red; carbon: black; nitrogen: blue; hydrogens: grey).

The carboxylate functions in **Th-abtc-2** show three types of coordination modes. There are two bridging bidentate carboxylates that bridge two thorium atoms (O3-C-O3' and O4-C-O4'), two chelating carboxylates for each thorium atom (O1-C-O2 and O5-C-O6) and one monodentate carboxylate (O7) (Figure IV-45). The distances between thorium and the bridging oxygens are 2.37(1) and 2.404(9) Å for Th-O3 and Th-O4 respectively. The oxygens atoms of chelating carboxylates have bigger distances from thorium. These distances are 2.456(7), 2.55(1), 2.525(8) and 2.52(1) Å for Th-O1, Th-O2, Th-O5 and Th-O6, respectively. The smallest distance is 2.335(8) Å and belongs to the one of thorium and the oxygen of monodentate carboxylate (Th-O7). The oxygens deriving from DMF molecules complete the nine-fold coordination state of thorium, with Th-O distances of 2.424(8) and 2.45(1) Å respectively. By taking into account the above bond lengths and according to bond valence calculations^[35], a value of 4.3 is found for the atom of Th1 which is in accordance with its charge of 4+.

In **Th-abtc-2**, there are two unique abtc ligands, one abtc^{4-} and one $\eta^1\eta^1\text{-abtc}$ that has two monodentate carboxylate functions. Both type of ligands are symmetrical with respect to the azo bond and $\eta^1\eta^1\text{-abtc}$ shows a disorder in the aromatic part as well, probably to the higher level of freedom in movement due to the monodentates carboxylates compared to the fully bidentates. In the monodentate carboxylate branch the bond distances carbon-oxygen between the coordinated and non-coordinated oxygen differs. The C-O7 distance is 1.25(1) Å, where the one of carbon with the non-coordinated oxygen is 1.24(1) Å. Actually, the structure of Th-abtc-2 did not reveal any additional organic linkers as we might expect with the addition

of formic acid or benzoic acid in the reaction medium and is built up from the association of thorium with abtc ligands only. However, the structures of **Th-abtc-1** and **Th-abtc-2** have things in common, as the carboxylate-bridged thorium atoms. Nonetheless, in **Th-abtc-1** there was additional one bridging benzoate (modulator) between thorium atoms, whereas in **Th-abtc-2** there are two bridging azobenzenecarboxylates (main ligand).

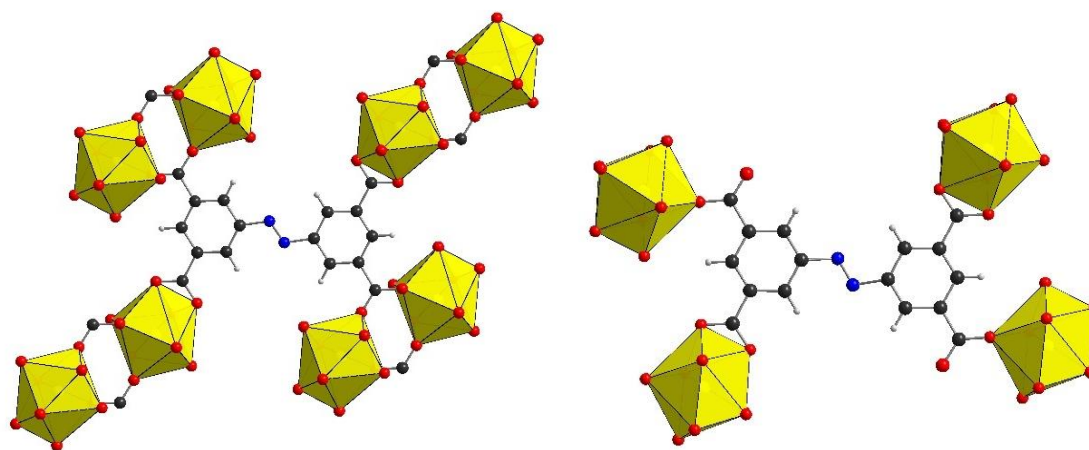


Figure IV-45. Bridging and bidentate carboxylates in **Th-abtc-2** (left) and monodentate (right) (color code: thorium: yellow; oxygen: red; carbon: black; nitrogen: blue; hydrogen: grey).

IV. 2.3.3. Characterization of **Th-abtc-2** by infrared and thermogravimetric analysis

Th-abtc-2-(form) and **Th-abtc-2-(bz)** was characterized by infrared spectroscopy and thermogravimetric analysis and the **Th-abtc-2-(form)** was also characterized by thermodiffraction. No significant differences were observed between the two samples by infrared spectroscopy, so only the characterization of **Th-abtc-2-(form)** will be presented here.

The infrared spectroscopy in Figure IV-46 shows weak bands at 3060 cm^{-1} and 2930 cm^{-1} that are assigned to the aromatic vibration $\nu(\text{C}=\text{H})$. The band at 1650 cm^{-1} and another one at 1103 cm^{-1} that correspond to a $\nu(\text{C}=\text{O})$ and a $\nu(\text{C}-\text{N})$ vibration respectively. These bands confirm the presence of coordinated DMF in **Th-abtc-2**, as they are characteristic for DMF molecules.^[17] The bands at 1600 cm^{-1} and at 1541 cm^{-1} correspond to the asymmetric and symmetric vibration $\nu(\text{COO})$ of the coordinated carboxylic acids. The vibration between aromatic carbons $\nu(\text{C}=\text{C})$ can be found at 1368 cm^{-1} and the torsion of OH and CH at 781 cm^{-1} .

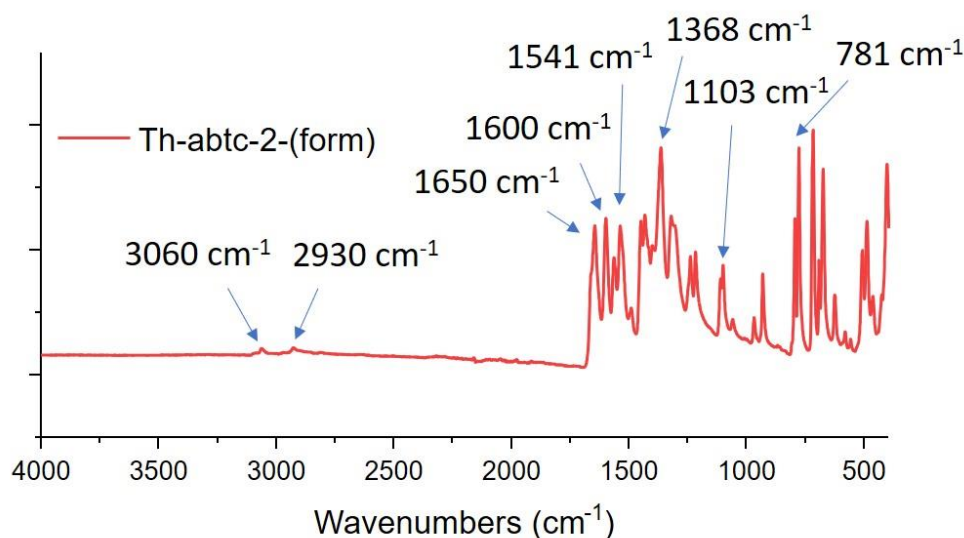


Figure IV-46. Infrared spectra of **Th-abtc-2-(form)** (red line).

The thermogravimetric analysis (TGA) of **Th-abtc-2-(bz)** and **Th-abtc-2-(form)** ($[\text{Th}_2(\text{abtc})(\eta^1\eta^1\text{-abtc})(\text{DMF})_4]$) has a main weight loss occurring at $\approx 400^\circ\text{C}$, which corresponds to the azobenzenetetracarboxylate ligand evacuation and the collapse of the framework to form ThO_2 . If we assume that this residue of 36.2 % corresponds to ThO_2 , then the experimental loss of 47.8 % and 49.2 % (calc.: 49.1 %) corresponds to the loss of 0.97 and 1.00 ligands accordingly and is in accordance with the structure of the **Th-abtc-2** that contains one organic linker for each thorium. The percentage missing can be due to defects in the structure by the addition of a modulator. By the weight loss in the thermogravimetric curve in Figure IV-47, we result that benzoic acid creates more defects in the structure than formic acid. There are also two coordinated DMF molecules for each thorium in the structure, that correspond to a theoretical loss of 20.0 %. Thus, the loss at 200°C , there is a two-step loss of 22.7 % and 17.7 % accordingly that corresponds to the loss of coordinated DMF (Figure IV-47, left).

According to the X-ray thermodiffractogram (Figure IV-47, right), the generation of the thorium oxide starts after 360°C , which is relatively in accordance with the TG analysis. As for the stability of the framework, it seems to be intact up to 180°C . Between 180 and 360°C , another weak diffracting phase is appeared, probably related to the removal of DMF (according to TGA). After $\approx 360^\circ\text{C}$, we see the collapse of the crystallinity of the framework to form thorium oxide.

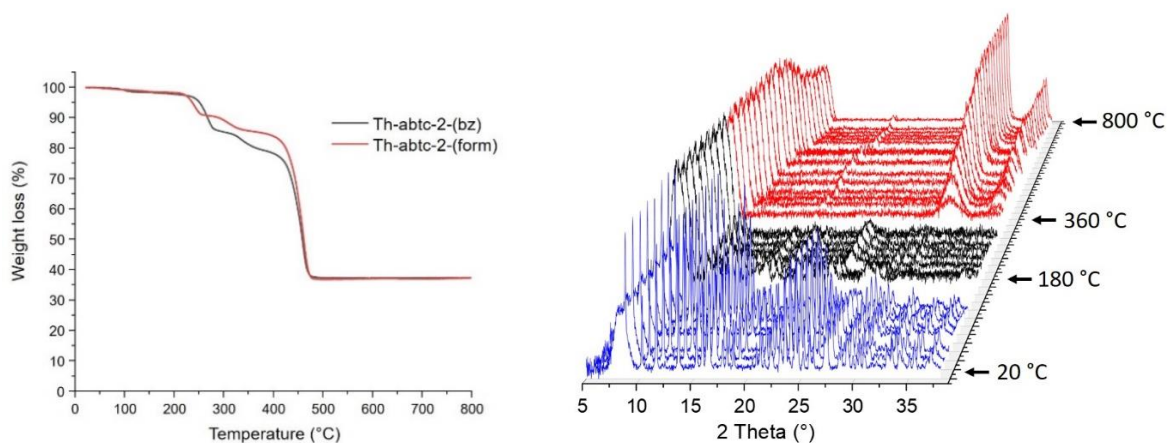


Figure IV-47. Thermogravimetric curves for **Th-abtc-2-(bz)** and **Th-abtc-2-(form)** (left) and X-ray thermodiffractogram for **Th-abtc-2-(form)** (right). X-ray source; Copper $K\alpha$ radiation; c ($\lambda_{CuK\alpha}=1.5406 \text{ \AA}$).

IV. 2.3.4. Gas sorption experiments and enthalpies of adsorption for **Th-abtc-2**

The structure of **Th-abtc-2** revealed a structure, potentially porous, and so gas sorption experiments were performed. According to its thermal stability, **Th-abtc-2** activated first at 120 °C, where no nitrogen sorption so BET surface area could not be measured. However, based on the kinetic diameter of gases, carbon dioxide has a smaller radius than nitrogen (3.30 Å instead of 3.64 Å in nitrogen, Table IV-6 in paragraph 1.7.4) and therefore CO₂ sorption was tested, without success. Then, **Th-abtc-2** was activated under secondary pump at 120 °C after pre-activation and washing steps that are provided in details in Table A1 in Appendix. Following this activation route, the Th-abtc-2 compound was able to adsorb CO₂, indicating that the DMF could be evacuated in order release enough porosity for its significant uptake (up to 17.7 cm³.g⁻¹ of CO₂ at 760 mmHg).

Carbon dioxide adsorption isotherm curves at three temperatures and the values of enthalpies depending on the amount of carbon dioxide adsorbed are shown in Figure IV-48. The values of enthalpies are higher than -60 kJ·mol⁻¹ and that indicates interactions between the surface of the pores and the carbon dioxide molecules.

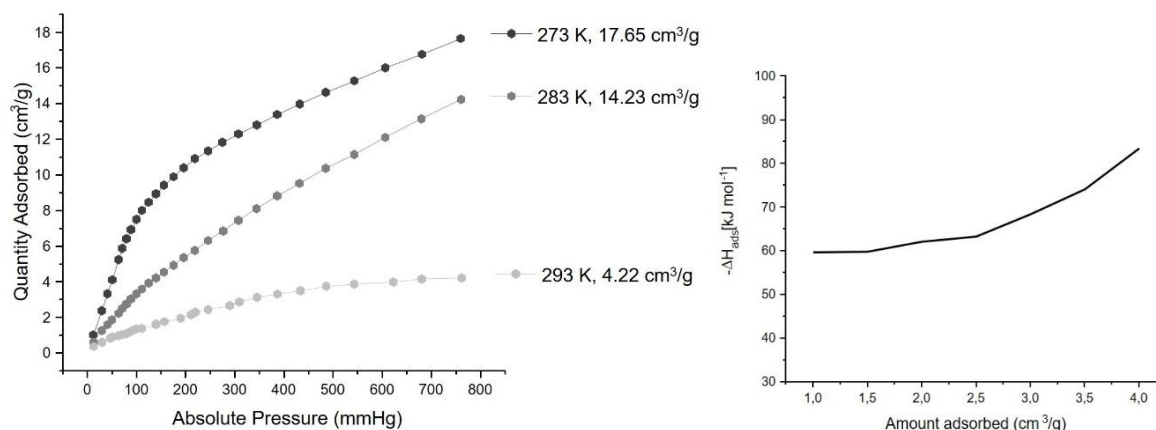


Figure IV-48. Isotherms of carbon dioxide adsorption for **Th-abtc-2(form)** at three different temperatures (top) and values of enthalpy depending on the volume of carbon dioxide adsorbed (bottom).

By comparing the results of carbon dioxide sorption into the three out the four phases presented in this chapter we will see that for **Th-abdc-1**, CO₂ uptake is more significant and that is due to its bigger pores (Table IV-16). The pores of **Th-abdc-2** may be bigger than **Th-abtc-2**, but the CO₂ uptake is lower. This can be explained by the values of enthalpies of adsorption. **Th-abtc-2** shows a higher value of enthalpy, which means there exist stronger interactions with CO₂ than **Th-abdc-2**.

Table IV-16. Pore size diameters, CO₂ uptake values (at 760 mmHg) and average enthalpies of adsorption for **Th-abdc-1**, **Th-abdc-2** and **Th-abtc-2**.

Compound	Pore size (Å)	CO ₂ sorption at 273K (cm ³ .g ⁻¹)	Average enthalpy (kJ.mol ⁻¹)
Th-abdc-1	14 and 18	40.30	-48
Th-abdc-2	11	10.40	-10
Th-abtc-2	3.8	17.65	-70

IV. 3 Conclusions

The richness of thorium's chemistry and reactivity is strongly demonstrated in this chapter. In total, four coordination network complexes were isolated, two with the azobenzene-derivatives dicarboxylic acid and two with the azobenzene-derivatives tetracarboxylic acid. One of them is an analogue of the well-known UiO family of MOFs. By small changes in the reaction conditions, different phases can be isolated. The type of modulator seems to play important role in the synthesis. For the phases with dicarboxylate, the use of naphthoic acid and formic acid results in the isolation of a 3D-framework of **Th-abdc-1**, whereas 2-fluorobenzoic acid is coordinated with Th(IV) and partially replace the main dicarboxylate ligands to form a 2D-network. For the phases with tetracarboxylate, benzoic acid helps in the crystallization of a 3D-network that is not stable and contains benzoic acids

in the pores, whereas when formic acid is used, another 3D-network is formed, more stable, where CO₂ uptake is possible. The same phase (**Th-abtc-2**) can be synthesized with benzoic acid, but when heating up at 170 °C. That can be explained, as by heating up we force the decomposition of DMF (organic solvent) to form formic acid and methylamine. This formic acid is then used as a modulator over benzoic acid, to isolate the more stable **Th-abtc-2** phase.

With the use of azobenzenedicarboxylate we observe that when we use the reported conditions in the literature to isolate the Zr-UiO-azo^[8], we obtain the thorium(IV) analogue (**Th-abdc-1**), for which a high BET specific surface area is observed compared to another similar structures (Table IV-17).

Table IV-17. Comparison of BET specific surface areas between similar well-known actinide MOFs

MOF	BET specific surface area
Th-UiO-67_NH ₂	1196 m ² /g
Np-UiO-67*	791 m ² /g
Th-UiO-66 ^[36]	730 m ² /g

*the measurement was performed with the thorium analogue.

However, by using another modulator (2-fluorobenzoic acid), the crystal structure changes dramatically (**Th-abdc-2**). In this new structure, the monocarboxylate modulators (fluorobenzoates) replace partially the azobenzenedicarboxylates. In that way, the number of connections between two hexameric thorium(IV) clusters decrease and with it, the dimensionality as well. The final structure of **Th-abdc-2** is a layered compound where each layer builds up triangular windows, where uptake of carbon dioxide is possible.

With the use of azobenzenetetracarboxylate, some MOFs have been synthesized with divalent metals like Co(II), Zn(II), Mn(II) and Cd(II).^[7] Only in the zinc compound, the abtc⁴⁻ ligands have two non-coordinated carbonyl function, like in **Th-abtc-1** and **Th-abtc-2** presented in this work. Except of this similarity the rest of the structures are quite different, as the zinc compound forms a paddlewheel-shaped inorganic building unit and in **Th-abtc-1,2** the SBU consists of two monomeric units bridged by azobenzenetetracarboxylates.

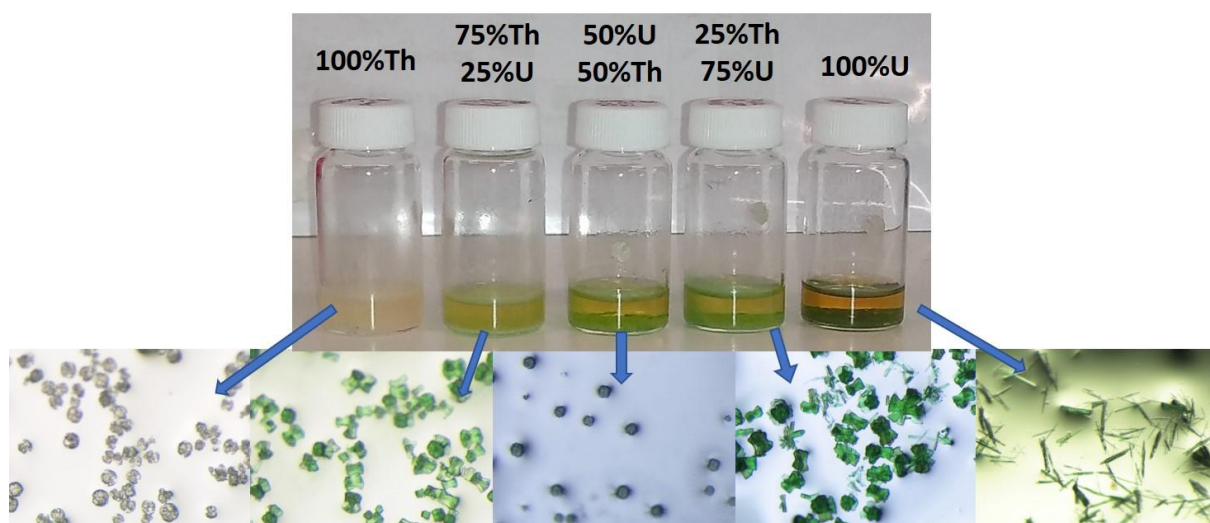
IV. 4 References

- [1] Z. Wang, K. Müller, M. Valášek, S. Grosjean, S. Bräse, C. Wöll, M. Mayor, L. Heinke, *J. Phys. Chem. C* **2018**, *122*, 19044–19050.
- [2] J. L. Zhuang, K. Lommel, D. Ceglarek, I. Andrusenko, U. Kolb, S. Maracke, U. Sazama, M. Fröba, A. Terfort, *Chem. Mater.* **2011**, *23*, 5366–5374.
- [3] R. Mogale, K. G. Akpomie, J. Conradie, E. H. G. Langner, *J. Environ. Manage.* **2022**, *304*, 114166.
- [4] H. Wang, X. Dong, V. Colombo, Q. Wang, Y. Liu, W. Liu, X.-L. Wang, X.-Y. Huang, D. M. Proserpio, A. Sironi, Y. Han, J. Li, H. Wang, Q. N. Wang, Y. Y. Liu, J. Li, W. Liu, X. L. Dong, Y. Han, V. Colombo, D. M. Proserpio, A. Sironi, X. Wang, X. Huang, *Adv. Mater.* **2018**, *30*, 1805088.
- [5] T. Chuusaard, S. Thammakan, N. Semakul, T. Konno, A. Rujiwatra, *J. Mol. Struct.* **2022**, *1251*, 131940.
- [6] B. Fernández, J. M. Seco, J. Cepeda, A. J. Calahorra, A. Rodríguez-Diéguez, *CrystEngComm* **2015**, *17*, 7636–7645.
- [7] S. Zhang, J. Ma, X. Zhang, E. Duan, P. Cheng, *Inorg. Chem.* **2015**, *54*, 586–595.
- [8] W. Y. Gao, T. Thiounn, L. Wojtas, Y. S. Chen, S. Ma, *Sci. China Chem.* **2016**, *59*, 980–983.
- [9] J. Li, I. Cvrtila, M. Colomb-Delsuc, E. Otten, S. Otto, *Chem. - A Eur. J.* **2014**, *20*, 15709–15714.
- [10] F. E. Chen, T. A. Pitt, D. J. Okong’o, L. G. Wetherbee, J. J. Fuentes-Rivera, P. J. Milner, *Chem. Mater.* **2022**, *34*, 3383–3394.
- [11] D. Bara, C. Wilson, M. Mörtel, M. M. Khusniyarov, S. Ling, B. Slater, S. Sproules, R. S. Forgan, *J. Am. Chem. Soc.* **2020**, *141*, 8346–8357.
- [12] W. Morris, S. Wang, D. Cho, E. Auyeung, P. Li, O. K. Farha, C. A. Mirkin, *ACS Appl. Mater. Interfaces* **2017**, *9*, 33413–33418.
- [13] C. L. Hobday, R. J. Marshall, C. F. Murphie, J. Sotelo, T. Richards, D. R. Allan, T. Düren, F. X. Coudert, R. S. Forgan, C. A. Morrison, S. A. Moggach, T. D. Bennett, *Angew. Chemie - Int. Ed.* **2016**, *55*, 2401–2405.
- [14] A. Schaate, S. Dühnen, G. Platz, S. Lilienthal, A. M. Schneider, P. Behrens, *Eur. J. Inorg. Chem.* **2012**, *2012*, 790–796.
- [15] J. H. Cavka, S. Jakobsen, U. Olsbye, N. Guillou, C. Lamberti, S. Bordiga, K. P. Lillerud, *J. Am. Chem. Soc.* **2008**, *130*, 13850–13851.
- [16] C. Falaise, J. S. Charles, C. Volkringer, T. Loiseau, *Inorg. Chem.* **2015**, *54*, 2235–2242.
- [17] G. Durgaprasad, D. N. Sathyanarayana, C. C. Patel, *Bull. Chem. Soc. Jpn.* **2006**, *44*, 316–322.
- [18] Z. J. Li, S. Guo, H. Lu, Y. Xu, Z. Yue, L. Weng, X. Guo, J. Lin, J. Q. Wang, *Inorg. Chem. Front.* **2019**, *7*, 260–269.
- [19] S. J. Lee, T. U. Yoon, A. R. Kim, S. Y. Kim, K. H. Cho, Y. K. Hwang, J. W. Yeon, Y. S. Bae, *J. Hazard. Mater.* **2016**, *320*, 513–520.
- [20] A. Abramova, N. Couzon, M. Leloire, P. Nerisson, L. Cantrel, S. Royer, T. Loiseau, C. Volkringer, J. Dhainaut, *ACS Appl. Mater. Interfaces* **2022**, *14*, 10669–10680.
- [21] Y. S. Bae, B. G. Hauser, Y. J. Colón, J. T. Hupp, O. K. Farha, R. Q. Snurr, *Microporous Mesoporous Mater.* **2013**, *169*, 176–179.
- [22] A. Nuhnen, C. Janiak, *Dalt. Trans.* **2020**, *49*, 10295–10307.
- [23] Y. Wang, W. Liu, Z. Bai, T. Zheng, M. A. Silver, Y. Li, Y. Wang, X. Wang, J. Diwu, Z. Chai, S. Wang, *Angew. Chemie - Int. Ed.* **2018**, *57*, 5783–5787.

- [24] M. A. Moreira, R. O. M. Dias, U. H. Lee, J. S. Chang, A. M. Ribeiro, A. F. P. Ferreira, A. E. Rodrigues, *J. Chem. Eng. Data* **2019**, *64*, 4724–4732.
- [25] D. P. Halter, R. A. Klein, M. A. Boreen, B. A. Trump, C. M. Brown, J. R. Long, *Chem. Sci.* **2020**, *11*, 6709–6716.
- [26] S. Peters, S. Renjith Pillai, E. Varathan, *Mater. Today Proc.* **2022**, *68*, 35–42.
- [27] A. M. Hastings, D. Ray, W. Jeong, L. Gagliardi, O. K. Farha, A. E. Hixon, *J. Am. Chem. Soc.* **2020**, *142*, 9363–9371.
- [28] M. A. Neumann, *J. Appl. Crystallogr.* **2003**, *36*, 356–365.
- [29] G. S. Pawley, *IUCr, urn:issn:0021-8898* **1981**, *14*, 357–361.
- [30] A. Altomare, C. Cuocci, C. Giacovazzo, A. Moliterni, R. Rizzi, N. Corriero, A. Falcicchio, *J. Appl. Crystallogr.* **2013**, *46*, 1231–1235.
- [31] R. Černý, V. Favre-Nicolin, J. Rohlíček, M. Hušák, *Cryst. 2017, Vol. 7, Page 322* **2017**, *7*, 322.
- [32] W. B. Jennings, B. M. Farrell, J. F. Malone, *Accounts Chem. Res. Res.* **2001**, *34*, 885–894.
- [33] S. E. Kentish, C. A. Scholes, G. W. Stevens, *Recent Patents Chem. Engeneering* **2008**, *1*, 52–66.
- [34] A. D. Wiersum, E. Soubeyrand-Lenoir, Q. Yang, B. Moulin, V. Guillerm, M. Ben Yahia, S. Bourrelly, A. Vimont, S. Miller, C. Vagner, M. Daturi, G. Clet, C. Serre, G. Maurin, P. L. Llewellyn, *Chem. – An Asian J.* **2011**, *6*, 3270–3280.
- [35] N. E. Brese, M. O’Keeffe, *IUCr, Acta Crystallogr. Sect. B* **1991**, *47*, 192–197.
- [36] C. Falaise, J. S. Charles, C. Volkringer, T. Loiseau, *Inorg. Chem.* **2015**, *54*, 2235–2242.

Chapter V

Elaboration of mixed thorium(IV)/uranium(IV) carboxylate compounds



This chapter describes the formation of different mixed U(IV)-Th(IV) polyoxo-hydroxo clusters and coordination polymers. Three different systems have been investigated: the already reported metal-organic framework UiO-67-NH₂ and two new chemical systems. One is based on the hexameric [An(IV)₆O₈] core stabilized by anthracene-9-carboxylate ligands and another one is characterized by an infinite 3D coordination network by means of fumarate linkers. These pure (Th or U) and the mixed (Th + U) compounds were characterized and primarily tested for the production of mixed oxides that can be potential new generation fuels for nuclear reactors.

CHAPTER V - Mixed U(IV)/Th(IV) compounds to produce mixed oxides

Many compounds of tetravalent thorium and uranium carboxylates have been reported so far, as they were detailed summarized in Chapter I (Paragraph I.4). The first studies to produce mixed actinide compounds were done with oxalates in order to synthesize mixed oxides for a potential future use as nuclear combustibles. Lately (2017), there is one study of the group of N. Shustova, who showed an incorporation of U(IV) into a Th(IV) UiO-n like framework ($\text{Th}_{5.65}\text{U}_{0.35}\text{-Me}_2\text{BPDC-8}$).^[1] In that study, the selected approach is a post synthetic goal. Even though they achieved this cation exchange, it remains a process where the final amount of the two cations in the framework is not predictable, because the amount inserted is not controlled. In this part, we aim to generate mixed Th/U coordination complexes/polymers by using a synthetic route based on the direct mixture of Th and U starting precursors and investigate the state of the final product as a potential solid-solution system of $\text{Th}_{1-x}\text{U}_x$ type. The further fate of this type of samples could be their behavior under thermal treatment to produce mixed (Th,U) oxides powders of fluorite-like structure, which would be then further studied for the sintering properties.

In this chapter, the controlled formation of mixed U(IV)/Th(IV) carboxylates, through a prior one pot synthesis, is studied (Figure V-1).

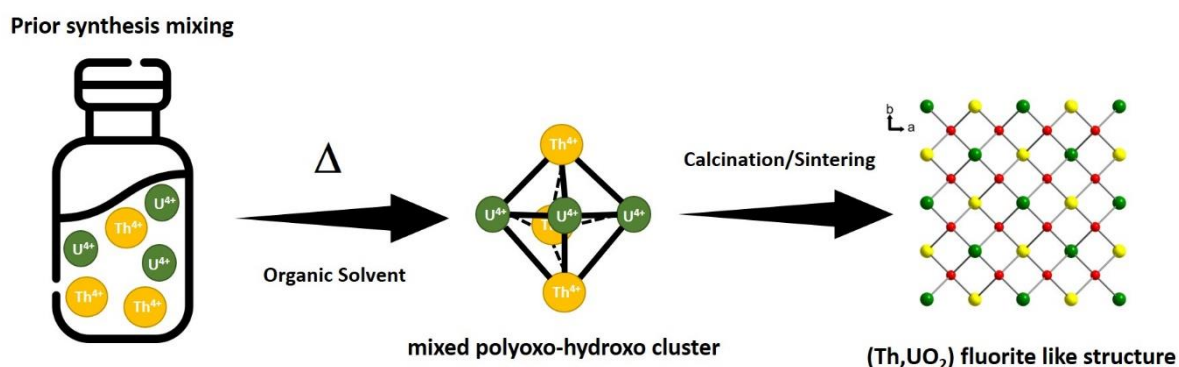


Figure V-1. Scheme of the synthetic strategy to obtain mixed Th/U compounds.

It is important to control the percentage of the final composition in order to synthesize a compound with a desirable ratio Th/U. The first step of our approach involves the isolation of each phase as pure uranium or thorium compound, characterized (if possible) by single-crystal X-ray diffraction. Since the synthesis of each pure phase is possible, the same synthesis is repeated but using a mixture of uranium and thorium chloride salts were added in the synthesis feed. For a compound that contains $\text{Th}_{1-x}\text{U}_x$, three different intermediate

compositions of reagents were tested in this work, $\text{Th}_{0.75}\text{U}_{0.25}$, $\text{Th}_{0.5}\text{U}_{0.5}$ and $\text{Th}_{0.25}\text{U}_{0.75}$. The composition after the precipitation of the mixed actinide carboxylates is studied with Energy-dispersive X-ray spectroscopy (EDX). Each material was also characterized by powder X-ray diffraction analysis and thermogravimetric analysis.

Three different actinide carboxylates were tested: a molecular hexameric cluster stabilized by anthracene-9-carboxylate (synthesized during the different modulator tests in Chapter IV), a well-known MOF (UiO-67-NH_2) obtained from a derived 4,4'-biphenyldicarboxylate ligand, and a new coordination polymer linked with fumarate species. This strategy aims to generate mixed actinide coordination polymers/polyoxo clusters as mixed actinide Th/U precursors used as potential nuclear combustibles. The organic ligands used in this chapter are summarized in Figure V-2.

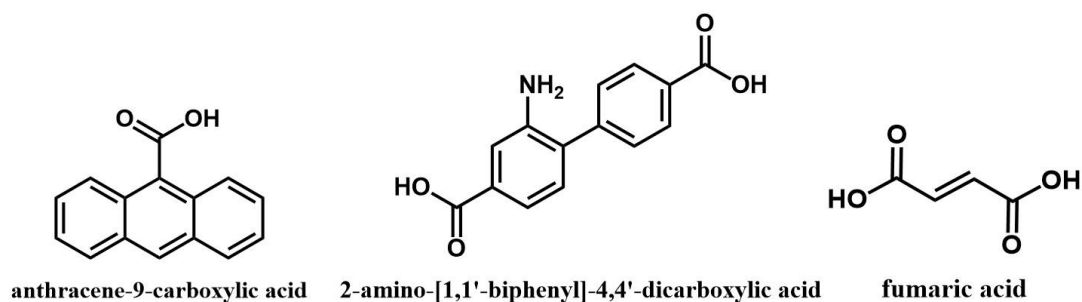


Figure V-2. The three main organic ligands used in this chapter for the three different series of mixed compounds.

V.1 Th(IV)/U(IV) hexameric cluster stabilized by anthracene-9-carboxylic acid

V. 1.1 Synthesis of actinide(IV) chloride precursors

About the experimental part of this chapter, all handlings before the thermal treatment, have been done in an inert atmosphere (Argon) in a glove box in order to avoid the oxidation of U^{4+} into U^{6+} . The source of tetravalent uranium is uranium tetrachloride (UCl_4) which has been synthesized from the reaction of UO_3 oxide with hexachloropropene, using a Schlenk line, under vacuum/argon.^[2]

Uranium tetrachloride (UCl_4) was prepared from a mixture of 5 g UO_3 (17.5 mmol) with 20 mL hexachloropropene (141 mmol) under inert atmosphere. The mixture was heated up slowly until an exothermic reaction ($\approx 180^\circ\text{C}$). This last step provokes the production of $\text{Cl}_2(\text{g})$ and the color change in the solution. The heating lasts around 4 hours and after cooling down

a green powdered well-crystalline solid (UCl_4) is isolated and washed with dichloromethane (≈ 40 mL).

Thorium tetrachloride tetrahydrate ($\text{ThCl}_4 \cdot 4\text{H}_2\text{O}$) was prepared by a solution of 5 g (10.4 mmol) thorium nitrate tetrahydrate ($\text{Th}(\text{NO}_3)_4 \cdot 4\text{H}_2\text{O}$) into 25 mL (81.7 mol) 37 % hydrochloric acid (HCl). The solution was refluxed, leading to the production of NO_x gases. The reflux is maintained until all NO_x gases leave the solution (≈ 6 hours). After the solution is cooled down, it is concentrated at room temperature to crystallize into $\text{ThCl}_4 \cdot 4\text{H}_2\text{O}$.

V. 1.2 Synthesis of the actinide(IV) anthracene-9-carboxylate : $\text{Th}_{6-x}\text{U}_x\text{-anth}$

The phase $\text{Th}_{6-x}\text{U}_x\text{-anth}$ is prepared in DMF with a specific amount of O-free water, which is a synthesis protocol usually followed in our group in order to generate the hexameric cluster $[\text{M}_6\text{O}_8]$.^[3] The pure uranium and thorium clusters were synthesized among the three different mixed ones. In order to simplify things, the compound's formula will be marked as $\text{Th}_{6-x}\text{U}_x\text{-anth}$, where x ranging from 0 to 6, and the same logic will be used for the other materials in this chapter. All synthesis protocols are summarized in Table V-1.

Table V-1. Synthesis protocols of $\text{Th}_{6-x}\text{U}_x\text{-anth}$.

Metal source		Ligand	Solvent		T	Time	Yield
$\text{ThCl}_4 \cdot 4\text{H}_2\text{O}$ 10.2 mg 23 μmol		9-Anthroic acid 195 mg 0.877 mmol	DMF 1 mL 13 mmol	H_2O 30 μL 0.82 mmol	100 °C	36 h	25%
$\text{ThCl}_4 \cdot 4\text{H}_2\text{O}$ 7.7 mg 17.3 μmol	UCl_4 2.4 mg 5.75 μmol	9-Anthroic acid 195 mg 0.877 mmol	DMF 1 mL 13 mmol	H_2O 30 μL 0.82 mmol	100 °C	36 h	27%
$\text{ThCl}_4 \cdot 4\text{H}_2\text{O}$ 5.1 mg 11.5 μmol	UCl_4 4.9 mg 13 μmol	9-Anthroic acid 195 mg 0.877 mmol	DMF 1 mL 13 mmol	H_2O 30 μL 0.82 mmol	100 °C	36 h	27%
$\text{ThCl}_4 \cdot 4\text{H}_2\text{O}$ 2.5 mg 5.75 μmol	UCl_4 7.4 mg 19.5 μmol	9-Anthroic acid 195 mg 0.877 mmol	DMF 1 mL 13 mmol	H_2O 30 μL 0.82 mmol	100 °C	36 h	28%
UCl_4 9.8 mg 26 μmol		9-Anthroic acid 195 mg 0.877 mmol	DMF 1 mL 13 mmol	H_2O 30 μL 0.82 mmol	100 °C	36 h	26%

After solvothermal treatment at 100°C of the five above synthetical protocols, plate-like crystals of 90-100 μm , with different colors based on their inorganic composition, appeared on the bottom of the 2 mL glass vial reactor (Figure V-3, top). Crystals of pure **Th₆-anth U₆-anth** compounds are transparent and the more uranium is added in the reaction mixture, the greener they crystals get. Optical microscopy revealed better the elongated plate-like shape and the size (100-150 μm) of the crystals (Figure V-3 bottom). This phase is stable under air for several months, even the pure uranium **U₆-anth** phase. As anthracenoates is a bulky and hydrophobic ligand, we may assume that it protects uranium(IV) sites from hydrolysis and oxidation.

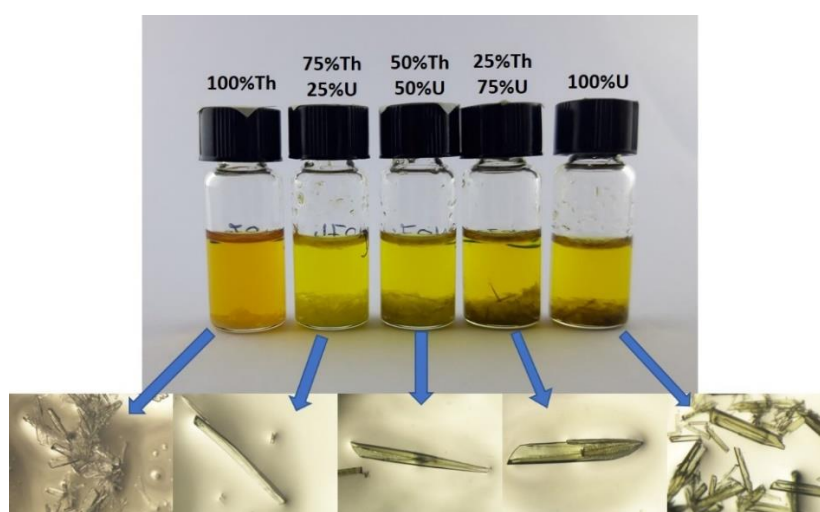


Figure V-3. Photograph of the 2 mL glass vial reactors after thermal treatment (top); Optical microscope images for the **Th_{6-x}U_x-anth** (bottom). The values represent the molar percentages related to the amounts of actinide salt precursors that were put in the feed.

V. 1.3 Structural description of **Th₆-anth**

The determination of the structure was obtained from the selection of crystals of pure thorium and pure uranium samples. Bragg intensities were collected under single crystal X-ray diffraction in a Bruker APEX DUO diffractometer of the lab ($\lambda_{\text{MoK}\alpha}=0.71 \text{ \AA}$) and the crystallographic data are presented in Table V-2. For the rest of the mixed samples this type of characterization was not performed, as thorium and uranium have a slight difference of two in their atomic numbers (90 and 92) and are hardly distinguished by single crystal X-ray diffraction technique. To overcome this difficulty, powder X-ray diffraction diagrams with a long exposure (3 s / 0.02° (2θ) step) were collected and indexed, in order to determine the cell parameters for all three materials with the intermediate compositions **Th_{6-x}U_x**.

Table V-2. Crystal data and structure refinements for *Th₆-anth*.

Th₆-anth	
Formula	C _{196.5} H ₁₃₆ N ₆ O ₃₉ Th ₆
Formula weight	4518.58
Temperature/K	100
Crystal type	plates
Crystal size/mm³	0.463 × 0.23 × 0.148
Crystal system	monoclinic
Space group	C2/c
a/Å	32.983(5)
b/Å	16.540(2)
c/Å	31.819(4)
α/°	90
β/°	101.338(6)
γ/°	90
Volume/Å³	17019(4)
Z, ρ_{calculated}/g.cm⁻³	4 / 1.764
μ/mm⁻¹	5.304
2θ range/°	2.518-52.8
Limiting indices	-35 ≤ h ≤ 41 -20 ≤ k ≤ 19 -39 ≤ l ≤ 39
Collected reflections	152387
Unique reflections	17409 [R _{int} = 0.0467]
Parameters	1114
Goodness-of-fit on F²	1.064
Final R indices [I > 2σ(I)]	R ₁ = 0.0409 wR ₂ = 0.0989
R indices (all data)	R ₁ = 0.0627 wR ₂ = 0.1093
Largest diff. peak and hole/e.Å⁻³	2.57 and -3.79

[Th₆O₄(OH)₄(anth)₁₂(DMF)₆]·DMF (**Th₆-anth**) crystallizes in monoclinic C2/c and exhibits a structure with four crystallographically unique thorium centers. Two of them (Th2, Th4) are at 100% occupancy (Wyckoff position "8f", 1 site only) and two of them (Th1, Th3) being in special positions "4e" (2 sites). In Th₆-anth, thorium is 9-fold coordinated (monocapped square antiprismatic geometry) with nine oxygen atoms: four of them come from four carboxylate oxygens deriving from anthracene ligands (Th-O_{carb} in the range 2.437(6)-2.539(5) Å), four others are μ₃-O or μ₃-OH bridging oxygens (Th-O_{oxo/hydroxo} in the range 2.320(6)-2.461(7) Å). More specifically there are four oxygens with shorter distances (in the range of 2.320(6)-2.344(6) Å) that correspond to μ₃-O and other four with longer ones (in the range of 2.435(7)-2.461(7) Å) that correspond to μ₃-OH. The coordination sphere is completed with a ninth oxygen coming from a terminal DMF molecule (Th-O_{DMF} in the range 2.499(7)-2.728(9) Å). The six thorium nodes are arranged along a slightly distorted octahedral geometry (point group O_h) and this cluster is stabilized by twelve anthracenoate molecules with the formula [Th₆(μ₃-O)₄(μ₃-OH)₄(O₂CC₁₄H₉)₁₂(DMF)₆] (Figure V-4). It results in a molecular assembly of [Th₆(μ₃-O)₄(μ₃-OH)₄(O₂CC₁₄H₉)₁₂(DMF)₆] entities and an additional intercalated free DMF molecule has been revealed from single-crystal analysis. (Figure V-4, right).

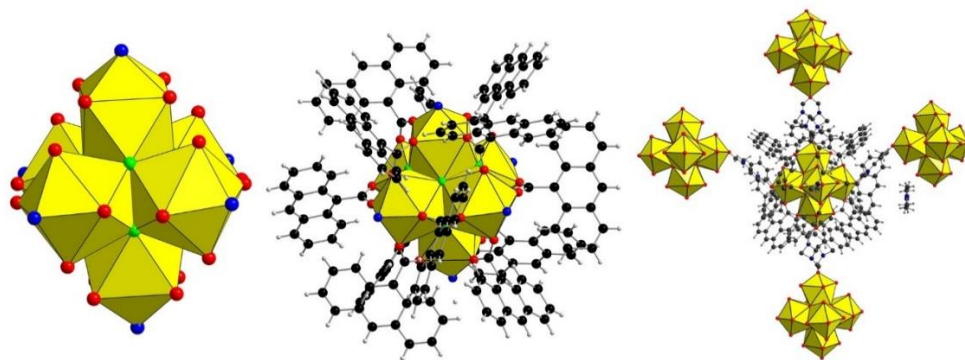


Figure V-4. Crystal structure of the hexameric cluster in **Th₆-anth** (left), the same cluster stabilized by anthracenates (middle) and the intercalated and free DMF molecules (right). Color code: thorium; yellow, O_{DMF} ; blue, O_{carb} ; red, μ_3-O_{oxo} ; green.

V. 1.4 Characterization of the **Th_{6-x}U_x-anth** compounds

The series of **Th_{6-x}U_x-anth** were characterized by powder X-ray diffraction, SEM-EDX analysis and thermogravimetric analysis.

Powder X-ray diffraction patterns show that all samples are pure and isostructural as the experimental as-synthesized patterns are compared with the simulated one from the crystallographic CIF file of **Th₆-anth** (Figure V-5). In the patterns we don't have double peaks for the mixed compounds which could be related to the juxtaposition of two pure **Th₆-anth** and **U₆-anth** forms, and that is a good signature that we observe a homogenous distribution of thorium and uranium as a solid-state solution for the mixed **Th_{6-x}U_x-anth** compounds. This indication will be proved later by SEM-EDX analysis.

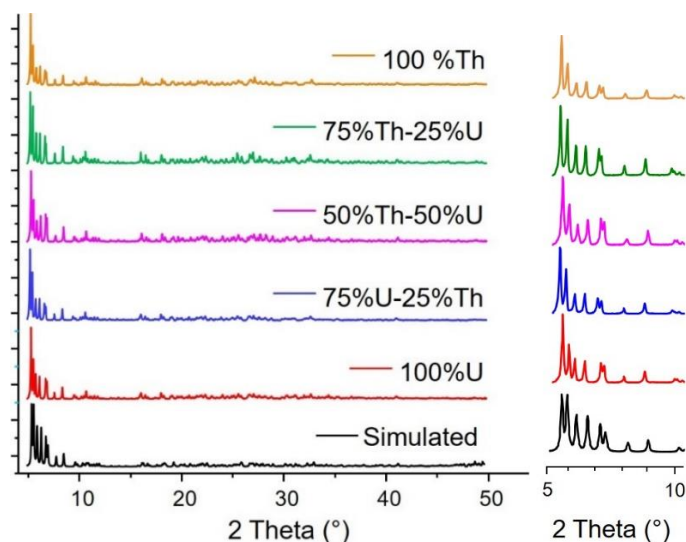


Figure V-5. Powder X-ray diffraction patterns of **Th_{6-x}U_x-anth** compared to the simulated one generated from the .cif file of **Th-anth** (left) and zoom on the patterns from 5 to 10.5 ° in order to observe better the single Bragg peaks for all samples (right). X-ray source; Copper K α radiation; ($\lambda_{CuK\alpha}=1.5406 \text{ \AA}$).

As mentioned before, it is not possible to obtain the crystal structure by single-crystal X-ray diffraction analysis for the mixed compounds, as thorium and uranium are close (^{90}Th , ^{92}U) and they cannot be distinguished. In this case, it is nevertheless interesting to index the powder X-ray diffraction diagrams, in order to extract the cell parameters of each compound for further comparisons and discussions. In the following Table V-3, the cell parameters of all $\text{Th}_{6-x}\text{U}_x\text{-anth}$ compounds have been extracted from le Bail refinement (Jana2006 software) of powder XRD patterns for $\text{Th}_{6-x}\text{U}_x\text{-anth}$ samples (by taking into account the real chemical formula from the starting (Th,U) precursor ratio). The related diagrams can be found in paragraph A3 in Appendix (Figure A2). It is observed, that the more uranium is added, the more the cell parameters decrease, which is logical as uranium(IV) possesses a smaller crystal ionic radius (1.19 Å) than that of thorium(IV) (1.23 Å) (ionic radii given for a 9-fold coordination).^[4]

Table V-3. Extracted cell parameters for $\text{Th}_{6-x}\text{U}_x\text{-anth}$ in the monoclinic system C2/c, from powder XRD patterns.

	a (Å)	b (Å)	c (Å)	β (°)	V (Å ³)
Th₆-anth	33.336(2)	16.434(1)	32.115(2)	101.920(6)	17215.4(1)
Th_{4.5}U_{1.5}-anth	33.254(3)	16.389(1)	32.036(2)	101.378(8)	17097.1(2)
Th₃U₃-anth	33.206(5)	16.347(2)	31.9111(5)	100.95(1)	17053.4(2)
Th_{1.5}U_{4.5}-anth	33.191(6)	16.312(3)	31.769(2)	100.56(1)	17023.4(3)
U₆-anth	33.149(3)	16.305(1)	31.432(3)	100.283(9)	17014.2(2)

For better visualize these changes, graphics with the evolution of the a , b , c , β and V parameters as a function of U content (x), starting from $x = 0$ up to $x = 6$ are presented in Figure V-6. The green line represents the values deriving from the Vegard law:

$$a_{A(1-x)B_x} = (1 - x)a_A + xa_B$$

where for example in the case of $\text{Th}_{0.52}\text{U}_{0.48}\text{O}_2$ the equation becomes

$$a_{\text{Th}_{0.52}\text{U}_{0.48}\text{O}_2} = 0.52a_{\text{ThO}_2} + 0.48a_{\text{UO}_2}$$

Whereas the black points represent the refined cell parameters for each composition according to EDX experiments (see hereafter) and with red line the fitting of these refined parameters. The fitting of these points is represented in black with R^2 values of 0.90 – 0.97. In order to verify if the EDX percentages that will be presented afterwards are trustworthy and close to reality, red points represent the refined cell parameters for each composition

according to the “theoretical” values added in the feed before the thermal treatment. The fitting of these points is presented in red with R^2 values of 0.91 – 0.99. It is a general trend, that the fitting of the red line is slightly better than the black one. From the consideration of the cell parameters measurements, this means that the real (Th,U) compositions are closer to the ones added in the feed, than from what found by the EDX analysis.

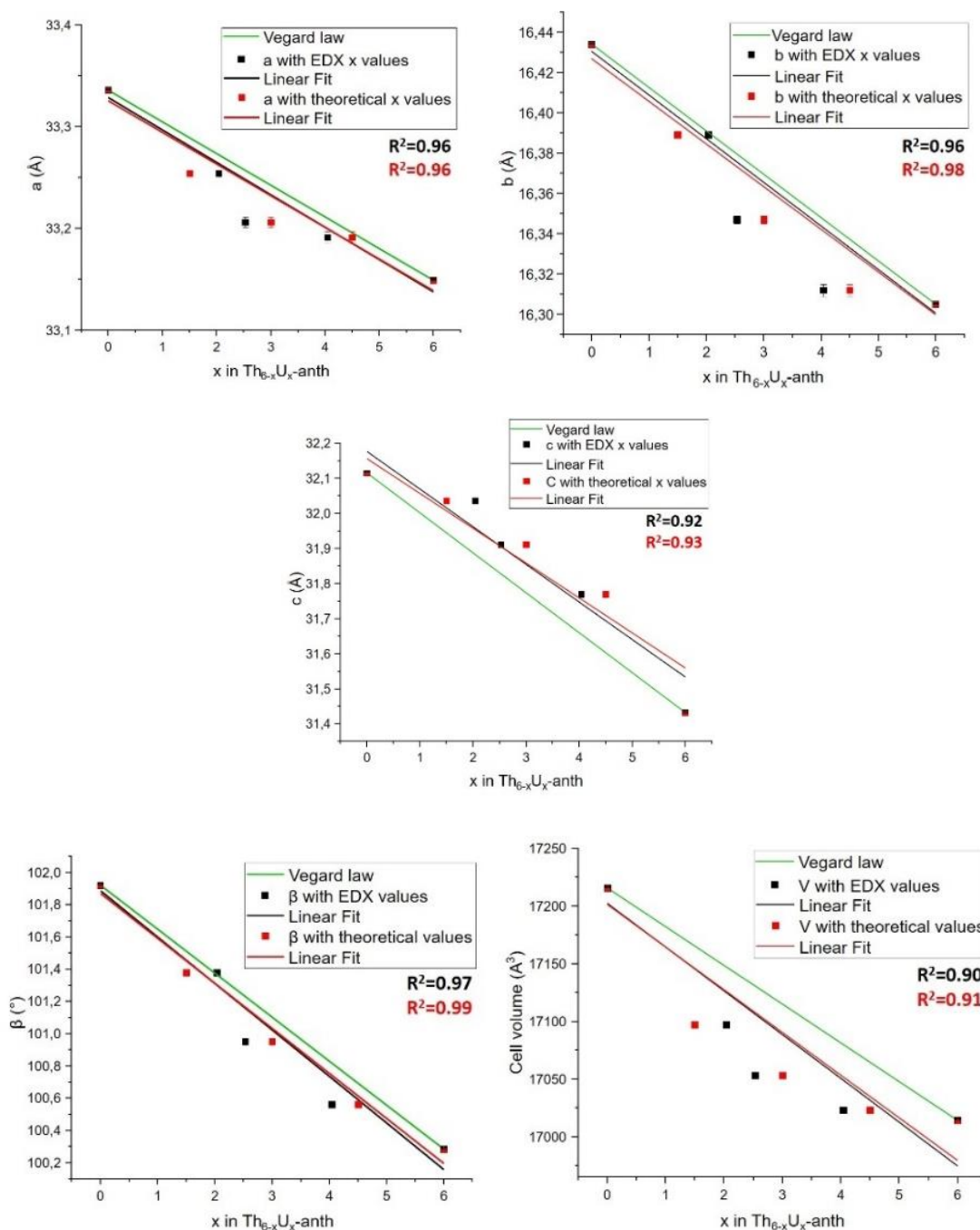


Figure V-6. Evolution of cell parameters a, b, c, β and V with the increasing content x of U in the mixed compounds $Th_{6-x}U_x-anth$. Fitting with the composition value x calculated from EDX experiments (black line). Fitting with the composition x that was put in the feed (red line).

The Th/U composition distribution of the actinides mixing was investigated by EDX (Energy Dispersion X-Ray spectroscopy) analysis including cartography experiments, coupled to a SEM machine. EDX analysis was performed for all the samples and most specifically the mixed ones for different crystals and at different spots in order to analyze the homogeneity of the metallic elements' distribution.

There are three different targeted compositions in the mixed samples with percentages 75% Th – 25 % U, 50 % Th – 50 % U and 25 % Th – 75 % U. Ideally, these metal molar compositions will lead to compounds with the formula **Th_{4.5}U_{1.5}-anth**, **Th₃U₃-anth**, and **Th_{1.5}U_{4.5}-anth** accordingly. Around twenty points in different crystals were tested with EDX analysis, in order to provide a more trustworthy average molar-based percentage for each compound of the series. The average weight-based (wt%) and molar based (at%) percentages with their standard deviations σ , are summarized in Table V-4.

Except of EDX, cartography experiments were conducted for all different samples in order to investigate the homogeneity of the uranium and thorium dispersion in the crystals (Figure V-7). Indeed, the distribution is homogeneous, as green (U) and red (Th) spots are equally distributed in the crystals' surfaces. In Table V-4, it is observed that for **Th_{4.5}U_{1.5}-anth** more uranium is inserted in the structure. However, when uranium gets more concentrated in the solution for **Th₃U₃-anth**, and **Th_{1.5}U_{4.5}-anth**, less uranium than expected is introduced in the structure. This behavior may happen due to the concentration of metals in solution. As a result, thorium and uranium can be located in the crystallites with molar-based percentages that deviate 7-10 % from the ones added in the feed.

Table V-4. Summary of the average of EDX (Th,U) compositions in the series of **Th_{6-x}U_x-anth**.

	Th _{4.5} U _{1.5} -anth 75% Th – 25 % U		Th ₃ U ₃ -anth 50% Th – 50 % U		Th _{1.5} U _{4.5} -anth 25% Th – 75 % U	
		σ		σ		σ
Th^{IV}	65.65 wt %	0.5	57.88 wt %	1.1	32.75 wt %	0.4
Th^{IV}	65.08 at %	0.3	57.25 at %	0.8	32.19 at %	0.4
U^{IV}	34.35 wt %	0.5	42.12 wt %	1.1	67.25 wt %	0.5
U^{IV}	34.92 at %	0.3	42.75 at %	0.8	67.81 at %	0.4
Final formula	Th_{3.96}U_{2.04}anth		Th_{3.47}U_{2.53}anth		Th_{1.96}U_{4.04}anth	

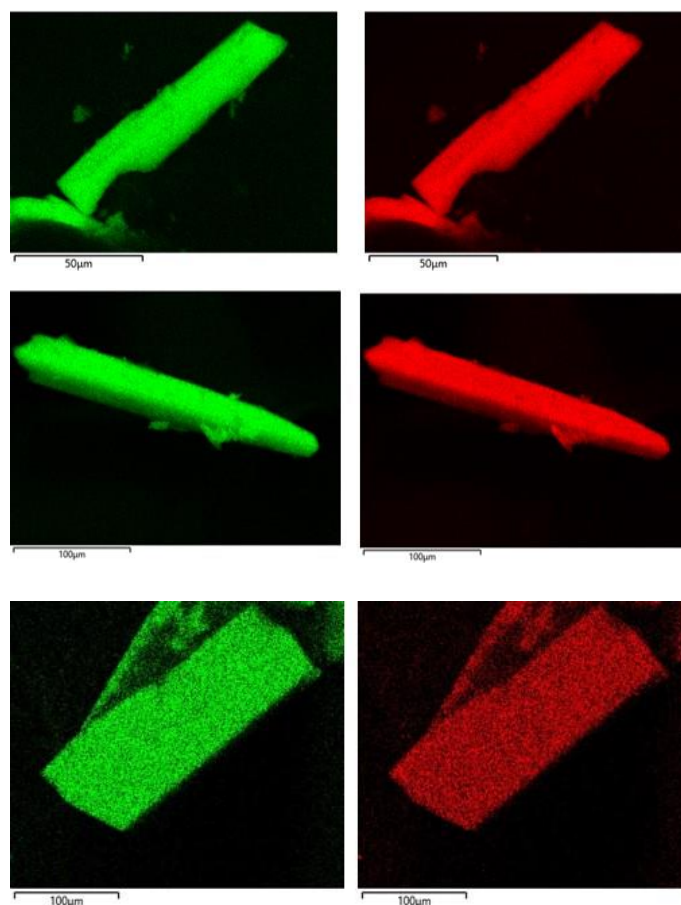
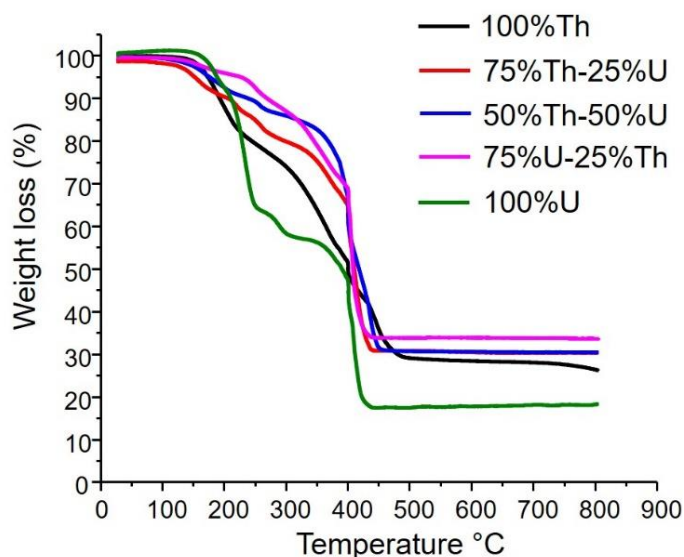


Figure V-7. Cartography of crystals of $\text{Th}_{3.96}\text{U}_{2.04}\text{-anth}$, $\text{Th}_{3.47}\text{U}_{2.53}\text{-anth}$ and $\text{Th}_{1.96}\text{U}_{4.04}\text{-anth}$ for uranium (green) and thorium (red) (from top to bottom), from EDX analysis.

The thermogravimetric analysis (TGA) in Figure V-8 of all five $\text{Th}_{6-x}\text{U}_x\text{-anth}$ samples ($[\text{Th}_6\text{O}_4(\text{OH})_4(\text{anth})_{12}(\text{DMF})_6]\cdot\text{DMF}$) has a main weight loss at $\approx 440^\circ\text{C}$ (from 350 to 450°C), which corresponds to the decomposition of the organic part (anthracenoate) and the formation of ThO_2 and/or UO_2 . For example, in the case of $\text{Th}_{3.96}\text{U}_{2.04}\text{anth}$, we assume that this residue of 30.7 % corresponds to $3.96x(\text{ThO}_2)$ and $2.02x(\text{UO}_2)$, then the experimental loss of 49.3 % (calc.: 51.6 %) at $\approx 400\text{-}440^\circ\text{C}$ corresponds to the loss of 11.5 ligands and is in accordance with the structure of $\text{Th}_{6-x}\text{U}_x\text{-anth}$ that contains 12 ligands for each hexameric cluster. There is another weight loss of 8.1 % (calc.: 8.5 %) at $\approx 250\text{-}300^\circ\text{C}$ that corresponds to the loss of 6 DMF molecules, the ones that are coordinated with thorium. Before 250°C there is a weight loss for each $\text{Th}_{6-x}\text{U}_x\text{-anth}$ that corresponds probably to the loss of free DMF. It is worth noticing that this loss is way more significant in $\text{U}_6\text{-anth}$ (green line in figure V-8), as uranium(IV) is more unstable (TGA is carried out under air atmosphere) than thorium(IV). This early weight loss is decreased with the addition of thorium into the structure and that fact indicates thorium as a potential stabilization factor in this series of molecular clusters.



Compound	1 st weight loss	2 nd weight loss		3 rd weight loss		Formation ThO ₂ /UO ₂ (> 440 ° C)
	(free DMF) (20-200 ° C)	(coordinated DMF) (250-300° C)		(anthracenoate ligands) (400 – 440 ° C)		
	Experimental	Experimental	Calculated	Experimental	Calculated	
Th₆-anth	13.2 %	9.6 %	7.8 %	46.1 %	46.9 %	28.2 %
Th_{3.96}U_{2.04}-anth	8.8 %	10.8 %	8.3 %	48.3 %	50.2 %	30.4 %
Th_{3.47}U_{2.53}-anth	9.4 %	8.1 %	8.5 %	49.3 %	51.6 %	31.1 %
Th_{1.96}U_{4.04}-anth	4.8 %	9.9 %	9.3 %	52.8 %	55.9 %	34.1 %
U₆-anth	32.3 %	6.2 %	4.8 %	32.1 %	29.0 %	17.8 %

Figure V-8. Thermogravimetric curves of Th_{6-x}U_x-anth (under air gas flow, 5 °C.min⁻¹ heating rate) and the calculations of the different weight losses on the table below.

In the first part of Chapter V, the well reported hexameric brick of [M₆O₄(OH)₄] was stabilized by anthracenoate molecules for different mixed compositions, containing thorium and uranium cations. The pure thorium structure was successfully resolved by single-crystal X-ray diffraction, whereas with the pure uranium analogue the quality of the crystals was not really good and the data not enough to resolve in total the crystal structure. For the three samples with mixed compositions, high-resolution powder X-ray diffraction patterns were collected and indexed in order to obtain and compare the cell parameters. It is observed that from Th-anth to U-anth, the more uranium added in the cluster, the smaller the cell parameters. EDX analysis shows a deviation of 10 % in the molar experimental percentages compared to the theoretical ones. A difference that is acceptable but not as precise as expected. Thus, in the next parts of this chapter, two other series of compounds (MOFs) will be tested in order to evaluate the efficiency of the same procedure. As for the future of these

compounds, they will be sent to the CEA Marcoule in order to be sintered and studied under thermal treatment to produced mixed Th,U oxides.

V.2 Study of the (Th, U) composition in the $\text{Th}_{6-x}\text{U}_x\text{-UiO-67_NH}_2$ series

V. 2.1 Synthesis of $\text{Th}_{6-x}\text{U}_x\text{-UiO-67_NH}_2$

The phase of $\text{Th}_{6-x}\text{U}_x\text{-UiO-67_NH}_2$ is prepared in DMF by means of amino-derivative 4,4-biphenyldicarboxylic acid as (noted $H_2\text{bpdc-NH}_2$) organic linker, with the addition of a calculated amount of water, according to the literature.^[5] The pure uranium and thorium compounds were synthesized among the three different mixed ones. All synthesis protocols are summarized in Table V-5; the different chemical reactants, including the use of a modulator (benzoic acid = $H\text{bza}$) were replaced in a closed glass vial (2 mL) and then heated in an oven at 130°C for 24-72 hours.

Table V-5. Synthesis protocols of $\text{Th}_{6x}\text{U}_{6y}\text{-UiO-67-NH}_2$.

Metal source		Ligand	Modulator	Solvent		T	Time	Yield
$\text{ThCl}_4 \cdot 4\text{H}_2\text{O}$ 10.2 mg 23 μmol		$H_2\text{bpdc-NH}_2$ 10 mg 0.039 mmol	$H\text{bza}$ 120 mg 0.98 mmol	DMF 1 mL 13 mmol	H ₂ O 30 μL 0.82 mmol	130 °C	24 h	12%
$\text{ThCl}_4 \cdot 4\text{H}_2\text{O}$ 7.7 mg 17.3 μmol	$\text{ThCl}_4 \cdot 4\text{H}_2\text{O}$ 7.7 mg 17.3 μmol	$H_2\text{bpdc-NH}_2$ 10 mg 0.039 mmol	$H\text{Bza}$ 120 mg 0.98 mmol	DMF 1 mL 13 mmol	H ₂ O 100 μL 2.73 mmol	130 °C	72 h	10%
$\text{ThCl}_4 \cdot 4\text{H}_2\text{O}$ 5.1 mg 11.5 μmol	$\text{ThCl}_4 \cdot 4\text{H}_2\text{O}$ 5.1 mg 11.5 μmol	$H_2\text{bpdc-NH}_2$ 10 mg 0.039 mmol	$H\text{Bza}$ 120 mg 0.98 mmol	DMF 1 mL 13 mmol	H ₂ O 100 μL 2.73 mmol	130 °C	72 h	12%
$\text{ThCl}_4 \cdot 4\text{H}_2\text{O}$ 2.5 mg 5.75 μmol	$\text{ThCl}_4 \cdot 4\text{H}_2\text{O}$ 2.5 mg 5.75 μmol	$H_2\text{bpdc-NH}_2$ 10 mg 0.039 mmol	$H\text{Bza}$ 120 mg 0.98 mmol	DMF 1 mL 13 mmol	H ₂ O 100 μL 2.73 mmol	130 °C	72 h	11%
UCl_4 9.8 mg 26 μmol		$H_2\text{bpdc-NH}_2$ 10 mg 0.039 mmol	$H\text{Bza}$ 120 mg 0.98 mmol	DMF 1 mL 13 mmol	H ₂ O 100 μL 2.73 mmol	130 °C	72 h	15%

After solvothermal treatment of the five above synthetical protocols, octahedral crystals of different sizes appeared on the bottom of the glass vial. As in the previous case, compounds have different colors based on their inorganic composition as it can be seen in Figure V-7 (top). Crystals of the pure Th-UiO-67_NH_2 solid are transparent and the more uranium is added in

the reaction mixture, the greener they crystals get. The octahedral shape of $\text{Th}_{6-x}\text{U}_x\text{-UiO-67-NH}_2$ can be seen perfectly even by optical microscopy for the pure thorium compound, as crystals are big enough (20-30 μm). For the mixed compounds and pure uranium one, the crystal size is smaller (5-10 μm) and SEM images were taken to confirm the shape (Figure V-9 bottom). This crystal size difference can be explained by the consideration of Lewis acidity of thorium and uranium, the latter being stronger acid, so crystallization process would be higher and does not favor the isolation of large single-crystals. The stability is observed under air for a few days only for the Th-UiO-67-NH_2 . The rest of the samples are not stable under air. This is logical, as uranium is sensitive to air and gets easily oxidized to U^{VI} .

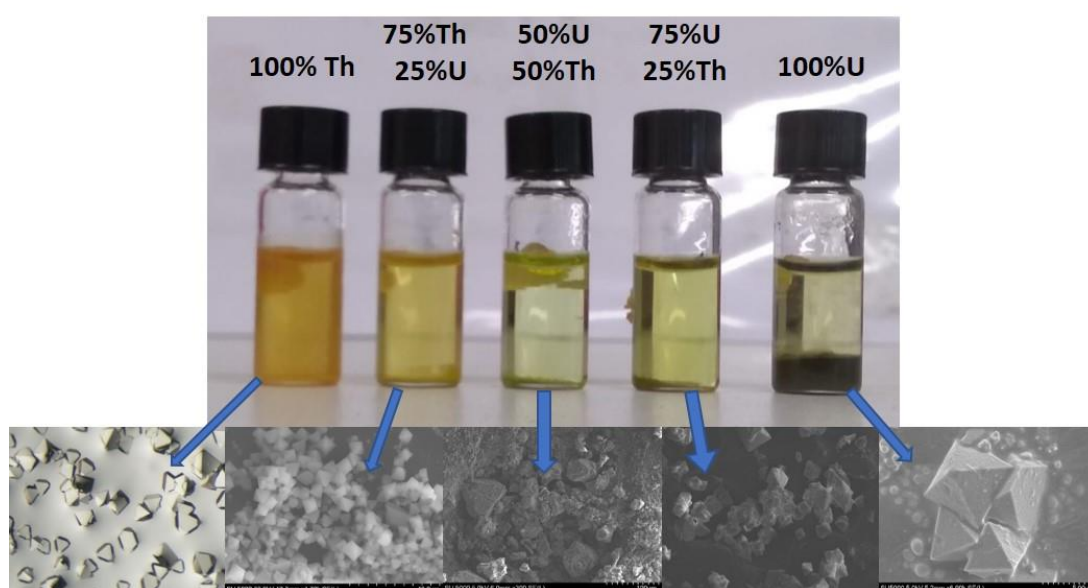


Figure V-9. Photograph of glass vials (2mL) after solvothermal treatment (top); Optical microscope and SEM images for $\text{Th}_{6-x}\text{U}_x\text{-UiO-67-NH}_2$ (bottom).

V. 2.2 Structural description of $\text{Th}_{6-x}\text{U}_x\text{-UiO-67-NH}_2$

The structure of Th-UiO-67-NH_2 ^[6], Th-UiO-67 ^[6], U-UiO-67 ^[7] and Zr-UiO-67-NH_2 ^[8] has been already reported in the literature. Inspired by these works, the thorium, uranium and mixed analogues to synthesize $\text{Th}_{6-x}\text{U}_x\text{-UiO-67-NH}_2$ will be presented in this part of Chapter V. The same protocol followed to synthesize successfully the thorium analogue $\text{Th}^{\text{IV}}\text{-UiO-67-NH}_2$. When the same synthesis tried to be reproduced with uranium, the resulted powder is amorphous. Thus, the synthetical conditions were modified in order to isolated the isostructural $\text{U}^{\text{IV}}\text{-UiO-67-NH}_2$ and indeed, it was achieved by adding more amount of water (100 $\mu\text{L}/\text{mL}$ DMF). Normally, uranium is more acidic than thorium, so it is expected to be more reactive. However, in this case, higher content of water is needed to be added in the reaction

mixture in order to obtain a crystalline precipitate. In order to explain this behavior, we may attribute this behavior to the thermal stability of thorium. The addition of higher water content in the reaction of uranium will speed up the reaction and will not destabilize uranium(IV) (competition with U(VI) oxidation) under thermal treatment for long time. Of course, this will result into smaller crystals, which was the case as seen in the previous paragraph. This latest change in the synthesis protocol was used to synthesized the mixed materials.

In this UiO-67-type structure reported in literature with zirconium(IV), the zirconium atom is 8-fold coordinated with eight oxygen atoms, coming from four carboxylate oxygens deriving from bpdc-NH₂ ligands, two μ_3 -oxo and two μ_3 -hydroxo bridging. Although, uranium(IV) and thorium(IV) in the analogous structures^[6,7] are linked to another oxygen molecule from a terminal water molecule resulting to a 9-fold coordination (Figure V-10, left). These hexameric clusters are surrounded by twelve bpdc or bpdc-NH₂ ligands with the formula [Th₆O₄(OH)₄(bpdc)₆(H₂O)₆]_n, [Th₆O₄(OH)₄(bpdc-NH₂)₆(H₂O)₆]_n, [U₆O₄(OH)₄(bpdc)₆(H₂O)₆]_n and [Zr₆O₄(OH)₄(bpdc-NH₂)₆]_n generating three-dimensional open structures (Figure V-10, right) with the typical cubic UiO-n topology.

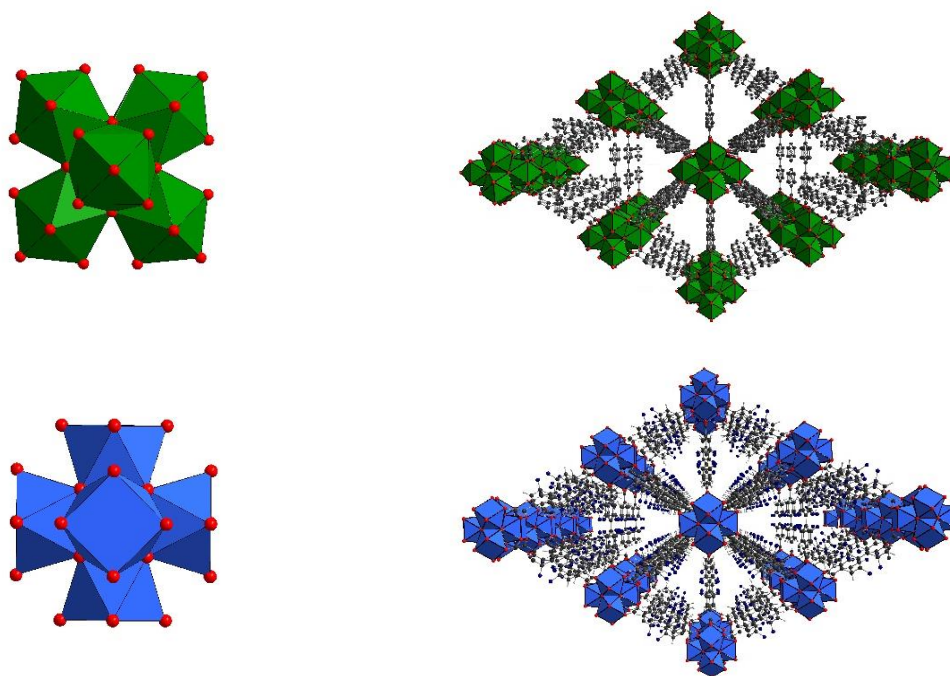


Figure V-10. The nine-fold hexameric cluster of [U₆O₄(OH)₄(H₂O)₆], [Th₆O₄(OH)₄(H₂O)₆] (top left) and the three-dimensional framework [U₆O₄(OH)₄(bpdc)₆(H₂O)₆]_n along the a,b plane (top right) and the eight-fold hexameric cluster of [Zr₆O₄(OH)₄] (bottom left) and the three-dimensional framework [Zr₆O₄(OH)₄(bpdc-NH₂)₆]_n along the a,b plane (bottom right).

V. 2.3 Characterization of $\text{Th}_{6-x}\text{U}_x\text{-UiO-67_NH}_2$

The series of $\text{Th}_{6-x}\text{U}_x\text{O}_4(\text{OH})_4(\text{bpdc-NH}_2)_6(\text{H}_2\text{O})_6$ were characterized by powder X-ray diffraction, SEM-EDX analysis and thermogravimetric analysis.

Powder X-ray diffraction patterns show that all samples are pure and isostructural as the experimental as-synthesized patterns are compared with the simulated one from the calculated crystallographic .cif file extracted from Th-UiO-67_NH_2 ^[6] (Figure V-11). In the patterns we do not have any double peaks for the mixed compounds and that indicates a homogenous distribution of thorium and uranium (Figure V-11, right). However, this remains an indication and will be proven later by SEM-EDX analysis.

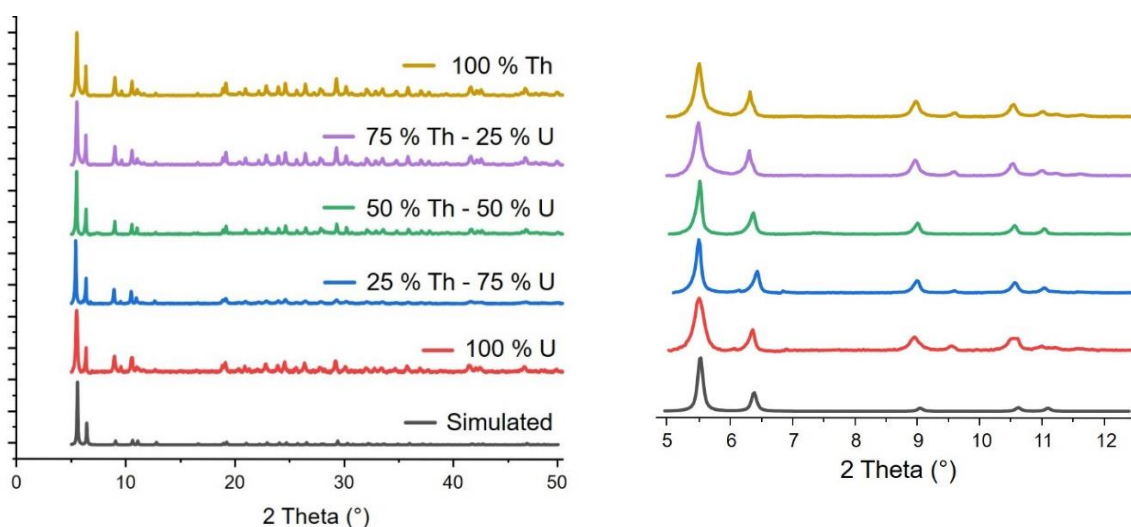


Figure V-11. Powder X-ray diffraction patterns of $\text{Th}_{6-x}\text{U}_x\text{-UiO-67_NH}_2$ compared to the simulated generated from U-UiO-67 ^[7] (left) and zoom on the patterns from 5 to 12.5° in order to observe better the single Bragg peaks at 5.5 and 6.4° (right). X-ray source; Copper K α radiation; ($\lambda_{\text{CuK}\alpha}$ =1.5406 Å).

This $\text{Th}_{6-x}\text{U}_x\text{-UiO-67_NH}_2$ phase is synthesized in low yields ($\approx 10\%_{\text{Ac}}$), without the possibility to scale up and is quite unstable even under inert atmosphere (powder XRD pattern becomes amorphous after some days). Due to these reasons, high-resolution powder X-ray diffraction diagrams, in order to extract the cell parameters of each compound was quite challenging. Therefore, the powder X-ray diffraction patterns in Figure V-11 (with 0.5 s of scan time per degree theta) were indexed, in order to observe if the same tendency is followed. In Table V-6, the cell parameters of all $\text{Th}_{6-x}\text{U}_x\text{-UiO-67_NH}_2$ compounds have been extracted from the Le Bail refinement (Jana2006 software) of powdered XRD patterns for $\text{Th}_{6-x}\text{U}_x\text{-UiO-67_NH}_2$ samples (by taking into account the real chemical formula from the starting (Th,U) precursor ratio). The related diagrams can be found in paragraph A3 in Appendix (Figure A2).

It is observed again, that the more uranium is added, the more the cell parameters decrease, as we encountered for the previous series of $\text{Th}_{6-x}\text{U}_x\text{-anth}$ compounds (paragraph V. 1.4).

Table V-6. Extracted cell parameters for $\text{Th}_{6-x}\text{U}_x\text{-UiO-67_NH}_2$ in the cubic system $Fm\text{-}3m$, from powder XRD patterns.

	a (Å)	V (Å ³)
$\text{Th}_6\text{-UiO-67_NH}_2$	28.085(9)	22396(9)
$\text{Th}_{4.5}\text{U}_{1.5}\text{-UiO-67_NH}_2$	27.855(3)	21612(2)
$\text{Th}_3\text{U}_3\text{-UiO-67_NH}_2$	27.827(1)	21549(1)
$\text{Th}_{1.5}\text{U}_{4.5}\text{-UiO-67_NH}_2$	27.799(6)	21484(1)
$\text{U}_6\text{-UiO-67_NH}_2$	27.719(1)	21465(1)

The evolution of the cell parameters (a and V) follows the same trend, with smaller cell parameters than expected from Vegard law. As for the series of $\text{Th}_{6-x}\text{U}_x\text{-anth}$, in Figure V-12 it is observed that the fitting with the theoretical values of x (uranium content) is better than the one with the experimental ones determined by EDX experiments.

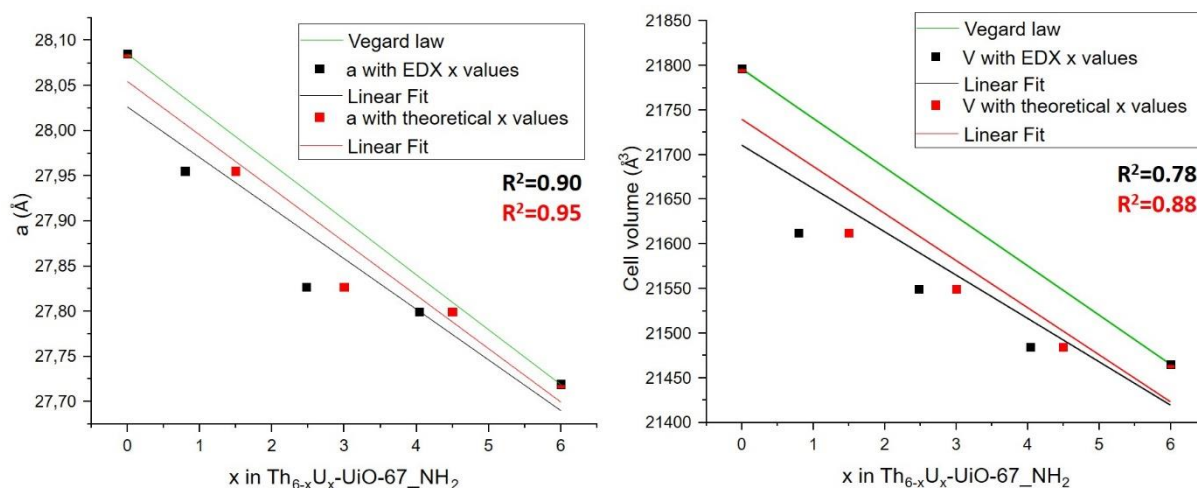


Figure V-12. Evolution of cell parameters a and V with the increasing content x of U in the mixed compounds $\text{Th}_{6-x}\text{U}_x\text{-UiO-67_NH}_2$.

There are three different molar compositions in the mixed samples with targeted percentages 75% Th – 25 % U, 50 % Th – 50 % U and 25 % Th – 75 % U. Around twenty points in different crystals were tested with EDX analysis, in order to provide a more trustworthy average molar-based percentage for each compound of the series. These average weight-based (wt%) and molar-based (at%) percentages, with their standard deviations σ , are summarized in Table V-7. Except of EDX, cartography experiments were conducted for all different samples in order to investigate the homogeneity of the uranium and thorium dispersion in the crystals (Figure V-13). Indeed, the distribution is homogeneous, as green (U)

and red (Th) spots are equally distributed in the crystals' surfaces. In this series, in all of the samples, thorium percentages are higher than expected, exceeded the desired percentages by a difference of around 20%.

Table V-7. Summary of the average of EDX measurements in the series of $Th_{6-x}U_xUiO-67_NH_2$.

	75% Th – 25 % U		50% Th – 50 % U		25% Th – 75 % U	
	$Th_{4.5}U_{1.5}UiO-67_NH_2$		$Th_3U_3UiO-67_NH_2$		$Th_{1.5}U_{4.5}UiO-67_NH_2$	
		σ		σ		σ
Th^{IV}	86.70 wt %	0.8	60.25 wt %	1.1	34.30 wt %	0.6
Th^{IV}	86.40 at %	0.9	59.63 at %	0.7	33.73 at %	0.7
U^{IV}	13.30 wt %	0.8	39.75 wt %	1.1	65.70 wt %	0.6
U^{IV}	13.60 at %	0.9	41.37 at %	0.7	66.27 at %	0.7
Final formula	$Th_{5.20}U_{0.80}UiO-67_NH_2$		$Th_{3.62}U_{2.48}UiO-67_NH_2$		$Th_{2.06}U_{4.04}UiO-67_NH_2$	

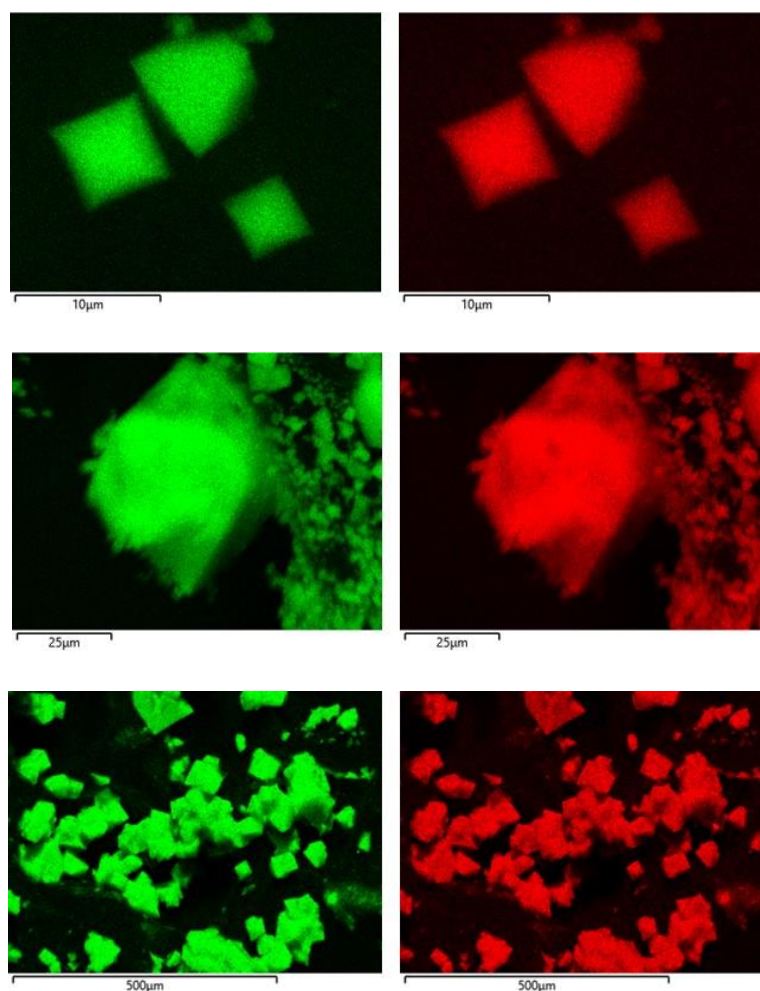
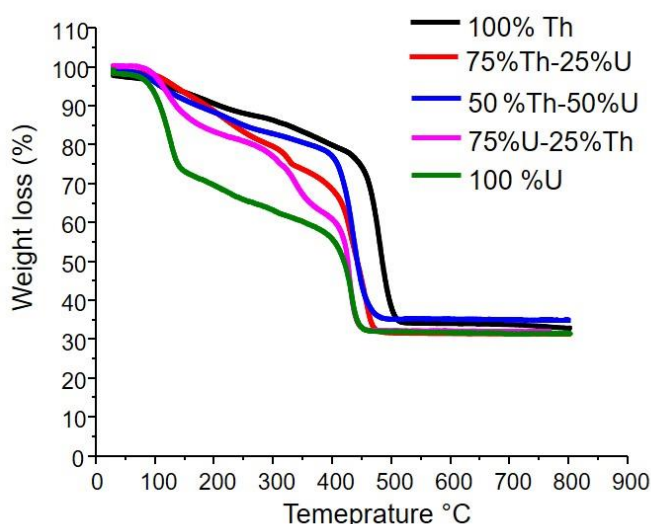


Figure V-13. Cartography of crystals of $Th_{4.5}U_{1.5}UiO-67_NH_2$, $Th_3U_3UiO-67_NH_2$ and $Th_{1.5}U_{4.5}UiO-67_NH_2$ for uranium (green) and thorium (red) (from top to bottom) from EDX analysis.

The thermogravimetric analysis (TGA) in Figure V-14 of $\text{Th}_{6-x}\text{U}_x\text{-UiO-67_NH}_2$ has a main weight loss at $\approx 440^\circ\text{C}$, which corresponds to the loss of the biphenyl ligands and the collapse of the framework to form ThO_2 and/or UO_2 . If we assume that for $\text{Th}_{3.62}\text{U}_{2.48}\text{-UiO-67_NH}_2$ the residue of 35.2 % corresponds to $3.62x(\text{ThO}_2)$ and $2.48x(\text{UO}_2)$, then the experimental loss of 39.8 % (calc.: 35.5 %) corresponds to the loss of around 6 biphenyl ligands and is in relative accordance with the structure of $\text{Th}_{3.62}\text{U}_{2.48}\text{-UiO-67_NH}_2$ that contains 6 for each Th_6 . There is another small weight loss of 5.4 % (calc.: 2.2%) that corresponds to the loss of coordinated water molecules, 6 for each hexameric cluster. A first weight loss is also present of around 11.5 % and is attributed to free solvent molecules in the pores of the framework. It is observed that for $\text{U}_6\text{-UiO-67_NH}_2$ (green line), the weight loss comes drastically faster than the rest of the samples of the series from 100 to 150 °C. Such behavior was also observed for the rest of the series of $\text{Th}_{6-x}\text{U}_x\text{-anth}$ previously in this chapter (paragraph 1.4, Figure V-8). This first weight loss, may indicate a thermal instability that can be prevented by thorium doping.



Compound	1 st weight loss	2 nd weight loss		3 rd weight loss		Formation ThO_2/UO_2 ($> 500^\circ\text{C}$)
	(free solvent) (0-250 ° C)	(coordinated H_2O) (300-400 ° C)	Calculated	(bpdc- NH_2 ligand) (430 – 500 ° C)	Calculated	
	Experimental	Experimental	Calculated	Experimental	Calculated	Experimental
$\text{Th}_6\text{-UiO-67_NH}_2$	8.3 %	4.4 %	2.4 %	39.4 %	35.4 %	34.6 %
$\text{Th}_{5.20}\text{U}_{0.80}\text{-UiO-67_NH}_2$	12.5 %	2.7 %	2.2 %	35.1 %	33.2 %	31.5 %
$\text{Th}_{3.62}\text{U}_{2.48}\text{-UiO-67_NH}_2$	11.5 %	4.8 %	2.4 %	39.8 %	35.5 %	35.2 %
$\text{Th}_{2.06}\text{U}_{4.04}\text{-UiO-67_NH}_2$	16.4 %	5.4 %	2.2 %	33.1 %	31.9 %	32.2 %
$\text{U}_6\text{-UiO-67_NH}_2$	26.4 %	7.1 %	2.2 %	28.4 %	32.2 %	32.2 %

Figure V-14. Thermogravimetric curves of $\text{Th}_{6-x}\text{U}_x\text{-UiO-67-NH}_2$ (under air gas flow, $5^\circ\text{C}\cdot\text{min}^{-1}$ heating rate) and the calculations of the different weight losses on the table below.

In this second part of Chapter V, the synthesis of An-UiO-67_NH₂ has been investigated with our synthetical approach to produce mixed Th,U-UiO-67_NH₂. The synthesis of Th-UiO-67_NH₂ was previously reported in literature by our group in Lille.^[6] Inspired by this work, this synthetical protocol was tested to synthesize the analogue U-UiO-67_NH₂ that is not previously reported with the amino derivative (only in the form of U-UiO-67^[7]). However, no crystalline powder was obtained and different parameters in synthesis were changed, as the temperature, the content of water and the content of modulator. When more water added (100 μL instead of 30 μL), then nanosized- octahedral crystal were isolated and the powder X-ray diffraction pattern revealed that it was indeed isostructural to Th-UiO-67_NH₂. Even if we overcame the barrier of the synthesis of U-UiO-67_NH₂, the yield of the reaction is low (10-15 %), the synthesis of this compound is not reproducible all the times, as well as the mixed that contain uranium(IV) species, shown a great instability. For all these reasons, characterization of the porosity with BET calculation and gas sorption experiments was not able to be performed. Thus, as a third series of compounds we chose to introduce a more stable MOF, where a full characterization and gas sorption experiments were conducted.

V.3 Study of the Th/U-fumarate series

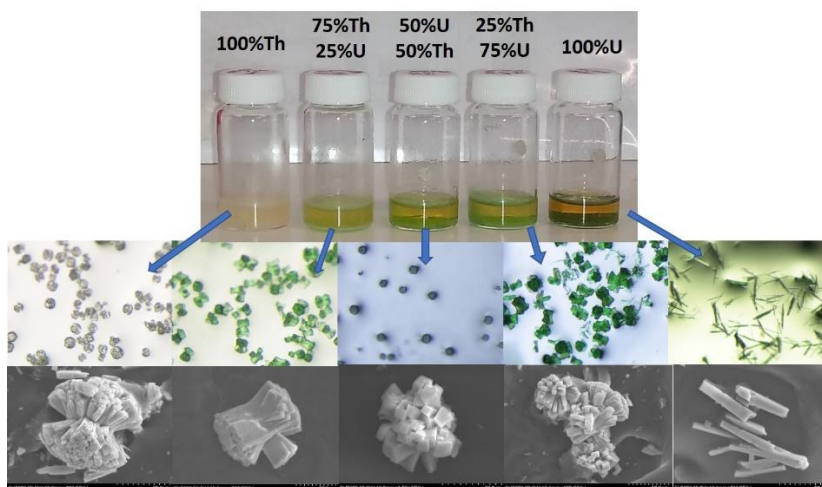
V. 3.1 Synthesis of Th_{1-x}U_x-fum

The phase **Th_{1-x}U_x-fum** is prepared by using fumaric acid as organic linker, in DMF without the addition of water or modulator, by using a 2mL glass vial heated at 120°C for 24 hours. This specific synthesis condition is of importance, since the protocol using water and modulator gives rise to the formation of the UiO-n compound as previously reported with the uranium-based MOF.^[7] The pure uranium and thorium materials were synthesized among the three different mixed ones. The synthesis protocols of **Th_{1-x}U_x-fum** are summarized in Table V-8. After the solvothermal treatment, all the powdered products have been washed with DMF, then three times with dichloromethane, and dried under primary vacuum for a few minutes, during the chamber transfer of the glovebox. The samples are finally left at room temperature, in the glove box and just exposed under ambient atmosphere for further characterization analysis.

Table V-8. Synthesis protocols of $Th_{1-x}U_x$ -fum compounds.

Metal source		Ligand	Solvent	T	Time	Yield
ThCl ₄ ·4H ₂ O 10.2 mg 23 μmol		Fumaric acid 122 mg 1.05 mmol	DMF 1 mL 13 mmol	120 °C	24 h	40%
ThCl ₄ ·4H ₂ O 7.7 mg 17.3 μmol	ThCl ₄ ·4H ₂ O 7.7 mg 17.3 μmol	Fumaric acid 122 mg 1.05 mmol	DMF 1 mL 13 mmol	120 °C	24 h	36%
ThCl ₄ ·4H ₂ O 5.1 mg 11.5 μmol	ThCl ₄ ·4H ₂ O 5.1 mg 11.5 μmol	Fumaric acid 122 mg 1.05 mmol	DMF 1 mL 13 mmol	120 °C	24 h	37%
ThCl ₄ ·4H ₂ O 2.5 mg 5.75 μmol	ThCl ₄ ·4H ₂ O 2.5 mg 5.75 μmol	Fumaric acid 122 mg 1.05 mmol	DMF 1 mL 13 mmol	120 °C	24 h	36%
UCl ₄ 9.8 mg 26 μmol		Fumaric acid 122 mg 1.05 mmol	DMF 1 mL 13 mmol	120 °C	24 h	35%

After solvothermal treatment of the five above synthetical protocols, plate-like agglomerated crystals of $\approx 20 \mu\text{m}$ appeared on the bottom of the vial. As in the previous case, compounds have different colors based on their inorganic composition as it can be seen in Figure V-15 (top). Crystals of pure **Th-fum** are colorless transparent and the more uranium is added in the reaction mixture, the greener the crystals get. The plate-like shape of the pure uranium-based compound can be seen better by optical microscopy (Figure V-15 bottom right). This phase is stable under air for months.

Figure V-15. Photo of vials after thermal treatment (top); Optical microscope and SEM images for the $Th_{1-x}U_x$ -fum (bottom).

V. 3.2 Structural description of $\text{Th}_{1-x}\text{U}_x\text{-fum}$

For the collection of crystallographic data, different crystals from all preparations were tested under single crystal X-ray diffraction. As can be observed from the photographs under optical microscope and maybe even more clear from the SEM images, in most samples, the crystals form agglomerates and that made it difficult to find a correct single-crystal in order to collect data. After many tries, crystals from **Th-fum** presented the most distinguished reflections and thus the data of this preparation were collected with a Bruker APEX DUO diffractometer. After data collection (Table V-9), solving the structure was more complicated than expected, as it is possible that the crystals consist of more than one single crystals, oriented with a tiltation. At this stage, it was not possible to obtain a proper structure ($R_1 = 0.1341$, $wR_2 = 0.3454$ for $I > 2\sigma(I)$), and we present hereafter only a model, which will need further analyzes in order to confirm the atomic arrangement.

Table V-9. Crystal data and structure refinements for **Th-fum** model.

	Th-fum
Formula	$\text{C}_8\text{O}_8\text{Th}$
Formula weight	267.05
Temperature/K	100
Crystal type	-
Crystal size/ mm^3	$0.463 \times 0.23 \times 0.148$
Crystal system	Tetragonal
Space group	$P4/ncc$
a/Å	16.578(1)
b/Å	16.578(1)
c/Å	9.3780(7)
$\alpha/^\circ$	90
$\beta/^\circ$	90
$\gamma/^\circ$	90
Volume/Å ³	2577.4(4)
Z, $\rho_{\text{calculated}}/\text{g}\cdot\text{cm}^{-3}$	8 / 2.372
μ/mm^{-1}	11.595
2 θ range/ $^\circ$	4.914-52.75
Limiting indices	$-14 \leq h \leq 14$ $-20 \leq k \leq 20$ $-11 \leq l \leq 11$
Collected reflections	22096
Unique reflections	4198 [$R_{\text{int}} = 0.0976$]
Parameters	37
Goodness-of-fit on F^2	1.298
Final R indices [$I > 2\sigma(I)$]	$R_1 = 0.1341$ $wR_2 = 0.3454$
R indices (all data)	$R_1 = 0.2073$ $wR_2 = 0.3956$
Largest diff. peak and hole/ $\text{e}\cdot\text{Å}^{-3}$	26.59 and -5.64

From the approaching model, **Th-fum** crystallizes in tetragonal $P4/ncc$ space group and results in a chemical formulation of $(\text{Th}(\text{C}_4\text{H}_2\text{O}_4)_2)$. It exhibits two inequivalent discrete mononuclear thorium(IV) units with 8-fold coordination. Each thorium is coordinated with eight oxygens deriving from carboxylate arms of the fumarate ligand (Figure V-16, left). These

oxygens adopt a distorted square antiprismatic geometry around each thorium and each mononuclear unit is bridged with each other with carboxylate groups from fumarate, resulting in the generation of infinite chains Th1...Th1...Th1 or Th2...Th2...Th2, along the *c* axis (Figure V-16, right). Th-O distances are Th1-O = 2.33(3) Å to 2.38(3) Å and Th2-O = 2.26(4) Å – 2.41(4) Å.

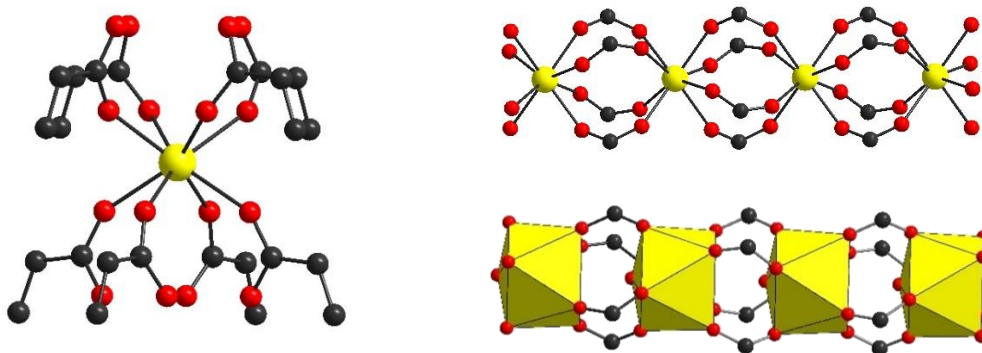


Figure V-16. The 8-fold coordination sphere of Th-fum (left), thorium chain bridged by fumarates along *c* axis (top right) and the same chain presented in polyhedral (bottom right).

These chains are further connected through the fumarate linkers to another type of chain along *a* and *b* axes constituted of mononuclear units, where thorium adopts an 8-fold coordination with a distorted square prismatic geometry. This connectivity leads to the formation of a three-dimensional framework with tetragonal 1D channels along the *c* axis with pore square-shaped diameter of around 3.5 Å. This value diameter was calculated by measuring the distance between two opposite carbons inside the pore and from this value two times the radii of carbon was subtracted. No other channels running along *a* or *b* axis, perpendicularly to the *c* axis are observed.

Interestingly, both chains are slightly different due to the coordination angle of the carboxylate function of the fumarate ligand. Upon looking at the network through the *c* axis, we can observe that the two C-O bonds constituting the carboxylate arms around the Th2 atoms are slightly twisted/turned while the ones surrounding the Th1 atoms are perfectly aligned (Figure V-17, bottom right). At this stage of refinement, there remain high electron densities of $\approx 26 \text{ e.}\text{\AA}^{-3}$ located nearby at 1.6 Å, and others of $\approx 11 \text{ e.}\text{\AA}^{-3}$ at 1.43 Å of one heavy atom (Th1), since the electron densities of $\approx 18 \text{ e.}\text{\AA}^{-3}$ located at 1.7 Å of the second thorium Th2 site.

Within the channels, remaining electron residue are visible ($\approx 17 \text{ e.}\text{\AA}^{-3}$) which could be attributed to DMF, but without observing the proper configuration of its expected geometry.

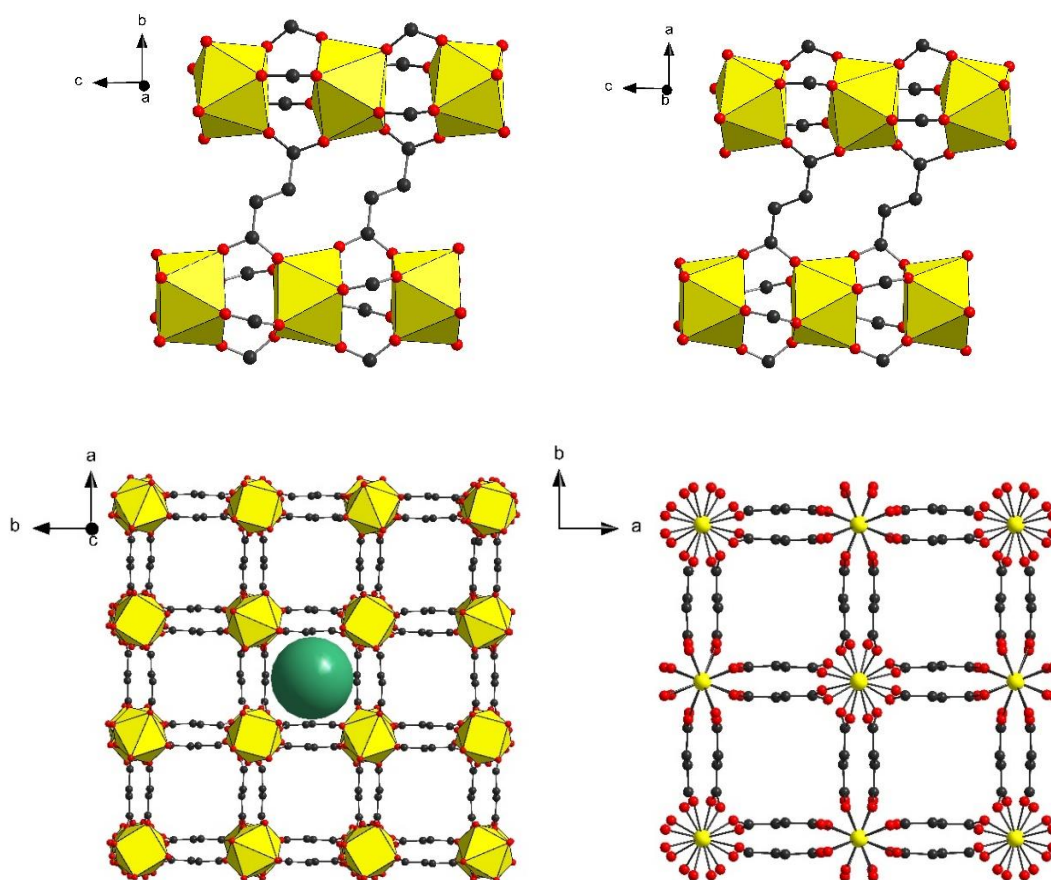


Figure V-17. Connectivity for *Th-fum* along *a* axis (top left) and *b* axis (top right) between 8-fold thorium(IV) coordination sites. Three-dimensional network of *Th-fum* with its tetragonal 1D channels of 3.5 Å diameter along *c* axis (bottom left) and the different Th1 and Th2 environments (bottom right).

V. 3.3 Characterization of $\text{Th}_{1-x}\text{U}_x\text{-fum}$

The series of $\text{Th}_{1-x}\text{U}_x\text{-fum}$ compounds were characterized by powder X-ray diffraction, SEM-EDX analysis and thermogravimetric analysis.

Powder X-ray diffraction patterns show that all samples are pure and isostructural as the experimental as-synthesized patterns are compared with the simulated one from the calculated cif of the model structure (**Th-fum**) (Figure V-18). In the patterns we do not have any double peaks for the mixed compounds indicating a homogenous distribution of thorium and uranium. This indication will be confirmed later by SEM-EDX analysis.

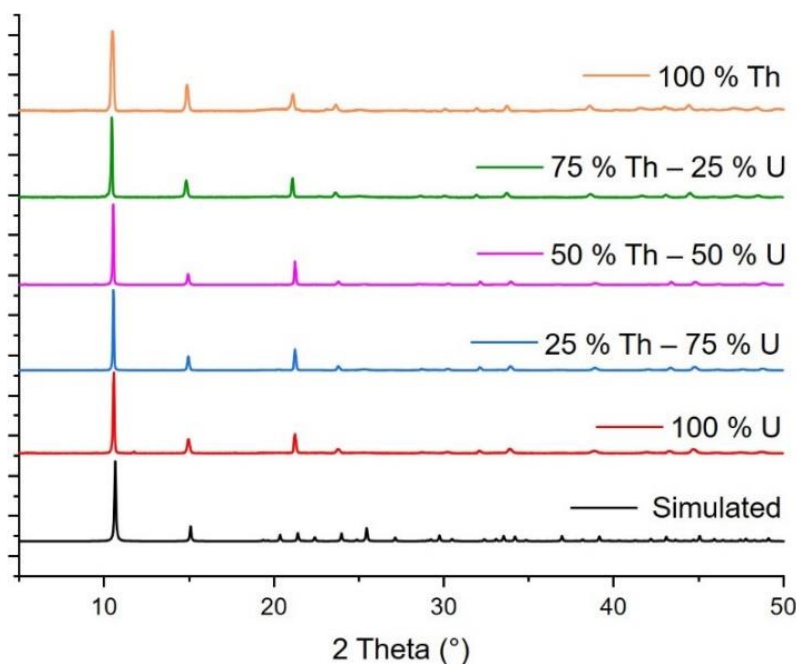


Figure V-18. Powder X-ray diffraction patterns of $\text{Th}_{1-x}\text{U}_x\text{-fum}$ compared to the simulated generated from Th-fum . X-ray source; Copper $K\alpha$ radiation; ($\lambda_{\text{CuK}\alpha}=1.5406 \text{ \AA}$).

Once again, powder X-ray diffraction diagrams were indexed, in order to extract the cell parameters (Table V-10) of all $\text{Th}_{1-x}\text{U}_x\text{-fum}$ compounds with the help of le Bail refinement (Jana2006 software) of powdered XRD patterns for $\text{Th}_{1-x}\text{U}_x\text{-fum}$ samples (by taking into account the real chemical formula from the starting (Th,U) precursor ratio). The related diagrams can be found in paragraph A3 in Appendix (Figure A2). The same trend is observed here as well, where the lengths a are decreased with the introduction of uranium, as well as the cell volume.

Table V-10. Extracted cell parameters for $\text{Th}_{1-x}\text{U}_x\text{-fum}$ with the tetragonal cell, from powder XRD patterns.

	a (Å)	c (Å)	V (Å ³)
Th-fum	16.912(7)	9.345(3)	1342(1)
Th_{0.75}U_{0.25}-fum	16.815(6)	9.291(1)	1317.3(8)
Th_{0.5}U_{0.5}-fum	16.754(6)	9.234(1)	1313.4(8)
Th_{0.25}U_{0.75}-fum	16.717(3)	9.155(1)	1273.1(5)
U-fum	16.672(7)	9.090(4)	1237.1(1)

These changes in the cell parameters seem to follow quite well the Vegard law (Figure V-19, green line) with some small deviations from the linear fitting of the refined cell parameters for each composition (Figure V-19, black line), where R^2 value is 0.95 – 0.96. In order to verify if the EDX percentages (see hereafter), that will be presented afterwards, are

trustworthy and close to reality, red points represent the refined cell parameters for each composition according to the theoretical values added in the feed before the thermal treatment. The fitting of these points is presented in red with R^2 values of 0.97 – 0.99. It is a general trend for this case as well, that the fitting of the red line is slightly better than the black one. This means that the (Th,U) composition real percentages are closer to the ones added in the feed, than from what found by the EDX experiments.

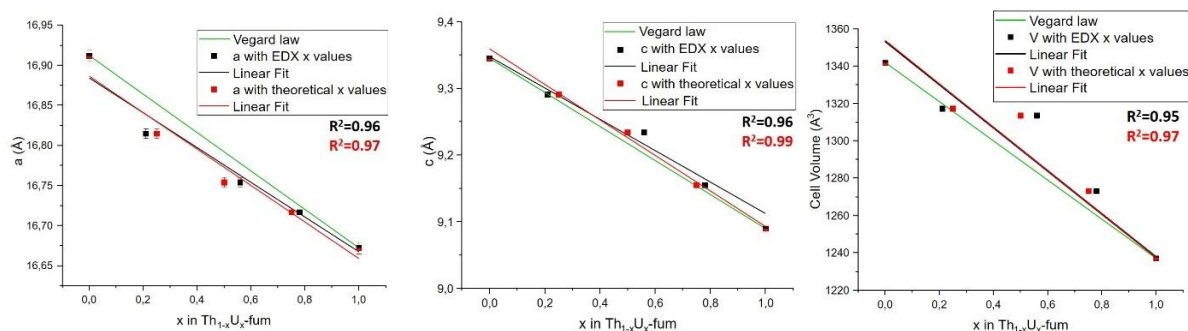


Figure V-19. Evolution of cell parameters a , c and V with the increasing content x of U in the mixed compounds $Th_{1-x}U_x\text{-fum}$.

There are three different compositions in the mixed samples with percentages 75% Th – 25 % U, 50 % Th – 50 % U and 25 % Th – 75 % U. Around twenty points in different crystals were tested with EDX analysis, in order to provide a more trustworthy average molar-based percentage for each compound of the series. These average weight-based (wt%) and molar-based (at%) percentages, with their standard deviations σ , are summarized in Table V-11. Except of EDX, cartography experiments were conducted for all different samples in order to investigate the homogeneity of the uranium and thorium dispersion in the crystals (Figure V-20). Indeed, the distribution is homogeneous, as green (U) and red (Th) spots are equally distributed in the crystals' surfaces. In Table V-11, it is observed that compared to the previous series of compounds, this time the percentages are closer to the molar ratios added in the feed, with a deviation of about 10% compared to the expected values. There are always some small deviations. When thorium is more concentrated ($Th_{0.75}U_{0.25}\text{-fum}$) it is incorporated in slightly higher percentages than uranium (79.7% for 75% added in the feed). However, the logic behind these deviations, does not follow a specific pattern and has to involve the chemistry that happens in solution.

Table V-11. Summary of the average of EDX measurements in the series of $\text{Th}_{1-x}\text{U}_x\text{-fum}$.

	75% Th – 25 % U		50% Th – 50 % U		25% Th – 75 % U	
	$\text{Th}_{0.75}\text{U}_{0.25}\text{-fum}$		$\text{Th}_{0.50}\text{U}_{0.50}\text{-fum}$		$\text{Th}_{0.25}\text{U}_{0.75}\text{-fum}$	
		σ		σ		σ
Th^{IV}	79.70 wt%	0.5	44.10 wt%	0.5	22.40 wt%	0.5
Th^{IV}	79.12 at%	0.5	43.48 at%	0.4	21.76 at%	0.4
U^{IV}	20.50 wt%	0.5	55.90 wt%	0.5	77.60 wt%	0.5
U^{IV}	20.88 at%	0.5	56.52 at%	0.4	78.24 at%	0.4
Final formula	$\text{Th}_{0.79}\text{U}_{0.21}\text{-fum}$		$\text{Th}_{0.44}\text{U}_{0.56}\text{-fum}$		$\text{Th}_{0.22}\text{U}_{0.78}\text{-fum}$	

If there is one observation we can make, is that in $\text{Th}_{6-x}\text{U}_x\text{-anth}$ and $\text{Th}_{6-x}\text{U}_x\text{-UiO-67-NH}_2$, thorium content is higher than expected (for instance $\text{Th}_{3.47}\text{U}_{2.53}\text{-anth}$ and $\text{Th}_{3.62}\text{U}_{2.48}\text{-UiO-67-NH}_2$), but it is the opposite for the $\text{Th}_{1-x}\text{U}_x\text{-fum}$ phase. Uranium may react faster in solution as a stronger Lewis acid, but the precipitation procedure is maybe favored by thorium, which is in a stable oxidation state. Finally, these results are only an indication that we have the two elements in one crystallite and there are limits posed by EDX measurements. Thus, the different chemical compositions indicate the trends, but in any case, the quantitative composition of the samples is not that accurate.

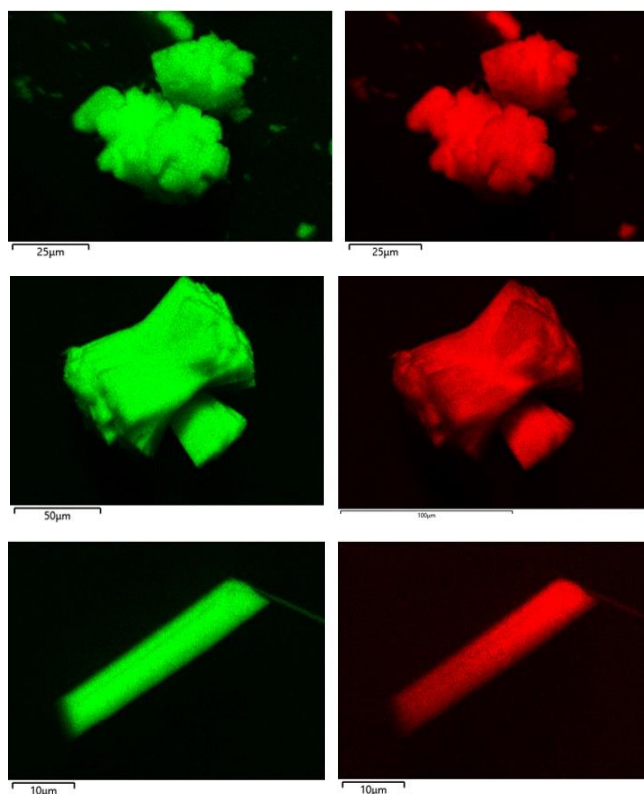
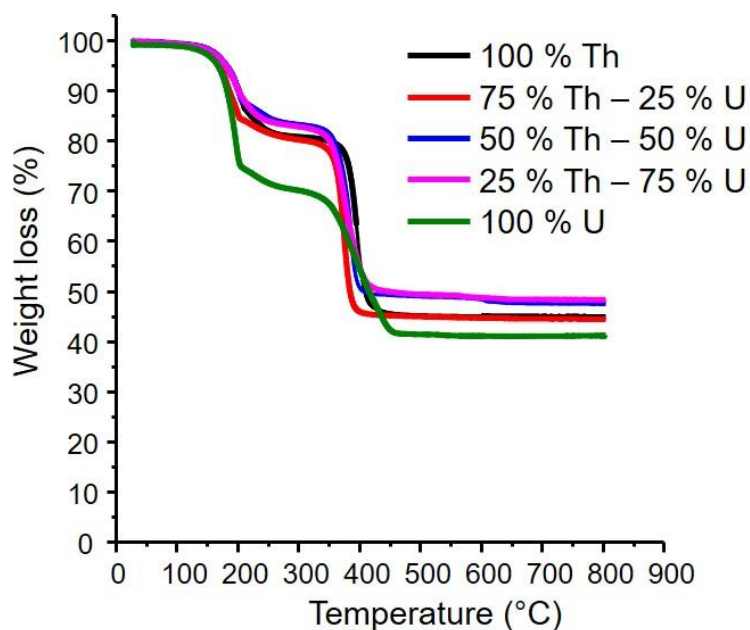


Figure V-20. Cartography of crystals of $\text{Th}_{0.75}\text{U}_{0.25}\text{-fum}$, $\text{Th}_{0.5}\text{U}_{0.5}\text{-fum}$ and $\text{Th}_{0.25}\text{U}_{0.75}\text{-fum}$ for uranium (green) and thorium (red) (from top to bottom) from EDX analysis.

The thermogravimetric analysis (TGA) in Figure V-21 of $\text{Th}_{1-x}\text{U}_x\text{-fum}$ has a main weight loss at $\approx 350\text{ }^\circ\text{C}$, which corresponds to the loss of fumarates and the collapse of the framework to form actinides oxide (ThO_2 and/or UO_2). If we assume that in $\text{Th}_{0.44}\text{U}_{0.56}\text{-fum}$ this residue of 47.5 % corresponds to $0.44x(\text{ThO}_2)$ and $0.56x(\text{UO}_2)$, then the experimental loss of 37.5 % (calc.: 40.4 %) corresponds to the loss of 1.92 fumarates / Th and is in agreement with the structure of $\text{Th}_{1-x}\text{U}_x\text{-fum}$ deduced from the structural model by single-crystal XRD calculations, showing the occurrence of 2 dicarboxylate ligands per thorium atom. The first loss starting from $170\text{ }^\circ\text{C}$ until $220\text{ }^\circ\text{C}$, of 14.3 % could be attributed to some free solvent into the 1D system of channels. However, from infrared spectroscopy we do not observe a band at around 1650 cm^{-1} to suggest that DMF could exist in the pores (Figure A23, Appendix). Due to the successive washing process with DMF and CH_2Cl_2 , one may suggest the replacement of encapsulated DMF by CH_2Cl_2 (named as “free solvent” in table from figure V-21). The same behavior is observed for the pure **U-fum**, as for the previous series. **U-fum** presents a bigger first weight loss, that is disappeared by the substitution of even 25 % of thorium in the structure. One possible explication can be that uranium(IV) is an unstable oxidation state and it can be easier oxidized under air (TGA is performed under air). On the other hand the presence of the stable thorium(IV) can help the thermal stabilization of the structures. This repeated motif in the thermogravimetric curves, is an important indication for the role of thorium as thermo-stabilizer and could be useful for the rest of future thermal characterization in the second part of the project.



Compound	1 st weight loss	2 nd weight loss		Formation
	("free solvent" in the pores)	(fumarate ligand)		ThO ₂ /UO ₂
	(170-220 ° C)	(350-400 ° C)		(> 400 ° C)
	Experimental	Experimental	Calculated	Experimental
Th-fum	15.3 %	37.4 %	38.8 %	44.9 %
Th_{0.79}U_{0.21}-fum	15.5 %	37.1 %	38.5 %	44.8 %
Th_{0.44}U_{0.56}-fum	14.3 %	37.5 %	40.4 %	47.5 %
Th_{0.22}U_{0.78}-fum	14.6 %	38.4 %	41.3 %	48.8 %
U-fum	19.8 %	31.7 %	34.0 %	40.3 %

Figure V-21. Thermogravimetric curves of **Th_{1-x}U_x-fum** (under air gas flow, 5 °C.min⁻¹) and the calculations of different weight losses on the table below.

V. 3.4 CO₂ sorption and enthalpies of adsorption for **Th_{1-x}U_x-fum**

The structure of **Th-fum** revealed voids, so gas sorption experiments were performed for the series of **Th_{1-x}U_x-fum** to identify a potential porosity. According to its thermal stability, the **Th_{1-x}U_x-fum** compounds have been activated under secondary vacuum at 250 °C for 5 hours, in order to evacuate the trapped DMF solvent molecules from the channels system (details in table A1 in Appendix). Unfortunately, nitrogen sorption has not been observed at 77 K, so BET surface area could not be estimated. The no adsorption of N₂ at 77 K, could be explained by the relative small size of **Th_{1-x}U_x-fum** tunnel diameters (3.5 Å) compared to the kinetic diameter of N₂ (3.64 Å).^[9] Therefore, we used carbon dioxide (CO₂), having a smaller radius (3.30 Å)^[9] than N₂ (Table V-12), and we were able to adsorb this gas molecule in the **Th_{1-x}U_x-fum** solid in order to characterize its porosity. Indeed, the possible carbon dioxide adsorption makes this MOF-like structure a good candidate for selective CO₂ adsorption due to its pore size, that is big enough to capture CO₂, but also small enough to prevent the capture of nitrogen. Since nitrogen sorption was not possible, no other gases like methane, krypton or xenon (bigger than nitrogen) were tested.

Table V-12. Kinetic diameters of nitrogen, methane and carbon dioxide.^[9]

Gas	Formula	Kinetic diameter (Å)
Nitrogen	N	3.64
Carbon dioxide	CO ₂	3.30
Methane	CH ₄	3.80

Carbon dioxide adsorption isotherm curves were measured by using the ASAP 2020 micromeritics apparatus, at three temperatures (273 K, 283 K and 293K) for the pure thorium and uranium compounds as well as the mixed **Th_{0.44}U_{0.56}-fum** one. In Figure V-22, the pores of **Th-fum** are presented with a space filling representation, so that the micropores can be better visualized.

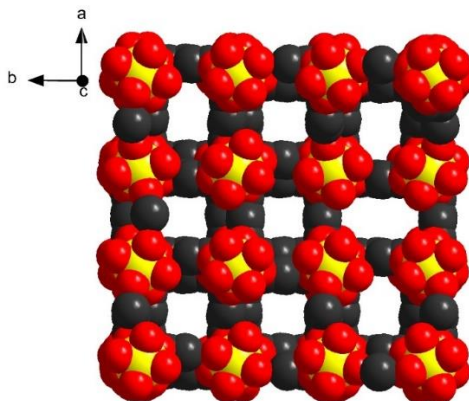


Figure V-22. Representation in space-filling of **Th-fum** micropores (3.5 Å) along *c* axis.

The fact that CO₂ is adsorbed and not N₂ or CH₄, gave us the opportunity to investigate the selectivity of CO₂/CH₄. Methane is widely used for the production of hydrogen and carbon dioxide is also a product of this reaction. It is important then to be able to separate and remove CO₂ from the reaction. This selectivity in **Th-fum** was calculated at 20.9 with the help of the isotherms of adsorption in Figure V-23 and the Henry's law:

$$\frac{S_{CO_2}}{S_{CH_4}} = \frac{k_H CO_2}{k_H CH_4}$$

Where k_H the Henry's constants.

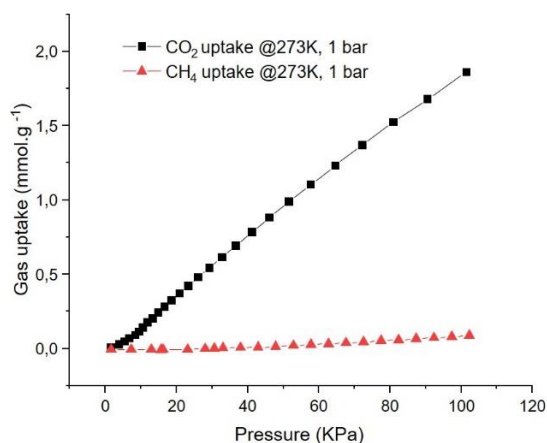


Figure V-23. Isotherms of adsorption for CO₂ and CH₄ at 273 K and 1 bar for **Th-fum**.

A near-perfect CO₂/CH₄ selectivity of 61 ± 4 in dynamic conditions reported in the literature.^[10] In fact, the multi-component gas adsorption experiments in this study of J. Long and his co-workers, shows that the single-component selectivity of the same sample was only 5.7. This example demonstrates the potential of the series of **Th_{1-x}U_x-fum** in selective CO₂ sorption.

Between the different samples, it is observed that the thorium **Th-fum** compound absorbs more CO₂ than the uranium **U-fum** analogue. This behavior is explained due to the ionic radius of the metallic source for an 8-fold coordination (Th(IV) = 1.19 Å versus U(IV) = 1.14 Å)^[4], leading to a larger cell and then larger pores. Based on the cell volumes, we calculated that the pore size of U-fum will decrease of approximately 7 %. As a result, by adding thorium into a uranium-based framework we can maximize the gas uptake values. Thus, in addition of thorium, not only the thermal stability is optimized, but also the adsorption capacity from 12 cm³/g for the pure **U-fum** to 42 cm³/g for the pure **Th-fum** (Figure V-24, top), or a ratio of x 3.5 for the CO₂ uptake capacity between the two solids.

In order to understand better this behavior, CO₂ sorption was evaluated at three different temperatures (273, 283 and 293 K), so that enthalpy values can be calculated (see for detail, chapter IV, paragraph IV 1.3.5). The sorption experiments were conducted for the pure U and Th compounds, as well as for the mixed **Th_{0.44}U_{0.56}-fum** one. The values of enthalpies are between -15, for the **Th-form** up to -40 kJ·mol⁻¹ for the **U-fum** (Figure V-24, bottom). These values are very different to each other, since the enthalpy values get higher the more uranium we introduce into the framework. Uranium(IV) has smaller ionic radius than thorium(IV) and thus uranium(IV) induces smaller size of tunnels. With smaller channels, CO₂ is found to be more confined as show the higher values of enthalpies measured for the U-form compound. Thus, the smaller the pores, the strongest the interactions between the adsorbent and the pores. This makes sense, as the more confined the space, the easier the adsorbent comes in contact with pores and interacts with them. According to studies^[11], enthalpy values up to -45 kJ·mol⁻¹ represent a reversible physio-sorption procedure. Thus, regardless the strong interactions, we still have a strong indication for a reversible carbon dioxide adsorption in **Th_{1-x}U_x-fum**.

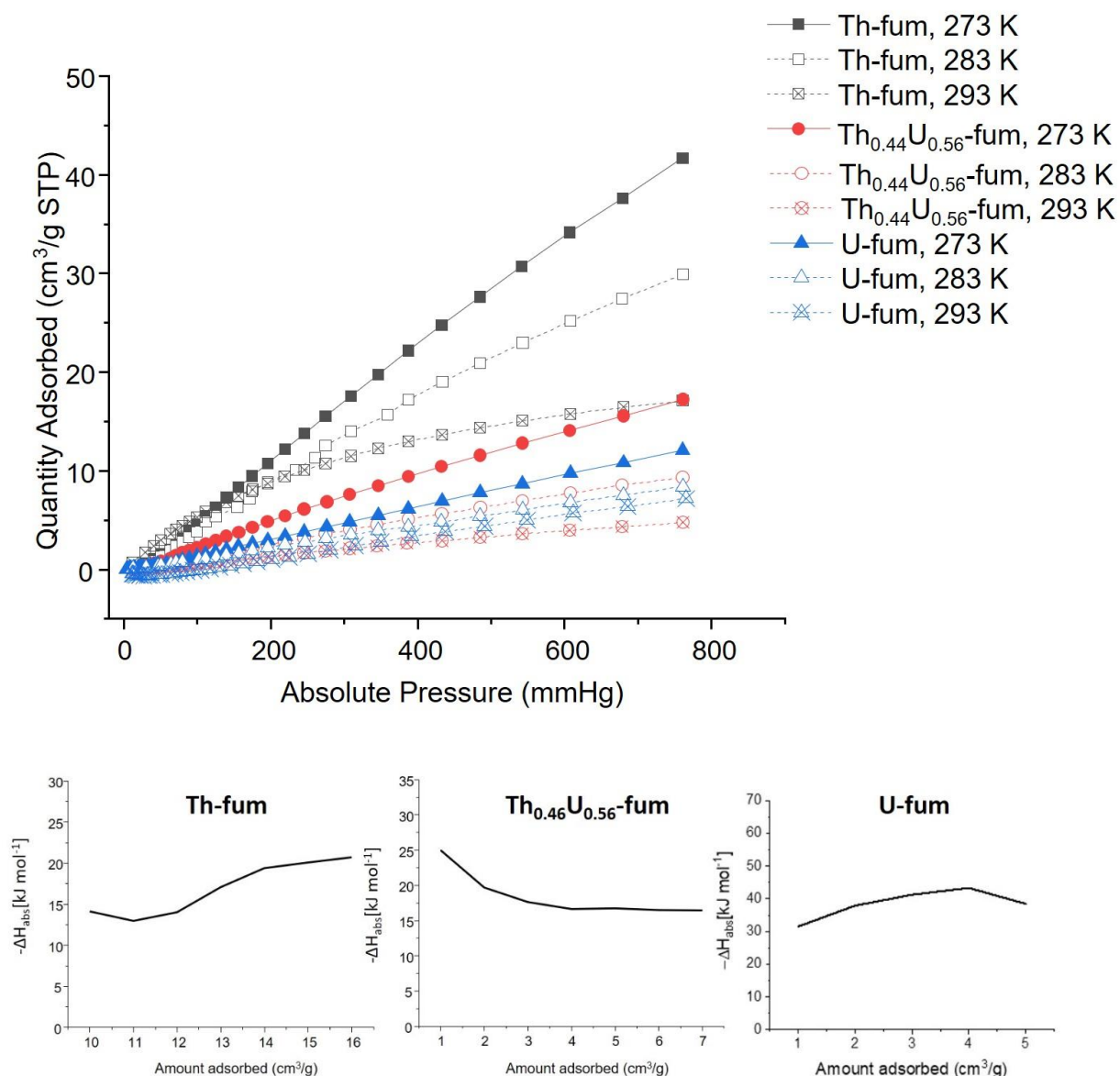


Figure V-23. Isotherms of carbon dioxide adsorption for *Th-fum*, *Th_{0.5}U_{0.5}-fum* and *U-fum* at three different temperatures (middle) and values of enthalpy depending on the volume of carbon dioxide adsorbed (bottom).

In this third part of Chapter V, a second type of a mixed actinide metal-organic framework was introduced, linked with fumarates. This series of compounds present higher yields than the previous materials in this chapter (35-40 %) and scale up (up to 5 times more) was achieved. EDX and cartography shown homogenous mixed samples with an average difference of around 5 % in the percentages. The quality of the crystals needs optimization so that sufficient data can be collected and solve the structure. The addition of modulator in the system is considered as the first step towards this direction of generating bigger single-crystals. Whereas in UiO-67-NH₂ phase, modulator and water were added in the system, in **Th_{1-x}U_x-fum**, none of them is used. In UiO-67-NH₂, the use of water leads to condensation of

actinide(IV) and isolation of the hexameric cluster. When this water content is not added (as in the case of fumarate), no there is no condensation and monomeric actinide(IV) SBUs are obtained. The smaller size of fumarates compared to aminobiphenyldicarboxylates, generates smaller pores, but with a much more thermally rigid framework as observed by TG analysis. These small pores demonstrate the perfect pore size for selective carbon dioxide to nitrogen sorption. Next step for the series of **Th_{1-x}U_x-fum**, is performing further thermal experiments, calcination and sintering to produce mixed Th,U-oxides.

V. 4 Conclusions

In this chapter, it was successfully investigated the synthetical strategy to achieve substitution of tetravalent actinide (Th,U) in coordination carboxylate complexes or carboxylate polymers. This strategy involves a prior to synthesis mixing of the metal sources of thorium(IV) and uranium(IV) chlorides. In order to have a proof of concept, it was tested in different type of carboxylate compounds, either a molecular hexameric cluster stabilized by monotopic anthracenoate species, or a large pore MOF of UiO-67_NH₂ type and a second one (Th,U-fumarate) with narrow pores. High-resolution powder X-ray diffraction was performed in order to extract the cell parameters for all compounds. It was thus observed that higher content of uranium in the system induces the decreasing of the crystal cell parameters. This conclusion was foreseeable as uranium is smaller than thorium by considering their ionic radii when going to heavier actinides in the periodic table. Furthermore, by comparing the powder X-ray diffraction patterns to each other, no double peak is observed so this is one indication that thorium and uranium were both successfully incorporated in the same crystallites, resulting in a typical solid-solution system of **Th_{1-x}U_x** composition.

This indication was further proved by EDX experimental mapping, for which thorium and uranium elements are homogeneously distributed through the crystallites, without any observation of local aggregates for a given actinide. However, we can distinguish some differences (up to 20% for some cases), as the order of doping accuracy, where the series of **Th_{1-x}U_x-fum** performed slightly better, as according to EDX analysis, the Th/U ratios were closer to the ones added in the feed compared to the series of **Th_{6-x}U_x-anth** and **Th_{6-x}U_x-UiO-67_NH₂**. On the other side, for the series of UiO-67-NH₂, the synthesis protocol was adjusted by adding more water in order to obtain the uranium analogue. In samples of **Th_{6-x}U_x-anth** and **Th_{6-x}U_x-UiO-67_NH₂**, thorium compositions were higher than the ones added in the feed.

The explanation of this tendency can be explained by the chemistry that happens in solution. For example, uranium(IV) species may react faster as a stronger Lewis acid, but perhaps the stability of Th(IV) wins over the sensible oxidation state of U(IV) during crystallization.

Thermal studies were conducted in order to determine the thermal stability and behavior of these materials. They were performed under air and so the general image of a less stable uranium(IV) compounds is normal, as uranium(IV) species are more sensible to air compared to the stable oxidation state of Th(IV). The addition of thorium(IV) into an uranium(IV) compound (molecular or not) shows to enhance the thermal stability under air and protect the sensible species of uranium(IV).

Finally, we highlight that all three series proved the concept of our “prior to synthesis” doping, to prepare mixed Th/U compounds. Most promising found to be the new coordination polymer connected with fumarate ligands (**Th,U-fum** series), as it presents the less charge in carbon, and that will be important for the next step of this study, which will be the calcination and sintering of these compounds to produce mixed Th/U oxides. In addition, it shows an efficient CO₂ sorption, without trapping N₂ due to the length of the organic ligand (fumaric acid) and the metal source (thorium). We also demonstrated, that by doping with thorium, the amount absorbed is increased. That can be interesting, as by doping in different percentages, we can modify the porosity and uptake capacities of U-MOFs.

V. 5 References

- [1] E. A. Dolgoplova, O. A. Ejegbavwo, C. R. Martin, M. D. Smith, W. Setyawan, S. G. Karakalos, C. H. Henager, H. C. Zur Loye, N. B. Shustova, *J. Am. Chem. Soc.* **2017**, *139*, 16852–16861.
- [2] C. Falaise, C. Volkringer, T. Loiseau, *Cryst. Growth Des.* **2013**, *13*, 3225–3231.
- [3] C. Falaise, J. S. Charles, C. Volkringer, T. Loiseau, *Inorg. Chem.* **2015**, *54*, 2235–2242.
- [4] R. D. Shannon, *Acta Crystallogr. Sect. A* **1976**, *32*, 751–767.
- [5] A. Schaate, P. Roy, A. Godt, J. Lippke, F. Waltz, M. Wiebcke, P. Behrens, *Chem. – A Eur. J.* **2011**, *17*, 6643–6651.
- [6] N. P. Martin, J. März, H. Feuchter, S. Duval, P. Roussel, N. Henry, A. Ikeda-Ohno, T. Loiseau, C. Volkringer, *Chem. Commun.* **2018**, *54*, 6979–6982.
- [7] C. Falaise, C. Volkringer, J. F. Vigier, N. Henry, A. Beaurain, T. Loiseau, *Chem. – A Eur. J.* **2013**, *19*, 5324–5331.
- [8] M. Kaposi, M. Cokoja, C. H. Hutterer, S. A. Hauser, T. Kaposi, F. Klappenberger, A. Pöthig, J. V. Barth, W. A. Herrmann, F. E. Kühn, *Dalt. Trans.* **2015**, *44*, 15976–15983.
- [9] S. E. Kentish, C. A. Scholes, G. W. Stevens, *Recent Patents Chem. Engineering* **2008**, *1*, 52–66.
- [10] M. K. Taylor, T. Runčevski, J. Oktawiec, J. E. Bachman, R. L. Siegelman, H. Jiang, J. A. Mason, J. D. Tarver, J. R. Long, *J. Am. Chem. Soc.* **2018**, *140*, 10324–10331.
- [11] A. Nuhnen, C. Janiak, *Dalt. Trans.* **2020**, *49*, 10295–10307.

General conclusions and perspectives

The work of the present thesis led to some advancements in the two different aspects in the field of the generation of hybrid organic-inorganic crystalline materials: the exploration of the chemistry and reactivity of niobium with carboxylates and the isolation of new actinide and mixed actinides coordination polymers.

In one part of this thesis, the emerging need for materials with new, little-studied metals has been highlighted. This challenging task has been assigned as a first pole of interest. Niobium was selected as an element for creating novel coordination networks, as only few examples of molecular niobium carboxylates exist in the literature. In order to study its reactivity towards organic ligands as carboxylic acids, many parameters were modified (oxidation state, nature of poly-carboxylic acids precursors, solvents, reaction temperature). Niobium salts are commercially available in Nb(III), Nb(IV) and Nb(V) chloride sources (usually stabilized by organic molecules, as THF) or as alkoxides (only for Nb(V)).

Nb(IV)Cl₄(THF)₂ precursor proved to have a good solubility in organic solvents and to react with pyridine-family carboxylate ligands. It seems that nitrogen in pyridine from dicarboxylate linker favors the coordination with Nb(IV) centers to result into a molecular assembly with an unusual eight-fold [NbO₄N₄] coordination environment. This molecular assembly presents a supramolecular structure derived by hydrogen bondings between the Nb(IV)-complex and the free solvent. By changing the reaction conditions (addition of an organic base, different ligand and solvent), the eight-fold dodecahedral environment [NbO₄N₄] is conserved, but however the crystal packing varies thanks to the formation of hydrogen bond networks with encapsulated organic solvent molecules (acetonitrile, pyridine, triethylamine and DMF). From this study, four new molecular Nb(IV) carboxylate complexes were isolated and deeply characterized by single-crystal and powder X-ray diffraction, IR, EPR, magnetism measurements and XPS, which confirm the d^1 configuration. According to EPR, this electron is delocalized between the d orbital of niobium and the p orbital of oxygen, but still has a d character, and can be observed to be localized in the d orbital for low temperatures (5K). At low temperatures, an unexpected antiferromagnetic transition occurs for the complexes where the interatomic Nb...Nb distances are lower than 10 Å. From the crystal structure point of view, it appeared that the niobium(IV) centers is always linked through a mixed N,O donors set, since the second free carboxylic acid of the ditopic molecule

functionality remains unbonded. This complexation mode and the keynote role of pyridine ligands can be a useful tool to develop polytopic organic spacers incorporating both N-acceptor and O-donor groups (Figure 1), in order to isolate niobium-based multidimensional coordination polymer networks.

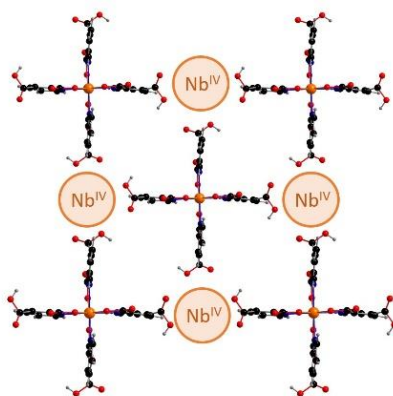


Figure 1. Nb(IV) centers with the possibility to generate a framework, by deprotonating the second carboxylic function.

In terms of applications, niobium cations may perform brightly as catalysts due to their many oxidation degrees. Therefore, these compounds can be tested as promoters in catalytical reactions. In recent studies, niobium(IV)oxide found to be perform well in the NRR reaction (Nitrogen Reductive Reaction), the procedure to synthesize ammonia from nitrogen.^[1] Another unstable oxidation degree of niobium is 3+, that is commercially available as NbCl₃(DME) (DME=1,2-dimehtoxyethane). As mentioned in the first chapter related to the literature, there are only four examples of Nb(III) carboxylates, some of them exhibiting a trinuclear motifs with a double μ_3 -oxo bridging species, which could be reminiscent to that of the other trivalent metals, with the single μ_3 -oxo bridge (see first raw of transition metals (Sc, V, Cr, Fe) or p elements (Al, Ga, In). This particular trimer is of great interest in MOF construction and is the basis of the generation of highly porous networks (see MIL-100/101 series for instance).^[2] From this brief literature survey, this field yet needs to be explored although the NbCl₃(DME) precursor was tested, but so far without some encouraging results. The stability of niobium(III) in term of redox would have to be controlled in order to investigate the conditions for further reacting such trinuclear units with polycarboxylate linkers for generating multidimensional networks.

Nb(V)ethoxide (Nb(OEt)₅) was also widely used as a niobium(V) precursor in this thesis. With a melting point at 5 °C, niobium(V) ethoxide is a viscous liquid precursor that was also

used as a solvent in many syntheses. Our work led to the isolation of twelve molecular niobium(V)-centered cores with various nuclearities, stabilized by arene or polyarene mono- and poly- carboxylates. Controlling hydrolysis in this system was challenging at first place, as niobium(V) cations are strong Lewis acid sites, subject to fast hydrolysis, resulting in Nb₂O₅ precipitation. However, we successfully controlled hydrolysis as the synthetic condition associating carboxylic acid with leaving ethanol groups allows for the slow production of ester species with releasing water molecules. This concept was proven by infrared spectroscopy and NMR experiments and this water molecule is the origin of the oxo-condensation bridges between the niobium centers in {Nb₂O}, {Nb₄O₄}, {Nb₈O₁₂} and {Nb₁₂O₂₁} moieties. It was also demonstrated that the occurrence of moisture atmosphere or/and elevated temperature (up 100 °C) favors the esterification process, which induce the formation of water and consequently the condensation of niobium(V) centers to result in niobium-based poly-oxo clusters with higher nuclearities ({Nb₄O₄}, {Nb₈O₁₂} and {Nb₁₂O₂₁}). All these different niobium(V) poly-oxo clusters can be viewed as prospective inorganic building units to generate multidimensional networks in combination with polydentate carboxylate ligands (Figure 2). Indeed, from the niobium(V)-oxygen bond distance consideration, we observed that Nb-O_{oxo} distances are quite shorter ($\approx 1.9 \text{ \AA}$) when compared to those observed in well-known MOF such as UiO-66 (2.23 Å)^[3] for instance, but Nb-O_{carboxylate} bond lengths are quite identical (Nb-O_{carboxylate} $\approx 2.10\text{-}2.20 \text{ \AA}$). With this purely metric view, we may expect a better chemical stability of the niobium-MOF compounds. What is interesting is that in the case of **Nb(V)-1** and **Nb(V)-7** compounds, the benzoates and naphthoates, respectively, are on the same plane and so, if a dicarboxylic acid is used, the resulting network will be a 2D layered structure. In order to increase the dimensionality, a polytopic ligand as pyromellitic acid, trimesic acid or other, should be considered. To overcome this barrier, the octameric brick of **Nb(V)-8** can be used instead, in which naphthoates exist in both two planes and thus a 3D network can be predicted, even with the use of a dicarboxylic acid.

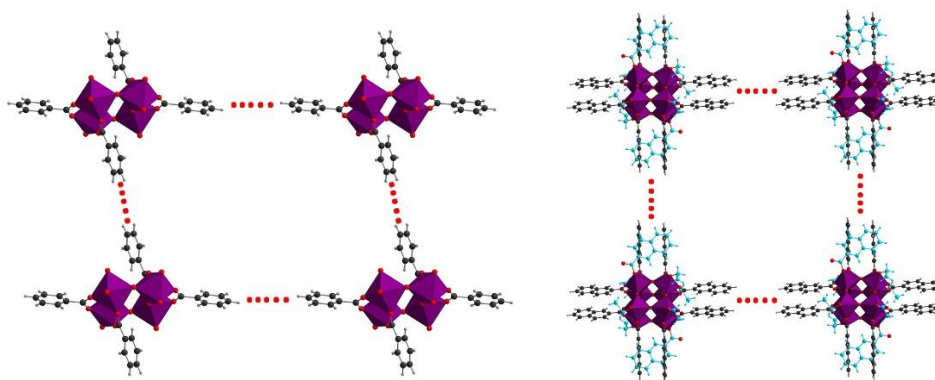


Figure 2. Possible configurations of niobium(V) multidimensional networks with the use of **Nb(V)-1** and **Nb(V)-8** as an inorganic building block (with red points, the places where a polytopic ligand can substitute the monotopic one).

Another field of exploration can be the use of a different precursor. In this study, a focus was given in Nb(V)ethoxide, but Nb(V)isopropoxide exist as well, adding a hydrophobic surrounding in niobium(V). It may be interested to see if this hydrophobicity can have an impact in condensation process through esterification. Except of alkoxide, other type of precursors can be used as well, as niobium(V) chloride (NbCl_5) and Nb(V)oxalate salts that are stable in aqueous media. The synthesis in water medium will minimize the difficulties in manipulation and may result to a whole new family of materials.

In terms of applications, metal alkoxides are known precursors for ceramic materials, as they are subject to hydrolysis and thus require much less energy to produce a high purity ceramic.^[4] Moreover, by altering the organic molecules that surround niobium(V) centers, the properties of the ceramic may change. In this study we proved that the replacement of ethoxy groups is easy and many different types of carboxylates can be introduced in their place. Thus, another interesting aspect will be to test these materials as precursors for ceramics through a sol-gel process.

So far, only molecular coordination complexes with relatively low niobium nuclearity were obtained at the end of the 2000s by associating the metal with oxo-donor organic ligands (containing mainly carboxylate functions). Due to the high valence of these two elements, the control of their reactivity appears challenging since several parasitic reactions (in particular hydrolysis due to water) can intervene and prevent the formation of high nuclearity complexes or coordination networks. The conclusive laboratory tests carried out in this thesis demonstrated that controlling hydrolysis with niobium(V) is possible and have led to a succession of clusters up to the octamer or dodecamer. Nevertheless, this research field

remains to be explored regarding the construction of extended coordination networks as well as the transposition to tantalum(V). This metal, although from the same family as niobium, generally appears less reactive and could therefore make it easier to obtain single crystals of a pure new tantalum(V)carboxylate networks.

A second part of this thesis was devoted to the isolation of new actinide(IV) carboxylate networks. In details, the first goal was to synthesize new thorium(IV) carboxylate networks by introducing home-made long chain organic linkers containing an azobenzene core. The second one was to determine a strategy to make mixed actinide (Th-U) carboxylate compounds that can be later converted to mixed actinide oxides and tested as potential nuclear combustibles.

For the first aspect of the work with actinides, two home-made long chain ligands belonging to the azobenzene family (noted 4,4'-azobenzenedicarboxylic acid and 3,3',5,5'-azobenzenetetracarboxylic acid) were synthesized. The rich chemistry of thorium(IV) is demonstrated by the isolation of four new thorium(IV) coordination polymers, two with each ligand. As with small changes (different modulator, different temperature) a second phase can be obtained. One of the four phases is an analogue to the well-known UiO-66 MOF with pores size 14-18 Å (BET $\approx 1200 \text{ m}^2.\text{g}^{-1}$) and possible to adsorb different gases like krypton, xenon, methane and carbon dioxide at RT. We demonstrated as well, that with the use of a smaller size modulator (formic acid), rather than a bigger one (2-naphthoic acid), BET specific area can be optimized ($1200 \text{ m}^2.\text{g}^{-1}$ instead of $850 \text{ m}^2.\text{g}^{-1}$). It was demonstrated that the chemistry of thorium(IV) is quite rich and many different structures can be isolated, by small changes in the reaction's conditions. The azobenzene family of ligands, is a quite unique type of photoactive ligands and since it can be linked to Th(IV)-centers, these photo-sensitive properties can be exploited.^[5] If one side of the ligand is non-coordinated (as it happens in the outer surface in MOFs), then the compound can be used in many photo-induced chemical procedures by a trans-cis photo-isomerization of the azo bond (N=N) that happens at 350 nm. Another target can be the organic synthesis of new architectures of azobenzene carboxylate linkers, where the azo bond will be free and all carboxylate branches will be placed in one side of the azo bond (Figure 4). This work requires a lot of time and a well-planned approach, but it is quite interesting as perspective for these systems. As long the results are supporting, more carboxylate compounds can be tested. For example, the addition of water in the system with fumarates will favorize the condensation of actinides and increase the ration metal/carbon.

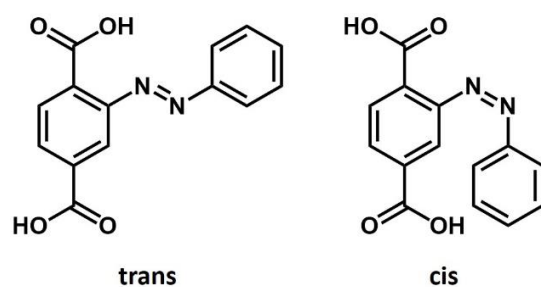


Figure 3. Trans and cis configuration of azobenzene linker with carboxylic functions that can be used in the future for photocatalytical applications.

The last part of this thesis was dedicated to a strategy to synthesize mixed-actinide carboxylate compounds, in different ratios between thorium(IV) and uranium(IV). Three different series of compounds were tested, a molecular hexameric actinide(IV) cluster stabilized by anthracenoates, a metal-organic framework (An)UiO-67-NH₂ and a new coordination polymer linked through fumarate. It was chosen to dope the reaction solution with both metals prior to synthesis, according to the desired final composition. Finally, indeed, that method was proven more accurate than others existing in the literature.^[6] As perspectives, advanced thermal analyses have been performed for these samples, starting with a thermogravimetric analysis under inert atmosphere (hydrogenated argon), in order to study the sintering capacity of the resulting mixed Th,U oxides. Further thermal analysis may include Raman and SEM experiments under heating, in order to follow their *in situ* the transformation of the mixed Th/U oxides. As a first step, the samples would be calcinated to remove the organic matter and then sintered. The series of Th(IV)/U(IV) fumarate, that showed better thermal stability and greater interest due to their low charge in carbon, would be expected to be transformed into pellets and tested as potential nuclear fuel in the case of the so-called mixed oxide (MOX) solid, containing both Pu and U.

References

- [1] L. Huang, J. Wu, P. Han, A. M. Al-Enizi, T. M. Almutairi, L. Zhang, G. Zheng, *Small Methods* **2019**, *3*, 1800386.
- [2] G. Férey, C. Serre, C. Mellot-Draznieks, F. Millange, S. Surblé, J. Dutour, I. Margiolaki, *Angew. Chemie* **2004**, *116*, 6456–6461.
- [3] J. H. Cavka, S. Jakobsen, U. Olsbye, N. Guillou, C. Lamberti, S. Bordiga, K. P. Lillerud, *J. Am. Chem. Soc.* **2008**, *130*, 13850–13851.
- [4] D. C. Bradley, *Chem. Rev.* **1989**, *89*, 1317–1322.
- [5] B. Tylkowski, A. Trojanowska, V. Marturano, M. Nowak, L. Marciniak, M. Giamberini, V. Ambroggi, P. Cerruti, *Coord. Chem. Rev.* **2017**, *351*, 205–217.
- [6] E. A. Dolgoplova, O. A. Ejegbavwo, C. R. Martin, M. D. Smith, W. Setyawan, S. G. Karakalos, C. H. Henager, H. C. Zur Loye, N. B. Shustova, *J. Am. Chem. Soc.* **2017**, *139*, 16852–16861.

Abstract:

In this thesis work, we explore the chemistry and reactivity of high valence transition metal cations (4+ and 5+) as well as tetravalent actinides towards carboxylate ligands and the possibility to isolate multidimensional metal-organic frameworks.

The first part deals with the chemistry of a poorly studied metal, the niobium at its +4 and +5 oxidation states. The reaction of niobium(IV) tetrachloride precursor towards pyridine-dicarboxylic acid ligands in different organic solvents leads to the isolation of four complexes with discrete 8-fold coordinated Nb(IV) mononuclear units, for which the d^1 configuration has been analyzed by magnetic measurements, EPR and XPS. The reactivity of the pentavalent ethoxide niobium(V) precursor has been investigated with a series of mono- and poly-carboxylic acids ligands, by controlling the hydrolysis rate. A total of twelve crystalline coordination complexes has been isolated with variable molecular $\{Nb_2O\}$, $\{Nb_4O_4\}$, $\{Nb_8O_{12}\}$ and $\{Nb_{12}O_{21}\}$ cores, by successfully controlling the condensation process.

The second part is dedicated to the crystal chemistry of four novel thorium(IV) coordination polymers, which were isolated by using 4,4'-azobenzenedicarboxylate and 3,3',5,5'-azobenzenetetracarboxylate ligands with the help of monocarboxylic acid ligands as modulators for improving the crystal growth process. In parallel, mixed Th-U carboxylate compounds were prepared with a 'prior to synthesis' substitution procedure, for three distinct systems, involving 9-anthropic acid, amino derived 4,4'-biphenyldicarboxylic acid and fumaric acid. They were studied under SEM-EDX to determine the efficiency of the substitution and thermal calcination led to the formation of solid solution $Th_{1-x}U_xO_2$ oxides. Full characterization study has been conducted for the different phases (single-crystal XRD, PXRD, IR, TGA, SEM). The adsorption capacities were analyzed with N_2 , Xe, Kr, CH_4 and CO_2 gases for the samples exhibiting porosity (mainly for Th-based compounds).

Résumé :

Dans cette contribution, nous explorons la chimie et la réactivité des cations métalliques de haute valence (4+ et 5+) vis-à-vis de ligands carboxylate ainsi que la possibilité d'isoler des metal-organic frameworks. La première partie traite de la chimie d'un métal peu étudié, le niobium à son degré d'oxydation +4 ou +5. La réaction du précurseur tétrachlorure de niobium(IV) ($NbCl_4 \cdot 2THF$) avec des ligands de la famille des acides pyridine-dicarboxyliques dans différents solvants organiques a conduit à l'isolation de quatre complexes avec des unités mononucléaires discrètes de niobium(IV) en coordinance huit, pour lesquelles la configuration d^1 a été analysée par des mesures magnétiques, RPE et XPS. La réactivité du précurseur pentavalent d'éthoxyde de niobium(V) ($Nb(OEt)_5$) a été étudiée avec une série d'acides mono- et poly-carboxyliques, en contrôlant le taux d'hydrolyse. Un total de douze complexes de coordination cristallins a été isolé avec des noyaux variables $\{Nb_2O\}$, $\{Nb_4O_4\}$ et $\{Nb_8O_{12}\}$. $\{Nb_{12}O_{21}\}$, en contrôlant avec succès le processus de condensation.

La deuxième partie est consacrée aux actinides tétravalents (thorium et uranium), où quatre nouveaux polymères de coordination du thorium(IV) ont été isolés en utilisant les ligands 4,4'-azobenzènedicarboxylate (noté $abdc^{2-}$) et 3,3',5,5'-azobenzènetétracarboxylate (noté $abtc^{4-}$) avec l'appui de ligands acides monocarboxylique comme modulateur. Une étude de caractérisation complète a été menée pour les différentes phases (DRX monocristal et poudre, IR, ATG, MEB) et les propriétés d'adsorption ont été étudiées avec les gaz N_2 , Xe, Kr, CH_4 et CO_2 . En parallèle, des composés mixtes Th-U ont été préparés avec une procédure de dopage "avant la synthèse". Ces composés ont été étudiés sous MEB-EDX pour déterminer l'efficacité de la substitution et seront utilisés à l'avenir comme précurseurs pour préparer des oxydes mixtes Th-U pour un combustible nucléaire potentiel.